Short Period Variable Stars in the *Kepler* Field

Adam Brooks

Supervisors

Professor Mark Cropper & Dr. Gavin Ramsay

Mullard Space Science Laboratory

Holmbury St. Mary - Dorking - Surrey

Armagh Observatory

Armagh, Northern Ireland

A Thesis submitted to UCL for the degree of Master of Philosophy

I, Adam Brooks confirm that the work presented in this thesis is my own. Where information has been derived from other sources, I confirm that this has been indicated in the thesis.

Abstract

The *Kepler* Satellite provides unique opportunities in stellar astrophysics, with its observations being of particular importance to the asteroseismology community. With *Kepler* having a limited target list due to data telemetry limitations, pre-launch time series and colour photometric surveys were undertaken to identify suitable targets for observation. However, none of these combined cadence and depth that matched that derived using *Kepler* itself. This meant that there were potentially many short period variable sources awaiting discovery which could be observed by *Kepler*. We therefore chose to initiate a deep, high cadence survey, RATS-*Kepler*, with a cadence of $\sim$1 minute and a depth of $g \sim 21$ with the aim of recovering astrophysically interesting sources to potentially be observed by *Kepler*. The work presented here details my role in developing a new data reduction pipeline process, a new variable stars selection algorithm and the subsequent selection of sources for proposals for *Kepler* short cadence observations. I present the results of our survey, which have been made publicly available to maximise their scientific impact and the *Kepler* data obtained for the 18 sources which we successfully obtained short cadence observations. I then go on to outline the future of the *Kepler* mission now that it is unable to continue with its initial mission.

Acknowledgments

First and foremost I would like to thank my supervisor, Gavin Ramsay. His guidance has helped me to learn how to evaluate things like a real scientist and has been invaluable.

I would also like to thank the friends who have made Armagh a great place to live these last few years, particularly Joachim Bestenlehner, Kamalam Vanninathan and Aswin Sekhar who were firm friends throughout my time here; as well as some of the more recent additions Will Mclean, Juie Shetye and Yanina Metodieva who have helped make these last few months a time I won't forget and kept me sane whilst writing my thesis.

Contents

Abstract **2**

Acknowledgments **3**

Contents **4**

List of Figures **8**

List of Tables **13**

1 Introduction **15**

1.1 The Variable Sky 15

1.2 Intrinsic Variables 19

1.2.1 δ-Scuti stars 28

1.2.2 Rapidly Oscillating Ap stars (roAp stars) 33

1.2.3 Subdwarf B (sdB) stars 34

1.2.4 White dwarfs 40
1.2.4.1 DAV or ZZ-Ceti stars 42
1.2.4.2 DBV or V777 Her stars 43
1.2.4.3 GW Vir or PG1159 stars 43
1.2.4.4 DQV stars 44
1.2.4.5 Extremely Low Mass Variables (ELMV) 45
1.2.5 Flare stars 47
1.2.6 Cataclysmic Variables (CVs) 48
1.3 Extrinsic Variables 52
1.3.1 Eclipsing and Contact binary systems 53
1.3.2 Planetary Transits 54
1.4 Ground Based Wide Field Variability Surveys 55
1.4.1 The RApid Temporal Survey (RATS) 58
1.5 Early Space-Based Variability Observations 59
1.5.1 Microvariability and Oscillations of Stars (*MOST*) 60
1.5.2 Convection Rotation et Transits (*COROT*) 60
1.6 The *Kepler* Satellite 61
1.7 Outline of Thesis 66

2 Observations and Data Reduction **68**

2.1 Observational Strategy 68
2.2 Telescopes and Instrumentation 71
2.2.1 Isaac Newton Telescope (INT) 71
2.2.2 MDM Telescope 72
2.3 Data Reduction 76
2.3.1 Extracting light curves 79

3 Selecting Variable Sources **85**

3.1 Variability Algorithms 85
3.1.1 Median Absolute Deviation from the Median (MAD) . . . 88
3.1.2 Chi-Squared Test 90
3.1.3 The Alarm Test 92
3.1.4 Analysis of Variance 94
3.1.5 Lomb-Scargle Periodogram 97
3.2 Selecting Candidate Variables 100
3.3 Follow-up Spectroscopic Observations 114
3.4 Sources Submitted for *Kepler* Proposals 115
3.5 Summary 121

4 *Kepler* Short Cadence Data **125**

4.1 *Kepler* Short Cadence Observations 125

4.2 δ-Scuti stars 133

4.2.1 Our Sample of δ-Scuti Stars 134

4.2.2 KIC 5623923: a δ-Scuti in a Contact/Eclipsing Binary . . 136

4.3 KIC 11911480: a Pulsating DA White Dwarf 144

4.4 KIC 7431243 (V363 Lyr): a Cataclysmic Variable 154

4.5 Contact/Eclipsing Binaries 156

4.6 KIC 5474065: an M Dwarf Flare Star 158

5 Summary of Thesis **173**

6 *Kepler* - Past, Present and Future **177**

6.1 *Kepler* - An Overview of the Initial Mission 177

6.2 *Kepler* - The Future and the K2 Mission 181

Bibliography **187**

List of Figures

1.1 Types of variable star 18

1.2 Variables across the Hertzsprung-Russell diagram 20

1.3 Typical pulsation modes in the spectral type versus absolute magnitude (M_V) plane 22

1.4 The effect of varying values of ℓ and m for $0 \leq \ell \leq 5$ 25

1.5 Seismic waves in geoseismology 28

1.6 Plot showing the δ-Scuti instability strip in the $\log T_{eff}$ - Luminosity plane with selected evolutionary tracks 29

1.7 Position of known δ-Scuti stars in the instability strip 31

1.8 Known sdBV and lpsdBV pulsators in the $\log g$ - T_{eff} diagram . . 37

1.9 Region of the $\log g$ - $\log T_{eff}$ plane where the compact pulsators are found 39

1.10 Examples of typical light curves of some compact pulsators 41

1.11 Predicted spectra of excited g-modes in DQV stars 46

1.12 The orbital period distribution of CVs 50

1.13 The *Kepler* light curve of the eclipsing U Gem catacylsmic variable, V447 Lyr 51

1.14 The region of space sampled by the *Kepler* satellite 61

1.15 A comparison of ground-based observations and *Kepler* observations 64

2.1 The location of our field centres 70

2.2 Image of the Isaac Newton Telescope 71

2.3 Image of the WFC camera on the INT 73

2.4 The transmission of the Sloan g and r filters and the quantum efficiency of the CCD on the WFC 74

2.5 Image of the MDM Observatory 75

2.6 Image of the MDM4k detector 77

2.7 The transmission of the Johnson B, V and R filters and the quantum efficiency of the MDM4k and red4k detectors 78

3.1 Example light curves of a variety of known variable sources 87

3.2 A comparison of variability tests 88

3.3 Distribution of chi-squared values 91

3.4 The distribution of Alarm values 93

3.5 The distribution of AOV values against period 96

3.6 The distribution of LS values against period 99

3.7 Plot showing cutoff levels and sources selected for $n = 18$ 102

3.8 Plot comparing methods for selecting candidate variable sources . 105

3.9 The RATS-*Kepler* light curves of 12 sources 106

3.10 Plot showing the cut-off to select variable sources for various values of n 108

3.11 Plot showing the $(g-r)$–$(u-g)$ colour-colour plane of all sources 110

3.12 Plot showing the $(r-i)$–$(r-\mathrm{H}_\alpha)$ colour-colour plane of all sources 111

3.13 The spectral fit to KIC 3223460 117

3.14 The INT light curve of those sources which *Kepler* Short Cadence data has been obtained for 119

3.15 The spectra of eight of our sources which have been observed by *Kepler* in short cadence mode 122

3.16 The spectra of seven of our sources which have been observed by *Kepler* in short cadence mode 123

3.17 The spectrum of KIC 5474065 124

4.1 The *Kepler* SC light curves of the eleven sources which appear to be δ-Scuti type stars 135

4.2 The power spectra of six of the sources shown in Figure 4.1 137

4.3 The power spectra of five of the sources shown in Figure 4.1 . . . 138

4.4 The location of our δ-Scuti sources in the δ-Scuti instability strip 139

4.5 A short section of Q14 *Kepler* data of KIC 5623923 140

4.6 A close up of the light curve of KIC 5623923 141

4.7 The power spectrum of the Q14 *Kepler* light curve of KIC 5623823 143

4.8 The RATS-*Kepler* light curve of the DA White dwarf KIC 11911480 and its Lomb-Scargle power spectrum 145

4.9 Colour-colour diagrams showing the position of KIC 11911480 and KIC 4552982 147

4.10 T_{eff} - $\log g$ distribution for a sample of DA white dwarfs 148

4.11 T_{eff} - Period distribution for a sample of DA white dwarfs 149

4.12 The Lomb-Scargle power spectrum of the *Kepler* light curve of the DA White dwarf KIC 11911480 151

4.13 A close up of the Lomb-Scargle power spectrum of KIC 11911480 153

4.14 The *Kepler* short cadence light curve of KIC 7431243 155

4.15 The *Kepler* short cadence light curves of the contact binaries KIC 7667885, KIC 9786165 and KIC 12553806 157

4.16 The *Kepler* Short Cadence light curve of KIC 5474065 161

4.17 Four day sections of the *Kepler* Short Cadence light curves of KIC 9726699 and KIC 5474065 162

4.18 The cumulative energy distribution of flares in KIC 5474065 and KIC 9726699 166

4.19 The mean folded light curves of KIC 5474065 and KIC 9726699 . 167

4.20 The cumulative flare frequency for a large group of M dwarfs . . . 169

6.1 A schematic overview of the *Kepler* mission lifetime 178

6.2 A histogram showing the number of exoplanet discoveries by year since 1995 179

6.3 *Kepler* planet candidate radii vs. orbital period 180

6.4 K2 mission observation strategy 183

6.5 Schematic representation of a typical K2 campaign timeline 184

6.6 Proposed K2 observation campaigns 185

List of Tables

1.1 Summary of a number of short period time-series photometry surveys 57

1.2 Summary of a number of short period surveys covering the *Kepler* field 66

2.1 A summary of our observations to date 69

2.1 List of fields observed using the INT in 2011 81

2.1 List of fields observed using the INT in 2011 82

2.2 List of fields observed using the INT in 2012 83

2.3 List of fields observed using the MDM 1.3m telescope in 2012 . . 84

3.2 Table showing all the variable stars selected using 'n=18' 112

3.2 Table showing all the variable stars selected using 'n=18' 113

3.3 Temperature and $\log g$ values of spectroscopically observed sources 116

3.4 The details of our sources which have been observed by *Kepler* in short cadence mode 120

4.1 The start and end times for *Kepler* short cadence observations . . 127

4.2 Table of sources observed in Q12 128

4.3 Table of sources observed in Q14 129

4.4 Table of sources observed in Q15 130

4.5 Table of sources observed in Q16 131

4.6 Table of sources observed in Q17 132

4.7 Pulsation modes in the DA white dwarf KIC 11911480 150

4.8 The absolute magnitude and luminosity of stars with spectral types M3 V – M5 V 159

4.9 Flare rates for KIC 5474065, KIC 9726699 compared to AD Leo . 165

6.1 Proposed K2 observation campaigns 184

Chapter 1

Introduction

1.1 The Variable Sky

In very early times Greek philosophers supposed that the heavens were a perfect creation of the Gods and that their most 'perfect' form would be as a constant, unchanging entity – but they were wrong. Over the centuries it has been found that stars vary in their light output on a wide variety of timescales, a journey of discovery that began with our Sun.

The first recorded observations of sunspots in 165 BC (Yau and Stephenson, 1998) showed that the light from our own Sun is not even constant with time, with observations by the Bendictine monk Adelmus in 807 AD then showing that these sunspots could appear and disappear over time (Wilson, 1917). Initially many of these observations were mistaken for planetary transits and it was not until Galilei et al. (1613) observed them directly with a telescope that they were

confirmed as being events on the Sun's surface. Since then the well known 11-year solar cycle has been determined (Schwabe, 1844) and a 25.38 day rotation period (Carrington, 1859).

Other signs that the heavens might not be constant came from supernova observations, with the earliest recorded supernova thought to be SN 185, which was observed by Chinese astronomers in 185 AD (Zhao et al., 2006). Over the next almost 2,000 years they recorded another 20 such events (Clark and Stephenson, 1982). Notable examples include: SN 1006 which was the brightest star ever to appear in the night sky, which has had its stellar remnant identified by modern astronomers at a distance of $7,100$ light years (Winkler et al., 2003); SN 1054 which produced the crab nebula stellar remnant and was visible in daylight for 23 days and visible in the night sky for 653 days (Collins et al. (1999); Brecher et al. (1983)); SN 1572, also known as Tycho's supernova due to the extensive observations performed by Tycho Brahe (Brahe and Kepler, 1602); SN 1604, also known as Kepler's supernova due to the extensive observations performed by Johannes Kepler (Kepler, 1606), which was the most recent supernova to occur within the Milky Way that was visible to the naked eye. The latter two events spurred Brahe and Kepler respectively to begin questioning the Aristotelian view that the heavens beyond the Earth were immutable. This was because if the new stars were contained within our known system of planets they should have had a measureable parallax with respect to the background stars as the planets did. However, they failed to measure one. Galileo also tried in vain to measure a parallax for Kepler's supernova, which spurred him to argue against the Aristotelian view in his revolutionary work 'Dialogue concerning the two

chief world systems, Ptolemaic & Copernican' (original in latin: Galilei (1635); Translated into english: Galilei (1953)).

Aside from novae, the first extrasolar truly variable star to be discovered was Mira (Campbell, 1946) when Fabricius noted a new third magnitude star in the constellation of Cetus the whale in August 1596 which disappeared again a few months later. However, Fabricius was murdered before he could gain fame for his discovery (Poggendorff, 1863), so it was not until 1638 when Holwarda noted that the star periodically became visible to the naked eye before becoming invisible even to telescopes, that its variability was truly well known (Campbell, 1946). Since at that time telescopes of sufficient aperture had not been constructed, it was not until 1660 that Mira was found to exhibit regular periodicity on a period of 11 months (Campbell, 1946).

Since then our understanding of what mechanisms power stars and their dynamics have improved drastically and now we know that stars vary in their brightness on many different timescales, whether that is the timescale of only a few minutes such as pulsating white dwarfs or close interacting binary systems; or the changes in output which occur over billions of years as the star passes along the main sequence determined by the changing rates/relative dominances, radial positioning and ignition of different fusion reactions which determine the variations. The continued development of telescopes over the centuries has lead to the discovery of at least 41,000 variable stars in our galaxy alone which can be split into over 100 distinct types (Samus et al., 2009). Stars which vary in their light output on timescales relevant to the advent of modern observational astronomy offer unique ways to probe the physics behind these far away systems and help further our

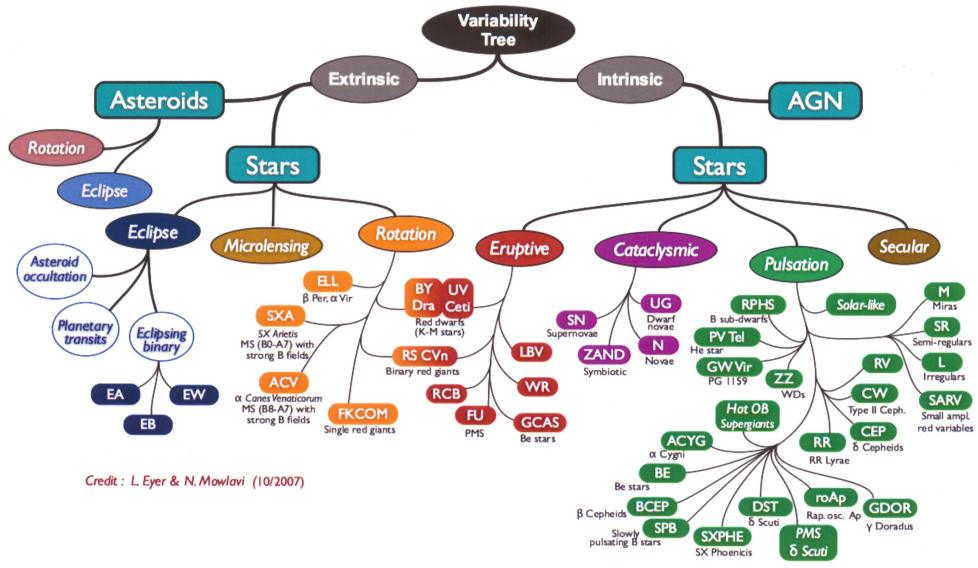

Figure 1.1: A breakdown of group (extrinsic/intrinsic), class of object, variability mechanism and types of variable stars. Image taken from http://www.ast.cam.ac.uk/research/milky.way.and.local.group.stars/variable.stars.

understanding of the behaviour of matter in these extreme environments which we cannot recreate in Earth-based laboratories, because they allow for the indirect determination of local physical parameters which can be used to construct stellar models.

The two most prevalent reasons why stars vary in their light output on observable timescales are physical pulsations of the stars and binary star systems. However, transient short-lived phenomena such as flares and sunspots can also cause irregular variations in the light output of stars. As such, variable stars can be broadly broken down into two classes - intrinsic and extrinsic - as shown in figure 1.1. Intrinsically variable stars are those for which the observed variation in flux is due to intrinsic fluctuations in the total luminosity of the system. They mostly

consist of pulsating stars, but also includes the outburst phases of interacting cataclysmic binary systems. Extrinsically variable stars are those where the observed variation in flux is not due to changes in the overall luminosity of the system, but rather due to mechanisms which change the amount of light which reaches Earth. Hence this class is composed almost entirely of binary systems, however it also includes rotating stars where the inhomogenous spread of sunspots across the star's surface is significant enough to cause observed variations in the flux. The work in this thesis will concentrate on those stars which exhibit variability on timescales of $\lesssim 2$ hours, with a particular focus on those which vary on timescales of <60 minutes, a number of which will be discussed in the following sections.

1.2 Intrinsic Variables

The intrinsically variable class of stars is mostly composed of pulsating stars, which populate a number of different regions in the Hertzsprung-Russell diagram as shown in figure 1.2. These pulsations are driven by instabilities due to ionisation of an abundant element at a critical depth (Cox, 1980), through a process known as the opacity change mechanism (κ-mechanism). In the case of the well-known instability strip, it is caused by the transition between ionised states of helium in regions known as helium ionisation zones. The two principle transitions involved are between neutral helium (He) and singly ionised helium (HeI) at temperatures of around 25,000–30,000K and the transition of HeI to doubly ionised helium (HeII) at temperatures of around 35,000–50,000K. If they are at a critical depth

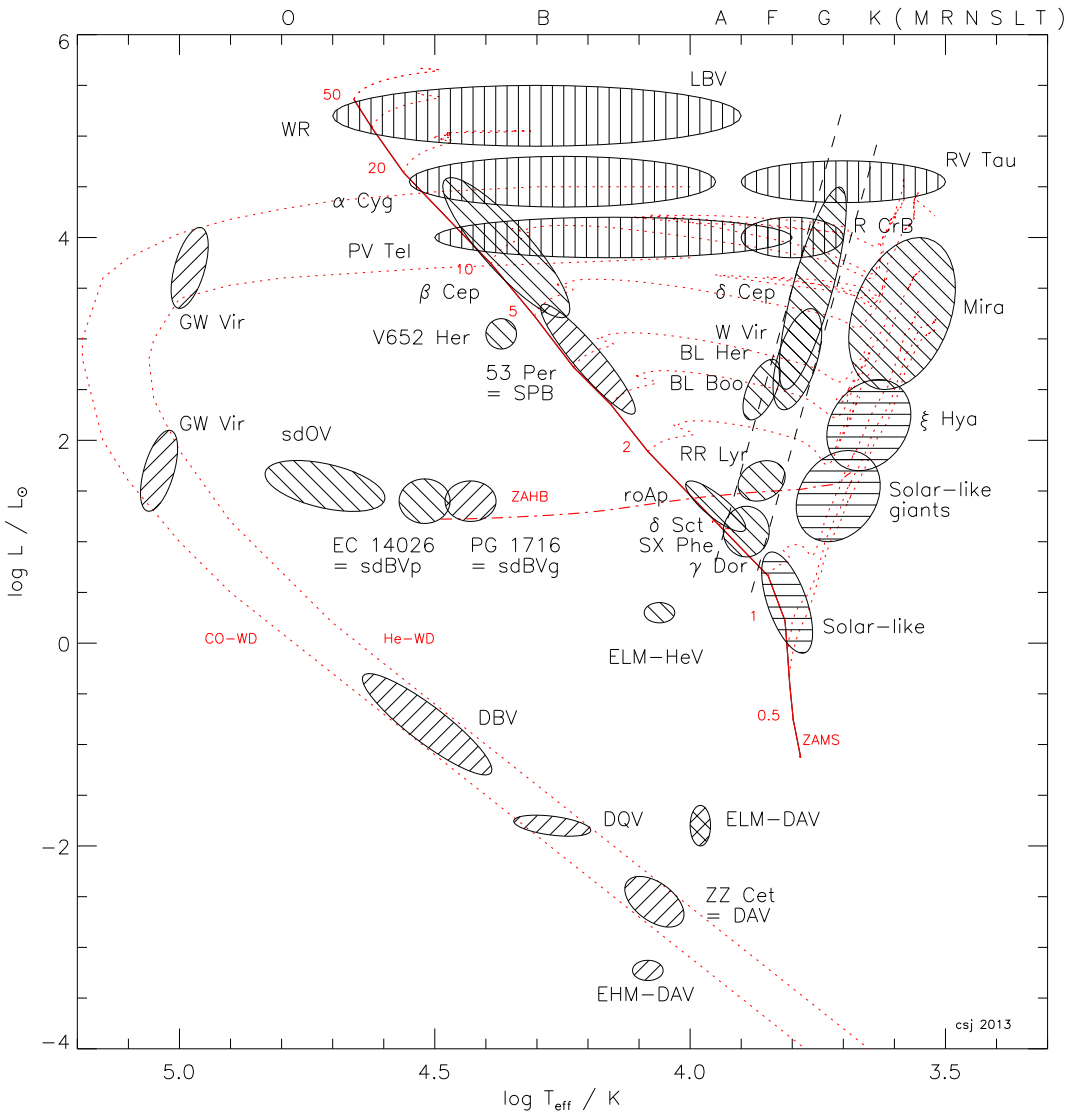

Figure 1.2: The Hertzsprung-Russell diagram showing regions where stars have the potential to exhibit pulsations due to their physical parameters, with a basic designation of pulsation modes and driving mechanism, where backward hatches represent p-mode pulsators; forward hatches represent g-mode pulsators; horizontal hatches represent solar-like oscillations; and vertical hatches represent stellar wind-driven variability. The solid red line indicates the zero-age main sequence; the dashed-dotted line indicates the zero-age horizontal branch; dashed tracks indicate evolutionary tracks for stars at a range of masses and for two types of white dwarf - carbon-oxygen and helium. Figure courtesy of Professor Simon Jeffery, Armagh Observatory/Trinity College Dublin.

then they can excite resonant pulsation modes via the cyclical process:

- The increase in the number of free electrons available increases opacity in the ionisation zone, causing more radiation to be absorbed which increases the temperature;
- The increase in temperature causes a thermal expansion which causes the temperature to decrease;
- This leads to a recombination of electrons, decreasing the opacity, causing the gas to cool and contract;
- This contraction leads to increased density and therefore the temperature rises once more, causing ionisation and the cycle continues;

When at a critical depth, the kinetic energy changes in this process can drive a variety of wave types. The allowed types of wave that can propagate depend on a number of factors, including temperature, composition, the existence of convective regions and modulating effects such as rotation. Figure 1.3 shows the dominant pulsation modes found in population I pulsating stars. Brief descriptions of some of the most commonly excited wave types are:

- p-modes – Acoustic waves driven by pressure differences, with speeds determined by the local speed of sound;
- g-modes – Gravity waves driven by buoyancy effects;

The propagation of these waves satisfies the wave equation,

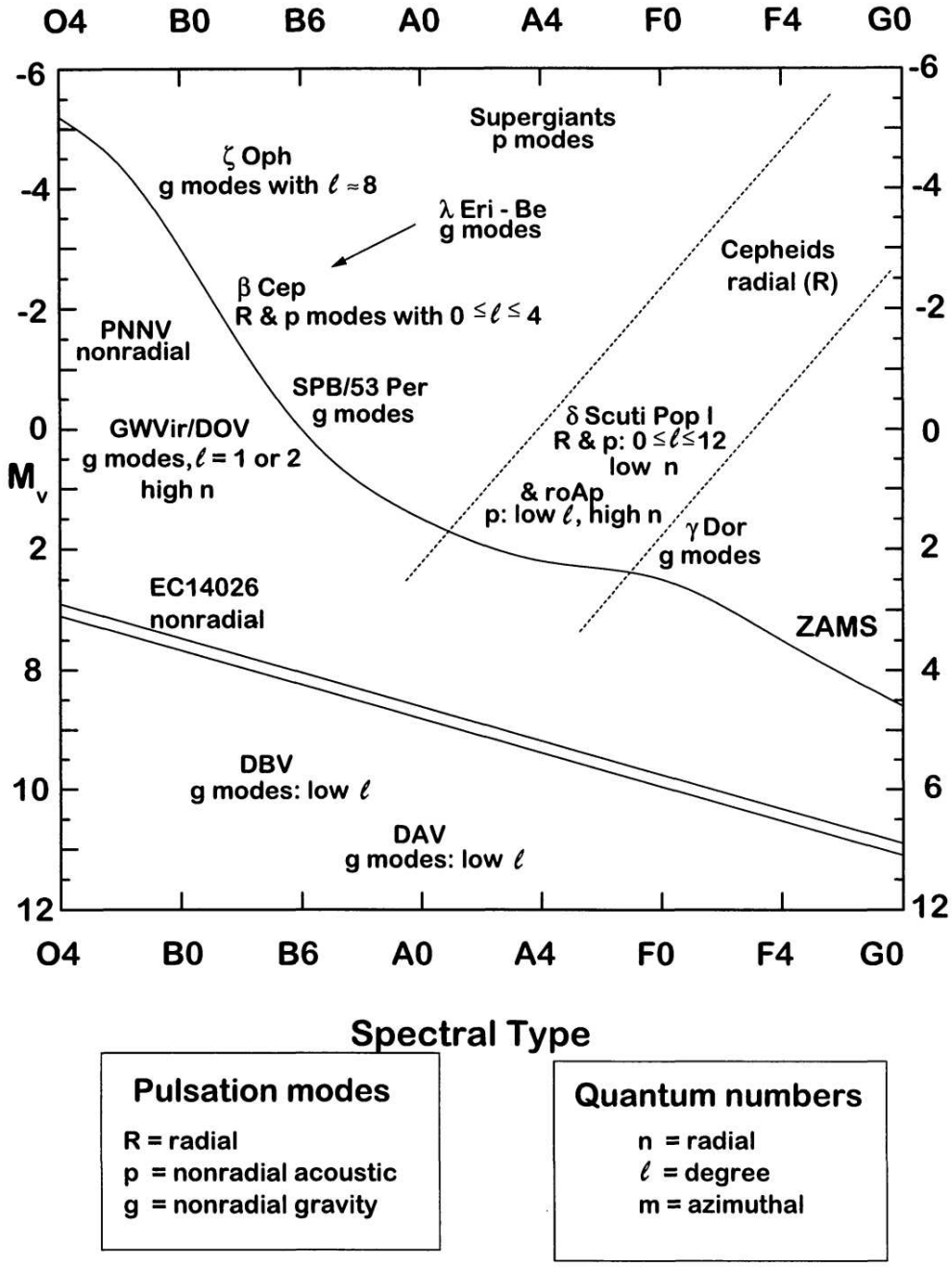

Figure 1.3: Illustration showing the approximate location of Population I pulsating stars in the spectral type versus absolute magnitude (M_V) plane and their typical pulsation modes. PNNV stars are a now defunct sub-class of GW Vir stars and EC14026 stars are now known as the subdwarf B variable stars. The quantum numbers are the eigenvalues described below. Note that some mode identification types may be speculative. Figure taken from Breger and Montgomery (2000).

$$\frac{1}{c^2}\frac{\partial^2 \mathbf{u}}{\partial t^2} = \nabla^2 \mathbf{u} \tag{1.1}$$

where $\mathbf{u}$ is a function which describes the propagation of the wave and is a function of $\mathbf{r}$, the radius; θ, the polar angle which is measured from the z-axis and takes values in the range $0 \rightarrow \pi$; ϕ, the azimuthal angle which is measured in the xy-plane and takes values in the range $0 \rightarrow 2\pi$; and time, t. ∇^2 is the laplacian operator which, in spherical polar coordinates, is defined as

$$\nabla^2 = \frac{1}{r^2}\frac{\partial}{\partial r}\left(r^2 \frac{\partial}{\partial r}\right) + \frac{1}{r^2 \sin\theta}\frac{\partial}{\partial \theta}\left(\sin\theta \frac{\partial}{\partial \theta}\right) + \frac{1}{r^2 \sin^2\theta}\frac{\partial^2}{\partial \phi^2} \tag{1.2}$$

through separation of variables the Helmholtz equation is derived and it can be shown (Boas, 2006) that the radial and angular components have general solutions of the form

$$A(r, \theta, \phi) = \sum_{\ell=0}^{\infty} \sum_{m=-\ell}^{\ell} (a_{\ell m} j_\ell(nr) + b_{\ell m} y_\ell(nr)) Y_\ell^m(\theta, \phi) \tag{1.3}$$

where $j_\ell(nr)$ and $y_\ell(nr)$ are the spherical Bessel functions of the first and second kind respectively; and $Y_\ell^m(\theta, \phi)$ are the spherical harmonics defined by

$$Y_\ell^m(\theta, \phi) = P_\ell^m(\cos\theta) e^{im\phi} \tag{1.4}$$

where $P_\ell^m(\cos\theta)$ are the associated Legendre polynomials. This solution is arrived at through the definition of eigenvalue problems, which gives rise to the eigenfunctions $j_\ell(nr)$, $y_\ell(nr)$ and $Y_\ell^m(\theta, \phi)$ which form complete orthogonal sets

on their domains (Boas, 2006). It is beyond the scope of this work to describe how these eigenfunctions are then related to the physical properties of stars, but it suffices to say that only discrete modes are allowed to propagate; which are uniquely described by the eigenvalues n, ℓ and m, which all take integer values and can be broadly described as:

- n – Often referred to as the 'radial order' of the mode. It determines the number of radial nodes of the wave, i.e. the number of stationary points in the wave in the radial direction. It is sometimes denoted by the symbol k;
- ℓ – Often referred to as the 'radial degree' of the mode, it is related to the angular momentum eigenstate exhibited by the wave. Mathematically speaking it determines the degree of the legendre polynomial and the order of the Bessel function describing the propagation of the wave, which corresponds physically to its shape. It determines the total number of nodes, ℓ, on the stellar surface (no radial motion takes place on these node lines);
- m – Eigenvalue related to the azimuthal projection of the angular momentum, often referred to as the 'azimuthal order' of the mode, it determines the number of nodes on the stellar surface, ℓ, which are orientated along the meridian. It can take values in the range $-\ell \leq m \leq \ell$, meaning for a given value of ℓ there are $2\ell + 1$ allowed values of m. Under the convention established in Unno et al. (1979) positive values of m denote azimuthal waves running in the same direction as the rotation of the star and represent prograde modes, whereas negative values of m represent retrograde modes;

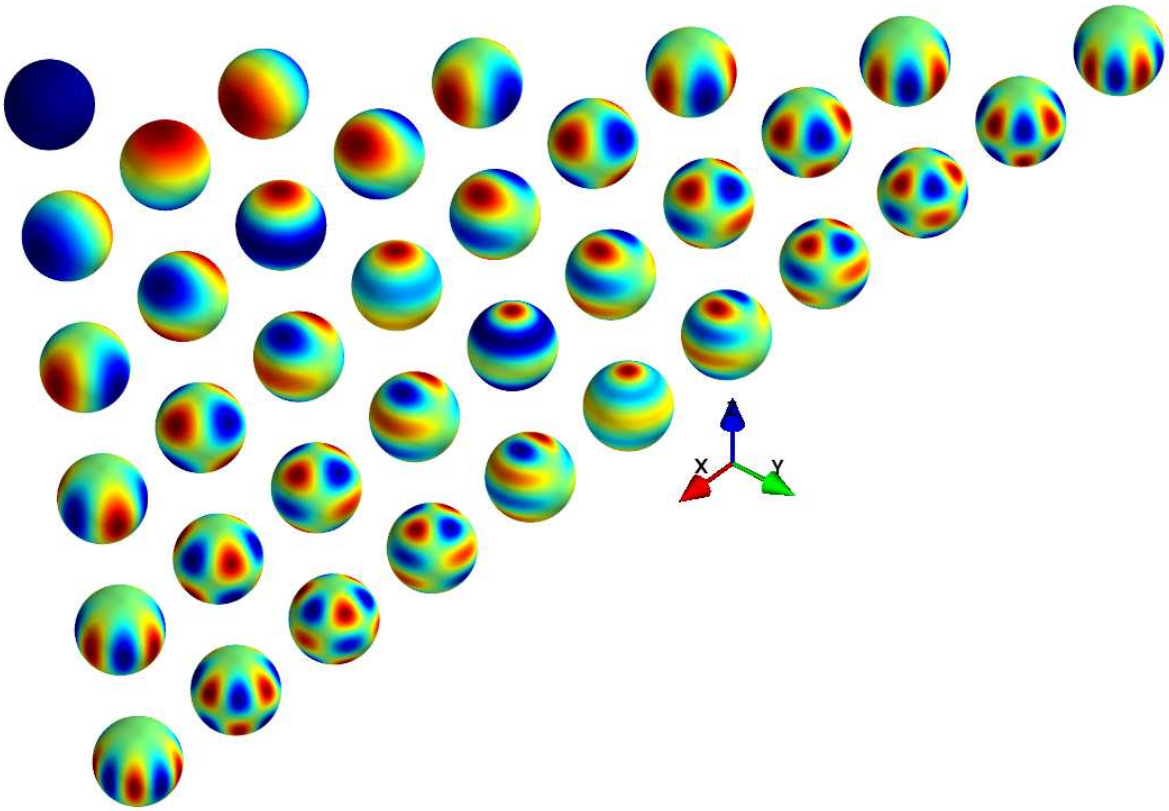

Figure 1.4: An illustration of how different wave modes cause varying deformations of stars depending on the ℓ and m values selected for $0 \leq \ell \leq 5$. The deformations are denoted by a heat map, where red indicates outward pulsations and blue indicates inward pulsations. These deformations oscillate between outward and inward (and vice versa) with time. The orientation of the axes is shown in the bottom right hand corner. ℓ values increase along the y-axis starting from $\ell = 0$ for the solid blue sphere in the top-left corner, m values are distributed along the x-axis. The wave nodes precess around the z-axis with time in a direction determined by the sign of m. Plot made using the Mayavi python package (Ramachandran and Varoquaux, 2011).

Due to the orthogonality of the eigenfunctions, it can be shown (Boas, 2006) that if two (or more) different solutions satisfy the wave equation within the star, then so too will a linear combination of them. Hence modes which are sums or any linear combination of these modes can also propagate.

Purely radial pulsations correspond to cases where $\ell = 0$ and $n = 0, 1, 2, \cdots, \infty$. Mathematically speaking this occurs because the spherical harmonics, $Y_\ell^m(\theta, \phi)$, are single valued for $\ell = 0$ (whereas the radial component is not for $\ell = 0$), hence there is no angular dependence for the resultant wave and motion is purely radial. In this case the variations in luminosity are wholly due to the changing surface temperature of the star as it expands and contracts radially. For the special case of the mode corresponding to $n = 0$ the Helmholtz equation reduces to Laplace's equation, whose angular solutions are still the spherical harmonics, $Y_\ell^m(\theta, \phi)$, but the radial component has solutions of the form

$$R(r) = a_{\ell m} r^\ell + \frac{b_{\ell m}}{r^{\ell+1}} \tag{1.5}$$

and is called the fundamental overtone; $n = 1$ is the first overtone; $n = 2$ the second overtone; and so on.

For non-zero values of ℓ the radial motion is perturbed by the angular dependance introduced by the spherical harmonics, $Y_\ell^m(\theta, \phi)$. Mathematically speaking this occurs because the associated Legendre polynomials have values in the range $-1 \rightarrow 1$, hence, radial motion will be modified by a factor in the range $-1 \rightarrow 1$ with a dependance on θ and ϕ. This is known as non-radial pulsation as the resultant waves are radially anisotropic. Figure 1.4 shows examples of the effect of a variety

of different modes of wave for values of ℓ in the range $0 \leq \ell \leq 5$, demonstrating how different values of ℓ and m can cause the star to be deformed in different ways. If we take the simple ℓ=1 modes as an example, it can be seen that for m=0 an alternate brightening of the north and south poles occurs; whilst the m=$\pm$1 cases result in waves of brightness travelling in opposite directions across the equator. In non-radially pulsating, non-rotating stars without a magnetic field, the frequency of all modes of a given ℓ have the same frequency for all $2\ell + 1$ allowed values of m, which is known as degeneracy. The presence of rotation or a magnetic field can cause this degeneracy to be broken into up to $2\ell + 1$ and $\ell + 1$ distinct frequencies respectively (Winget et al., 1991), which is analagous to the Zeeman effect in atomic physics.

Effects such as rotation, non-axisymmetric internal magnetic fields and other perturbing effects can cause different m values to be prefered or to be excluded from being excited. Analysis of pulsations to derive the resonant energy levels being excited in this process offers a unique opportunity to probe the interiors of such stars through the science of asteroseismology, in a similar way to that which is used to determine the internal composition of the Earth through the science of geoseismology, as demonstrated in figure 1.5. What questions can be answered depends on the nature of the object in question, but includes probing properties such as temperatures in different regimes, internal rotation, the extent of the core and envelope sections of the star and the mechanisms driving the pulsations themselves, where the higher the number of different excited modes, the more information can be extracted. There are a wide variety of stars for which these pulsations occur over timescales of less than 1–2 hours, including δ-Scuti stars,

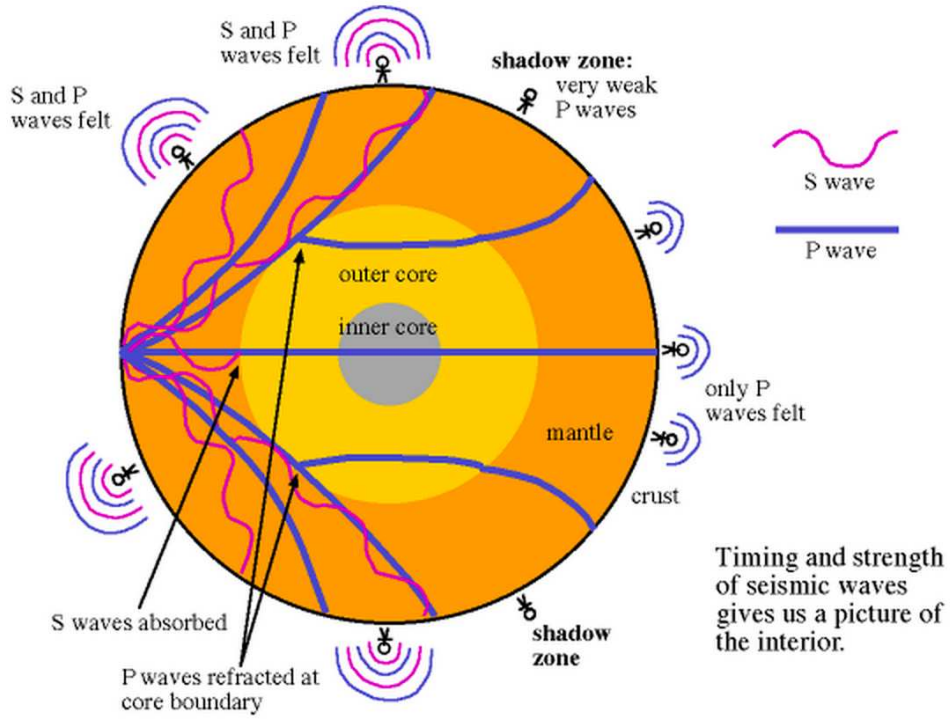

Figure 1.5: A basic illustration showing how geoseismology uses different types of wave to probe the interior of the Earth, a method which has been extended to probe the interiors of stars through the science of asteroseismology. Figure taken from http://simostronomy.blogspot.co.uk/2010/01/surfs-up-astronomers-ride-stellar-waves.html, copyright Nick Strobel.

Subdwarf B stars, PG1159 stars and white dwarfs, which will be discussed in more detail in the following sections.

1.2.1 δ-Scuti stars

δ-Scuti stars are the second most populous variable star in the galaxy after the white dwarfs (Breger, 1979), they have spectral types between A and F, masses in the range 1.5–2.5$M_{\odot}$ (Breger and Montgomery, 2000) and occupy the classical instability strip near where it crosses the zero-age main sequence on the

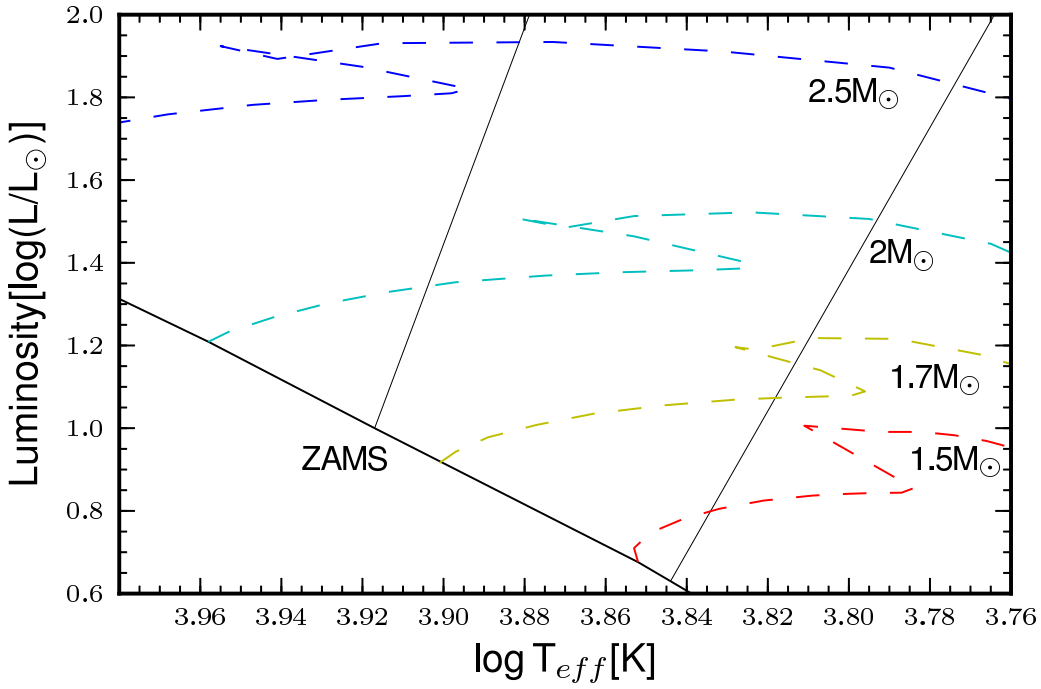

Figure 1.6: Plot showing the δ-Scuti instability strip in the $\log T_{eff}$ - Luminosity plane, where the δ-Scuti instability strip is contained in the region between the two near vertical lines extending upwards from the zero-age main sequence (ZAMS). The evolutionary tracks for stars of initial mass $1.5M_{\odot}$, $1.7M_{\odot}$, $2M_{\odot}$ and $2.5M_{\odot}$ are shown, which illustrate how the δ-Scuti stars can be either main sequence stars or evolved sub-giants whilst in their pulsation phase. The values of the δ-Scuti instability strip were taken from Dupret et al. (2004); whilst the stellar evolutionary tracks were taken from Schaller et al. (1992) and were provided by the Geneva group.

Hertzsprung-Russell Diagram as shown in Figure 1.6. They show photometric variations in their light curves on periods in the range 18 minutes (HD34282, Amado et al. (2004)) up to 7 hours (SS Piscium, McNamara and Redcorn (1977)), vary with amplitudes in the range 0.002–1.30 mag (Rodríguez et al., 2000), with effective temperatures and $\log g$ values in the range T_{eff} = 6300–8300 K and $\log g$ = 3.2–4.3 (Rodríguez and Breger, 2001). It has been theorised that all stars in this region should pulsate, with the deficiency of detected systems attributed to these variations being below the level of current photometric accuracy and hence are unmeasurable, resulting in observations finding 33–50% of stars found in this region showing variation in their light curve (Breger and Montgomery, 2000), as shown in figure 1.7 (note that most δ-Scuti stars have not been discovered in surveys and are not shown in this figure so as to show an unbiased sample. Consequently, the stars used in this figure were restricted to those studied in unbiased variability surveys which treated variable and non-variable sources similarly). As can be seen in figure 1.6 their positioning so close to the zero-age main sequence means that stars of different initial mass may be either main sequence stars or evolved sub-giants during their phase of exhibiting δ-Scuti type pulsations. This is in contrast to the longer period pulsators in the instability strip which have always evolved off the main sequence before pulsating, such as Cepheids and RR Lyrae stars. This causes two distinctive classes in the population I δ-Scutis:

- High Amplitude δ-Scutis (HADS) - composed of the higher temperature, more massive, evolved sub-giants which pulsate predominantly in high ℓ, radially isotropic modes, often only at the fundamental overtone, but more typically show pulsations in a few different modes.

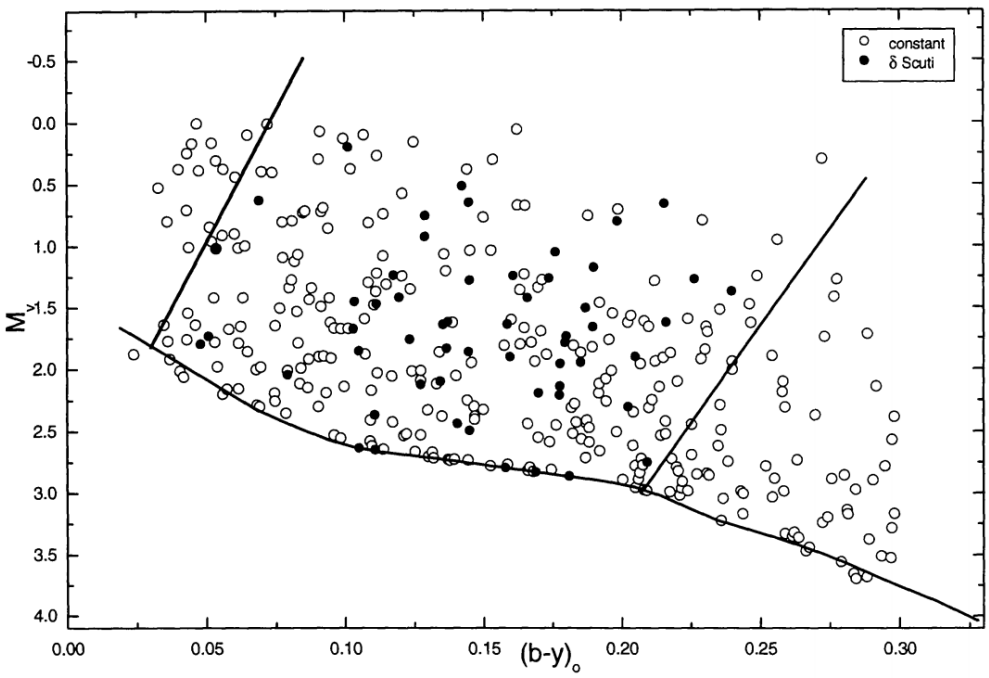

Figure 1.7: Position of known δ-Scuti and constant (to a detection limit varying between 0.003 and 0.010 magnitudes) stars in and around the instability strip in a colour-magnitude diagram. Approximately 33–50% of stars in this region show photometrically measurable variability. Figure taken from Breger and Montgomery (2000).

- Low Amplitude δ-Scutis (LADS) - composed of the lower temperature, lower mass stars which are on the main sequence when they pass through the instability strip. As well as the radially isotropic modes seen in HADS, LADS also exhibit lower ℓ, radially anisotropic modes which cause asymmetric pulsations of the star.

The multiple types of modes excited in the LADS sub-group makes these stars of particular interest to asteroseismologists, as the greater number of excited modes allows for more information about the interior of the star to be obtained, however, long-term near-continuous observations are required to do this well.

One of the advantages of the HADS only showing pulsations on a small number of modes means that they have a well-defined period-luminosity relation derived by McNamara et al. (2000), meaning they can be used as distance indicators. Added to these sub-classes of δ-Scutis, there are metal-poor stars known as SX Phoenicus (SX Phe) stars which pulsate via the same mechanism as δ-Scutis, with their lower metallicity causing lower amplitude pulsations on a period range of 56–172 minutes (Rodriguez et al. (1990); Poretti et al. (2008)) with amplitude variations of 0.050–0.80 mag. They show a tendency to have larger amplitude pulsations for longer period ranges, a phenomenom not seen in δ-Scutis (Nemec and Mateo, 1990). Their origin is also largely unknown, their lower metallicity might imply that they are population II objects, but they do not show the same age, typically being 2–5 billion years old (Nemec and Mateo, 1990). The majority are found in globular clusters, where they appear as blue stragglers. Due to their pulsation modes being similar to those of the HADS, they too have a well-defined period-luminosity relationship.

Currently, the main open question in the field of δ-Scutis concerns the selection and excitation of the different p and g modes available (Uytterhoeven et al., 2011a), which are affected by the internal composition of the star and the pulsation mode driving mechanisms. Before recent space-based programs there were only a small number of well-studied cases due to the limitations of ground-based data and the need for a long-term study to build effective asteroseismological models, especially for the LADS which show multiple pulsation modes.

1.2.2 Rapidly Oscillating Ap stars (roAp stars)

roAp stars are A-spectral type stars which are chemically peculiar and show photometric variability in their light curve over an observed period range of 4–23.6 minutes (Dupret et al. (2008); Alentiev et al. (2012)). They have abundances of some rare-earth metals sometimes exceeding 10^6 times that of solar abundances, magnetic fields in the range 1–25 kG (Kurtz et al., 2011) and T_{eff} in the range 6600–8500K (Paunzen et al., 2012). They show rapid oscillations in both their photometric flux (which also show frequency multiplets (Baldry et al., 1998)) and their radial velocities. The current best model to explain the observed variations in flux is the κ-mechanism operating in the hydrogen ionisation zone (Balmforth et al., 2001), with the obliquely rotating magnetic field playing a key role in mode selection and driving (Paunzen et al., 2012). The theoretical instability strip of these stars was computed by Cunha (2002), however, not all stars within this region show variability (Paunzen et al., 2012) and the observed cool edge of this instability strip is cooler than that computed (Kurtz et al., 2011). Were the pulsations simple axisymmetric spherical harmonics, measurements of the changing pulsational amplitude with rotation (the pulsation axis is generally not aligned with either the rotational or magnetic axes) would allow for a simple determination of the degree, ℓ and put constraints on the relative inclinations of the rotational and magnetic axes (Kurtz et al., 2011). However, it has been shown (Takata and Shibahashi (1994, 1995); Dziembowski and Goode (1996); Cunha (2006); Saio and Gautschy (2004); Bigot et al. (2000)) it is far from a simple spherical harmonic. This makes it difficult to treat both of the competing effects of rotation and magnetism. Add to this the relatively small sample of 45 currently

known systems (Paunzen et al., 2012) and the limitations of ground-based work, the need for more systems being observed over longer periods of time to improve our understanding of these objects is clear. The benefit of this is not just limited to our understanding of these objects though, the observed vertical stratification of metal abundances in these stars has applications in atomic diffusion theory, with applications in solar physics, stellar cluster age determination, pulsation driving in main sequence and sdB stars and a possible solution for frequency anomalies in β Cep stars (Kurtz et al., 2011).

1.2.3 Subdwarf B (sdB) stars

Subdwarf B stars are degenerate objects which have a helium burning core and a thin atmosphere typically dominated by hydrogen and occupy the blue end of the horizontal branch (c.f. Figure 1.2). They have effective temperatures in the range $20,000\,\mathrm{K} \lesssim T_{eff} \lesssim 35,000\,\mathrm{K}$ (Østensen et al., 2010a) and typically have a mass of $\sim 0.5\mathrm{M}_{\odot}$ and $\log g \sim 5.8$ (Saffer et al., 1994), with an extremely thin ($\mathrm{M}_{Env} \leq 0.02\mathrm{M}_{\odot}$) inert hydrogen dominated envelope (Heber (1986); Saffer et al. (1994)). Their main formation mechanisms are thought to be the expulsion of the envelope via stellar winds or the result of one or two common envelope phases. However, the exact mechanism and timescales of this remains an unresolved issue as the mass loss mechanism in the progenitor has to remove all but a tiny fraction of the hydrogen, as well as needing to have enough hydrogen to fuse until this time to produce a core that reaches sufficient mass ($\sim 0.47\mathrm{M}_{\odot}$) to initiate the helium flash (Østensen et al., 2010a). Approximately half of the known sdB systems are in close binary systems with a white dwarf or M-dwarf companion (Maxted

et al. (2001); Napiwotzki et al. (2004)). A significant fraction of the rest are in binary systems with a main sequence F–K companion (Østensen et al., 2010a). Hence mass transfer in close binary evolution must be an important evolutionary pathway for sdB stars (Han et al., 2002, 2003).

Pulsating sdB stars were found by Kilkenny et al. (1999) with the discovery of short period variability in the light curve of V361 Hya and are now known as sdBVs or V361 Hya stars. Typically V361 Hya stars exhibit short period (∼1–10 minutes), low amplitude variations attributed to low order p-modes and typically have pulsation amplitudes in the range of ∼10 mma[1](Østensen et al., 2010a). They have been observed to be as high as ∼60 mma in V338 Ser (Kilkenny et al. (1999), Oreiro et al. (2004)) and as low as 2mma in LM Dra (Silvotti et al., 2000). The number of detected modes in these systems varies from one, to more than fifty and is strongly correlated to measurement accuracy (Østensen et al., 2010a). Then in 2001 V1093 Her was found to exhibit long period (∼1 hour) variations in its light curve (Green et al., 2003) which are attributed to high radial order g-modes and are now known as long period sdBVs (lpsdBVs) or V1093 Her stars. These longer period pulsators are cooler than their short period counterparts and exhibit lower amplitude variations in their light curve, with example light curves for both class of object shown in Figure 1.10. Two instabililty regions were successfully found for these subclasses in the $\log \mathrm{T}_{eff}$–$\log g$ plane (see below), however, in 2006 DW Lyn/HS 0702+6043, which was between the boundaries of these instability regions, was found to exhibit both long and short period variations simultaneously (Schuh et al., 2006). At least four more sdB stars have

[1]The mma units are 10^{-3} of the Fourier amplitudes of a lightcurve in normalised intensity units. One mma translates to a peak-to-peak amplitude of two millimodulation intensity (mmi) units in the light curve.

since been found to show both long and short period variability (Østensen et al., 2010b) and populate a region centred around $29k$ K, as shown in figure 1.8. These stars are known as DW Lyn or hybrid sdBVs.

The iron-opacity bump constitutes a significant contribution to stellar opacity for iron group elements (chromium, manganese, iron, cobalt and nickel) at temperatures of ∼200,000 K (Rogers and Iglesias (1992); The Opacity Project Team (1995)). Radiative levitation and gravitational settling is operative in sdB stars (Chayer et al., 1995) and can cause sufficient accumulation of iron group elements in layers at ∼200,000 K to excite pulsations. It was predicted using computational models that low degree (ℓ), low radial order (n) pulsation modes could be driven by an iron opacity bump driving zone at ∼200,000 K in sdB stars of effective temperatures in the range $29,000\,\mathrm{K} \lesssim T_{eff} \lesssim 36,500\,\mathrm{K}$ (Charpinet et al., 1996, 1997). Their simultaneous and independent detection was considered a major success of pulsational theory (Fontaine and Brassard, 2008). This mechanism has been used to successfully explain p-mode pulsations in sdBVs and g-modes in lpsdBVs (Fontaine et al., 2003), but the hybrid pulsators remained unexplained. With the addition to the models of more accurate opacity statistics for iron and nickel by Jeffery and Saio (2006), the iron opacity effect was enhanced and the nickel opacity temperature range moved to within the temperature range of the driving zone, the instability regions were expanded to the point that the two instability regions overlap, thus explaining the hybrid sdBVs.

Around 10% of the sdBVs pulsate (Charpinet et al., 2001), whilst undocumented reports suggest that around 50% of the lsdBVs pulsate (Jeffery and Saio, 2007). Radiative levitation and gravitational settling have been shown to be effective at

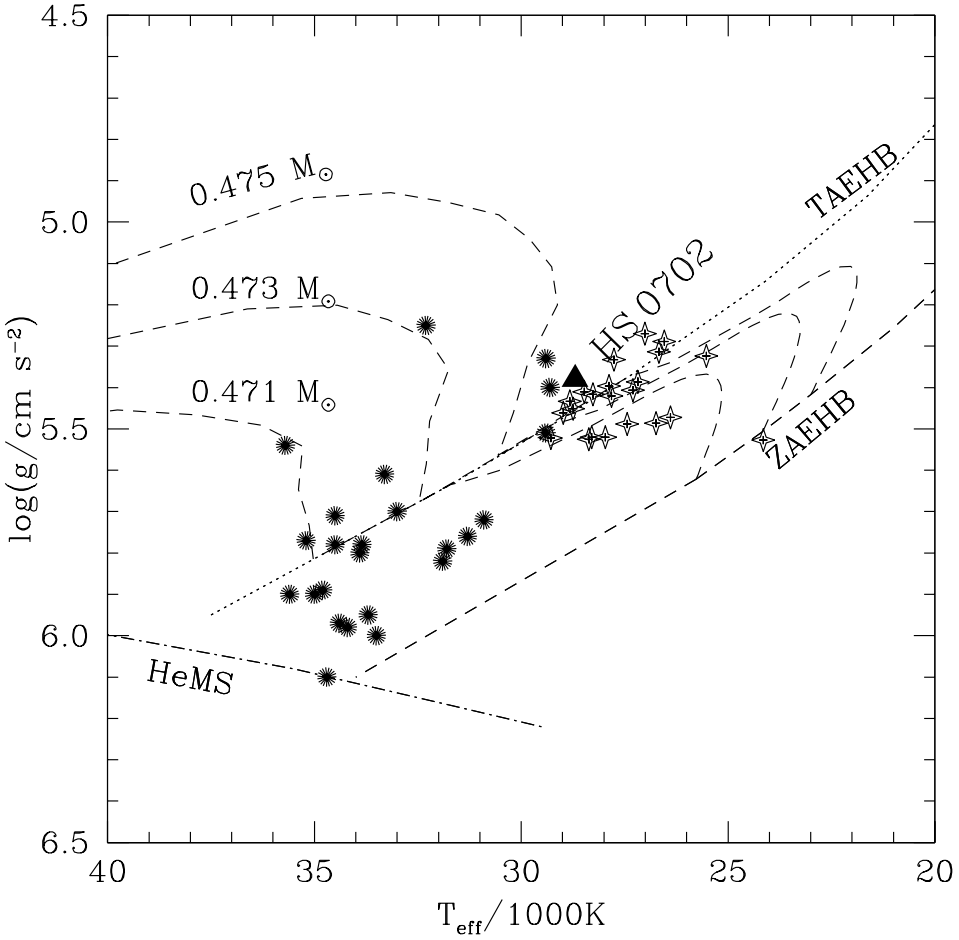

Figure 1.8: Known sdBV and lpsdBV pulsators in the $\log g$ - T_{eff} diagram: sdBV populate the higher-temperature region and are plotted as filled circles, lpsdBV populate the lower-temperature region and are plotted as open stars. The helium main sequence (HeMS), zero (ZAEHB) and terminal (TAEHB) age extended horizontal branches are marked; also shown are evolutionary tracks off the extended horizontal branch by Dorman et al. (1993). The position of HS 0702+6043, the prototype of the hybrid sdBVs, is plotted as a triangle. Figure taken from Schuh et al. (2006).

accumulating sufficient iron group elements within the driving zone within 10^6 years (Fontaine et al., 2006). Since this is such a short fraction of the typical sdB evolutionary lifetime of $\sim 10^8$ years (Dorman et al., 1993), it is an unresolved mystery as to why all of the sdBs located within the instability strip have not been found to pulsate (Østensen et al., 2010b). Most sdBVs that have been monitored regularly have shown varying amplitudes of pulsation with time, with some pulsation modes having been reported to disappear completely (Kilkenny, 2010). Jeffery and Saio (2007) have speculated that pulsations may disrupt local elemental enhancements on timescales much shorter than the diffusion timescale on which they accumulate. Hence, once enough iron and nickel have accumulated in the driving zone to trigger pulsational instability, pulsations may redistribute iron and nickel away from the driving zones. Furthermore, since p-modes operate primarily vertically and g-modes operate mostly horizontally, the shorter period p-mode pulsators may redistribute the iron to hotter and cooler regions on shorter timescales than their longer period counterparts, which may explain the large discrepancy between the fractions of sdB stars found to pulsate in the hot and cool instability regions. In recent years theoretical models of sdB stars have become capable of accurately predicting the pulsation frequencies in sdB stars (Hu et al., 2008, 2009). Hence, new high-precision, long-term observations of these objects will help distinguish the individual formation channels and finally allow for their complete evolutionary history to be unravelled (Østensen et al., 2010a).

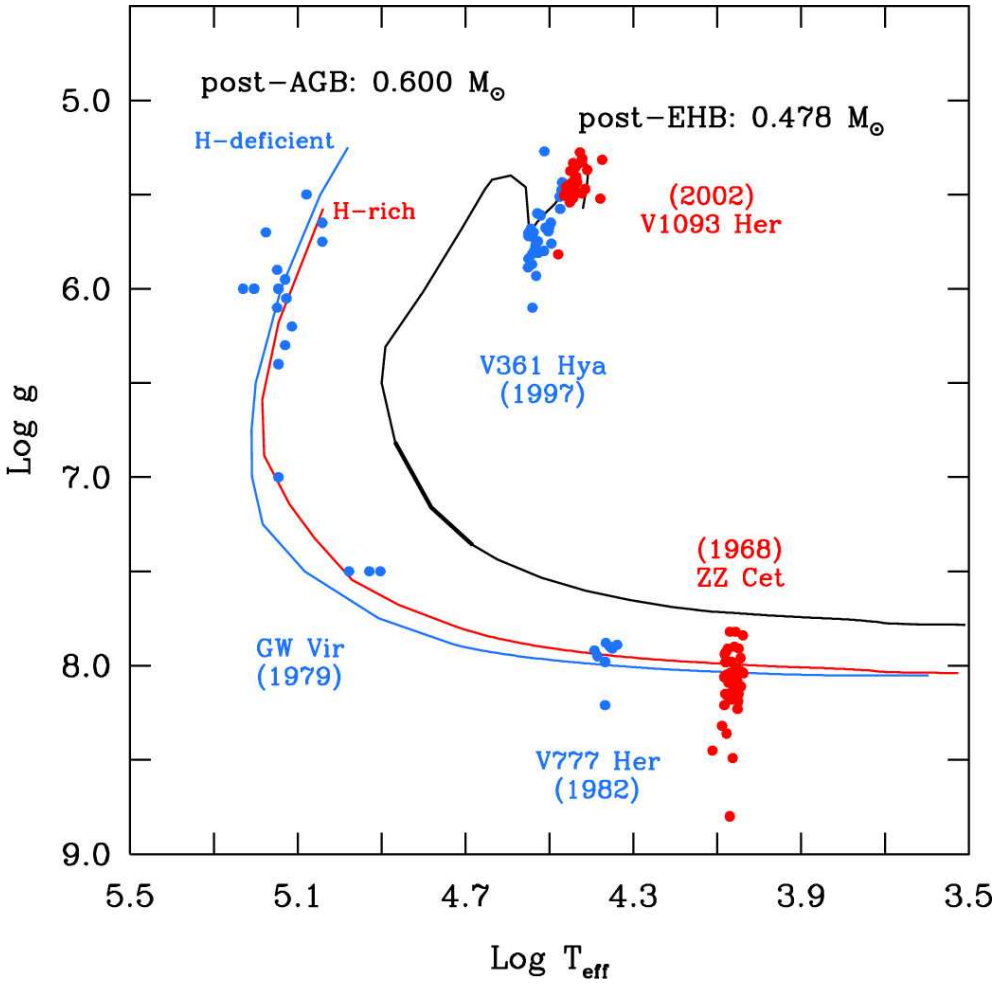

Figure 1.9: Region of the $\log g$ - $\log \mathrm{T}_{eff}$ plane where the compact pulsators are found. Each of the five distinct families is identified by its official IAU name, and the year of the report of the discovery of the prototype of each class is also indicated. Typical evolutionary tracks are plotted showing (1) the track followed by a $0.6\mathrm{M}_{\odot}$ post-AGB, H-rich star, which becomes a H-atmosphere white dwarf (red curve), (2) the path followed by a $0.6\mathrm{M}_{\odot}$ post-AGB, H-deficient star, which becomes a He-atmosphere white dwarf (blue curve), and (3) the path followed by a $0.478\mathrm{M}_{\odot}$ post-EHB model, which leads to the formation of a low-mass H-atmosphere white dwarf (black curve). Figure taken from Fontaine and Brassard (2008).

1.2.4 White dwarfs

White dwarfs are degenerate objects which are supported against gravitational collapse by electron degeneracy pressure and typically consist of degenerate carbon or oxygen cores with a thin hydrogen or helium atmosphere. They are known to have masses ranging from $0.17M_{\odot}$ (Kilic et al., 2007) up to $1.33M_{\odot}$ (Kepler et al., 2007), where the mass distribution is strongly peaked around $0.6M_{\odot}$ with the majority lying in the range 0.5–$0.7M_{\odot}$. They have radii typically in the range 0.008–$0.02R_{\odot}$ (Shipman, 1979), which is comparable to the Earth's radius of $0.009R_{\odot}$. They are the endpoint of the stellar lifecycle for all stars with initial masses of $< 10.5M_{\odot}$ (in the single star evolution scenario), or more precisely, when the core mass is $< 1.44M_{\odot}$ once all fusion reactions cease (Werner et al., 2005). As such $\sim$97% of stars in the Galaxy will eventually evolve into white dwarfs (Fontaine et al., 2001). They begin their life when nuclear fusion in a star ceases and the outer layers have been shed, after which they cool on timescales of 10^9 years from initial temperatures of up to 200,000 K (Kurtz et al., 2008). As they cool they have the potential to exhibit pulsations as they pass through a number of instability regions in the HR-diagram, as shown in Figure 1.9, with all pulsations found to be due to the propagation of g-mode waves (Fontaine and Brassard, 2008). This leads to five sub-classes of pulsating white dwarf, example light curves of some of which can be seen in Figure 1.10, which will be described in the following sections.

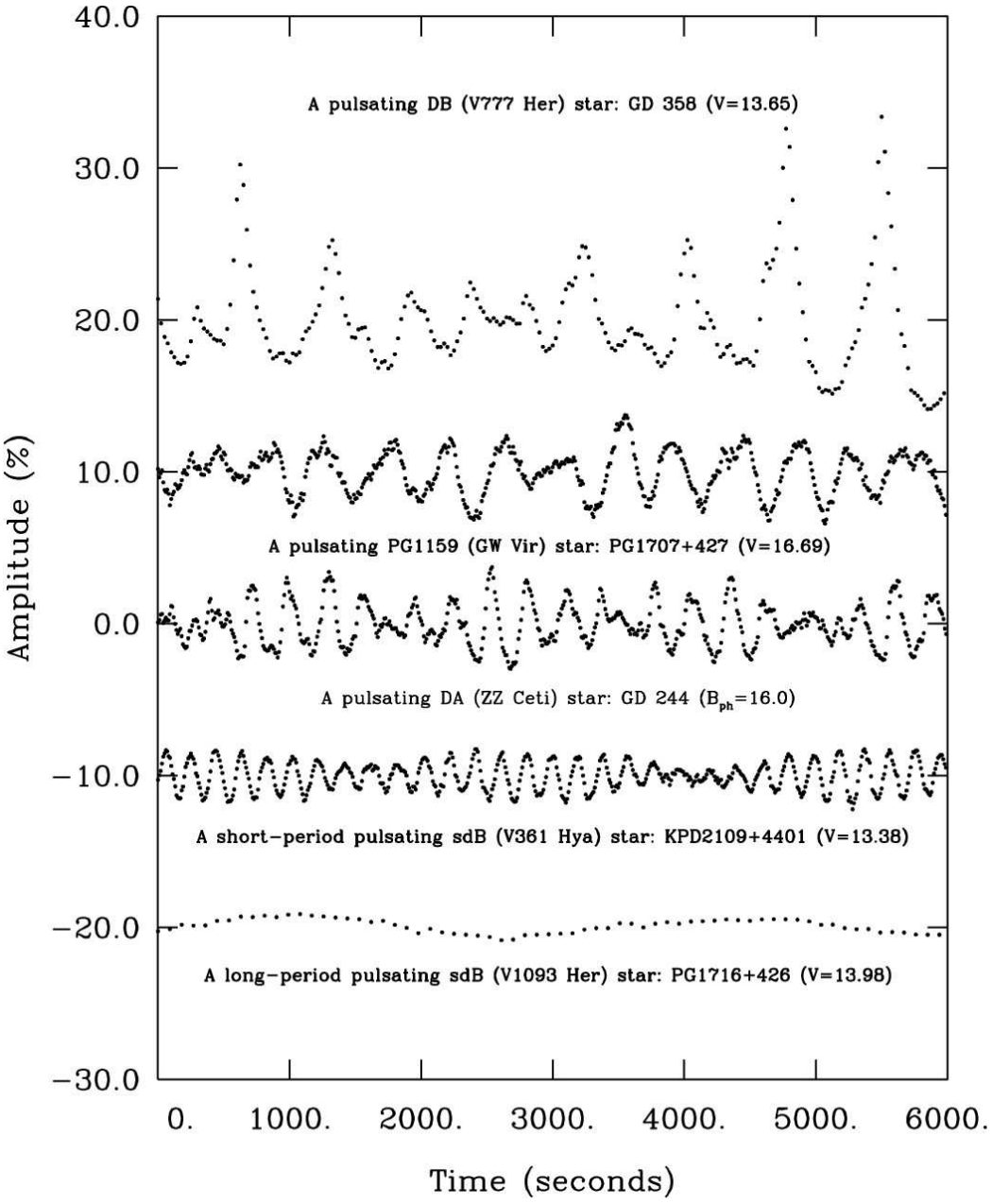

Figure 1.10: Examples of typical optical light curves of some compact pulsators. Each light curve is displaced up by 10% starting from the lpsdBV star at –20%. Note the quasi-periodic behaviour which implies a beat frequency between multiple propagating modes. Figure taken from Fontaine and Brassard (2008).

1.2.4.1 DAV or ZZ-Ceti stars

Hydrogen (or DA) white dwarfs comprise ∼80% of all white dwarfs. As they cool, they pass through an instability strip centred around 11,800 K, starting at T_{eff} ∼13,000 K and ending at ∼10,000 K (Fontaine and Brassard, 2008). The first photometrically variable DA white dwarf discovered was HL Tau 76 in 1976 (Landolt, 1968). Their pulsations are driven via a combination of the κ-mechanism in the hydrogen ionisation zone and a superficial convection zone induced by this process. This convection zone is important as it leads to non-uniform period distributions (Brassard et al., 1992). This excites g-mode oscillations (Chanmugam (1972); Warner and Robinson (1972)), which are highly sensitive to chemical stratification and propagate easily in the outer layers, but are suppressed in the highly degenerate core. Since they are the coolest of the Carbon/Oxygen core pulsating white dwarfs this means that of the various varieties of variable white dwarf, the least can be probed about the core. This is due to the lower core temperature causing a higher degree of degeneracy in the core than the other, hotter pulsating white dwarfs; however, the envelope can be more readily probed than their hotter counterparts. Extensive studies of the DAV, G29-38, have shown that to be able to construct comprehensive asteroseismic models, as many of these different competing modes must be observed as possible (Kleinman et al., 1994, 1998). Hence, the longer such systems can be observed continuously, the more comprehensive asteroseismic models of their interior can be developed.

1.2.4.2 DBV or V777 Her stars

Helium (or DB) white dwarfs comprise almost all of the remaining ∼20% of all white dwarfs. As they cool, they pass through an instability strip centred around T_{eff} ∼25,000 K, starting at ∼27,000 K and ending at ∼23,000 K. Variable DB white dwarfs were predicted by Winget (1981) by direct analogy with the DAV white dwarfs. The first photometrically variable DB white dwarf discovered was GD 358 by Winget et al. (1982). The higher temperature of pulsation seen here is due to the element driving the κ-mechanism being helium for transitions between HeII and HeIII (Fontaine and Brassard, 2008), with transitions being driven at the base of the helium convection zone (Beauchamp et al., 1999). From adiabatic modelling (Winget et al. (1983); Bradley and Winget (1994)) it was found that the blue edge of the instability strip for DBVs is a sensitive function of the convective efficiency of the envelope and the total stellar mass; and is independent, to first approximation, of the helium envelope mass and the core composition (Beauchamp et al., 1999). Given this dependence of important structural and asteroseismological parameters, it is clear how an improved set of long time-series, high precision observations could improve theoretical models.

1.2.4.3 GW Vir or PG1159 stars

These stars are actually a transitionary, short lived state between the Asymptotic Giant Branch phase of stellar evolution and the birth of a white dwarf where the outer envelope has been shed, but helium fusion has reignited until mass loss and cooling cause it to make the final transition to a hot white dwarf. They exhibit

pulsations as they pass through an instability strip centred around 120,000 K. Pulsations in these stars are driven by the κ-mechanism through the ionisation of K-shell electrons in carbon and oxygen (Fontaine and Brassard, 2008). The first photometrically variable PG1159 star to be discovered was PG 1159-035 by McGraw et al. (1979). They typically have a very rich pulsation spectrum, with over 100 modes found in the prototype (Winget et al., 1991). Their hotter temperature means there is a lower degree of degeneracy in the core than the other types of pulsating white dwarf, hence g-mode waves are not so suppressed in the core as they are in other more degenerate classes of pulsating white dwarf. This allows for the greatest degree of probing of the degenerate core of the pulsating white dwarfs.

1.2.4.4 DQV stars

Dufour et al. (2007) reported the discovery of a new type of white dwarf which they recovered during work on the SDSS project. They were found to have carbon-rich atmospheres and populated a narrow range of effective temperature around 20,000 K in the range ∼18,000–24,000 K (Dufour et al., 2008). It had been known theoretically for quite some time that if such carbon-rich atmosphere white dwarfs existed they would have a superficial convection zone (see, e.g. Fontaine and van Horn (1976)) similar to that which drives pulsations in the H and He pulsators. Hence Fontaine et al. (2008) undertook a survey of theoretical models to find if pulsations could be driven in these stars. They successfully found it was possible for g-modes to be driven in these stars, but that for the range of effective temperatures that real DQs populated, a large fraction of helium contamination

(X(He)>0.25) was required, with theoretical calculations of allowed pulsation modes for a variety of compositions shown in figure 1.11. Simultaneously and independently Montgomery et al. (2008) completed a survey of 6 DQs and were able to report that SDSS J1426+5752 pulsates in at least one mode with a period of 417s.

1.2.4.5 Extremely Low Mass Variables (ELMV)

In May 2012 Hermes et al. reported the discovery of an extremely low mass variable white dwarf which showed high amplitude, non-sinusoidal variations in its light curve on a period exceeding 4000s. With $T_{eff} = 9100 \pm 170$ K and log g = 6.22 ± 0.06, this corresponds to a mass of $\sim 0.17 M_{\odot}$. Since the age of the galaxy is not long enough for the evolution of white dwarfs of mass $< 0.5 M_{\odot}$ via single star evolution, a white dwarf of this mass can have only been produced via binary evolution (Marsh et al. (1995); Brown et al. (2011c)). This makes it highly likely that enough mass is removed to prevent helium fusion into carbon or oxygen (Hermes et al., 2012). There is little direct evidence that low-mass white dwarfs have such a composition, but if they do and they pulsate, it offers unique opportunities. Steinfadt et al. (2010) emphasised that if such stars pulsated in g-modes, these waves would be able to globally probe the core in a way not possible in normal pulsating white dwarfs, which would significantly improve our knowledge of the interiors of white dwarfs.

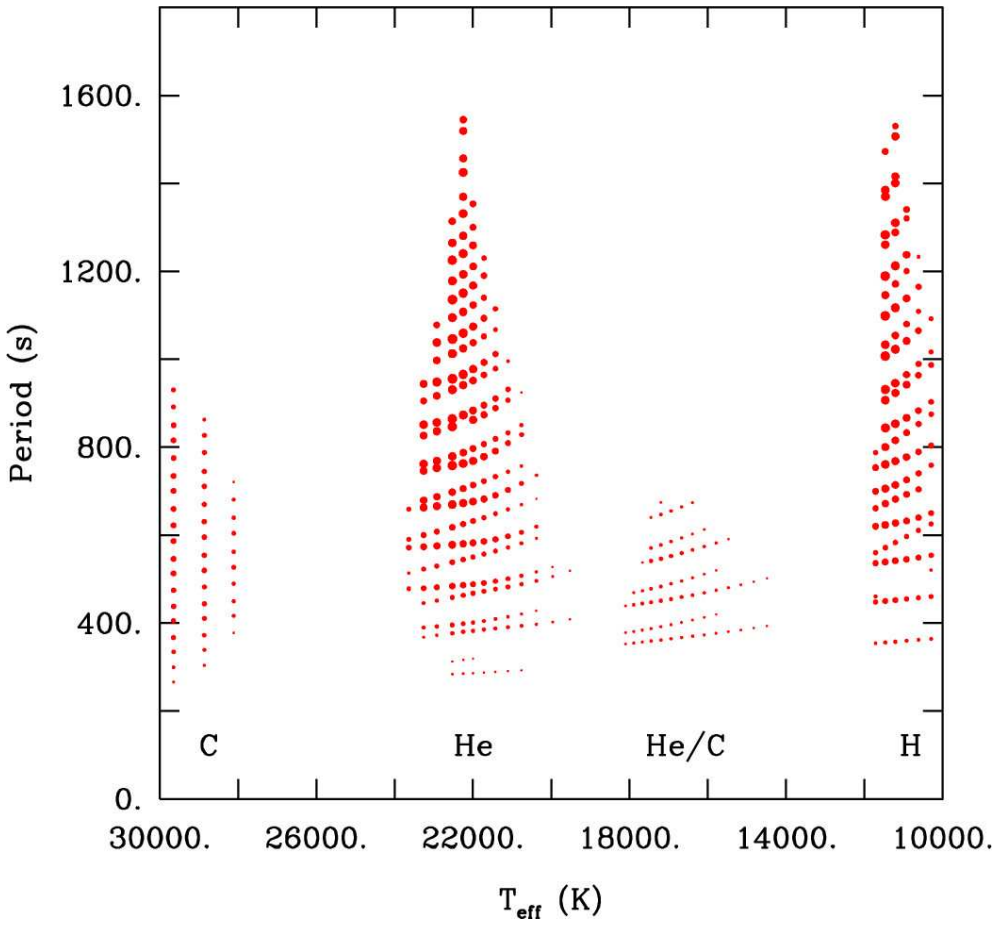

Figure 1.11: Predicted spectra of excited g-modes computed from four distinct evolutionary sequences, each characterized by a total mass of $0.6M_{\odot}$, but with a different envelope composition: pure C, pure He, X(He)=X(C)=0.5, and pure H, from left to right. Each dot gives the period of a mode, and its size represents a logarithmic measure of the modulus of the imaginary part σ_I of the complex eigenfrequency. The bigger the dot, the more unstable the mode. The so-called ML2/α=0.6 version of the mixing-length theory was used in these calculations. Figure taken from Fontaine and Brassard (2008).

1.2.5 Flare stars

Solar flares were first observed by Carrington (1859) and are well observed phenomena on our Sun, which release massive amounts of magnetic energy stored in magnetic loops on the surface and emit large amounts of radiation in optical, UV and X-ray through the process of magnetic reconnection (Haisch et al., 1991). Such events have also been observed on other stars (Kowalski et al., 2009), with events typically lasting a few minutes, during which the optical brightness of the star can be observed to increase by as much as 100 times (e.g. Kowalski et al. (2010)). Their similarity to Solar flares implies they are likely powered by the same mechanism. Historically, the study of stellar flares was performed by observing known M dwarf stars, though they have also been observed in stars of earlier spectral type (e.g. Andrews (1967)).

M-type stars are of particular interest to the exoplanet community since they are a good candidate for hosting easily detectable planets in the habitable zone (see, e.g. Scalo et al. (2007)). This is because the transit of Earth-mass planets across lower radii stars is easier to detect and that the habitable zone (a radially defined zone where the temperature of a planet would make it habitable. One of the key criteria for this is that the temperature allows for the presence of liquid water, thought to be a key parameter for planets to be able to support life) is closer to the star and hence has a shorter orbital period, meaning more potential transit detections in a given period of time. For example, the habitable zone for an M4 V dwarf is 0.04–0.14 AU (Kopparapu et al., 2013), which would imply a relatively short orbital period. However, the prevalence of flaring in M-type stars could be a problem for the potential habitability of planets in the habitable

zone of such stars (Segura et al., 2010). If flares happen too frequently then the atmosphere of such a planet may not be able to prevent damaging amounts of hard radiation from reaching the planet's surface. Further observation of a sample of these stars would help to place constraints on the flaring rate and intensity so that the effect on habitability could be quantified.

1.2.6 Cataclysmic Variables (CVs)

Cataclysmic variable stars consist of a white dwarf primary accreting matter from a secondary star, with the presence of hydrogen in the spectra of all but one sub-class implying that the secondary must be on (or near) to the main sequence. As CVs evolve over time they lose angular momentum through magnetic braking (Verbunt and Zwaan (1981); Rappaport et al. (1983)) and gravitational wave radiation (Faulkner (1971); Paczyński and Sienkiewicz (1981)), which causes their orbital period and radius to reduce. This continues until the donor star loses enough mass such that hydrogen burning can no longer be sustained, causing it to become semi-degenerate and increase in size, which increases the angular momentum of the system and the orbital period begins to increase. Hence, a strong prediction of CV evolution theory is the existence of a minimum orbital period (Rappaport et al. (1982); Paczyński and Sienkiewicz (1983)). Early work predicted this minimum to occur at around $P_{min} \approx 60 - 80$ mins (Paczyński and Sienkiewicz (1981); Rappaport et al. (1982)), whilst more recent work utilising improvements in the modelling of low-mass stars gives a value of $P_{min} \approx 65 - 70$ mins (Kolb and Baraffe (1999); Howell et al. (2001)). Observationally, a period minimum is found in the known sample of CVs at $\sim$76 mins (Knigge,

2006), which is significantly longer than the theroretical value, which implies there may be additional sinks of angular momentum loss other than gravitational wave radiation (e.g. Patterson (1998)).

Furthermore, binary evolution models (e.g. Kolb and Baraffe (1999)) imply that there should be a significant accumulation of CVs near the minimum period, as this is theorised to be the longest-lived stage of their evolution, which is often referred to as the 'period minimum spike'. For many years this was not found observationally (Patterson (1998); Gänsicke et al. (2002); Knigge (2006)) and was a source of frustration for the CV community. However, Gänsicke et al. (2009) finally detected it in a sample of SDSS spectroscopically selected sources, with a significant accumulation of sources found in the range 80–86 minutes, as shown in Figure 1.12, finally resolving this discrepancy. The previous lack of systems found in this period range was attributed to the vast majority of systems previously identified being discovered when they were in outburst, which happens much less often in these systems; lower mass transfer rate meaning intrinsically fainter luminosity; and complex selection effects (Gänsicke, 2005).

There is also a significant lack of CVs detected in the range $2\text{h} < P_{Orb} < 3\text{h}$, which is known as the 'period gap'. The conventional explanation (e.g. King (1988)) for this is that the orbital timescale approaches the thermal timescale for the secondary star, causing it to become fully convective at this point and no longer fills its Roche lobe, causing mass transfer to cease until the system reaches $P_{Orb} \sim 2\text{h}$ and is found observationally (e.g. Szkody et al. (2003, 2007); Southworth et al. (2006, 2007); Gänsicke et al. (2009)).

The exceptions to the period minimum are two groups of helium rich accreting

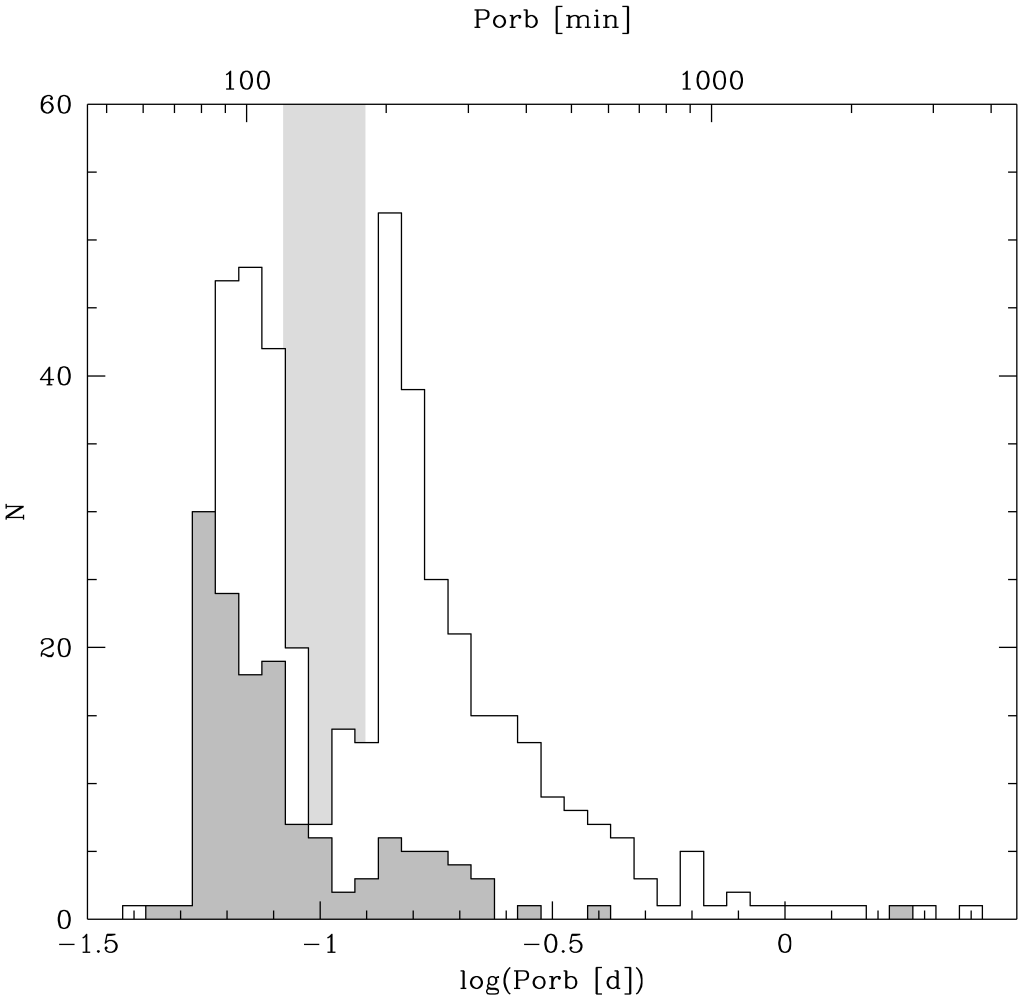

Figure 1.12: The orbital period distribution of 454 CVs from Ritter and Kolb (2003), V7.6, which have no spectroscopic observation in SDSS DR6 (white) and the distribution of 137 SDSS CVs from Gänsicke et al. (2009) (grey). The grey shaded area represents the 2–3 h orbital period gap. These distributions exclude the hydrogen-deficient AM CVn systems. Figure taken from Gänsicke et al. (2009).

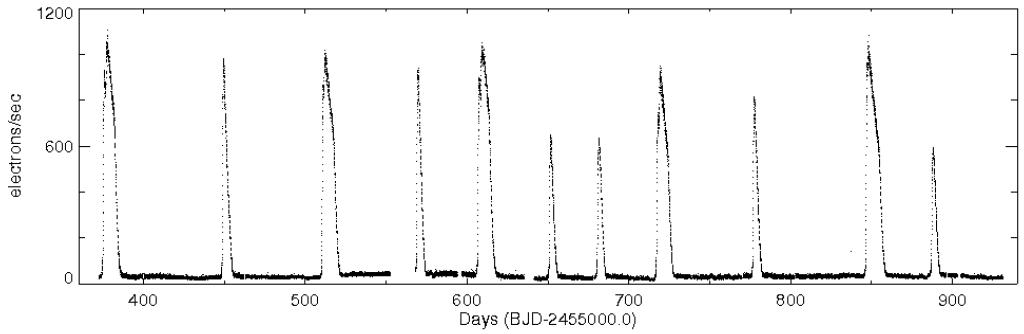

Figure 1.13: The *Kepler* light curve of the eclipsing U Gem catacylsmic variable, V447 Lyr spanning 1.5 years, taken from Ramsay et al. (2012), where the time unit is BJD - 2455000.0. The longer, brighter super-outburst phases can be seen as distinct from the shorter, fainter outburst phases.

binary systems. The helium-dominated, hydrogen deficient AM Canum Venaticorum (AM CVn) stars where the shortest period system identified so far has a period of just 5.4 minutes (Ramsay et al. (2002); Roelofs et al. (2010)), whilst the upper period limit is 65 minutes for these systems to exhibit mass transfer (Solheim, 2010). From their spectra and spatial constraints inferred by their orbital period, both objects must be degenerate or semi-degenerate (Paczyński (1967); Paczyński and Sienkiewicz (1981)), making them an important system in their own right. There is also a much smaller group of evolved hydrogen-rich accreting binaries which exhibit outbursts and in contrast to the AM CVn's, exhibit hydrogen lines as well as helium lines (e.g. Breedt et al. (2012); Carter et al. (2013)).

As well as showing variability in their light curve due to their binarity, CVs also typically exhibit periodic/quasi-periodic 'outbursts' in which their brightness can increase by up to 19 magnitudes in the most extreme cases of the classical novae, with increases of the order of 10 magnitudes more typical (Warner, 1995) and can be further divided into the sub-classes - Classical novae, Recurrent novae, Dwarf

Novae, Polars, Nova-like variables, and Magnetic CVs. The various systems behave differently in outburst and can be satisfactorily modelled by sufficent hydrogen being accreted onto the white dwarf's surface to ignite thermonuclear runaways; or the accretion flow reaching a critical temperature at which the viscosity of the hydrogen significantly reduces, leading to a sudden massive transfer of matter onto the white dwarf, causing a large temperature increase and possibly ignition of fusion (Warner, 1995). Some systems (SU Uma and U Gem) also exhibit outbursts and 'super-outbursts', with figure 1.13 showing the Kepler light curve of the dwarf nova V447 Lyr exhibiting such outbursts. The origin of these two separate scenarios is still yet to be fully understood and long-term, continuous observations of these systems will help further our understanding of accretion physics, which also has implications in the study of other accreting systems such as active galactic nuclei, blackholes and X-ray binaries.

1.3 Extrinsic Variables

The extrinsically variable group of stars is primarily composed of systems which are variable due to eclipses or rotation (c.f. Figure 1.1). For eclipsing systems, the observed variation in luminosity is solely due to eclipses along the line of sight and therefore depends on the angle of inclination of the system to the line of sight, it also means that to detect such a system it needs to be observed at the time of an eclipse. It is generally accepted that a large fraction of all stars are contained within binary systems, with many estimates giving a fraction as high as 57% (Duquennoy and Mayor, 1991). Identifying and studying such systems

is important because they allow for an accurate measurement of local properties such as mass and radius which can be used to improved stellar models and cannot be determined with direct observations in single star systems.

1.3.1 Eclipsing and Contact binary systems

Of all binary systems, a few percent (Duquennoy and Mayor, 1991) eclipse each other as viewed from Earth. They can be seen as a distinct drop in the amount of light observed coming from the system as one star passes in front of the other, the width and depth of which are determined by the transit time of the eclipsing star and the relative differences in radii and brightness between the two stars. To determine the orbital period, eclipses of both stars need to be observed, all these parameters together then allow for the calculation of orbital separation, the velocity of the stars and the stellar radii and luminosities. The duration of eclipses can range from a few 10's of minutes for close binary systems, up to days for wide binaries (Budding et al., 2004). Observations of these systems are important as they are one of the few ways that stellar radii and masses can be directly measured which help to constrain stellar models.

Contact binaries, or W Ursae Majoris systems, are binary systems where the two stellar components are so close together as to be in physical contact with each other and account for $\sim$1% of main sequence star systems (Rucinski (1998), estimates are made excluding stars of spectral type K5 and later), with periods in the range of 0.21–0.7 days (Rucinski and Pribulla (2008); Pribulla et al. (2003)). Their physical point of contact means not only that the stars are close enough together to be deformed to spheroids by each other's gravity, but they can also

exchange material at the point of contact, meaning they are essentially in thermal equilibrium. The observed variation in flux is due to our view of the system changing from the cooler sides of the stars opposite the point of contact, to the hotter contact point of the two stars. This variation happens continuously across the whole orbital phase, so unlike eclipsing binaries where an eclipse has to be observed to confirm the nature of the target, an observation of any phase of a contact binary system allows for its identification.

1.3.2 Planetary Transits

The first exoplanets to be discovered were found around pulsars by virtue of their effect on the arrival time of radio pulses from the pulsar (Wolszczan and Frail, 1992; Wolszczan, 1994). The first exoplanet was found around normal stars in 1995 with the discovery of a Jupiter mass companion of the star 51 Pegasi (Mayor and Queloz, 1995), whilst the first observation of an exoplanet's transit across its host star was observed in late 1999 (Henry et al. (2000); Charbonneau et al. (2000)). By the time of the launch of the *Kepler* satellite around 400 exoplanets were known (Borucki et al., 2010). When a planet transits across the face of its host star as seen from Earth it causes a characteristic dip in the observed flux coming from the star. Planetary transit is not the only way that an exoplanet can be detected in orbit of another star, but it is the simplest method to find it in unknown systems, hence many surveys targeted at detecting exoplanets use the planetary transit method to detect them. By finding and characterising more exoplanets the population synthesis models of planet formation and evolution can be tested (e.g. Mordasini et al. (2012a,b)).

1.4 Ground Based Wide Field Variability Surveys

In recent years there have been a number of wide field time series photometric surveys with the aim of detecting a variety of variable phenomena over many different timescales, as shown in table 1.1. Typically these have had the primary aims of detecting supernovae or exoplanets. For supernova surveys this leads to the selection of long cadence (the time between observations) observations since these events are relatively infrequent and the fact that these events are typically quite faint means high depth. A well known example of such a survey is the Palomar Transient Factory (PTF, Law et al. (2009)), which uses a wide field camera with a 7.78 $\deg^2$ field of view which is used to survey up to 2700 $\deg^2$ every 5 days to a depth of $R = 21.0$ in its primary observation mode. Typically these observations are used to identify novae (super, classical and dwarf), gamma-ray burst afterglows and have even identified a number of AM CVn systems in outburst. In contrast exoplanet surveys tend to concentrate on brighter sources as they require higher accuracy on their photometry to confirm a planetary transit. An example is the SuperWASP survey (Pollacco et al. (2006)) which covers the whole sky to a depth of $V = 15$ at a typical cadence of 40 minutes every night. PTF and SuperWASP both have a mode of observation with just 1 minute cadence, however these modes are only used for a limited amount of sky, in the case of PTF this mode is used for just 50,000 stars (Law et al., 2009). Until 2001 there were very few surveys that combined both high cadence and depth, with the highest cadence survey of the faint sky being provided by the Faint Sky Variability Survey at 12 minutes. However, with a Nyquist frequency corresponding to a period of 24 minutes, this left a number of potentially variable

sources undetectable, a parameter space which contains a number of astrophysically interesting sources. Hence there was a clear need for a new survey to discover such sources. A project which aimed to address this was the RApid Temporal Survey (RATS).

Survey	FoV (sq. deg.)	Cadence	Limiting mag (R)	Coverage (sq. deg. night^{-1})	Lifetime	Total Coverage (sq.deg.)	Reference
Palomar Transient Factory	7.78	1min–5d[a]	21.0	1000	ongoing	∼10,000[e]	Law et al. (2009)
ROTSE-III	3.42	1d	18.5[b]	450	ongoing	∼1,100	Quimby (2006)
Palomar-Quest	9.4	30 min–days	21.0[c]	500	2003–08	∼15,000[e]	Djorgovski et al. (2008)
SDSS-II Supernova search	1.5	2d	22.6	150	2005–08	∼300	Frieman et al. (2008)
Cataline Real-time Transient Survey	8	10 min – yr	19.5[d]	1200	ongoing	∼33,000[e]	Drake et al. (2009)
Supernova Legacy Survey	5.7	3d–5yr	24.3	2	2003-08	∼580[e]	Astier et al. (2006)
SkyMapper	5.7	0.2d–1yr	19.0	1000	ongoing	∼21,000[e]	Keller et al. (2007)
Pan-STARRS 3π	7	7d	21.5	6000	ongoing	∼30,000	Young et al. (2008)
Large Synoptic Survey Telescope	9.62	3d	24.5	3300	2020+	∼21,000	Ivezic et al. (2008)
Rapid Temporal Survey	0.28	1 min	23.0[b]	1	2003-10	∼46	Barclay et al. (2011)
Faint Sky Variability Survey	0.28	12 min	24[d]	1	1998-2001	∼23	Groot et al. (2003)
SuperWasp	482	1–40 min[a]	15[b]	whole sky	ongoing	∼41,000[e]	Pollacco et al. (2006)

[a]Only a small amount of sky is observed at 1 min cadence
[b]Unfiltered
[c]RG610 filter
[d]V-band filter
[e]Applies to the longest cadence mode only

Table 1.1: Summary of a number of short period time-series photometry surveys. Columns show the name of the survey; field of view (square degrees); cadence; Limiting magnitude (depth) in the R-band unless otherwise stated; coverage (square degrees per night); the dates when the survey has or is taking place; The total intended or completed sky coverage; and the reference. This is a modified version of a Table taken from the Ph.D. thesis of Barclay (2011).

1.4.1 The RApid Temporal Survey (RATS)

RATS was a deep, high cadence optical light survey which took place between 2003-2010, which surveyed 164 individual fields covering 46 square degrees of sky, the majority of which were near the Galactic plane, see Barclay et al. (2011) for details. So far light curves of 3 million stars have been identified, with 120,000 assigned as significantly variable, 28,000 of which show variability on a period of less than 40 minutes. The observation strategy consisted of pointing at one area of sky and taking 30s exposures every minute over a 2 hour time period in white light, with single exposures taken of each field in a variety of filters to provide basic colour information to aid in object identification. This gave a faint limit of $g \sim 23$ and a cadence of $\sim$1 minute (30s exposure time, $\sim$30s CCD read-out time). This meant that the survey was capable of identifying stars which showed variations in their optical flux in the range 2 minutes up to a few hours. The primary aim was to find and identify AM CVn systems, primarily to place constraints on the binary evolution models of (Nelemans et al., 2001, 2004) but also to increase the number of identified systems beyond the 18 systems known previous to the initiation of RATS, such that they can be studied further to increase our understanding of these systems and place constraints on stellar population models. However, the study was also capable of identifying a variety of types of variable systems. Some of the more notable results include a rare hybrid pulsating sdB star (Ramsay et al. (2006); Baran et al. (2011)), which is currently the second highest known amplitude pulsating sdB, the first dwarf nova to be discovered in quiescence through detection of Quasi-periodic oscillations (Ramsay et al., 2009), a pulsating white dwarf with a hot companion

and a number of δ-Scuti/SX Phoenicus stars (Ramsay et al., 2011).

1.5 Early Space-Based Variability Observations

Ground-based observations have serious limitations in the study of variable stars, most notably due to their limited duration. This makes identification of multiple modes and measuring competition between then difficult, which limits the extent to which asteroseismic models can be tested. This difficulty can be reduced by making multiple observations from the same sight, but gaps in the data cause mode aliases in the data. To remove these, long time series continuous observations are essential. Campaigns such as The Whole Earth Telescope (Nather et al., 1990), which has achieved near continuous observation of sources on timescales of several days to weeks, mitigate these issues to some extent, but the difficulties obtaining coordinated telescope time for such projects on a regular basis still leaves this approach with limitations. Also, due to absorption and scattering by the atmosphere, ground-based observations are limited in their precision. This lead to the pursuit of making observations of variable objects from space-based telescopes where long time series continuous observations can easily be made at precision levels of the order of a few parts per million (ppm) (equivalent to a $\sim \mu$mag level of precision in magnitude space (Rowe et al., 2006)). With many objects varying in this regime, or exhibiting changes to higher amplitude, dominant variability at this level, this shift towards space-based observations offered unprecedented new opportunities in the science of variable stars.

1.5.1 Microvariability and Oscillations of Stars (*MOST*)

The *MOST* satellite was designed to observe oscillations in solar-like stars, observe roAp stars, detect reflected light from large, short orbital period exoplanets and the turbulent variability in the winds of Wolf-Rayet stars (Walker et al., 2003). It was launched in 2003 and continues to operate to this day. It consists of a 15cm optical telescope which has one broadband filter (350–750nm) and a cadence as low as 6s (Rowe et al., 2006). It operates in a polar, solar-synchronous orbit at a height of 820km above Earth, which allows for stars to be observed continuously for a period of up to 60 days in a continuous viewing zone in the declination range $+36^\circ \geq \delta \geq -19^\circ$ (Walker et al., 2003). In its high precision mode it is limited to observing targets of $V < 6.5$, with the low precision mode extending the observation range to $6.5 \geq V \geq 13$ with a precision on the order of millimag level (Rowe et al., 2006).

1.5.2 Convection Rotation et Transits (*COROT*)

COROT was launched in December 2006 with the primary objective of detecting exoplanets, with a specific focus on attempting to detect exoplanets smaller than previously known systems (Fridlund, 2007) and ran with a duty cycle exceeding 90% until a computer failure in November 2012. It could observe up to 10 targets with a sensitivity range of V=5.5–9.4 over periods of 150 or 20 days (Gutiérrez-Soto et al., 2007). It had two alternate pointings which are placed at the intersection between the equatorial plane and the galactic plane and have a radius of 10 degrees (Gutiérrez-Soto et al., 2007).

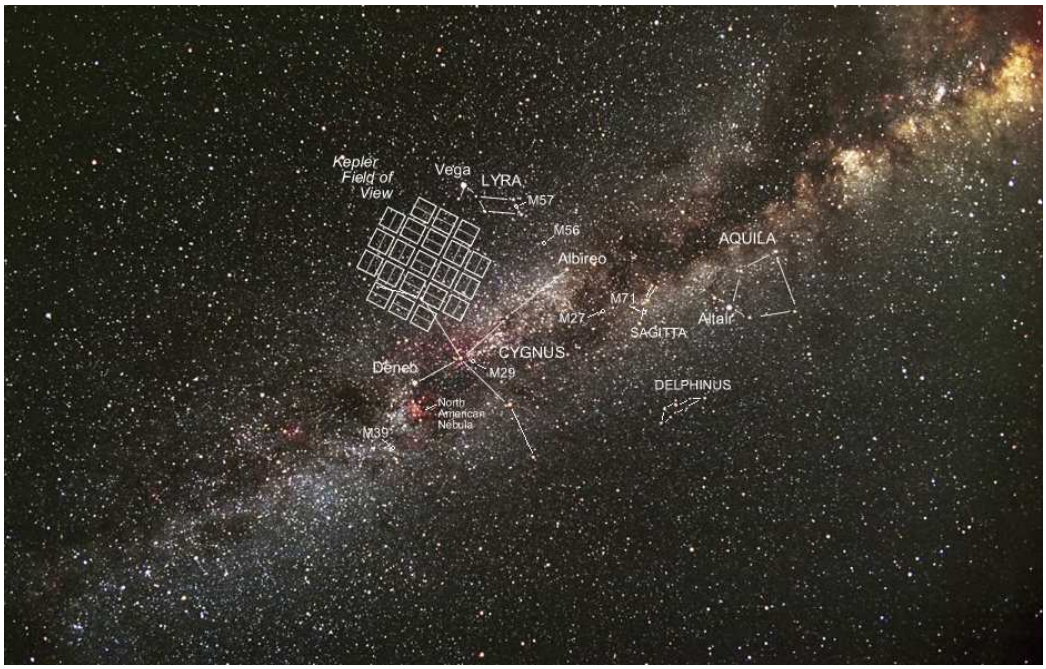

Figure 1.14: Figure showing the region of space sampled by the *Kepler* satellite. Figure taken from http://kepler.nasa.gov/Science/about/targetFieldOfView/.

1.6 The *Kepler* Satellite

The *Kepler* Satellite[2] was launched on March 6^{th} 2009 with the primary objective of discovering exoplanets via their transit of their host star (Borucki et al., 2010), with a particular focus on identifying Earth-like planets in the 'habitable zone' around solar-like stars (c.f. Section 1.2.5). To achieve this aim *Kepler* points continuously at an area of sky in the constellations of Cygnus, Lyra and Draco, as shown in Figure 1.14. This region was selected to balance the need to have a large number of stars in the field of view, but without causing the confusion which would occur for a pointing within the galactic plane, with the exact pointing chosen to maximise the number of objects brighter than K_p=15. It is also far

[2]Technical specifications and details of observations taken from Kjeldsen et al. (2010) and http://keplergo.arc.nasa.gov/DataAnalysisProducts.shtml unless otherwise stated

enough away from the ecliptic plane that the Sun does not shine into the telescope at any time throughout the year, allowing for year round observations, with the only gaps occuring during monthly data transmission to the ground, with a full frame image of the *Kepler* field also taken during this period; and the quarterly rolls performed by the telescope. It samples a region of the extended Solar neighbourhood pointing towards the Orion arm and contains 10 million stars brighter than the *Kepler* confusion limit. *Kepler* has a shutter-less 42 chip CCD mosaic with a total of 95 million pixels, each corresponding to a size of 3.98 x 3.98 arcseconds and a 3.1–7.5 arcsecond full width at half maximum. An exposure is taken once every 6.5s, which are then summed onboard and stored at 1765.5s (29.4 minutes) and 58.89s intervals. This provides both a long and short cadence observation mode respectively, with the number of stars that can be observed at any one time being 170,000 and 512 respectively. It is sensitive to stars in the range $11.5 \leq g \leq 21$, with brighter stars being saturated and the confusion limit being approximately 20–21. It was initially launched with a planned mission lifetime of at least 3.5 years, which came under review in 2012 and was extended until 2016, including a review of the mission's scope in 2014.

In addition to the primary aim of exoplanet detection, there was also the secondary aim of studying variable stars, with the much greater depth and the uninterrupted pointing offering unprecedented opportunities for the study of variable stars that exceed even those offered by *MOST* and *COROT*. The opportunity to obtain detailed, near continuous light curves up to a timescale of years offers unprecedented opportunities in the field of asteroseismology. The difference in quality and quantity of data between ground based observations and those

made by *Kepler* can easily be seen in figure 1.15, with the near continuous data collection especially effective in identifying any changes in period of variation with time and for identifying multiple pulsation modes in pulsating stars beyond the dominant period. Due to storage and bandwidth limitations on the data telemetry, only 5.4 million of the 95 million pixels ($\sim$5.7%) can have their data transmitted to the ground. This means that if *Kepler* is to be exploited to its full potential in the study of variable stars, potential targets need to be pre-selected. This leads to the use of target lists which are regularly reviewed and have a number of channels open to the scientific community to submit proposals of potential interest.

The differing observation modes and the near continuous observation mode in combination, mean that the data collected by *Kepler* allows for a wide range of results to be obtained. These range from ensemble results quantifying trends in general populations such as those found by (Chaplin et al., 2011) on Solar-type stars, but also for individual objects, with the short cadence mode being of particular interest as it allows the study of some of the shortest period variable objects. This data can be used to probe the details of stellar structure and test accretion disk models in a way not previously possible. Examples include those on catacylsmic variable (CV) systems (Cannizzo et al. (2012)), studies on δ-Scuti systems (Antoci et al. (2011); Uytterhoeven et al. (2011b)), or the many opportunites afforded in the study of white dwarfs, with the detection of at least one DAV & DBV white dwarf in the *Kepler* field (Hermes et al. (2011); Bischoff-Kim and Østensen (2011a)) which will allow tests of models such as the extent of radiative levitation and diffusion of heavy metals (Charpinet et al.,

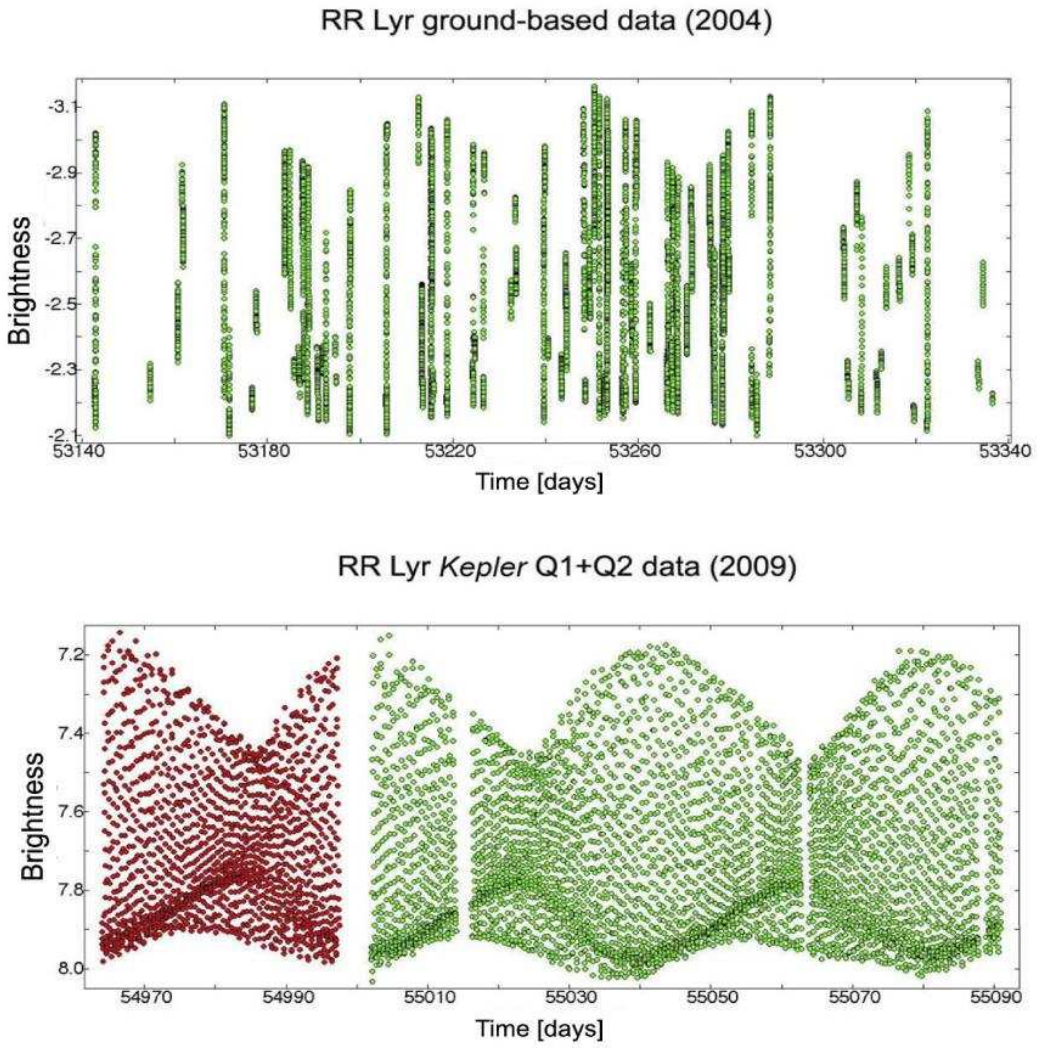

Figure 1.15: A comparison of one of the most accurate sets of ground-based observations (top) and *Kepler* observations (bottom) of RR-Lyrae, demonstrating the dramatic increase in data acquisition rate provided by *Kepler*. Figure taken from http://kepler.nasa.gov/news/nasakeplernews/20101026webcast/.

2008) and the neutrino flux from DBV white dwarfs (Bischoff-Kim and Østensen, 2011b).

Prior to the launch of *Kepler*, several programmes were put in place to identify bright Solar-like stars which exhibited low amplitude optical variability in their flux, to identify potential targets for the primary objective of exoplanet detection. However, these surveys left large portions of the *Kepler* parameter space unexplored, so there were various surveys initiated to try to find astrophyscially interesting sources across the full range, the details of which can be seen in Table 1.2. As can be seen, these surveys suffer from a number of limitations, with the highest cadence of $\sim$4 minutes being limited to a small field of view and the depth of 18.5 leaving a significant fraction of stars in the field of view that could be observed by *Kepler* undetected. Indeed, the only survey which approaches the confusion limit of *Kepler* is the KIS colour survey (Greiss et al., 2012a,b), however, since this is a colour survey, separate time-series data are also needed to confirm if a source is variable and suitable for the limited observation allocations of *Kepler*. With none of these surveys combining high cadence and depth, this implies that a large subset of potentially astrophyscially interesting sources remain undetected. With the unprecedented opportunities offered by *Kepler*, in particular in its short cadence mode of observation, it is of great importance to the study of variable stars to identify as many of these targets as possible to offer as wide as possible a variety of objects from which to select those that should be observed and have the invaluable *Kepler* observations collected for them. For this reason we initiated a deep, high cadence survey with the primary aim of identifying suitable targets to observe using *Kepler* in short cadence mode. To achieve this we used an

Survey	Cadence	Limiting mag	Filters	Coverage	Reference
HATNet	5 minutes	8–14 (I)	I	67 deg^2	Hartman et al. (2004)
All Sky Automated Survey	2-4 days	7–15 (V), 6–14 (I)	V, I	whole Kepler field	Pojmanski (2002)
BOKS	225–345s	14–18.5 (r)	r, V	1.39 deg^2	Feldmeier et al. (2011)
UBV Colour Survey	n/a	18.7 (U), 19.3 (B), 19.1 (V)	U, B, V	whole Kepler field	Everett et al. (2012a)
KIS Survey	n/a	20 (all filters)	$U, g, r, i, \mathrm{H}\alpha$	50 deg^2	Greiss et al. (2012a,b)

Table 1.2: Summary of a number of short period surveys covering the *Kepler* field. Columns show the name of the survey; cadence; limiting magnitude (depth) ; Filters; coverage and the reference

adapted version of the RATS strategy (c.f. Section 1.4.1), with the primary aim of detecting and selecting sources which exhibit short period optical variations which are suitable for *Kepler* observations in short cadence mode to answer key science questions as described previously in this thesis.

1.7 Outline of Thesis

I now briefly outline the work presented in this thesis, which primarily describes my work on the RATS-*Kepler* project. I have lead the development of a new data reduction pipeline and a new algorithm for selecting candidate variable stars which reduces the false positive selection rate to provide a more manageable sample size for manual inspection. The data reduction process and instrumentation will be described in chapter 2. Chapter 3 will outline various algorithms for detecting variable sources from a large sample, the process used to select variable sources from our data and those sources which were selected to be part of bids

for short cadence observations by *Kepler*. In chapter 4 the details of our *Kepler* observations will be presented and analysed, with chapter 5 summarising the initial *Kepler* mission and its future now it is no longer able to continue its original mission with only 2 reaction wheels operational.

Chapter 2

Observations and Data Reduction

2.1 Observational Strategy

Our strategy was a modified version of that used in the RATS project, which obtained a series of short (30 second) exposures of the same field for 2 or more hours and covered 40 square degrees (see Barclay et al. (2011) for further details). Our new strategy was driven by the relatively large area of the *Kepler* field of view (116 square degrees) and the *Kepler* confusion limit $g \sim 21$. Since the *Kepler* field covers an area almost 3 times that which the RATS project obtained data for in 10 epochs of observations over 7 years and our goal is to survey as much of the *Kepler* field as possible within *Kepler*'s scientific lifetime, it was clear that there was a need to increase our sky coverage rate. Hence, we chose a 1 hour observation length per field, to give an observation rate twice that used by RATS. RATS had a depth of $g \sim 23$, which left it sensitive to a wider range of sources. However, the photometric accuracy of *Kepler* SC observations reduces

Dates	Telescope	No. Fields
11–17 Jul 2011*	INT	49
01–10 Aug 2011*	INT	58
16–22 May 2012	MDM	26
03–12 Aug 2012	INT	55

Table 2.1: A summary of our observations to date, detailing the number of fields observed in each run and the telescope used. Observation runs marked with an asterisk indicate those which I participated in.

from 12.9% at $g = 19$, to 32.4% at $g = 20$ (compared to 0.85% at $g = 16$)[1]. Hence, observations of targets fainter than $g = 20$ by *Kepler* would give high photometric errors and would not aloow for detections of variability at $> 3\sigma$ level. Therefore we reduced the exposure time such that we were sensitive to targets in the range $13.5 \lesssim g \lesssim 20$ and used a filter to eliminate fringing, unlike RATS which did not use a filter. Our observations were made between July 2011 and August 2012 using the 2.5m Isaac Newton Telescope located on the island of La Palma in the Canary islands at the Spanish Observatorio del Roque de los Muchachos of the Instituto de Astrofisica de Canarias (IAC), operated with financial support from the UK Science and Technology Facilities Council; and the 1.3m MDM telescope at Kitt peak observatory, in the USA which is operated by Dartmouth College, Columbia University, Ohio State University, Ohio University, and the University of Michigan. These observations are summarised in table 2.1 and shown in equatorial coordinates in figure 2.1 (see tables 2.1, 2.2 and 2.3 at the end of this chapter for a full list of field centres).

[1]http://keplergo.arc.nasa.gov/CalibrationSN.html

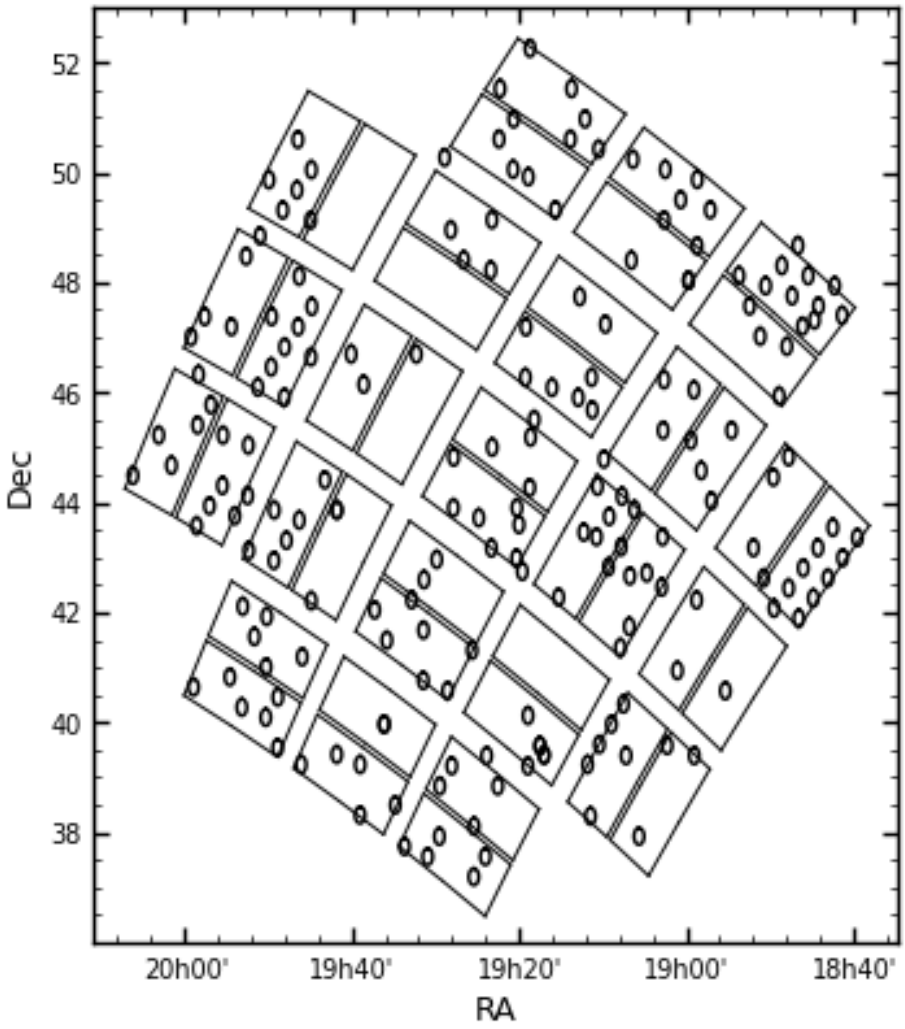

Figure 2.1: The location of our field centres in equatorial coordinates along with the field of view of the *Kepler* satellite, where each circle corresponds to a point in the centre of the telescope pointing. The outline of the *Kepler* field of view shows the positions of the 42 CCD chips at a given point, their orientation would change with each quarterly roll. Figure produced courtesy of Sandra Greiss, Warwick University.

Figure 2.2: Image of the building housing the Isaac Newton Telescope, located on the island of La Palma in the Canary islands. Image taken from http://en.wikipedia.org/wiki/Isaac_Newton_Telescope.

2.2 Telescopes and Instrumentation

2.2.1 Isaac Newton Telescope (INT)

The instrument used to record photometric observations at the 2.5m Isaac Newton Telescope (INT, as shown in Figure 2.2) is the Wide Field Camera (WFC) as shown in Figure 2.3, which consists of a 4 chip mosaic of thinned AR coated EEV devices and is placed at the prime focus of the INT; it has an on sky (taking into account the space between chips) field of view of $33'$ x $33'$(0.55 square degrees))[2]. Each of the four chips consists of 4096x2048 pixels, each with dimensions 13.5 x 13.5 microns, corresponding to a pixel scale of 0.333 arcsec/pixel. We made use of the Sloan g filter for our main observations, with a single exposure taken for each

[2]Information in this section taken from http://catserver.ing.iac.es/filter/list.php?instrument=WFC and http://www.ing.iac.es/Engineering/detectors/ultra_wfc.htm

field using the Sloan r filter to provide basic colour information. The detector is cooled by liquid nitrogen and has an operating temperature of 153 K; at this temperature the quantum efficiency is $>70\%$ in the range of the filters used, as shown in Figure 2.4. We made use of the fast (30s) readout mode, which has an average noise of 8.8 electrons per chip. Using the INT exposure time calculator[3] an exposure time of 20s was chosen, with 80 exposures of each field taken, which left us sensitive to targets in the range $13.5< g <21$, with a cadence of $\sim$50s over the duration of $\sim$1 hour. For such a short exposure time the autoguider on the INT cannot be used. This is because a fault with the autoguider which cannot be fixed due to obsolete equipment causes cross-talk between the CCDs of the WFC and the autoguider. For observations with a longer exposure time this is mitigated by reading out the autoguider CCD 1 minute before the WFC CCD, a solution which could not be used for our observations whilst still maintaining our desired cadence. Hence it could not be used to maintain pointing for our observations and manual corrections had to be made where we aimed to maintain the pointing accuracy to a level of <10 pixels ($\sim$3 arcseconds).

2.2.2 MDM Telescope

For observatory scheduling reasons two different detectors were used for our observations on the 1.3m MDM telescope (as shown in Figure 2.5), with the red4k detector used for two nights and the MDM4k detector used for the other 5, which is shown in Figure 2.6. The MDM4k detector[4] is a Silicon Technology

[3]http://catserver.ing.iac.es/signal/

[4]Information in this section taken from http://mdm.kpno.noao.edu/

Figure 2.3: Image of the WFC camera which is situated at the prime focus of the INT, shown here in the park position. Image taken from http://www.ing.iac.es/astronomy/instruments/wfc/.

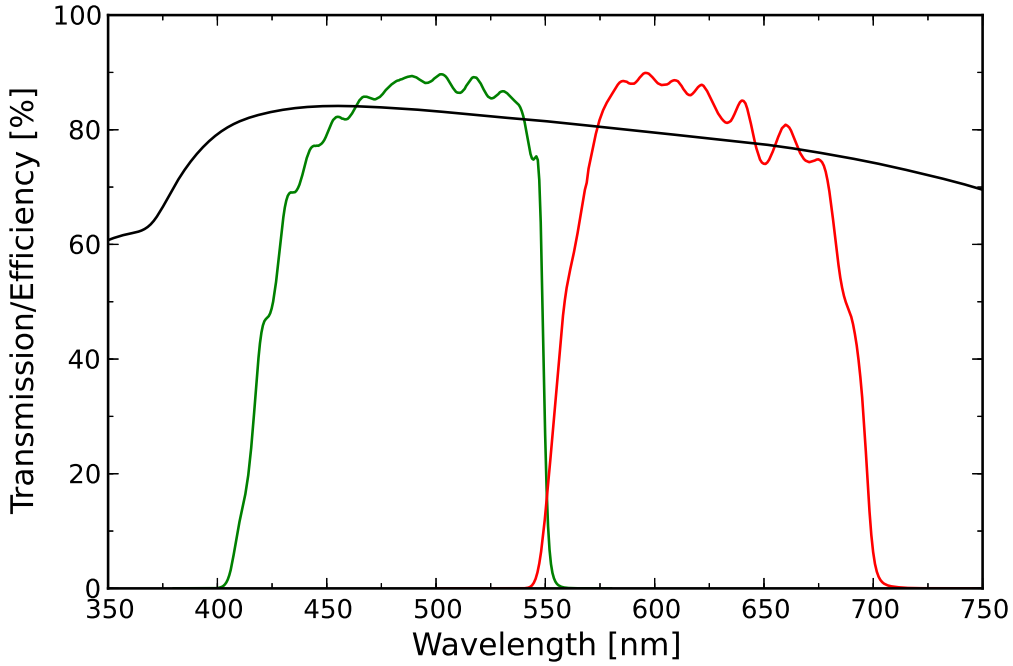

Figure 2.4: The transmission of the Sloan g and r filters used for our INT observations plotted in green and red respectively, along with the quantum efficiency of the CCD on the WFC over this wavelength range plotted in black. Figure produced using data from http://catserver.ing.iac.es/filter/list.php?instrument=WFC and http://www.ing.iac.es/Engineering/detectors/ultra_wfc.htm.

Figure 2.5: Image of the building housing the MDM Observatory, in the USA. The 1.3m MDM telescope, which is the white domed telescope at front-left, was used for our observations. Image taken from https://dept.astro.lsa.umich.edu/obs/mdm/.

Associates STA-0500 CCD with 4064x4064 15μm pixels. The detector is cooled by liquid nitrogen and has an operating temperature of 149 K, with a noise of 5 electrons (rms). The red4k detector is a fully depleted LBNL CCD, which is notable for its increased quantum efficiency at redder wavelengths, as shown in Figure 2.7. It is 250μm thick and has 4096x4096 15μm pixels. It is cooled by liquid nitrogen and has an operating temperature of 140–170 K, with a typical noise value of 3 electrons. Both detectors have a field of view of 21.3′ x 21.3′(0.35 square degrees) and a pixel scale of ∼0.315 arcsec/pixel.

The Johnson V band filter was used for our main observations and a single exposure of each field taken in each of the Johnson B and R filters to provide basic colour information. Both detectors have a quantum efficiency of >60% across all filters used and >70% in the V band range of our main observations, as shown in figure 2.7. For our main observations we took 60 30s exposures in the V band on both detectors. The readout time of the MDM4k detector was 40s giving a cadence of 70s, with the red4k readout time at 55s, giving a cadence of 85s.

2.3 Data Reduction

Our images were bias subtracted and flat-fielded using evening twilight flats in the usual fashion using `Starlink`[5] and `ftools` software[6]. We then made use of software provided by astrometry.net (Lang et al., 2010) to embed sky coordinates into our images, with the resulting positions typically agreeing with the 2MASS catalogue within 0.4 arcseconds. To obtain magnitudes from our observations,

[5]http://starlink.jach.hawaii.edu/starlink
[6]http://heasarc.gsfc.nasa.gov/ftools

Figure 2.6: Image of the MDM4k detector which was used for the majority of our observations on the MDM telescope. Image taken from http://mdm.kpno.noao.edu/index/Instrumentation.html.

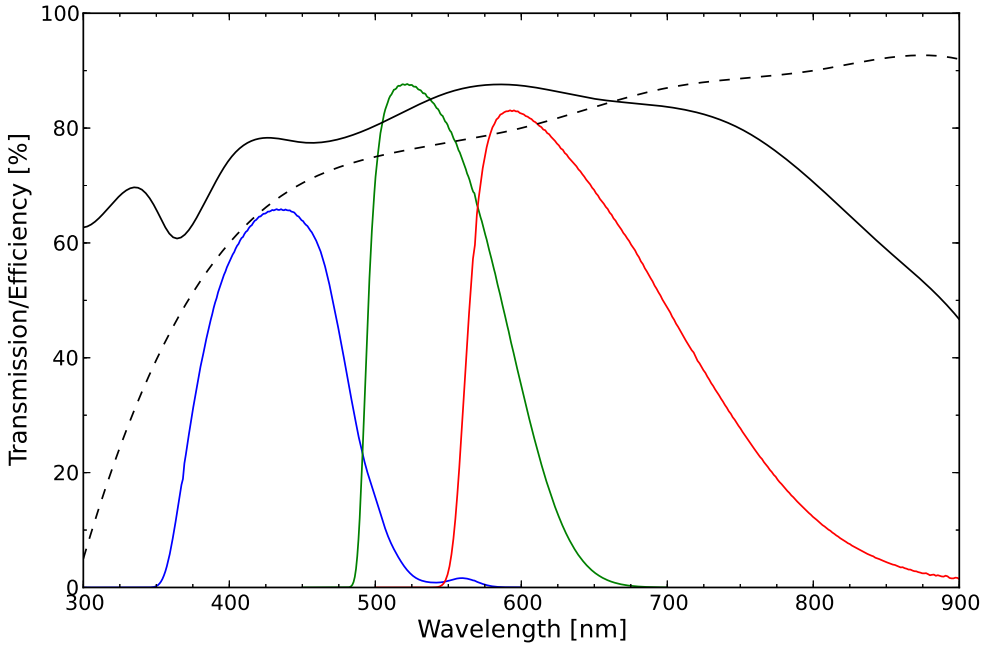

Figure 2.7: The transmission of the Johnson B, V and R filters used for our MDM observations, plotted in blue, green and red respectively; along with the quantum efficiency of the MDM4k and red4k detectors over this wavelength range, plotted in solid and dashed black respectively. Figure produced using data from http://mdm.kpno.noao.edu/index/Instrumentation.html.

exposures of standard star fields were taken each night and magnitudes obtained using the Vega system, transformed to the AB system. For our MDM observations our B, V and R magnitudes were converted to g and r magnitudes using the work of Jester et al. (2005). Colour information was then normalised to the KIS catalogue (Greiss et al., 2012a,b), which was also used to obtain further colour information through their U, i and H_α observations.

2.3.1 Extracting light curves

Since the *Kepler* field extends 6–21 degrees above the Galactic plane, our fields at low latitudes were crowded and high latitudes were sparse. For sparse fields light curves were obtained using `sextractor` (Bertin and Arnouts, 1996). This used aperture photometry to extract magnitudes, with differential photometry obtained by comparing the magnitude of each star with the mean brightness of the 3^{rd}–10^{th} brightest stars in the image. Tests performed on randomly selected fields using, for example, the 4^{th}–20^{th} brightest did not yield significantly different results.

For denser fields we used the Difference Imaging package `DIAPL2`, an updated version of `diapl` (Wozniak, 2000), as this method is more suited to accounting for systematic differences between images such as differences in the seeing across the course of the observations (Alard and Lupton, 1998). This required the production of a new data pipeline to process our data as we had not used this program before, which I developed. The seeing was determined for each field on a chip by chip basis by calculating the point-spread function (PSF) across the image and then the mean Full Width at Half Maximum of brighter stars in the image.

Those images which have the best seeing and lowest background (we combined up to six images) were then used to make a reference image. After determining the PSF, this reference image was convolved with the PSF of each individual image and subtracted, with any variation in the PSF across the image taken into account by determining the PSF over 2 or 8 sub-sections of the image, where two sub-sections were used for lower density fields, as using 8 in these instances meant there were too few stars per sub-section for `DIAPL2` to complete properly. Aperture photometry was then performed on the location of stars in the residual image. Despite the use of difference imaging there were still some systematic trends present in our data caused by factors such as differences in seeing, air mass and atmospheric extinction (cf. Cameron et al. (2006)), the SYSREM algorithm (Tamuz et al., 2005) was applied to each CCD individually using a varying number of cycles as described in (Tamuz et al., 2006), with a maximum limit of 6 cycles to limit degradation of signals in true variable sources. After detrending had been performed analysis of light curves with periodograms indicated reduced period aliasing, particularly for periods around $\sim$20 minutes which was the typical duration between manual corrections of the pointing, and reduced the number of light curves assigned a high probability of being significantly variable (cf. Chapter 3), with manual inspection on a randomly selected sample of these verifying that the variability previously present in the light curve was due to systematic trends.

Table 2.1: List of fields observed using the INT in 2011, field ID corresponds to our own internal designations, field centres correspond to a point in CCD 4. Observations made by Adam Brooks and Gavin Ramsay between 11^{th}-17^{th} July and by Adam Brooks 1^{st}-10^{th} August.

Date (dd-mm-yy)	Field ID	RA DEC (J2000)	Date(dd-mm-yy) (dd-mm-yy)	Field ID	RA DEC (J2000) (J2000)
11-07-11	522	19:46:51 +49:43:35	17-07-11	28	18:48:05 +44:52:19
11-07-11	542	19:45:05 +47:36:21	17-07-11	27	18:49:54 +44:30:19
11-07-11	541	19:46:43 +47:14:21	17-07-11	133	18:59:24 +46:05:28
11-07-11	349	19:39:18 +39:16:51	17-07-11	55	18:59:05 +42:16:18
11-07-11	539	19:49:56 +46:30:21	17-07-11	412	19:28:28 +49:00:06
11-07-11	567	19:57:19 +43:59:07	17-07-11	436	19:32:35 +46:44:27
11-07-11	570	19:52:40 +45:05:09	17-07-11	439	19:38:53 +46:11:30
12-07-11	94	18:44:31 +47:36:58	01-08-11	36	18:55:39 +40:37:18
12-07-11	100	18:45:45 +48:09:58	01-08-11	238	19:02:58 +49:10:54
12-07-11	93	18:46:25 +47:14:58	01-08-11	139	19:02:58 +46:16:28
12-07-11	234	18:57:27 +49:21:54	01-08-11	131	19:03:05 +45:21:28
12-07-11	575	19:55:42 +45:16:09	01-08-11	376	19:21:01 +50:06:03
12-07-11	503	19:53:20 +42:09:20	02-08-11	240	18:59:00 +49:54:54
12-07-11	488	19:53:27 +40:19:20	02-08-11	151	19:03:09 +43:25:19
13-07-11	99	18:47:40 +47:47:58	02-08-11	141	19:08:12 +41:24:19
13-07-11	105	18:48:54 +48:20:58	02-08-11	154	19:09:37 +42:52:19
13-07-11	92	18:48:18 +46:52:58	02-08-11	390	19:22:35 +51:34:03
13-07-11	157	19:15:34 +42:19:19	02-08-11	382	19:22:42 +50:39:03
13-07-11	469	19:43:31 +44:27:24	02-08-11	408	19:23:33 +49:11:06
13-07-11	446	19:40:23 +46:44:30	03-08-11	46	19:01:23 +40:59:18
13-07-11	354	19:42:06 +39:27:51	03-08-11	63	19:05:58 +37:58:36
14-07-11	104	18:50:50 +47:58:58	03-08-11	260	19:11:38 +46:19:02
14-07-11	97	18:51:29 +47:03:58	03-08-11	73	19:11:46 +38:20:36
14-07-11	103	18:52:45 +47:36:58	03-08-11	259	19:13:14 +45:57:02
14-07-11	110	18:54:01 +48:09:58	03-08-11	380	19:14:02 +51:34:03
14-07-11	204	19:24:20 +37:36:28	03-08-11	373	19:14:10 +50:39:03
14-07-11	214	19:29:50 +37:58:28	04-08-11	72	19:02:36 +39:37:36
14-07-11	213	19:31:14 +37:36:28	04-08-11	236	19:06:53 +48:26:54
15-07-11	8	18:46:20 +42:51:19	04-08-11	264	19:16:22 +46:08:02
15-07-11	7	18:48:05 +42:29:19	04-08-11	296	19:18:56 +45:13:52
15-07-11	12	18:51:04 +42:40:19	04-08-11	277	19:19:29 +47:14:02
15-07-11	18	18:52:17 +43:13:19	04-08-11	269	19:19:33 +46:19:02
15-07-11	321	19:31:44 +41:43:30	04-08-11	406	19:26:55 +48:27:05
15-07-11	297	19:28:09 +43:56:55	05-08-11	245	19:02:50 +50:05:54
15-07-11	328	19:31:40 +42:38:30	05-08-11	76	19:07:31 +39:26:36
16-07-11	114	18:57:18 +44:04:28	05-08-11	281	19:20:36 +43:01:58
16-07-11	120	18:58:32 +44:37:28	05-08-11	223	19:28:21 +39:15:28
16-07-11	126	18:59:46 +45:10:28	05-08-11	325	19:36:07 +41:32:30
16-07-11	314	19:31:45 +40:48:30	05-08-11	583	20:06:28 +44:32:07
16-07-11	309	19:28:51 +40:37:30	05-08-11	585	20:03:23 +45:16:09
16-07-11	338	19:35:06 +38:32:48			
16-07-11	219	19:34:00 +37:47:28			

Table 2.1: (continued) List of fields observed using the INT in 2011, field ID corresponds to our own internal designations, field centres correspond to a point in CCD 4. Observations made by Adam Brooks and Gavin Ramsay between 11^{th}-17^{th} July and by Adam Brooks 1^{st}-10^{th} August.

Date (dd-mm-yy)	Field ID	RA DEC (J2000)	Date(dd-mm-yy) (dd-mm-yy)	Field ID	RA DEC (J2000) (J2000)
06-08-11	578	20:01:52 +44:43:09	09-08-11	473	19:49:34 +43:54:24
06-08-11	555	19:59:31 +47:03:21	09-08-11	477	19:49:10 +39:35:20
06-08-11	499	19:59:13 +40:41:20	09-08-11	484	19:49:09 +40:30:20
06-08-11	566	19:58:51 +43:37:09	09-08-11	521	19:48:33 +49:21:35
06-08-11	580	19:58:44 +45:27:07	09-08-11	533	19:48:22 +45:57:19
06-08-11	588	19:58:37 +46:22:09	09-08-11	540	19:48:20 +46:52:21
06-08-11	556	19:57:53 +47:25:21	09-08-11	466	19:48:07 +43:21:23
07-08-11	581	19:57:09 +45:49:09	10-08-11	530	19:46:45 +50:38:35
07-08-11	494	19:54:53 +40:52:20	10-08-11	548	19:46:36 +48:09:21
07-08-11	550	19:54:41 +47:14:21	10-08-11	467	19:46:35 +43:43:23
07-08-11	562	19:54:17 +43:48:09	10-08-11	486	19:46:14 +41:14:17
07-08-11	559	19:52:56 +48:31:21	10-08-11	516	19:45:13 +49:10:35
07-08-11	563	19:52:45 +44:10:09	10-08-11	535	19:45:11 +46:41:21
07-08-11	471	19:52:37 +43:10:24	10-08-11	454	19:45:09 +42:15:24
08-08-11	538	19:51:32 +46:08:21			
08-08-11	560	19:51:16 +48:53:21			
08-08-11	483	19:50:35 +40:08:20			
08-08-11	490	19:50:33 +41:03:20			
08-08-11	497	19:50:28 +41:58:18			
08-08-11	528	19:50:12 +49:54:35			
08-08-11	465	19:49:37 +42:59:24			

Table 2.2: List of fields observed using the INT in 2012, field ID corresponds to our own internal designations, field centres correspond to a point in CCD 4. Observations made by Gavin Ramsay and Onur Şatir.

Date (dd-mm-yy)	Field ID	RA DEC (J2000)	Date (dd-mm-yy)	Field ID	RA DEC (J2000)
03-08-12	5	18:39:52 +43:24:19	08-08-12	1010	19:20:19 +43:38:30
03-08-12	67	18:59:22 +39:26:36	08-08-12	203	19:25:43 +37:14:28
03-08-12	144	19:03:15 +42:30:19	08-08-12	251	19:06:41 +50:16:54
03-08-12	300	19:23:31 +45:02:56	08-08-12	289	19:19:02 +44:18:58
05-08-12	463	19:42:05 +43:54:24	08-08-12	383	19:20:57 +51:01:03
05-08-12	1001	18:45:00 +47:21:36	09-08-12	1005	19:12:34 +43:30:14
05-08-12	1007	18:59:02 +48:42:37	09-08-12	1006	19:17:19 +39:27:18
05-08-12	155	19:08:06 +43:14:17	10-08-12	1006	19:17:19 +39:27:18
05-08-12	568	19:55:46 +44:21:07	10-08-12	1008	19:11:33 +45:43:44
05-08-12	463	19:42:05 +43:54:24	10-08-12	210	19:25:41 +38:09:28
05-08-12	546	19:49:53 +47:25:22	10-08-12	222	19:29:47 +38:53:28
05-08-12	523	19:45:08 +50:05:35	10-08-12	365	19:15:57 +49:22:03
06-08-12	1	18:46:52 +41:56:18	10-08-12	368	19:10:48 +50:28:03
06-08-12	1002	19:04.62 +42:45:48	10-08-12	374	19:12:25 +51:01:03
06-08-12	168	19:10:56 +44:20:19	11-08-12	1009	19:09:59 +47:17:07
06-08-12	175	19:17:49 +39:37:14	11-08-12	1011	19:18:30 +45:33:11
06-08-12	181	19:19:14 +40:10:15	11-08-12	1012	19:19:12 +49:57:51
06-08-12	305	19:28:07 +44:52:02	11-08-12	292	19:25:07 +43:45:58
06-08-12	342	19:39:19 +38:21:51	11-08-12	359	19:46:21 +39:16:51
07-08-12	1013	19:29:12 +50:19:02	11-08-12	392	19:19:00 +52:18:03
07-08-12	226	19:00:03 +48:04:54	11-08-12	401	19:23:41 +48:16:06
07-08-12	239	19:00:59 +49:32:54	12-08-12	10	18:42:48 +43:35:20
07-08-12	311	19:25:55 +41:21:30	12-08-12	2	18:45:08 +42:18:20
07-08-12	327	19:33:09 +42:16:30	12-08-12	3	18:43:23 +42:40:20
07-08-12	332	19:37:34 +42:05:30	12-08-12	4	18:41:38 +43:02:20
07-08-12	351	19:36:26 +40:00:51	12-08-12	496	19:51:57 +41:36:20
08-08-12	1003	19:06:31 +43:54:48	12-08-12	6	18:49:50 +42:07:20
08-08-12	1004	19:19:55 +42:47:29	12-08-12	9	18:44:35 +43:13:20

Table 2.3: List of fields observed using the MDM 1.3m telescope in 2012, field ID corresponds to our own internal designations, field centres correspond to a point approximately in the centre of the chip. Observations made by Gavin Ramsay and Thomas Barclay.

Date (dd-mm-yy)	Field ID	RA DEC (J2000)	Date (dd-mm-yy)	Field ID	RA DEC (J2000)
16-05-2012	81	19:12:07 +39:16:50	21-05-2012	174	19:19:15 +39:15:15
16-05-2012	82	19:10:42 +39:38:50	21-05-2012	175	19:17:49 +39:37:15
16-05-2012	83	19:09:16 +40:00:51	21-05-2012	226	19:00:03 +48:04:55
16-05-2012	84	19:07:49 +40:22:55	21-05-2012	351	19:36:26 +40:00:51
17-05-2012	85	18:49:13 +45:58:48	22-05-2012	212	19:22:51 +38:53:28
19-05-2012	135	19:10:10 +44:50:04	22-05-2012	218	19:24:11 +39:26:28
19-05-2012	142	19:07:08 +41:47:26	22-05-2012	273	19:13:03 +47:47:02
19-05-2012	149	19:07:04 +42:42:34	22-05-2012	95	18:42:35 +47:58:58
19-05-2012	89	18:41:41 +47:26:48	23-05-2012	106	18:46:58 +48:42:58
20-05-2012	122	18:54:54 +45:21:28	23-05-2012	286	19:23:37 +43:12:58
20-05-2012	160	19:11:03 +43:25:19	23-05-2012	288	19:20:34 +43:56:58
20-05-2012	161	19:09:32 +43:47:19	23-05-2012	329	19:30:09 +43:00:30
20-05-2012	162	19:08:00 +44:09:19			

Chapter 3

Selecting Variable Sources

3.1 Variability Algorithms

Selecting stellar variable sources from a large selection of sources is a non-trivial task. Variables typically comprise only a small fraction of stars in a survey; for example Barclay et al. (2011) found only 4.1% of stars in the RATS project to be variable in the period range relevant to these observations, 4-115 minutes. There are a number of selection effects such as survey cadence, observation length and sensitivity which affect what types of system a survey can detect. Furthermore, the fact that variable sources can exhibit a wide variety of forms of variability in their light curve, as shown in Figure 3.1, means that it is difficult to find a single means of detection that is capable of identifying all forms of variability. These include periodic sinusoidal variation where the peaks in the light curve have approximately equal sizes, such as δ-Scuti stars; periodic sinusoidal variation with asymmetric peaks in the light curve, such as eclipsing

or contact binaries; quasi-periodic sinusoidal variations, such as pulsating white dwarfs; quasi-periodic non-sinusoidal variations, such as CVs; and transient modulations, such as flare stars.

As discussed in Chapter 1, there are many types of stars which are variable on timescales that our survey is sensitive to and which we expect to be able to detect in our data. There are also a number of systematic effects that can cause variability in a light curve which is not due to an astrophysical process, such as imperfections in the CCD and variations in seeing and transparency. Therefore a two stage process whereby a number of variability tests are first applied to identify a set of candidate variable sources and then a process of manual quality assessment is applied to remove spurious detections.

To perform statistical tests on the RATS-*Kepler* data the `VARTOOLS` suite of software (Hartman et al., 2008) was used, which allows the parameterisation of large numbers of light curves using many different statistical tests in a quick and simple manner. The following tests were applied on each of the light curves: the LS Periodogram; the Alarm test and the AOV test. The χ^2 value and standard deviation (σ) were also determined for each light curve. A 5σ clipping was applied to each light curve before determining the χ^2 and σ. As an example of how the different tests discussed in this section compare, Figure 3.2 shows the results of the σ, LS and AOV tests on a field which contains KIC 3223460, which has a dominant pulsation period of 24.2 mins (see Table 3.4). Plotting the σ of each light curve as a function of g mag shows that KIC 3223460 has a greater σ than the main distribution of sources with similar magnitude. However, there is (naturally) no information on the timescale of variability. On the other hand,

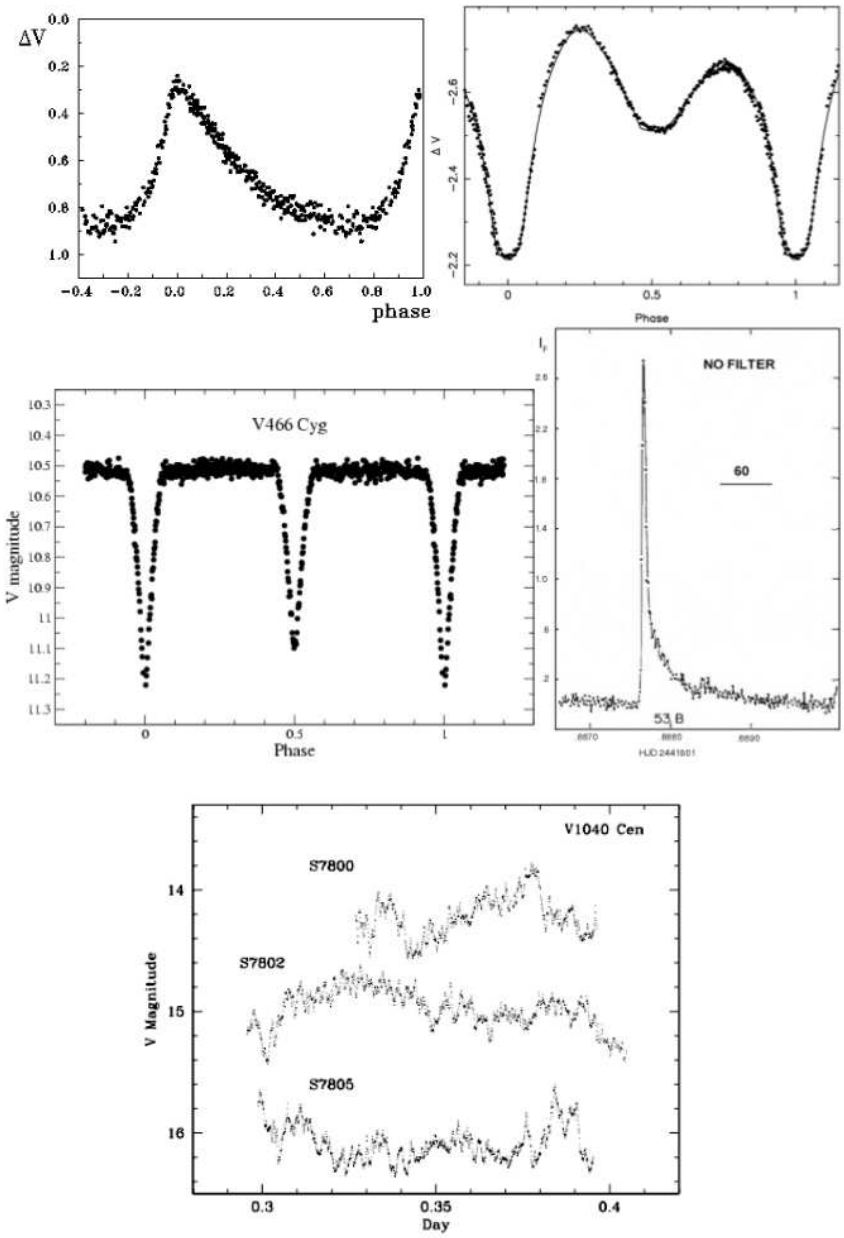

Figure 3.1: Example light curves of a variety of known sources demonstrating the wide variety of forms of variability. From top left - the phased light curve of the High Amplitude Delta Scuti star USNO-A2.0 0975-09853705 (Antipin et al., 2007), the phased light curve of the near-contact detached binary GR Tau (Zhang et al., 2002), the phased light curve of the Algol type eclipsing binary V466 Cyg = HD 331473 (Mas-Hesse et al., 2003), the flare star UV Ceti (Moffett, 1974) and the CV V1040 Cen (3 separate observing runs shown in one plot) (Woudt and Warner, 2010).

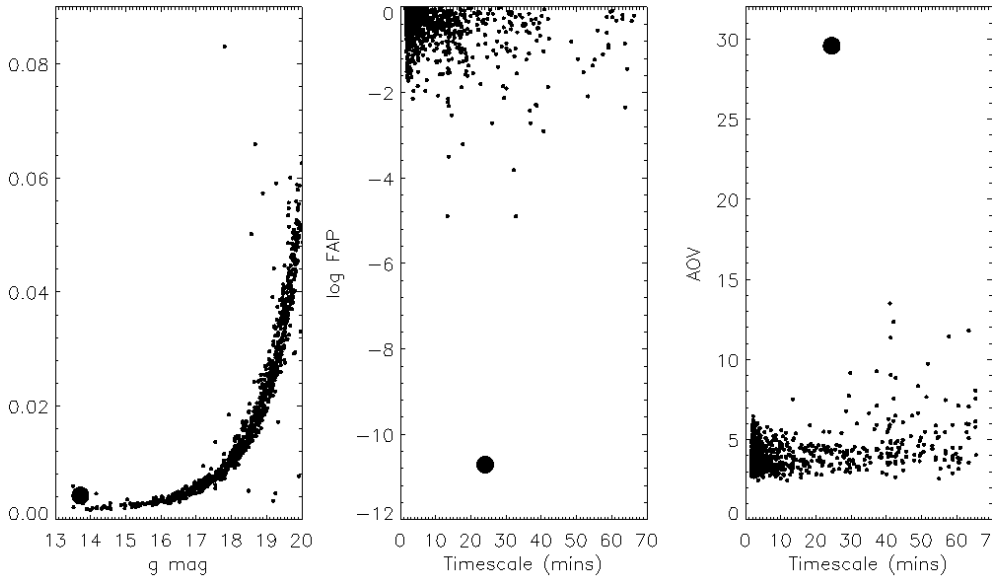

Figure 3.2: From left to right, the plot for all stars in field 73 chip 4 (which includes the short period blue variable KIC 3223460) the σ of each light curve as a function of g mag; the log FAP (False Alarm Probability, see Section 3.1.4) as a function of the period of the highest peak in the LS power spectrum; and the AoV value as a function of the AoV period. Figure taken from Ramsay et al. (2014).

the LS and AOV test clearly identify KIC 3223460 as being strongly variable on a period of 24 mins.

3.1.1 Median Absolute Deviation from the Median (MAD)

Much of the output from the variability algorithms approximates a Gaussian with a long tail of outliers to one side of the peak of the distribution, as the vast majority of sources are non-variable and fill the peak of the Gaussian-like portion of the distribution, whilst the small number of variable sources will only occupy an area to one side of this peak. Due to this large amount of asymmetric outliers,

the typically used parameters for describing variance in a dataset - the mean and standard deviation - are inadequate parameters for describing these distributions because of their sensitivity to the presence of outliers (Press et al. (1992)). This sensitivity is easily shown by considering what would happen if one data point in a distribution of values were replaced by infinity - the mean and standard deviation would both be infinite and therefore useless in any analysis or description of the set of parameters. The median and median absolute deviation from the median (MAD, Hampel (1974)) are more robust statistics in this instance, since they are largely unaffected by the presence of outliers. In the above example the median and MAD would remain unaffected by replacing one of the values in the distribution with infinity and hence can remain robust descriptors of variance in a distribution when there are significant numbers of outliers present. This robustness is well demonstrated by the median's 50% breakdown point (Donoho and Huber, 1983), i.e. how much of a dataset would have to be replaced by infinity before the median value is affected. The MAD is calculated by finding the median value of the absolute deviations from the median of the dataset and is defined for a set of parameters $\{x_1, \cdots, x_n\}$ as:

$$\mathrm{MAD}_n = \mathrm{b} \times \mathrm{median}_i(|x_i - \mathrm{median}_j(x_j)|) \tag{3.1}$$

Where $\mathrm{median}_j(x_j)$ denotes the median of the set of parameters and b is a constant which can be used to make the MAD a consistent estimator of the standard deviation for use in statistical analysis. It is defined as: $\mathrm{b} = 1/\mathrm{Q}(0.75)$, where $\mathrm{Q}(0.75)$ refers to the 0.75 quartile of the underlying distribution (Huber, 1981); if a normal distribution is assumed for simplicity, b takes a value of 1.4826.

3.1.2 Chi-Squared Test

The Chi-squared test is a method for 'goodness of fit' of a set of data to a given model. When applied to a light curve with n points, it does this by measuring the deviation of points from the mean observed brightness, $\bar{O}$, i.e. it compares the variation in the light curve to a constant, non-variable light curve at brightness $\bar{O}$ and is defined as:

$$\chi^2 = \sum_{i=1}^{n} \frac{(O_i - \bar{O})^2}{\sigma_i^2} \tag{3.2}$$

Where O_i is the observed brightness of the ith point in the light curve and σ_i is the corresponding error. It is particularly proficient at detecting flare stars, however, it has limited use when trying to select sources of astrophysical interest from a large dataset, both because it does not give any information about the period; and that a short duration, high amplitude change in the observed brightness would give a similar χ^2 value to a long duration, low amplitude variation. Hence, I have not used it to select variable sources in this work, however, it does have some use in describing the overall variability of the dataset.

The distribution of chi-squared values for the RATS-*Kepler* data approximates a Gaussian distribution with a long tail, as shown in Figure 3.3, with a peak around unity, as one would expect. For the RATS-*Kepler* data I find a median chi-squared value of 1.543 and a MAD of 0.626 (with b in equation 3.1 equal to 1.4826). Of the 7.1×10^5 sources, I find that 35,525 sources have a chi-squared value 3 times the MAD or more above the median and 4,642 light curves to have a chi-squared value 5 times the MAD or more above the median. This

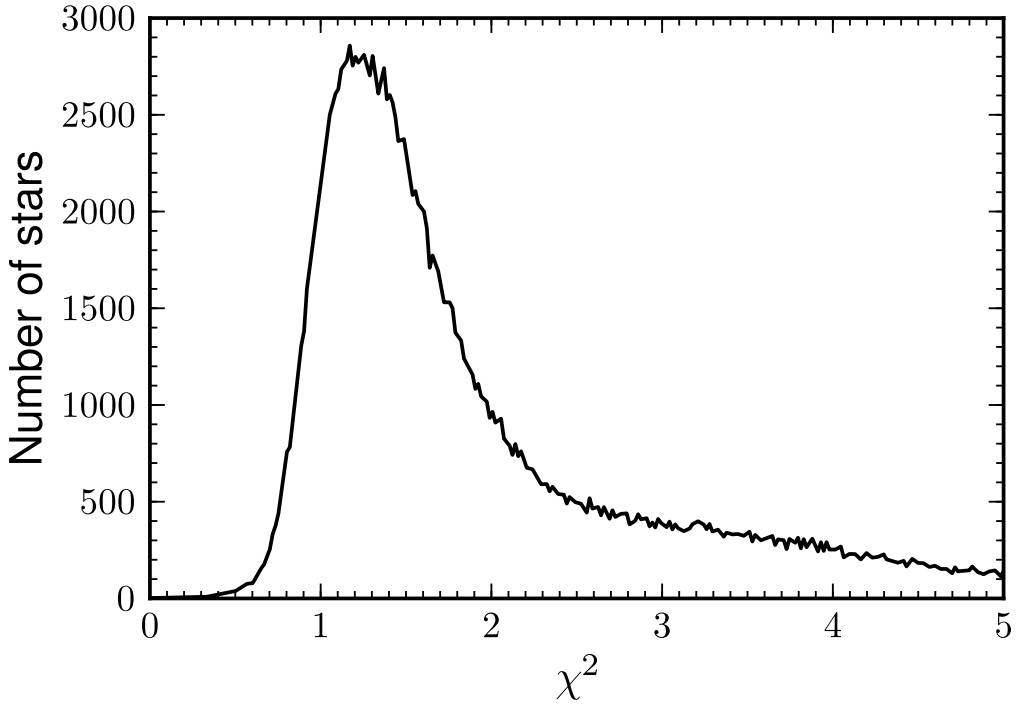

Figure 3.3: The distribution of chi-squared values for the RATS-*Kepler* dataset. Data are binned with a bin width of 0.01 in chi-squared.

implies that our data should contain of the order of 10^3 or less light curves which show significant variation in their light curve (whether due to true astrophysical variability or otherwise).

3.1.3 The Alarm Test

The Alarm variability statistic (Tamuz et al., 2006) was originally designed to improve upon the performance of the χ^2 statistic in the analysis of residuals after fitting binary models to sources identified in OGLE data of the small and large Magellanic clouds (Udalski et al., 1998, 2000). Specifically it has the advantage over the χ^2 in that it takes into account the sign and order of the residuals for a given fit, whereas the χ^2 does not take into account the order or sign of residuals. In the `VARTOOLS` application, it measures the residuals from a fit to the mean brightness of the light curve, $\bar{O}$, as defined in the previous section. A run of residuals is defined as the number of consecutive residuals which have the same sign. If k_i is the number of consecutive residuals in the ith run, then the Alarm, $\mathcal{A}$, is defined as:

$$\mathcal{A} = \frac{1}{\chi^2} \sum_{i=1}^{M} \left(\frac{r_{i,1}}{\sigma_{i,1}} + \frac{r_{i,2}}{\sigma_{i,2}} + \cdots + \frac{r_{i,k_i}}{\sigma_{i,k_i}} \right)^2 - \left(1 + \frac{4}{\pi} \right) \tag{3.3}$$

where $r_{i,j}$ is the jth measurement of the ith run, with $\sigma_{i,j}$ being the corresponding uncertainty. The sum is executed over all elements of a run and then over all M runs contained in the light curve. The chi-squared is defined by:

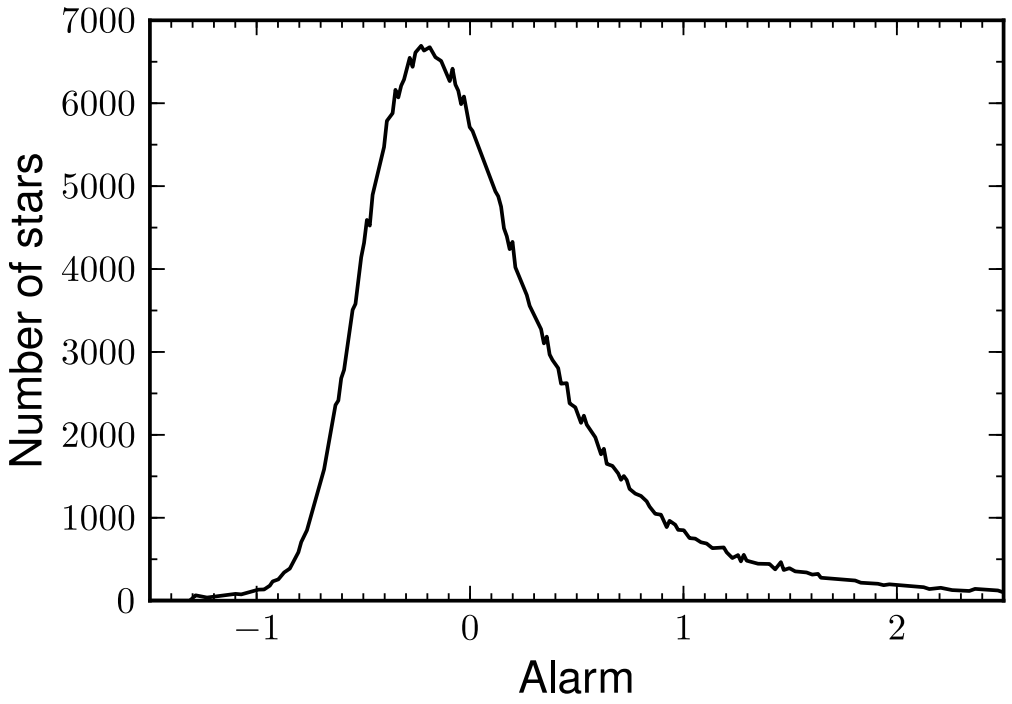

Figure 3.4: The distribution of Alarm values for the RATS-*Kepler* dataset. Data are binned with a bin width of 0.01 in Alarm.

$$\chi^2 = \sum_{i=1}^{N} \left(\frac{r_i}{\sigma_i} \right)^2 \tag{3.4}$$

where the sum is over all N observations. The division by chi-squared means that $\mathcal{A}$ is not sensitive to a systematic overestimation or underestimation of the uncertainties.

If the residuals alternate between positive and negative values then the alarm statistic will be low; and long runs with large residuals will lead to a higher value of $\mathcal{A}$.

The Alarm statistic is proficient at identifying eclipsing or contact binaries, or transient phenomena such as flare stars. However, as with the chi-squared

statistic it has the disadvantage of giving no information about the period, hence I do not use it to select an initial sample of candidate variable sources from the whole dataset, but as with the chi-squared it is useful in giving a measure of the variability of the whole dataset. The distribution of Alarm statistic values approximates a Gaussian distribution with a long tail, as shown in Figure 3.4, with a peak around zero, as one would expect. For the Alarm I find that the median is -0.029 and the MAD is 0.467. I find that 30,057 sources have an Alarm value 3 times the MAD or more above the median and 6,789 light curves to have an Alarm value 5 times the MAD or more above the median, which is consistent with the expectation from the chi-squared that I can expect to find of the order of 10^3 or less significantly variable light curves in the RATS-*Kepler* data.

3.1.4 Analysis of Variance

The analysis of variance (AOV) periodogram (Schwarzenberg-Czerny (1989, 1996); Devor (2005)) works by folding a light curve on a number of test periods and measuring the variance around a linear regression from a sinusoid within each of eight phase bins. For a periodically variable light curve, where the fold period is not equal to the intrinsic period there will be a high level of scatter, whereas scatter will be minimised on the intrinsic period. The AOV periodogram has been shown to be suitable for the detection of sharp periodic signals (Schwarzenberg-Czerny, 1989), such as eclipsing or contact binaries, though it should be noted that this method leaves the AOV prone to detecting aliases of the true period. The statistic Θ_{AOV} gives a measure of the goodness of fit to the best fitting period. However, a more useful statistic is the formal false alarm probability (FAP) of the detected

period being due to random noise, AOV-FAP, as the value of Θ_{AOV} for the most significant peak in the periodogram on its own does not give any information about the significance of that peak within the rest of the periodogram, which is important in determining if a source is truly exhibiting variability in its light curve and what level of confidence can be assigned to the period detected. This can be calculated by the method shown in Press et al. (1992). If the periodogram exhibits a peak at a frequency, ω, then the probability that it lies between some positive values z and $z + dz$ is $e^{-z}dz$. It should be noted that this requires that the periodogram be normalised by the total variance of the light curve to give the desired e^{-z} probability behaviour, as described in Horne and Baliunas (1986). Therefore, if M independent frequencies are scanned then the probability that none are greater than z is $(1 - e^{-z})^M$. The AOV-FAP is then defined as:

$$\text{AOV} - \text{FAP} = 1 - (1 - e^{-z})^M \tag{3.5}$$

Which gives probability values in the range 0 (no chance that the peak in the periodogram is due to random noise) to 1 (the peak in the periodogram is certainly due to random noise). Since the vast majority of sources are non-variable, the distribution is heavily weighted towards 1, hence `VARTOOLS` outputs the negative of the natural logarithm of the AOV-FAP. The distribution of AOV-FAP against period for the RATS-*Kepler* data is shown in Figure 3.5. As can be seen, the distribution is heavily weighted towards lower values of FAP, especially at short periods, with a long, narrow peak in FAP values at a period of around 3–4 minutes, which implies these are spurious period detections.

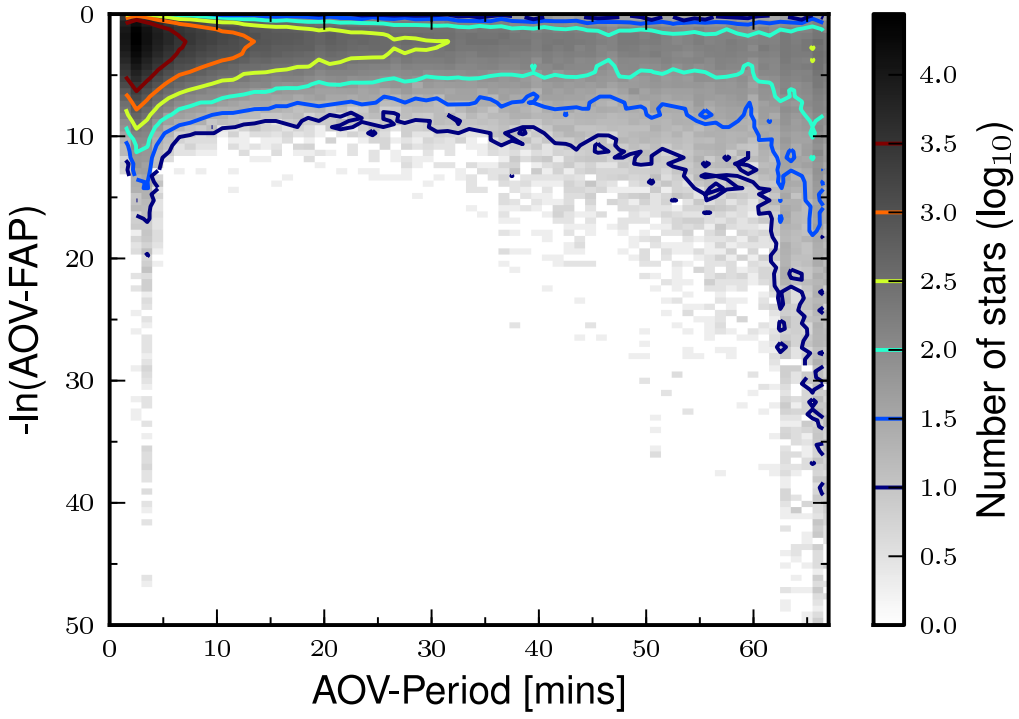

Figure 3.5: The distribution of AOV values against period for the RATS-*Kepler* dataset shown in greyscale with contours. Data are binned with a bin width of 1 minute in period and 0.5 in AOV-FAP. Contours are plotted at $\mathrm{Log}_{10}(\mathrm{count}) = 1$ and then at increments of 0.5 to make trends more readily apparent. The colour of the greyscale represents density of stars and values are shown in the colourbar on the right, along with the position of the contours. The y-axis is inverted by convention and higher values of AOV-FAP imply a greater chance of variability.

3.1.5 Lomb-Scargle Periodogram

The Lomb Scargle (LS) Periodogram (Lomb (1976); Scargle (1982); Press and Rybicki (1989)) is an algorithm which performs least squares fitting of sinusoids on unevenly sampled data to recover periodic sources. This method has the advantage over Fourier methods in that it is only evaluated at points where there is an actual measurement, whereas Fourier methods have to interpolate missing data to create an evenly sampled dataset (Press et al., 1992). It requires start and end frequencies and frequency steps to be selected to evaluate the equation:

$$P_N(\omega) = \frac{1}{2\sigma^2}\left(\frac{(\sum_j (h_j - \bar{h})\cos\omega(t_j-\tau))^2}{\sum_j \cos^2\omega(t_j-\tau)} + \frac{(\sum_j (h_j - \bar{h})\sin\omega(t_j-\tau))^2}{\sum_j \sin^2\omega(t_j-\tau)}\right) \tag{3.6}$$

Where $P_N(\omega)$ is the spectral power as a function of ω, where $\omega = 2\pi f$, f is the frequency, h_j is a flux measurement taken at time t_j and $\bar{h}$ is the mean flux of the light curve. σ^2 is the variance of the data points where:

$$\sigma^2 = \frac{1}{N-1}\sum_1^N (h_j - \bar{h})^2 \tag{3.7}$$

τ is defined by:

$$\tan(2\omega\tau) = \frac{\sum_j \sin(2\omega t_j)}{\sum_j \cos(2\omega t_j)} \tag{3.8}$$

which is an offset that makes $P_N(\omega)$ independent of shifting the values of t_j by

an arbitrary constant (Press et al., 1992), as well as making solving Equation 3.6 equivalent to fitting

$$h(t) = A\cos\omega t + B\sin\omega t \tag{3.9}$$

using linear least-squares fitting at a frequency ω. Using the same method as the AOV, a formal false alarm probability (LS-FAP) can be calculated to give a measure of the significance of the peak in the periodogram and is output by `VARTOOLS` as the $\log_{10}$ of the FAP. The distribution of LS-FAP against period for the RATS-*Kepler* data is shown in Figure 3.6. As can be seen, the distribution is heavily weighted towards less negative values of log FAP, especially at short periods, though not as significantly as with the AOV-FAP. There is clearly period dependent noise, with a wider distribution of log FAP values at longer periods, the lack of a peak in the contours at longer periods implies the sensitivity of LS decreases as the test period approaches the duration of the light curve.

The main disadvantage to the LS-FAP is that a short duration modulation in the light curve will be denoted as a significantly variable light curve, which causes a number of false positive detections where light curves have just a small number of spurious outliers. However, it also leaves it sensitive to short-lived transient phenomena such as flares, as well as periodic or quasi-periodic sources. Since the variable selection process requires a manual inspection process to remove sources which have been selected due to non-astrophysical effects anyway and it does not lead to a significant number of false positive selections, the possibility of being sensitive to a wider variety of sources is of greater importance. I found

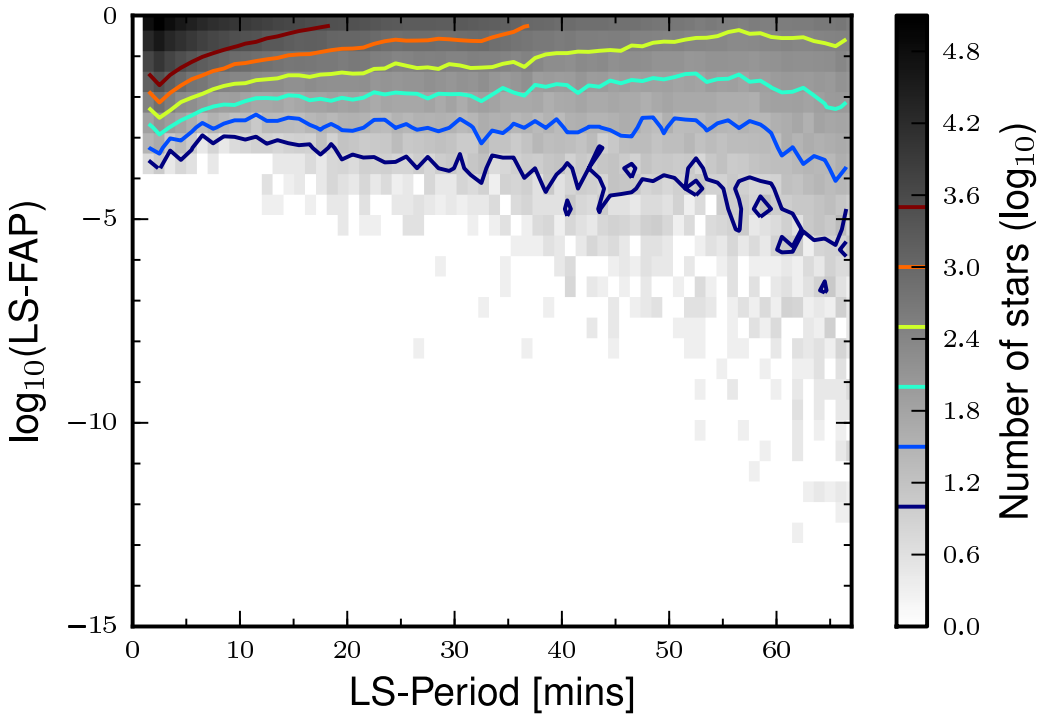

Figure 3.6: The distribution of LS values against period for the RATS-*Kepler* dataset. Data are binned with a bin width of 1 minute in period and 0.5 in LS-FAP. Contours are plotted at $\mathrm{Log}_{10}(\mathrm{count}) = 1$ and then at increments of 0.5 to make trends more readily apparent. The colour of the greyscale represents density of stars and values are shown in the colourbar on the right, along with the position of the contours. Increasingly negative values of LS-FAP imply a greater chance of variability.

through manual inspection that the LS algorithm is able to assign a high enough significance to recover a wide range of variable sources. Hence, I chose to use the LS algorithm to select a subset of candidate variable sources, from which truly variable sources can be selected.

3.2 Selecting Candidate Variables

The main goal of the RATS-*Kepler* survey is to identify short period variable sources in the *Kepler* field which would then have been the subject of bids to observe them in Short Cadence mode using *Kepler*. The RATS-*Kepler* data contains 7.1×10^5 sources and inspecting all the light curves to identify such sources would not only be an impractical task, it is also a gross waste of time given that it can be expected that only of the order of 10^{-1}–10^{0} % of all sources will be truly variable sources. Hence, an initial selection of candidate variable sources is performed to provide a sample size which can practically be manually inspected.

Firstly, light curves which could lead to spurious detections of variability needed to be removed - namely those which had fewer than 40 data points (as light curves with <2/3 of the total possible number of data points cause false positive selections) and those which were within 10 pixels of dead pixel lines and horizontal charge leakage lines on the CCD (this corresponds to the accuracy of pointing we aimed to maintain via manual corrections, c.f. Section 2.2.1). The LS Periodiogram as implemented in `VARTOOLS` determines the frequency of the highest peak in the power spectrum (which henceforth will be defined as the 'Period' of variability even if the source cannot be verified as strictly periodic) and the False Alarm Probability of this peak being statistically significant. It should be noted that it is physically impossible to detect any period greater than half the observation length, however, the purpose of this work is to identify sources which warrant further investigation, not necessarily to unambiguously define parameters for sources. For each light curve an LS power spectrum is obtained and the AOV

test is performed in the frequency interval corresponding to the Nyquist frequency (847.1 cycles/day – which equates to a period of 1.7 mins – for the INT data and 600 cycles/day – which equates to a period of 2.4 mins – for the MDM data) and 21.49 cycles/day – which equates to a period of 67 mins – (which is the mean duration of the INT light curves).

As mentioned in Section 3.1.5 I chose to use the LS test for the purposes of selecting an initial sample of candidate variables. In the absence of red noise and systematic trends, a peak in the power spectrum with log FAP = –2.5 is likely to be significantly variable at the 3σ confidence level. However, since the seeing and sky brightness can vary from field to field, the success of the detrending algorithim can vary from chip to chip and there is period dependent noise in the data, the threshold for identifying variables can be more negative than log FAP = –2.5. To set this threshold I made a number of adaptations to the method used in Barclay (2011).

The first adaptation I made was to the set of stars on which the selection of candidate variables was made. Barclay (2011) made a 'global' selection from all stars in a given epoch of data, which contained many different fields which had been observed over a number of nights and therefore in a variety of different seeing conditions, air masses etc. This meant that fields with widely different spreads in the log FAP values were being combined together. This method had been chosen since there are too few stars in each individual field-chip combination to perform an acceptable statistical selection, but it also meant that fields were being combined together where a given value of log FAP at a given period would have vastly different levels of significance in terms of true variability. This meant

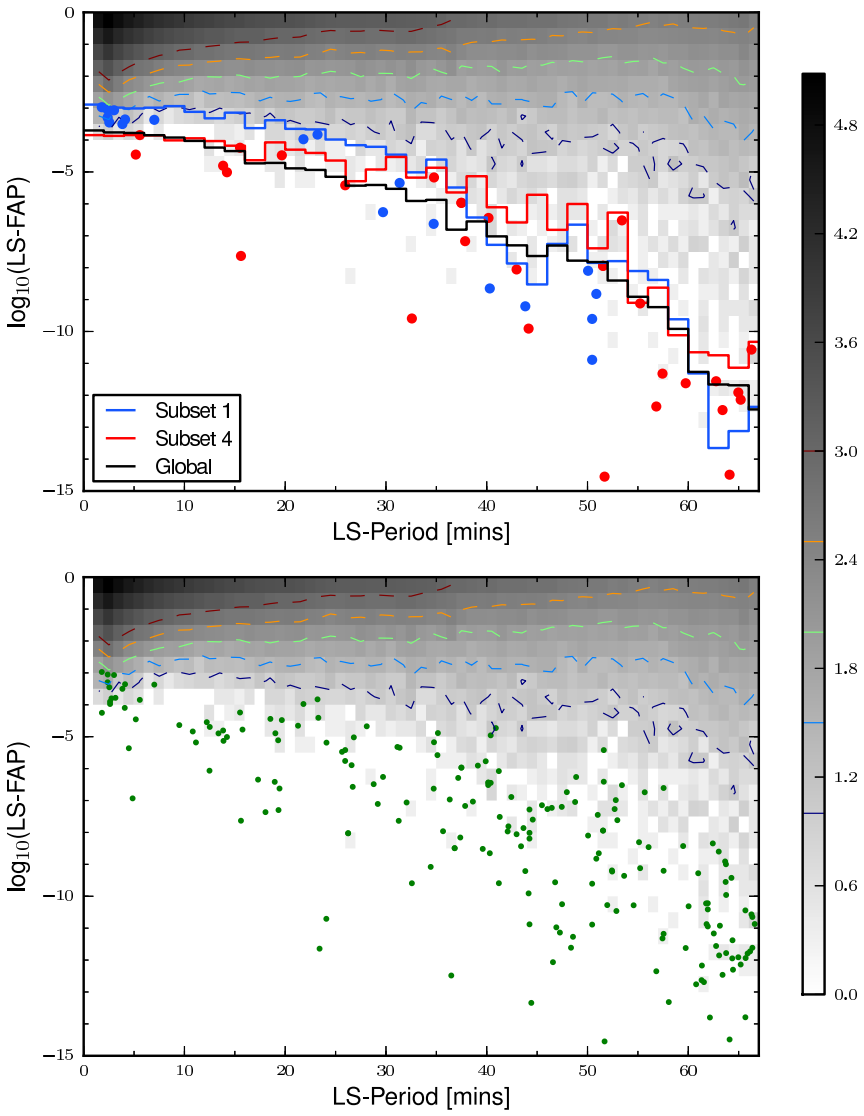

Figure 3.7: The top panel shows the FAP cutoffs (solid lines) and those stars selected as variable (circles) for $n = 18$ for those 10^5 stars located in field-chip combinations which have the least negative median log FAP (Subset 1) and those located in the central field-chip combination of the 7 subsets created (Subset 4) in blue and red respectively. The FAP cutoff level obtained via a global selection on all sources is shown for comparison in black (Global). The bottom panel shows all of the stars selected as variable for $n = 18$ indicated by green circles. Both are shown on a plot of the False Alarm Probability (FAP) as a function of the period of the most prominent peak in the Lomb Scargle power spectrum for all sources. The greyscale is binned with a bin width of 1 minute in period and 0.5 in LS-FAP. Contours are plotted as dashed lines at $\mathrm{Log}_{10}(\mathrm{count}) = 1$ and then at increments of 0.5 to make trends more readily apparent. More negative values of log FAP imply a greater chance of intrinsic variability.

some variable sources from fields with low levels of noise in the log FAP values were not selected and that some non-variable sources were being selected because the number of sources at lower log FAP values from fields with less noise in the log FAP values was unduly increasing their significance.

Therefore, to more robustly take into account varying systematic trends in different field-chip combinations, the median value of the log FAP statistic for the light curves in each field-chip combination was determined. The sources were then ordered by this median log FAP and seven sub-sets containing 10^5 stars each were selected by decreasing value of median log FAP (the remaining 8,787 stars which were in field-chip combinations with the most negative median log FAP were discarded). For the subset with the least negative median value for log FAP, there were 911 sources which have a log FAP< -2.5, or 0.91 percent of sources in the sub-set, demonstrating the heavy weighting of the distribution to less negative values of FAP and therefore non-variability. The effect of this change can be seen in Figure 3.7, which shows the log FAP cutoff levels and those stars selected as variable for those 10^5 stars located in field-chip combinations which have the least negative median log FAP (Subset 1) and those located in the central field-chip combination of the 7 subsets (Subset 4), along with the FAP cutoff which would be derived from a global selection performed on all stars (Global). As can be seen, had a global selection been performed, many candidate variable sources would not have been recovered and the selection on the subsets has lead to better taking into account the FAP spread in both subsets, as demonstrated by the often large difference between the global cutoff value and those for the subsets. Furthermore, there are many regions where both the subsets exhibit differing trends to each

other, as well as each having differing trends to those found in the global selection, implying that the use of individual subset selection of candidate variable source has had some degree of success in better taking into account the local systematic trends in each subset. Of the 30 sources selected from Subset 4 with $n = 18$, 12 passed our manual verification stage, with their light curves shown in Figure 3.9.

The second adaptation I made to the method of Barclay (2011) was the correction of an error in the code used to select variable sources. The methodology was otherwise very similar to that described below, but an errant minus sign in the code lead to it not sufficiently taking into account the spread in log FAP values, especially at longer periods, as shown in Figure 3.8. This lead to a dramatic reduction in false positive selections of variable sources, especially at longer periods. Further to this, I added in a condition that on top of the requirements described below, a source must have log FAP< -2.5 to be selected as a candidate variable source.

Since there is period dependent noise in the FAP values (see figure 3.6), using a fixed threshold to select candidate variable sources will either select a larger number of false positives with increasing period, or exclude potentially astrophysically interesting sources at shorter periods. Hence, rather than using a fixed threshold for the log FAP to provide an initial selection of candidate variables, I used the Median Absolute Deviation (MAD) (see equation 3.1) applied to period bins to provide a means of identifying sources which were 'outliers' in the Period - log FAP distribution for each of the subsets of the field-chip combinations with similar median FAP values. Since the use of the MAD in this context was to provide a relative measure of variance in the distribution and not to approximate

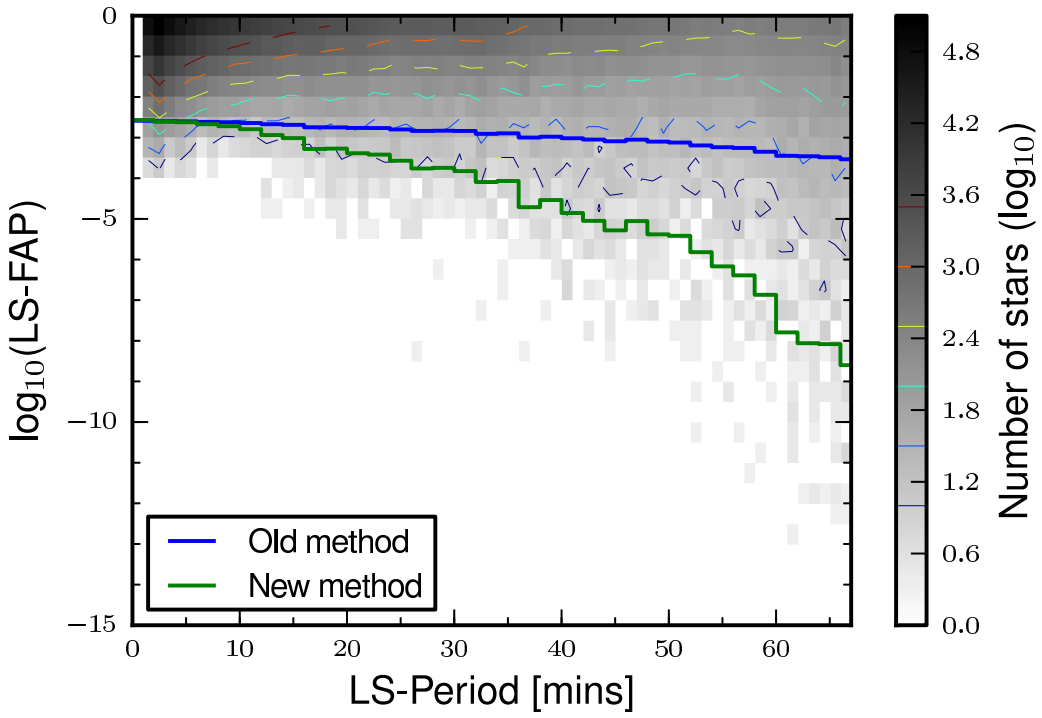

Figure 3.8: Plot showing the cut-off in each period bin for the 'Old method' of Barclay (2011) with n=500 (blue solid line) and my corrected, 'New method' with n=12 (green solid line) for selecting variable sources. Values of n for each method were selected such that the cut-off levels were approximately equal at lower periods to aid in comparison, the large difference between them is due to a difference in methodology and as such, values of n for each method are not directly comparable. Plotted on a graph of log of the False Alarm Probability (FAP) as a function of the period of the most prominent peak in the Lomb Scargle power spectrum for all sources. The greyscale is binned with a bin width of 1 minute in period and 0.5 in LS-FAP. Contours are plotted as dashed lines at Log_{10}(count) = 1 and then at increments of 0.5 to make trends more readily apparent. More negative values of log FAP imply a greater chance of intrinsic variability.

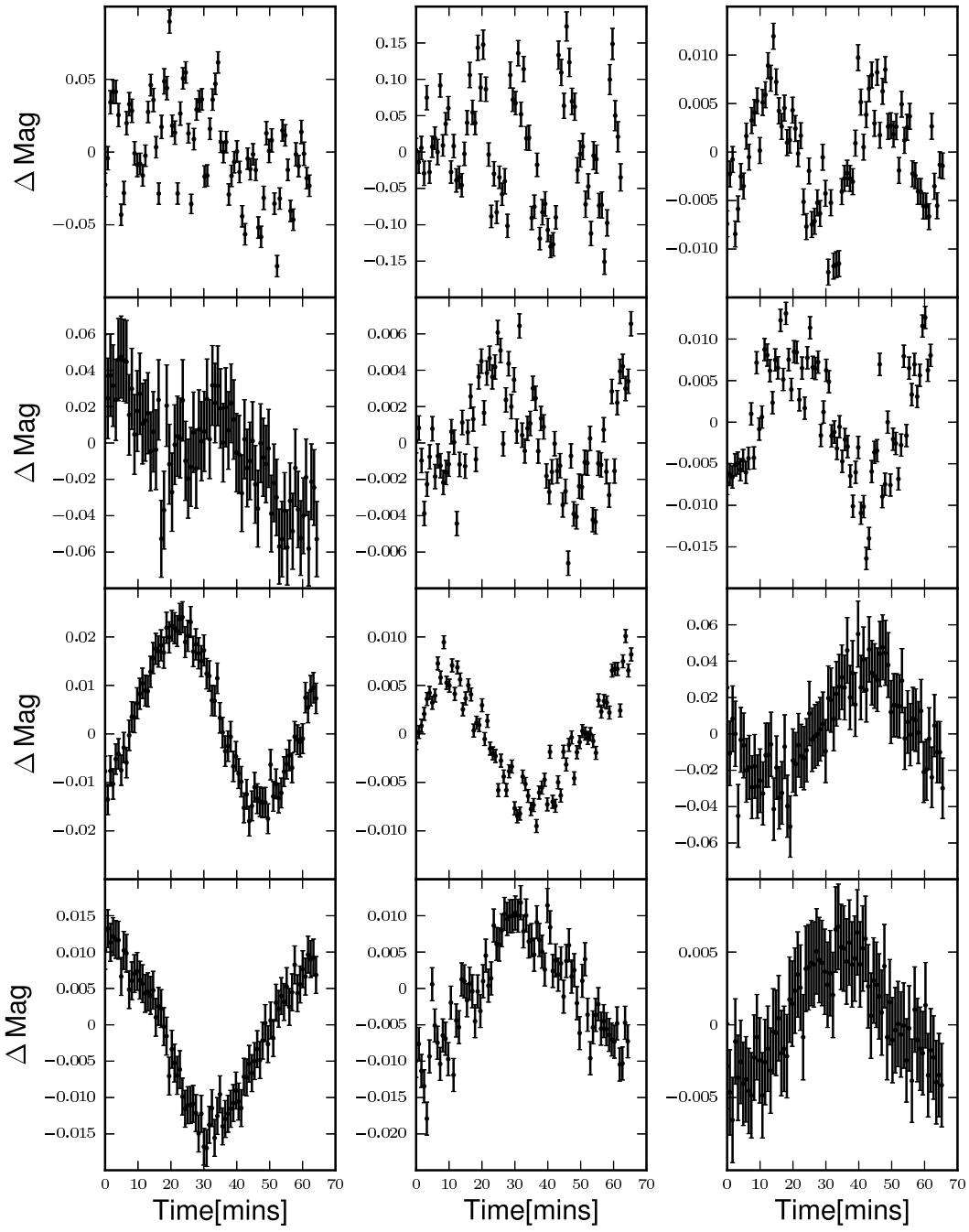

Figure 3.9: The RATS-*Kepler* light curves of the 12 sources selected from Subset 4 with $n = 18$ and which passed our manual verification stage.

the standard deviation, the constant b in equation 3.1 was set to 1. The data were ordered by Period then binned at 2 min time intervals and the MAD and median were derived for each bin. Candidate variables were then selected in each bin so that variable sources obey

$$(\text{logFAP}) < (\text{MAD}_{\text{logFAP}} \times n) + \text{Median}_{\text{logFAP}} \tag{3.10}$$

where n is an integer which defines how far a source is from the local median log FAP.

The value of n is selected largely by trial and error through manual inspection of light curves around the threshold in FAP given by various values of n – too high a value of n will select only the most strongly variable sources, but too low a value of n will produce large quantities of candidate variables, all of which require manual verification. The effect of changing the value of n can be seen in Figure 3.10. Higher values of n will decrease the threshold log FAP value to select fewer and fewer stars; and with the change in cut-off level roughly reflecting the change in contour levels and greyscale, this implies the use of the MAD seems to have performed effectively at taking into account the period dependent noise. Note that to be selected as a candidate variable, a source also has to have log FAP< -2.5; this threshold has been omitted from Figure 3.10 to show more clearly the difference in threshold for various values of n, but would omit some stars from being selected at shorter periods for lower values of n. The selection of variables using the MAD statistic was done on each subset of 10^5 stars separately then combined according to the n value that was used. We found that for n=18,

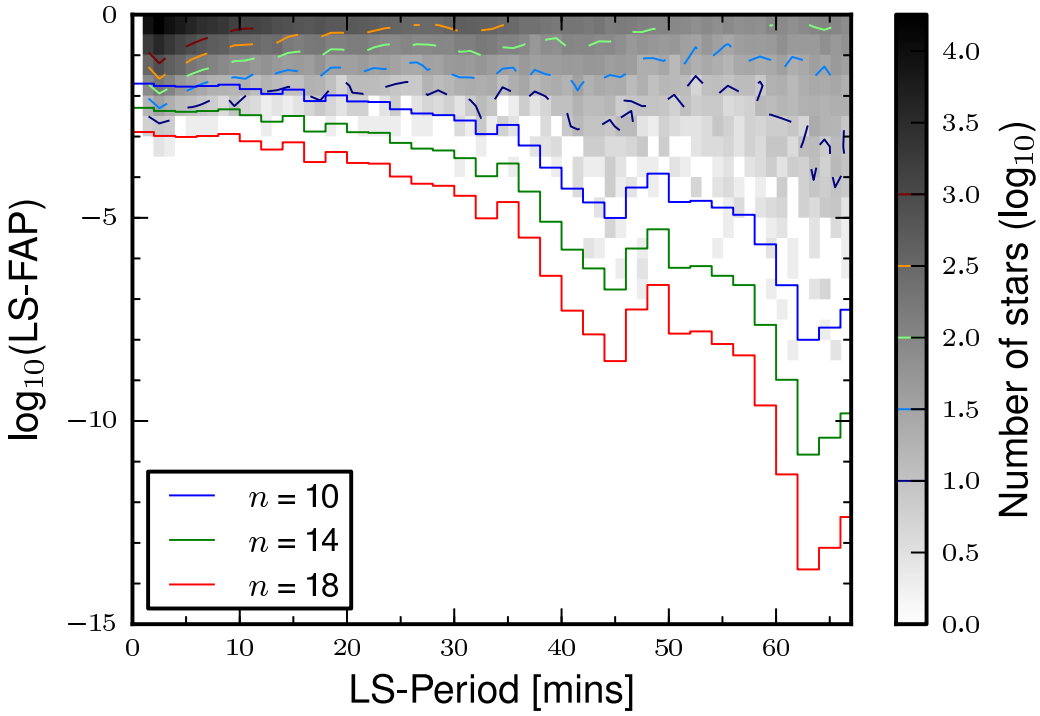

Figure 3.10: Plot showing the cut-off in each period bin for varying values of n to designate a star as a candidate variable on a graph of log of the False Alarm Probability (FAP) as a function of the period of the most prominent peak in the Lomb Scargle power spectrum for those 10^5 stars located in field-chip combinations which have the least negative median log FAP. The greyscale is binned with a bin width of 1 minute in period and 0.5 in LS-FAP. Contours are plotted as dashed lines at $\mathrm{Log}_{10}(\mathrm{count}) = 1$ and then at increments of 0.5 to make trends more readily apparent. More negative values of log FAP imply a greater chance of intrinsic variability.

227 stars (or 0.032 percent of the total) were selected as candidate variables, as shown in Figure 3.7 (n=16 $\rightarrow$ 368 stars, n=14 $\rightarrow$ 642, n=12 $\rightarrow$ 1187, n=10 $\rightarrow$ 1999). It should be stressed that this selection simply identifies those stars which are most likely to be variable.

Each source was then subject to a manual inspection of the light curve and the corresponding relevant images to verify their variable nature. Where appropriate, additional light curves were obtained from our observations using the optimal aperture photometry routine `autophotom` (Eaton et al., 2009) to verify the authenticity of the `DIAPL2` light curve. For the n=18 sample we found that after a second stage verification process there were 65 sources which could be classed as highly likely to be variable using the LS statistic as a first screening stage. A summary of these sources are shown in Table 3.2, which has also been made publicly available at star.arm.ac.uk/rats-kepler along with our light curves and other photometric products to maximise the potential scientific impact of our survey. The colours of our sources are shown in Figures 3.11 and 3.12, with these colours then used to provide a tentative identification of sources to aid in selection of sources suitable to be observed by *Kepler* in short cadence mode, particularly in the case of those which were far from the main sequence. It was found that a high fraction of sources (71 percent) of the n=18 sample were unlikely to be truly variable sources and hence were removed in this manual verification process. Many of these spurious variables were caused by residual systematic trends in the light curves - for instance sources from the same chip showed very similar trends in their light curves. This is almost certainly a result of using manual corrections in the guiding process in the INT observations (which was due to instrumental

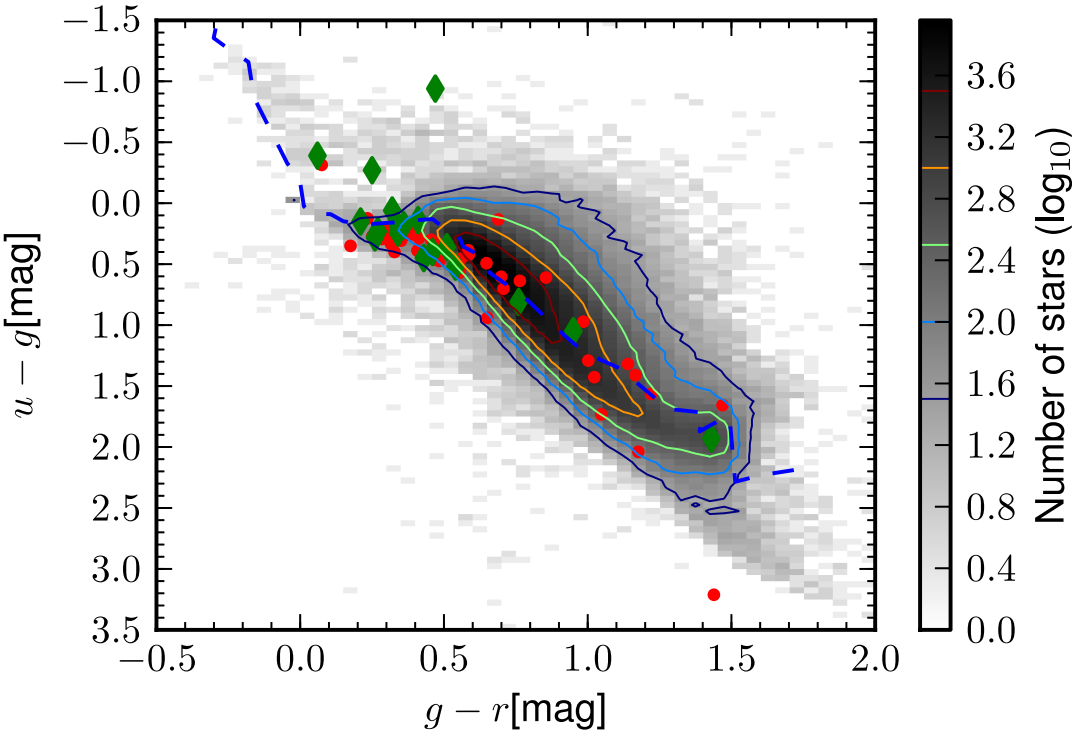

Figure 3.11: Plot showing the $(g - r)$–$(u - g)$ colour-colour plane of all sources where the greyscale is binned at 0.05 in magnitude for both colours, the colour of the greyscale indicates the number of stars along with the solid contour lines, both of which are shown in the colour bar at the side. The dashed blue line shows the unreddened main sequence (taken from Groot et al. (2009)), around which the majority of stars are located, as would be expected. Red circles indicate the colours of sources shown in Table 3.2 while green diamonds indicate the colours of those sources for which we have obtained *Kepler* Short Cadence data (Table 3.4).

limitations as detailed in Section 2.2.1) and for the fact that the light curves only covered a short time (typically 1 hr).

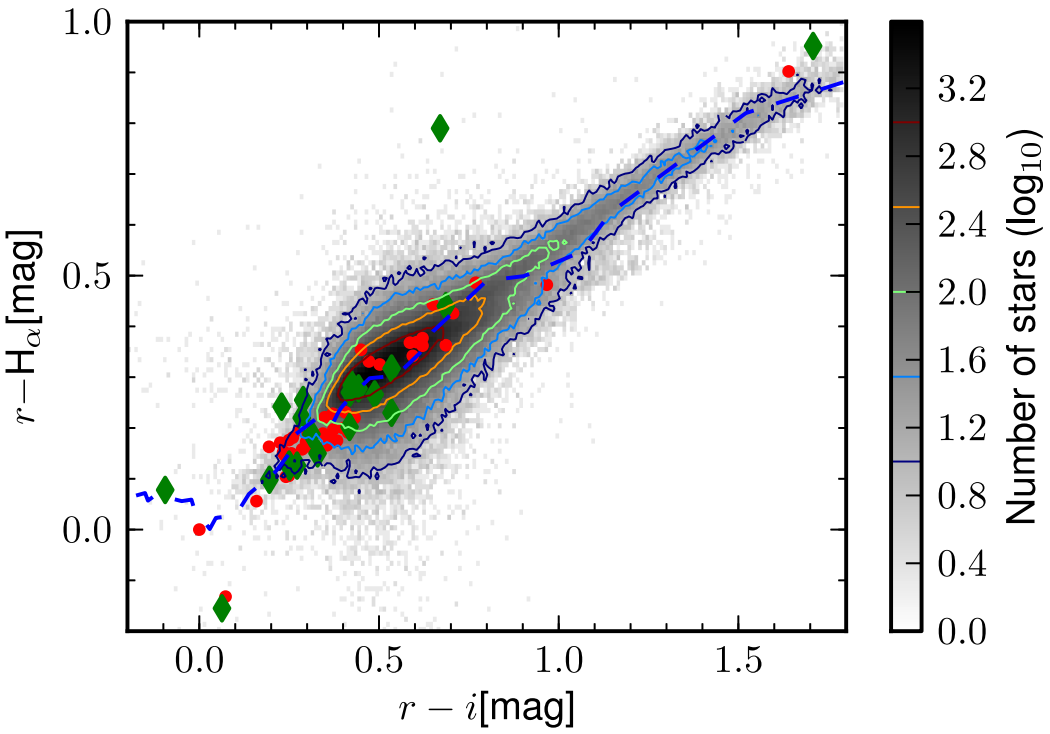

Figure 3.12: Plot showing the $(r-i)$–$(r-\mathrm{H}_\alpha)$ colour-colour plane of all sources where the greyscale is binned at 0.01 in magnitude for both colours, the colour of the greyscale indicates the number of stars along with the solid contour lines, both of which are shown in the colour bar at the side. The dashed blue line shows the unreddened main sequence (taken from Drew et al. (2005)), around which the majority of stars are located, as would be expected. Red circles indicate the colours of sources shown in Table 3.2 while green diamonds indicate the colours of those sources for which we have obtained *Kepler* Short Cadence data (Table 3.4).

Table 3.2: Table showing all the variable stars selected using 'n=18' and which passed the manual verification phase along with a selection of parameters.

KIC ID	RA J2000	DEC J2000	g_{KIS} mag	$(U-g)_{KIS}$ mag	$(g-r)_{KIS}$ mag	g_{rats} mag	$(g-r)_{rats}$ mag	Alarm	AOV Period mins	AOV	LS_Per mins	LS_Log_FAP
11911480	19:20:24.91	+50:17:22.4	18.09	-0.39	0.06	18.13	-0.05	0.02	4.89	14.75	4.9	-6.93
8293193	19:17:55.25	+44:13:26.1	18.42	-0.31	0.08	18.41	0.00	1.88	5.17	5.81	5.2	-4.46
	19:29:00.80	+44:56:59.2				13.95		1.43	9.93	9.29	10.1	-5.51
12647528	19:22:50.90	+51:45:31.5	14.31	1.73	1.05	14.35	0.99	2.75	43.4	10.36	10.8	-4.83
10728590	19:23:18.49	+48:02:09.0	19.14		0.97	19.37	1.01	4.25	13.9	8.73	13.8	-4.81
10936077	19:52:53.44	+48:19:35.6	15.85	0.70	0.70	15.90	0.56	2.62	31.8	12.19	16.2	-4.80
7356523	19:19:30.70	+42:58:08.5	19.20	0.94	0.65	19.20	0.65	2.00	18.8	6.91	18.5	-4.44
9899481	19:41:00.84	+46:44:58.3	19.66	0.49	0.64	19.61	0.53	2.99	36.4	10.77	19.3	-5.11
6665002	18:46:27.78	+42:10:34.9	19.50	0.13	0.68	19.45	0.64	3.34	21.0	9.38	21.2	-4.66
8123702	19:57:39.81	+43:55:07.7	13.46	2.04	1.17	13.50	1.11	4.54	64.9	8.78	21.8	-3.98
	18:55:13.43	+43:57:31.6	19.75			19.61	1.08	2.21	22.9	8.10	23.2	-3.83
6109859	19:07:56.19	+41:26:33.1	16.19	0.35	0.17	16.19	0.17	8.22	23.1	39.38	23.4	-11.64
3223460	19:12:32.15	+38:23:00.1	13.71	0.27	0.25	13.74	0.16	7.58	24.4	29.58	24.0	-10.71
	19:53:11.03	+48:39:39.1				14.79	0.63	4.06	44.6	14.76	25.9	-5.42
	19:18:03.08	+39:26:21.8						5.28	26.4	16.88	26.2	-8.03
11360026	19:45:03.62	+49:06:01.0	15.01	0.24	0.29	14.99	0.16	9.25	32.9	18.47	32.5	-9.59
9813390	18:49:08.86	+46:40:04.2	16.86	1.30	1.14	16.98	1.04	10.29	66.2	24.35	34.7	-5.17
10031075	19:54:21.16	+46:57:39.9	15.17	0.63	0.76	15.18	0.64	2.71	38.2	9.62	35.1	-5.57
8118210	19:52:18.66	+43:58:11.8	17.02	0.46	0.47	17.09	0.33	3.98	65.4	12.07	35.4	-6.31
7960631	19:28:05.53	+43:45:45.5	15.31	0.30	0.31	15.32	0.18	7.28	63.5	23.15	35.6	-7.96
9479634	19:48:39.16	+46:03:47.1	14.65	0.39	0.32	14.63	0.20	11.23	36.0	51.00	36.4	-12.4
5772488	19:00:07.98	+41:02:51.8	17.67	0.21	0.33	17.70	0.16	9.54	65.5	22.88	37.3	-8.15
11723564	19:47:11.37	+49:53:13.7	12.81	0.38	0.40	12.74	0.17	7.47	66.4	18.83	38.0	-7.91
10253681	18:46:40.86	+47:18:28.1	17.22	0.60	0.69	17.04	0.63	5.61	37.6	25.38	39.6	-8.51
9786930	19:51:01.55	+46:34:24.6	19.00	1.29	1.00	19.03	0.77	8.33	47.3	18.77	41.1	-6.77
10975348	19:26:46.09	+48:25:30.9	18.88	0.19	0.34	18.72	0.07	13.32	54.0	32.84	41.2	-9.59
9364179	19:56:24.52	+45:48:24.1	14.38	0.44	0.43	14.42	0.36	6.93	43.4	17.11	41.2	-7.51
9294308	19:47:09.39	+45:44:32.1	13.66	0.25	0.34	13.64	0.19	6.09	44.7	17.89	42.9	-8.05
7698266	19:46:50.79	+43:19:02.3	13.22	0.21	0.41	13.26	0.32	6.54	43.7	18.00	43.6	-7.86
10353926	19:47:53.67	+47:26:56.3	14.89	0.22	0.28	14.90	0.31	9.32	45.0	26.15	44.1	-9.90
7625723	19:47:11.80	+43:16:37.4	14.18	1.42	1.02	14.21	0.95	8.22	48.7	19.43	44.2	-7.70
9417741	19:47:39.58	+45:55:07.6	14.72	0.29	0.28	14.78	0.20	15.78	45.3	75.25	44.4	-13.3

Table 3.2: (continued) Table showing all of our variable stars selected using 'n=18' and which passed our manual verification phase along with a selection of parameters.

KIC ID	RA J2000	DEC J2000	g_{KIS} mag	$(U-g)_{KIS}$ mag	$(g-r)_{KIS}$ mag	g_{rats} mag	$(g-r)_{rats}$ mag	Alarm	AOV Period mins	AOV	LS_Per mins	LS_Log_FAP
4262791	19:26:48.06	+39:20:35.7	15.74	4.82	0.26	15.71	0.21	13.49	62.9	23.15	44.5	-7.60
12406812	19:23:33.80	+51:17:58.9	17.24	0.17	0.36	17.24	0.21	14.47	46.8	47.66	46.5	-12.06
7548311	19:48:28.48	+43:06:12.3	14.55	0.47	0.48	14.52	0.34	10.56	66.5	32.02	46.7	-9.56
5623923	19:32:01.53	+40:51:16.8	16.61	0.23	0.27	16.57	0.15	10.30	45.3	23.26	47.4	-10.24
6418095	18:44:56.53	+41:50:28.1	13.20	0.12	0.23	13.14	0.23	10.41	47.4	35.16	48.3	-11.61
7770746	19:49:00.55	+43:26:06.4	18.84	1.41	1.16	19.20	1.35	17.02	47.6	72.20	48.5	-13.46
9640005	19:09:46.28	+46:20:04.1	18.39	0.15	0.21	18.39	0.15	18.18	63.9	50.71	48.5	-11.27
9786165	19:50:10.98	+46:34:40.8	17.66	0.81	0.76	18.39	1.12	16.50	47.3	47.53	49.7	-10.19
5474065	19:53:02.53	+40:40:34.6	18.77	1.93	1.43	18.76	1.39	12.75	51.3	105.44	49.9	-6.32
9672731	19:59:30.69	+46:23:06.7	17.47	0.97	0.98	17.95	1.16	8.185	66.2	18.77	51.1	-8.65
8840638	19:55:35.07	+45:04:46.0	14.63	0.52	0.54	14.71	0.42	22.33	49.8	98.99	51.6	-14.54
9720306	19:43:03.19	+46:25:56.0	15.45	0.28	0.33	15.50	0.23	15.80	49.7	30.96	51.9	-10.27
6029053	19:08:02.00	+41:22:12.6	17.51	3.21	1.43	17.51	1.43	13.82	55.1	76.53	52.9	-7.61
8117771	19:51:52.82	+43:55:00.1	13.24	0.26	0.36	13.22	0.25	17.99	54.2	59.45	53.4	-12.18
8387281	19:54:08.13	+44:22:16.5	15.65	1.65	1.47	15.64	1.46	7.73	45.5	49.45	55.6	-6.74
4389023	19:47:47.78	+39:29:41.5	13.63	0.21	0.36	13.64	0.25	18.31	52.3	59.75	56.8	-12.35
5818101	19:54:18.14	+41:04:07.1	17.52	0.25	0.39	17.48	0.28	17.61	65.1	32.50	57.4	-11.32
7839261	19:48:18.90	+43:34:22.1	14.77	0.39	0.40	14.77	0.31	22.00	57.2	92.79	58.0	-13.31
8118471	19:52:35.03	+43:56:42.3	15.72	0.45	0.56	15.75	0.46	12.94	60.8	28.50	59.2	-10.42
5179693	19:18:32.80	+40:22:51.3	17.60	0.17	0.32	17.74	0.29	19.35	65.8	64.82	61.3	-12.62
7768746	19:47:00.08	+43:28:22.2	13.23	0.38	0.58	13.18		18.11	54.1	78.36	61.5	-12.69
3350736	19:34:23.34	+38:24:30.5	15.47	0.30	0.45	15.53	0.33	23.04	64.3	41.69	62.1	-11.50
10284901	19:43:46.41	+47:20:32.8	15.72	0.06	0.31	15.59	0.11	19.40	64.4	161.97	62.1	-13.80
8255272	19:53:55.44	+44:11:49.4	13.24	0.28	0.41	13.18	0.44	17.86	62.1	49.52	63.0	-11.85
9364721	19:57:04.39	+45:48:41.1	19.06	0.60	0.85	19.06	0.71	10.03	64.2	19.32	63.7	-8.99
8908767	19:56:07.19	+45:08:50.8	14.30	0.56	0.55	14.35	0.46	21.59	66.4	118.8	64.0	-14.48
9905251	19:48:41.25	+46:43:33.9	16.11	0.30	0.35	16.13	0.18	17.04	55.9	40.88	64.4	-12.30
9812716	18:47:14.89	+46:36:38.4	13.95	0.28	0.29	13.91	0.14	13.67	52.7	38.82	64.9	-11.91
	19:16:43.60	+39:31:27.8						17.24	62.2	61.85	65.2	-12.21
8254486	19:53:11.74	+44:07:43.2	14.76	0.42	0.58	14.59	0.48	17.17	56.6	47.02	65.2	-12.13
4916020	19:17:58.54	+40:04:54.6	14.57	0.33	0.31	14.53	0.28	13.69	61.9	47.96	65.8	-11.79
4149801	19:18:07.97	+39:15:42.0	19.51	1.56	1.21	19.74	2.04	18.62	54.2	58.62	66.1	-11.72
8561192	19:29:05.17	+44:41:50.8	16.43	0.34	0.49	16.40	0.48	17.05	66.5	62.97	66.5	-10.86

3.3 Follow-up Spectroscopic Observations

To help ascertain the nature and various parameters of some of the sources, low and medium resolution optical spectroscopy was performed for over 50 sources which were either identified as being variable on a short timescale or had unusual colours. This included one very blue ($g - r = -0.5$) source in our sample, KIC 10449976, which has been reported as an extreme helium star (Jeffery et al., 2013). We obtained data using the INT and 10.4 m Gran Telescopio Canarias (GTC), both of which are located at the Observatorio Roque de los Muchachos in La Palma, Canary Islands, Spain.

The observations at the INT were made using the Intermediate Dispersion Spectrograph (IDS) and the R400 grism between 26–28 June 2012. The individual exposure time ranged from 180 to 360 sec and had a spectral resolution of $\sim$2Å . The observations at the GTC were made using the Optical System for Imaging and Low Resolution Integrated Spectroscopy (OSIRIS) tunable imager and spectrograph (Cepa et al., 2003) and the R1000R grism during March – June 2013. The individual exposure time ranged from 40 to 400 sec and had a spectral resolution of $\sim$8Å . The spectra were reduced using standard procedures with the wavelength calibration being made using a CuNe+CuAr arc taken shortly after the object spectrum was taken. At least two spectra were obtained of each source and a flux standard was observed so that the resulting combined spectra of each source could be flux calibrated in the case of the IDS spectra and to remove the instrumental response in the OSIRIS spectra (the observing programme through which we obtained our observations utilises poor observing conditions).

Spectra of stars which were of the spectral type A/F were modelled using a grid of LTE models calculated using the ATLAS9 code (Kurucz, 1992) with convective overshooting switched off. Other spectra were calculated with the LINFOR line-formation code (Lemke, 1991). Data for atomic and molecular transitions were compiled from the Kurucz line list. The stellar temperatures were estimated from the hydrogen Balmer lines of the stars (Hβ to Hδ) using the FITSB2 routine (Napiwotzki et al., 2004). No gravity sensitive features are accessible in the low resolution spectra. McNamara (1997) finds that SX Phe and large amplitude δ-Scuti stars have a range in $\log g$ of 3.0–4.3. Hence we chose to fix $\log g$=4.0, although the resulting temperature is only weakly sensitive to this parameter, so any effect of this choice is minimal. The metallicity was allowed to vary although this was not strongly constrained in the fits. The error of the fit parameters were determined with a bootstrapping method. An example of these fits can be seen in Figure 3.13, which shows the fit to the spectrum of KIC 3223460. Table 3.3 shows the temperature derived for all the stars for which spectra were obtained.

3.4 Sources Submitted for *Kepler* Proposals

In total 18 sources were selected that would be suitable for short cadence *Kepler* observations and had the potential for high impact science goals. In brief, they are:

- KIC 11911480 is a pulsating DA white dwarf, which at the time of submission was only the third known pulsating white dwarf in the *Kepler* field;
- KIC 5474065 is an M4 V dwarf which showed a flare with a duration of 8

KIC	RA (J2000)	Dec (J2000)	g (mag)	Timescale (mins)	T_{KIC} (K)	log g	T_{IDS} (K)	T_{GTC} (K)
7173839	18:44:40.31	+42:43:13.0	13.2	34.5	8098	3.96	8147 (38)	
8733545	18:48:07.34	+44:57:31.2	14.2	37.1	N/A	N/A	6249 (31)	
6923743	18:48:26.20	+42:29:01.3	16.8	21.1	8210	4.15	8331 (121)	
8733715	18:48:32.17	+44:54:03.9	13.7	35.5	N/A	N/A	6399 (20)	
8733904	18:49:01.37	+44:54:06.0	13.3	37.1	6493	4.21	6457 (22)	
10516812	18:51:17.89	+47:43:17.9	16.5	4.3	6730	4.17	6486 (90)	
10648468	18:54:01.17	+47:54:56.3	15.0	31.4	6512	4.24	6481 (69)	
	19:05:21.79	+38:00:24.4	15.5	27.2			6330 (50)	
2694706	19:05:36.02	+37:56:06.4	14.9	25.3	6465	4.25	6425 (38)	
2971944	19:05:59.91	+38:06:19.2	16.2	44.7	8338	3.92	8198 (68)	
6109859	19:07:56.23	+41:26:34.2	16.0	23.4	8155	4.04	8099 (58)	
3223460	19:12:32.15	+38:23:00.1	13.7	24.1	7932	4.08	8209 (45)	
	19:18:44.39	+42:59:48.2	14.9	37.5			6373 (29)	
7960410	19:27:44.29	+43:42:40.1	13.2	27.1	6566	4.38	6762 (47)	
	19:27:57.02	+40:40:43.0	13.7	24.7			5692 (58)	
7960631	19:28:05.53	+43:45:45.5	15.3	35.7	7824	3.83	7800 (85)	
11297693	19:28:54.57	+49:01:32.4	17.0	30.9	7841	4.11	7996 (217)	
2857323	19:29:49.16	+38:01:21.8	13.7	60+	7725	4.03	7372 (68)	
6207136	19:30:06.47	+41:30:28.6	16.1	34.0	8215	4.05	8075 (72)	
	19:30:37.89	+40:34:35.7	14.1	24.7			6964 (35)	
6211901	19:35:51.20	+41:33:55.4	15.5	34.4	8629	4.11	8155 (59)	
4377815	19:39:08.10	+39:27:35.9	14.8	45.2	7743	4.02	7815 (42)	
5808231	19:45:57.42	+41:00:49.7	13.8	31.6	8181	4.04	8135 (40)	
5977736	19:46:04.83	+41:13:58.8	13.3	33.9	7661	3.81	7889 (42)	
11723564	19:47:11.37	+49:53:13.7	12.7	60+	6847	4.33	7006 (37)	
	19:48:21.86	+46:40:55.3	13.5	15.0			6665 (30)	
9479634	19:48:39.18	+46:03:46.8	14.6	36.7	7865	3.91	8168 (53)	
7909392	19:49:53.14	+43:38:19.5	13.8	44.2	7793	3.83	7859 (47)	
	19:52:18.66	+43:58:11.8	17.1	35.4			8309 (169)	
5301952	19:53:09.20	+40:28:48.7	14.0	30.5	6310	4.45	6731 (50)	
6547396	19:53:18.25	+41:58:26.9	14.8	25.3	7484	3.95	8238 (46)	
	19:53:23.21	+44:09:21.8	15.8	32.6			8070 (71)	
6804054	19:53:26.55	+42:13:39.2	15.6	43.1	7238	3.98	8043 (74)	
8120184	19:54:11.93	+43:59:20.1	14.1	34.4	7293	3.73	7719 (59)	
6719649	19:54:17.72	+42:06:41.4	14.5	34.0	7334	4.06	7738 (36)	
9364179	19:56:24.52	+45:48:24.1	14.4	41.6	7004	4.01	7835 (55)	
10230546	19:56:59.42	+47:12:37.5	14.0	44.2	N/A	N/A	7317 (54)	
8914189	20:02:28.68	+45:11:26.6	14.4	37.5	N/A	N/A	7159 (78)	
8526451	20:05:31.72	+44:34:42.1	13.0	41.5	7532	4.01	8098 (39)	
3223460	19 12 32.2	+38 23 00.1	13.7	24.1	7930	4.10		8180 (110)
9640005	19 09 46.3	+46 20 04.1	18.4	48.6				7730 (180)
8840638	19 55 35.1	+45 04 46.0	14.6	51.7	6310	3.80		7860 (120)
4636671	19 01 52.2	+39 45 59.3	15.7	53.0	7640	4.00		7950 (120)
12406812	19 23 33.8	+51 17 58.9	17.2	46.6	7370	4.10		7660 (140)
5623923	19 32 01.5	+40 51 16.8	16.6	47.5	8300	3.90		7970 (110)
10284901	19 43 46.4	+47 20 32.8	15.7	62.1	8420	4.00		7710 (180)
10975348	19 26 46.1	+48 25 30.8	18.9	41.2				7080 (210)

Table 3.3: Stars which were observed using the IDS on the INT in June 2012 and OSIRIS on the GTC during March – June 2013 along with the temperature and $\log g$ taken from the *Kepler* Input Catalog (Brown et al., 2011a). The values in parenthesis are the formal 3σ confidence interval. Including systematic uncertainties, which have not been included, the realistic 3σ uncertainties are around ± 300 K. The uncertainties for T_{KIC} and $\log g_{KIC}$ are ± 250 K and ± 0.25 dex respectively (c.f. Brown et al. (2011a) and Pinsonneault et al. (2012)).

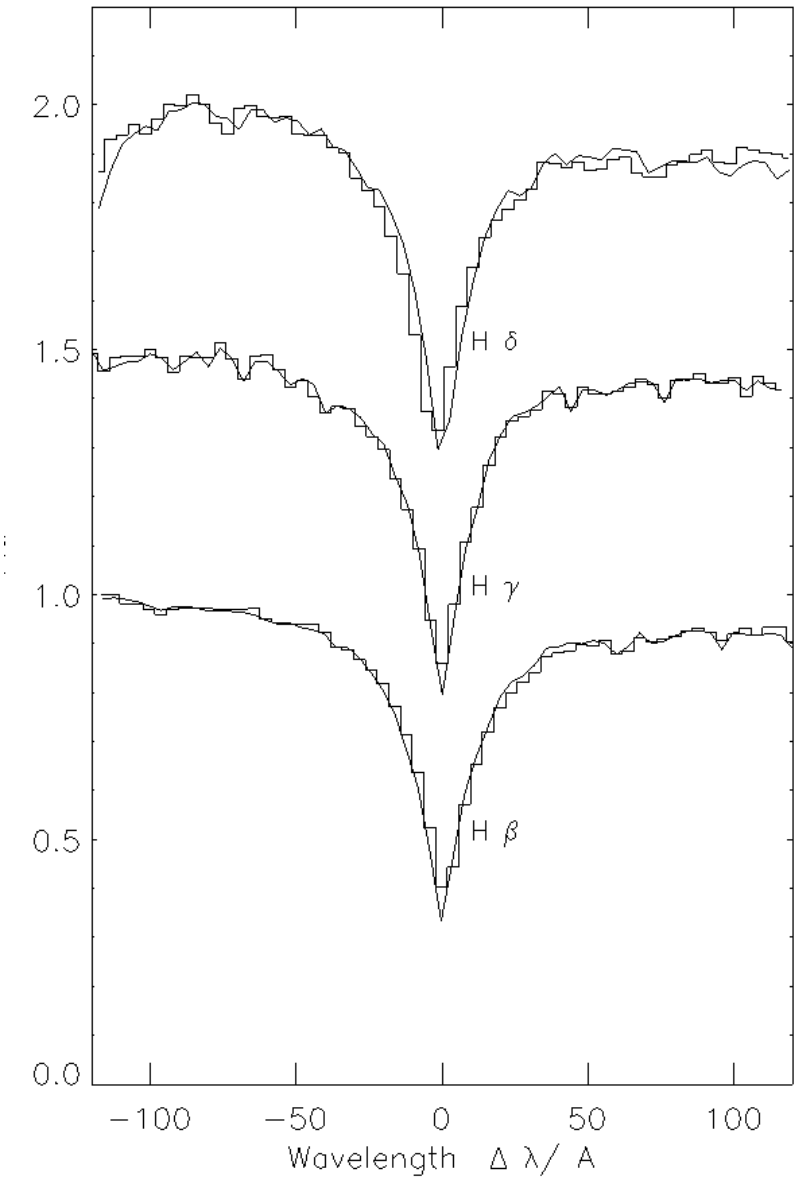

Figure 3.13: The spectral fit to KIC 3223460, as an example of the spectral fits used. For each spectral line, the continuum has been normalised to unity and each spectrum after H_β has been shifted up by 0.5 flux units.

minutes in our RATS-*Kepler* observations, a flare shorter than any observed on the other flare stars being observed at the time (Hawley et al., 2011) and which would not be detected in long cadence observations (Walkowicz et al., 2011);

- KIC 7431243 is a cataclysmic variable which matches the known variable source V363 Lyr;
- KIC 7667885, 9786165 and 12553806 are contact binaries;
- The remaining 12 objects all appear to be δ-Scuti stars (one of which has since been determined from *Kepler* observations to be part of an eclipsing binary), which cover a range of temperature and $\log g$ values mostly across the blue edge of the δ-Scuti instability strip. Due to our observation strategy they naturally mostly come from the short period extreme of the δ-Scuti period range ($\sim$0.25–7 hours Rodríguez and Breger (2001)).

Successful bids to have them observed by *Kepler* in short cadence mode were made through the *Kepler* Guest Observer Programme and Directors Discretionary Time Programme, with each source being observed in at least one quarter. The INT light curves of these sources are shown in Figure 3.14 whilst their sky coordinates, magnitude and colours are shown in Table 3.4, along with an approximate spectral classification using our INT and Gran Telescopio Canarias (GTC) spectra, which are shown in Figures 3.15, 3.16 and 3.17.

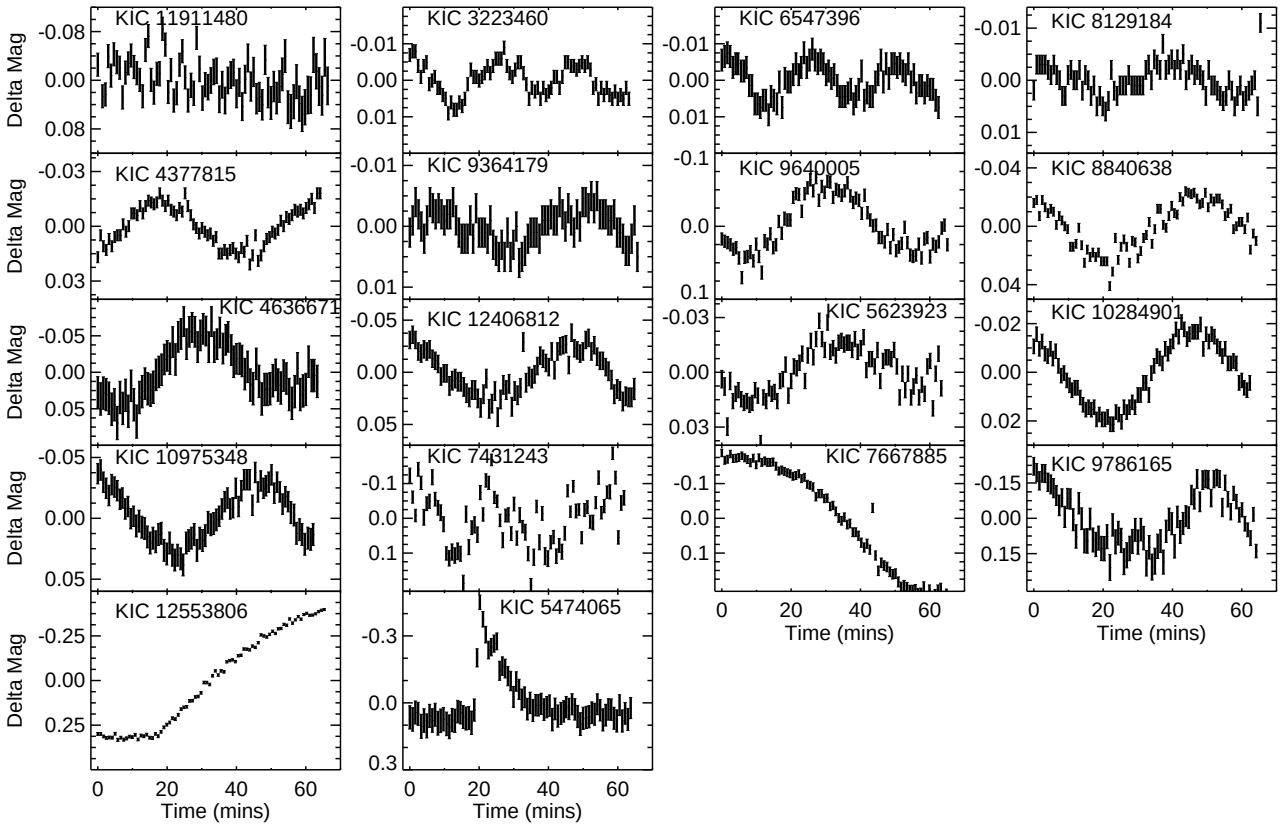

Figure 3.14: The INT light curve of those sources which have been identified as variable in the RATS-*Kepler* survey and which *Kepler* Short Cadence data have been obtained for. The details of these sources are shown in Table 3.4.

KIC	RA (J2000)	DEC (J2000)	g	$U-g$	$g-r$	*Kepler* SC Data	Period *Kepler*	Spectra	Spectral Type	Variable Type
11911480	19 20 24.9	+50 17 22.4	18.13	–0.39	0.06	12,16	290 sec			DAV (1)
3223460	19 12 32.2	+38 23 00.1	13.74	–0.27	0.25	14	24.2 min	GTC	mid-late A	δ Sct
6547396	19 53 18.3	+41 58 26.9	14.84	0.40	0.46	16	26.6 min	INT	mid-late A	δ Sct
8120184	19 54 11.9	+43 59 20.1	14.27	0.36	0.51	15	42.6 min	INT	mid-late A	δ Sct
4377815	19 39 08.1	+39 27 35.9	14.83	0.24	0.34	15	45.7 min	INT	mid-late A	δ Sct
9364179	19 56 24.5	+45 48 24.1	14.38	0.45	0.43	15	46.8 min	INT	mid-late A	δ Sct
9640005	19 09 46.3	+46 20 04.1	18.40	0.15	0.21	14–16	49.5 min	GTC	mid A	δ Sct
8840638	19 55 35.1	+45 04 46.0	14.63	0.52	0.54	14–16	49.6 min	GTC	mid-late A	δ Sct
4636671	19 01 52.2	+39 45 59.3	15.67	0.28	0.26	14–16	50.0 min	GTC	mid A	δ Sct
12406812	19 23 33.8	+51 17 58.9	17.24	0.18	0.36	14–16	50.4 min	GTC	mid-late A	δ Sct
5623923	19 32 01.5	+40 51 16.8	16.62	0.23	0.27	14–16	50.5 min	GTC	mid-late A	EB+δ Scuti
10284901	19 43 46.4	+47 20 32.8	15.73	0.06	0.32	14,16	75.8 min	GTC	mid-late A	δ Sct
10975348	19 26 46.1	+48 25 30.8	18.89	0.19	0.34	14–16	2.35 hrs	GTC	mid A	δ Sct
7431243	19 08 51.6	+43 00 31.5	19.10	–0.94	0.47	16	4.68 hrs			CV (2)
7667885	19 03 30.2	+43 23 22.7	17.64	1.05	0.95	14–16	7.56 hrs	GTC	mid G	W UMa
9786165	19 50 11.0	+46 34 40.8	17.67	0.81	0.76	14,16	7.98 hrs	GTC	mid G	W UMa
12553806	19 14 41.0	+51 31 08.9	17.52	0.14	0.41	14–16	11.12 hrs	GTC	A+F?	W UMa
5474065	19 53 02.5	+40 40 34.6	18.77	1.93	1.43	14	Flare	GTC	M4 V	Flare star (3)

Table 3.4: The details of our sources which have been observed by *Kepler* in short cadence mode. Indicated are their KIC ID; their RA and Dec; the g mag, $(U-g)$ and $(g-r)$ colours, which have been taken from the KIS (Greiss et al., 2012a,b). The Quarter in which *Kepler* Short Cadence (SC) data were obtained is also shown and what the dominant period was in the power spectrum of the *Kepler* light curve. In the 'Spectra' column it is shown if we obtained a spectrum of the source using the INT or GTC, what the approximate spectral type was and in the last column what the type of variable star the source is. EB: Eclipsing Binary. Notes: (1) Greiss et al. (2014), (2) Cataclysmic Variable, Scaringi et al. (2013), (3) Ramsay et al. (2013).

3.5 Summary

In this Chapter I have outlined a number of algorithms which can be used to detect variable sources from a large set of sources. I then go on to describe how a set of sources is selected which is likely to contain significantly variable sources from the output of the LS-periodogram, which was chosen due to its versatility, using the MAD statistic. The manual screening process used to exclude false positive detections is then detailed, which resulted in 227 stars (or 0.032 percent of the total) being selected using our most stringent criteria and 1,999 stars (or 0.28 percent of the total) being selected using our least stringent criteria. The results of follow-up optical spectroscopic observations are then shown, followed by the presentation of the sources eventually selected to be the subject of proposals to be observed by *Kepler* in short cadence mode. The next chapter will go on to present these observations and show the results of their preliminary analysis.

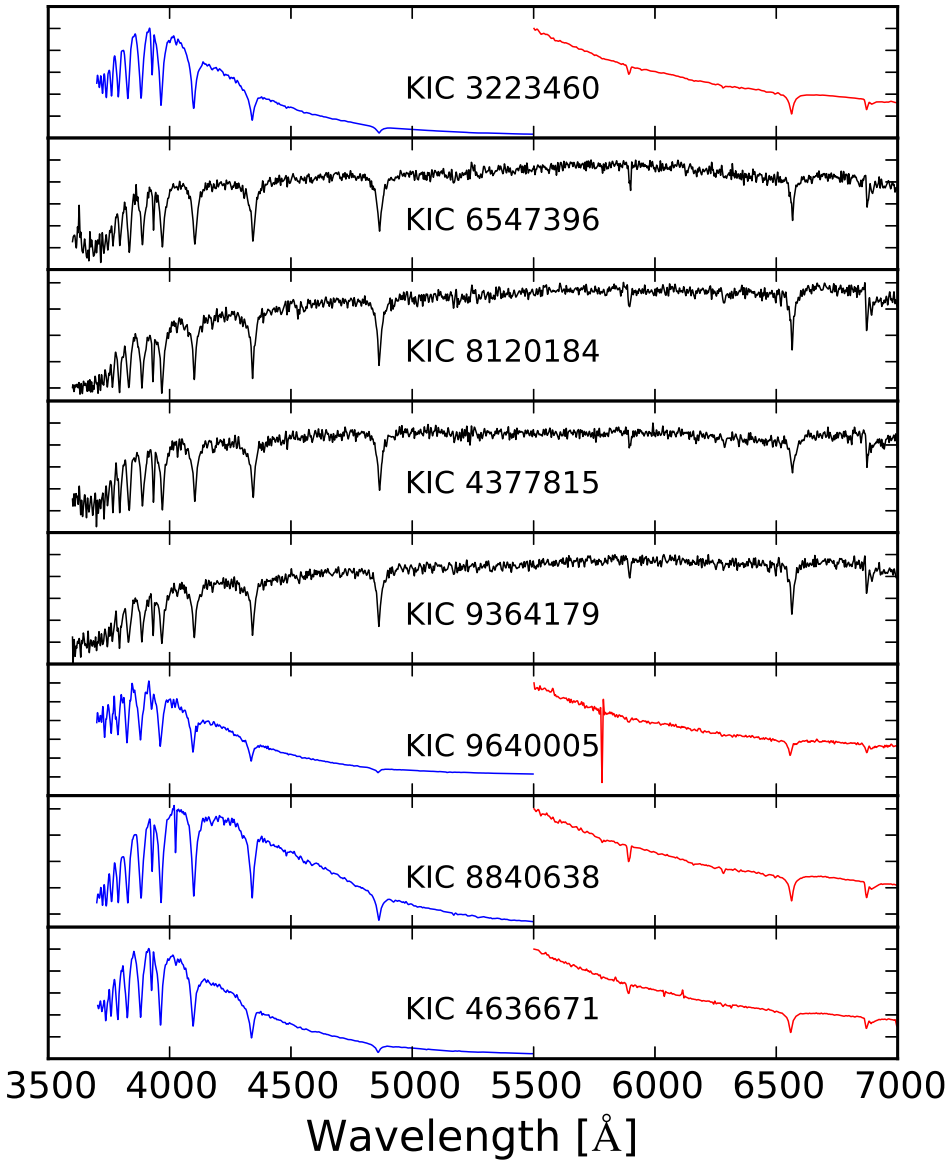

Figure 3.15: The spectra of eight of our sources which have been observed by *Kepler* in short cadence mode. The 4 sources for which IDS spectra have been obtained have been flux calibrated and normalised and are plotted in black. The remaining spectra were obtained with GTC. Since these were taken utilising a program which makes use of poor observing conditions, it was not possible for them to be flux calibrated. Therefore to more readily show spectral lines each half of the spectra have been normalised separately, with each half plotted in blue and red.

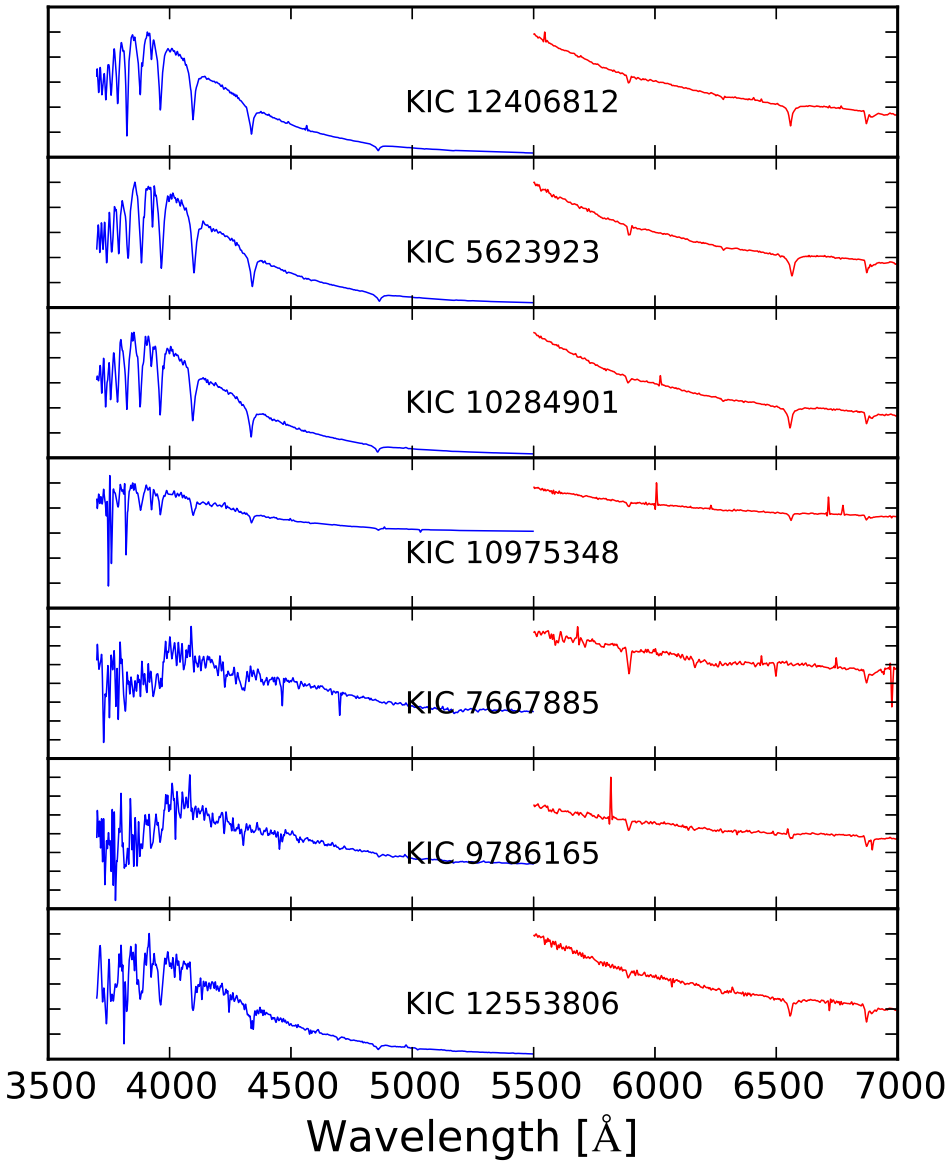

Figure 3.16: The spectra of seven of our sources which have been observed by *Kepler* in short cadence mode. These spectra were all obtained with GTC. Since these were taken utilising a program which makes use of poor observing conditions, it was not possible for them to be flux calibrated. Therefore to more readily show spectral lines each half of the spectra have been normalised separately, with each half plotted in blue and red.

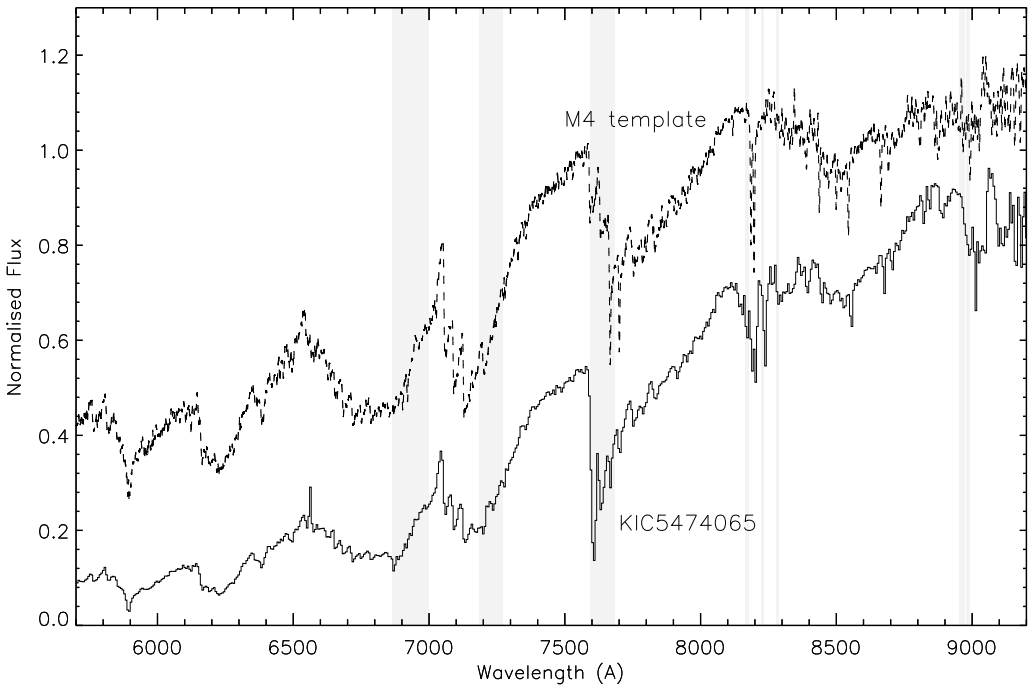

Figure 3.17: The lower spectrum (solid line) shows the spectrum of the flare star KIC 5474065 taken using GTC. As this is a red source ($g-r=1.43$), a different grism was used to the rest of the spectra. The wavelength of telluric absorption features are indicated as light grey vertical bands (taken from Kirkpatrick et al. (1991)) and it has not been attempted to remove them. The upper spectrum (dashed line) shows the M4 template spectrum provided by Bochanski et al. (2007). Figure taken from Ramsay et al. (2013).

Chapter 4

Kepler Short Cadence Data

4.1 *Kepler* Short Cadence Observations

As described in Section 1.6. *Kepler* takes exposures every 6.5s which are then summed onboard at 1765.5s (29.4 minute) and 58.89s intervals. This provides both a long and short cadence observation mode, with 170,000 and 512 targets able to be observed in each mode respectively. With its primary aim being the detection of exoplanets, it was decided that *Kepler* would have a continuous pointing to maximise the period of time for which sequential data could be obtained. This meant an unprecedented opportunity for the study of asteroseismology, which exceeds those provided even by *COROT* and *MOST*. As outlined in section 1.6, we initiated the RATS-*Kepler* survey with the explicit aim of exploiting this unique opportunity for the study of short period variable stars. This chapter will outline the data obtained for the targets from our survey for which we were able to obtain *Kepler* short cadence data.

The Kepler light curves were produced by the *Kepler* Science Operations Center Pipeline which uses simple aperture photometry and are made available for download from the MAST website[1]. These are then reduced using the methods described on the *Kepler* data analysis website[2]; where notes are also provided on issues specific to particular quarters amongst other things.

Each quarter lasts for 3 months, within each quarter there were three monthly target lists (though each 'month' did not necessarily correspond to the exact length of a month). At the end of each month, data acquisition is paused while the data from that month are downloaded, to obtain a full frame image of the entire *Kepler* field and to upload the next month's target lists. The start and end times of the quarters and months during which we had sources observed by *Kepler* in short cadence mode are shown in Table 4.1, whilst the sources we had observed and in what cadence mode during each quarter and month are shown in Tables 4.2, 4.3, 4.4, 4.5 and 4.6. The most significant events affecting our observations were:

- The failure of Reaction wheel 2 during Q14 generated a safemode event which lead to a loss of ∼6 days of data during the 1st month of this quarter.
- A loss of fine pointing during Q15 generated a safemode event which lead to the loss of ∼4 days of data during month 2 of this quarter.
- A safemode event generated during Q16 lasting ∼12 days during month 1 in an attempt by the *Kepler* spacecraft to prolong the lifetime of its reaction wheels, lead to the decision to switch to the month 2 target list when this

[1]http://archive.stsci.edu/kepler/publiclightcurves.html
[2]http://keplerscience.arc.nasa.gov/DataAnalysis.shtml

Quarter	Month	Start Time(UT)	End Time(UT)
Q12	1	21:49:54 5^{th} Jan 2012	09:38:08 1^{st}Feb 2012
	2	02:48:58 2^{nd} Feb 2012	11:56:40 29^{th} Feb 2012
	3	09:32:20 1^{st} Mar 2012	12:46:56 28^{th} Mar 2012
Q14	1	15:03:34 28^{th} Jun 2012	12:02:49 29^{th} Jul 2012
	2	15:31:34 30^{th} Jul 2012	19:20:59 29^{th} Aug 2012
	3	15:57:48 30^{th} Aug 2012	19:54:23 3^{rd} Oct 2012
Q15	1	23:24:53 5^{th} Oct 2012	19:25:19 5^{th} Nov 2012
	2	18:29:14 6^{th} Nov 2012	21:19:47 6^{th} Dec 2012
	3	17:27:10 7^{th} Dec 2012	15:32:29 11^{th} Jan 2013
Q16	1	14:06:57 12^{th} Jan 2013	19:38:37 17^{th} Jan 2013
	2	03:50:07 29^{th} Jan 2013	11:16:17 6^{th} Mar 2013
	3	14:45:02 7^{th} Mar 2013	11:16:41 8^{th} Apr 2013
Q17	1	17:12:31 9^{th} Apr 2013	02:11:14 2^{nd} May 2013
	2	07:15:26 7^{th} May 2013	12:15:52 11^{th} May 2013

Table 4.1: The start and end times for each quarter and month during which we had sources observed by *Kepler* in short cadence mode.

safemode ceased, such that there would be a short (5.2 days) set of month 1 observations and a long (37 days) set of month 2 observations.

- A ∼6 day safemode event due to excess friction experienced by the reaction wheels towards the end of month 1 in Q17 lead to an early end to month 1 and a changeover to the month 2 target list. The failure of reaction wheel 4 4 days into month 2 eventually lead to the need to end the *Kepler* mission in its original format, as sufficient pointing accuracy whilst observing the *Kepler* field could not be achieved with only 2 reaction wheels.

I will now go on to present the *Kepler* short cadence data we obtained, along with a preliminary analysis.

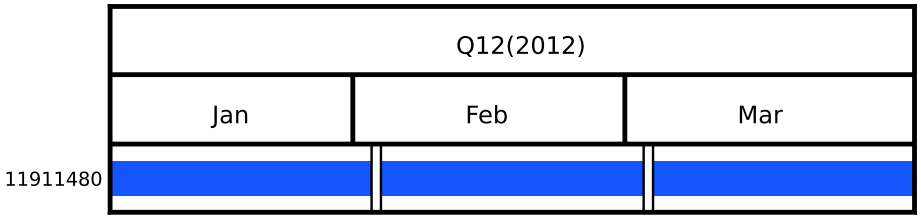

Table 4.2: Table showing the source that was observed by *Kepler* in short cadence mode during Quarter 12, with its KIC identifier shown on the left-hand side. Blue regions indicate those where short cadence observations were obtained. Blank regions indicate monthly download pauses.

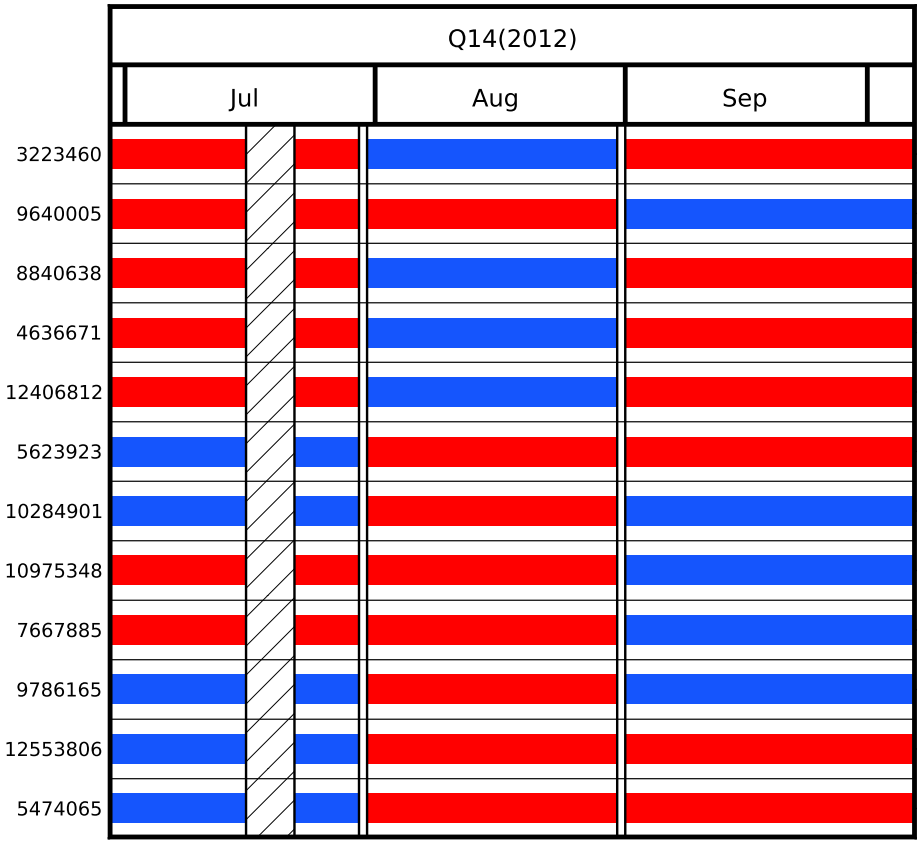

Table 4.3: Table showing the sources that were observed by *Kepler* in short cadence mode during Quarter 14, sources are arranged by the dominant period in their *Kepler* light curve from shortest to longest, with their KIC identifier shown on the left-hand side. Blue regions indicate those where short cadence observations were obtained, whilst red regions indicate those where long cadence observations were obtained. Blank regions indicate monthly download pauses. The hatched region was a safe mode event generated when the 1^{st} of four reaction wheels broke, reaction wheel 3.

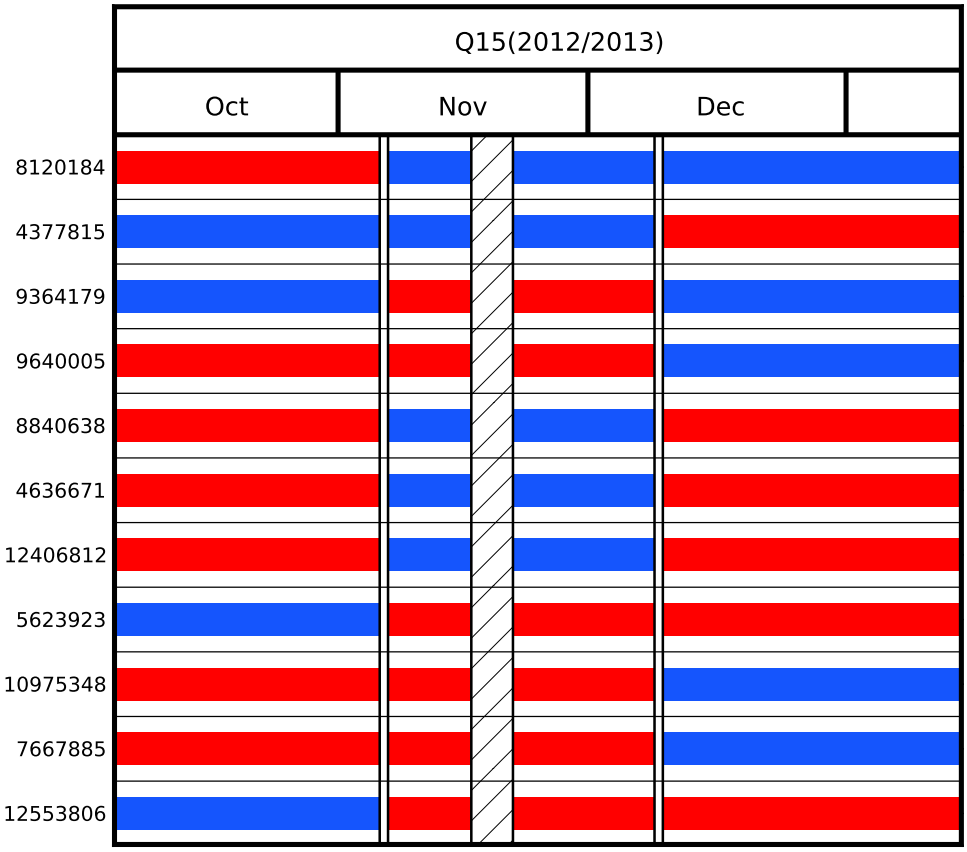

Table 4.4: Table showing the sources that were observed by *Kepler* in short cadence mode during Quarter 15, sources are arranged by the dominant period in their *Kepler* light curve from shortest to longest, with their KIC identifier shown on the left-hand side. Blue regions indicate those where short cadence observations were obtained, whilst red regions indicate those where long cadence observations were obtained. Blank regions indicate monthly download pauses. The hatched region was a safe mode event generated when there was a loss of fine pointing.

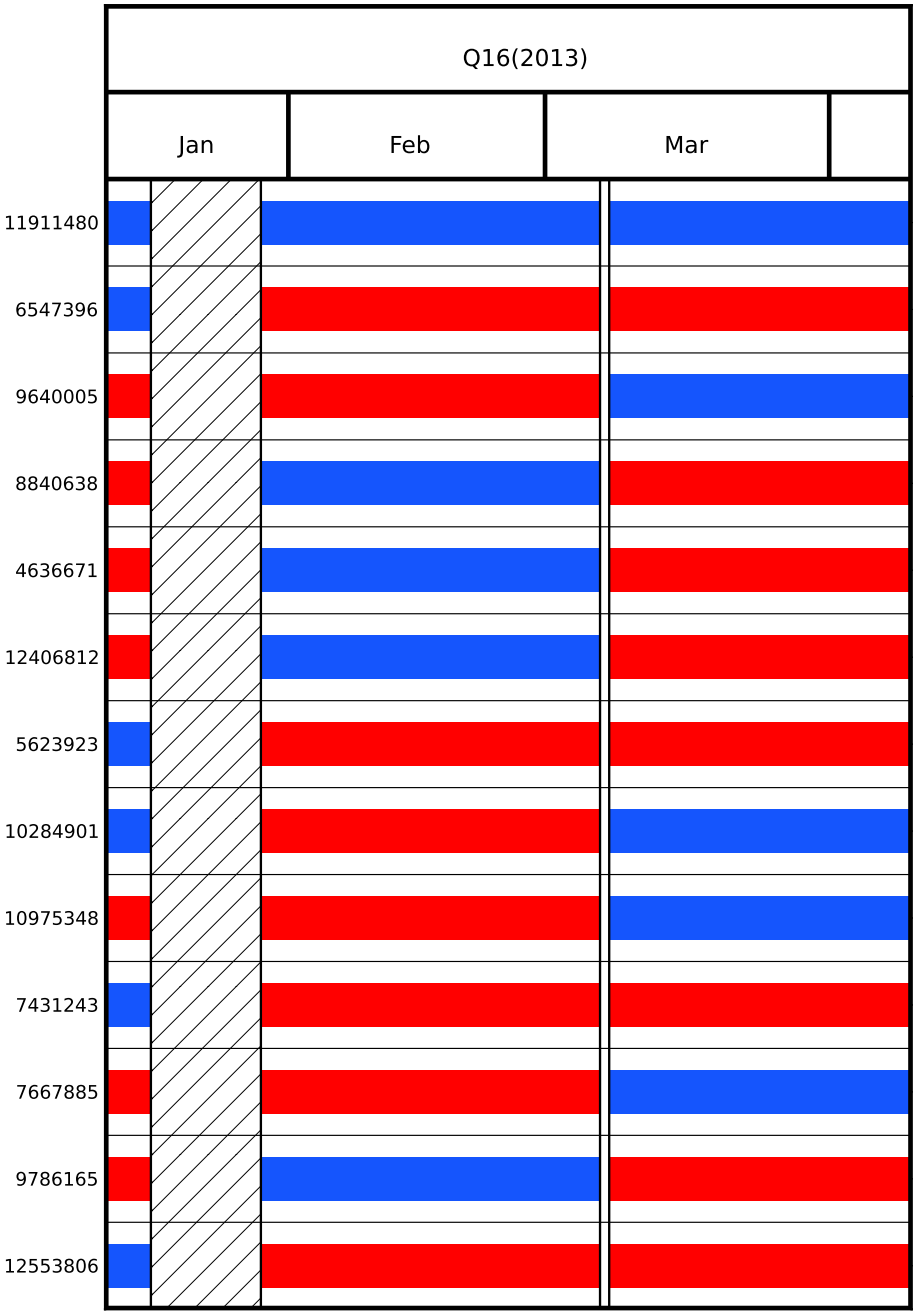

Table 4.5: Table showing the sources that were observed by *Kepler* in short cadence mode during Quarter 16, sources are arranged by the dominant period in their *Kepler* light curve from shortest to longest, with their KIC identifier shown on the left-hand side. Blue regions indicate those where short cadence observations were obtained, whilst red regions indicate those where long cadence observations were obtained. Blank regions indicate monthly download pauses. The hatched region was a safe mode event generated to attempt to prolong the lifetime of the remaining reaction wheels.

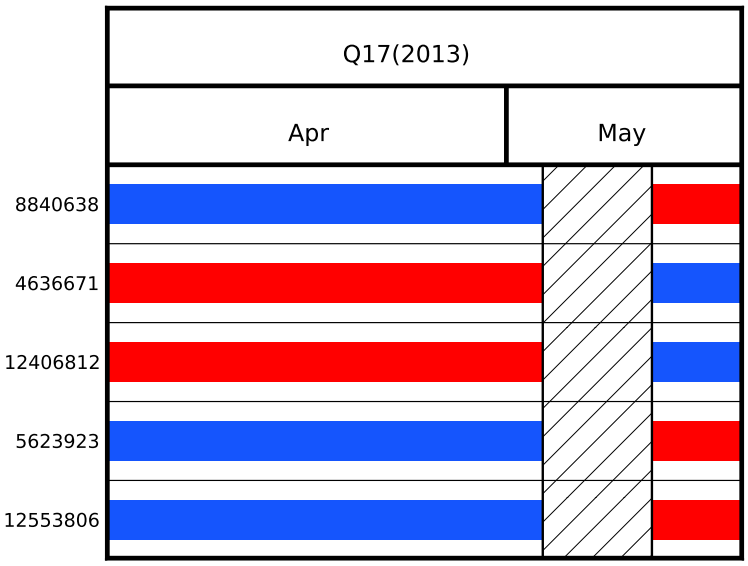

Table 4.6: Table showing the sources that were observed by *Kepler* in short cadence mode during Quarter 17, sources are arranged by the dominant period in their *Kepler* light curve from shortest to longest, with their KIC identifier shown on the left-hand side. Blue regions indicate those where short cadence observations were obtained, whilst red regions indicate those where long cadence observations were obtained. The hatched region was a safe mode event generated by problems with the reaction wheels. The second month was interrupted by another safe mode event, after reaction wheel 4 failed.

4.2 δ-Scuti stars

As described in Section 1.2.1, δ-Scuti stars are A/F-type stars which exhibit pulsations due to p and g-modes which are thought to be driven by the opacity change mechanism in the helium ionisation zone (Baker and Kippenhahn, 1962). This makes them interesting astrophysical laboratories as they exhibit physical phenomena that can be used to test theoretical models about the internal structure of stars based on observational data that can be obtained here on Earth. Furthermore, the high amplitude δ-Scuti stars have a period-luminosity relationship (McNamara et al., 2000) and can be used to measure galactic and extragalactic distance scales, including those for the Small and Large Magellanic clouds as well as other local galaxies and globular clusters (McNamara, 2011). Refinement of theorectical models describing them therefore helps to more accurately determine the Galactic distance scale and calibrate some of the lower rungs of the 'cosmic distance ladder'.

However, in many δ-Scuti stars it is difficult to uniquely identify modes in the power spectra of the light curve. An exception is slow rotators such as 44 Tau (Lenz et al., 2010) where a large variety of pressure and gravity modes were identified. For the majority of these stars, when it comes to modelling their power spectra, a major difficulty is that the mechanisms, such as rotation or internal magnetic fields, which select or dampen which modes are excited to observable amplitudes is not well understood (Dziembowski and Krolikowska, 1990). In other words, some modes are excited while others are not, which makes identifying the specific spherical harmonic mode for each peak in the frequency spectra difficult. From *CoRoT* and *Kepler* observations, however, it seems that

the opacity mechanism alone cannot excite the entire range of observed modes. This means that either the models are incomplete or that there is an additional mechanism contributing to the driving. Such an alternative explanation would be the presence of stochastically excited modes, like in the Sun. Theoretical models in fact predict the convective envelopes of δ-Scuti stars are still deep and effective enough to drive Solar-like oscillations. Recently, Antoci et al. (2011), suggested the detection of such a hybrid star, showing κ-mechanism and stochastically driven modes. However, longer observations revealed that the interpretation is more complicated than initially anticipated Antoci et al. (2013). Previous research in this area has been hindered by the difficulty in obtaining continuous light curves which span long time periods. With *Kepler* able to obtain light curves over months or even years of these sources, there is the potential for significant advances in this area of research using *Kepler* data.

4.2.1 Our Sample of δ-Scuti Stars

In total, we successfully obtained short cadence observations of eleven sources which appear to be δ-Scuti type stars, as well as one which appears to be part of an eclipsing binary, which will be presented in Section 4.2.2, which were all observed in at least 1 quarter and some for 3 continuous quarters. A short section (1 day) of each of the *Kepler* light curves of these δ-Scuti type stars is shown in Figure 4.1. Their power spectra are complex and show many frequencies, with the power spectrum obtained for each source using one month worth of data shown in Figures 4.2 and 4.3. The δ-Scuti stars with the shortest pulsation periods in our sample are KIC 3223460 (24 min) and KIC 6547396 (26 min). Indeed, they are

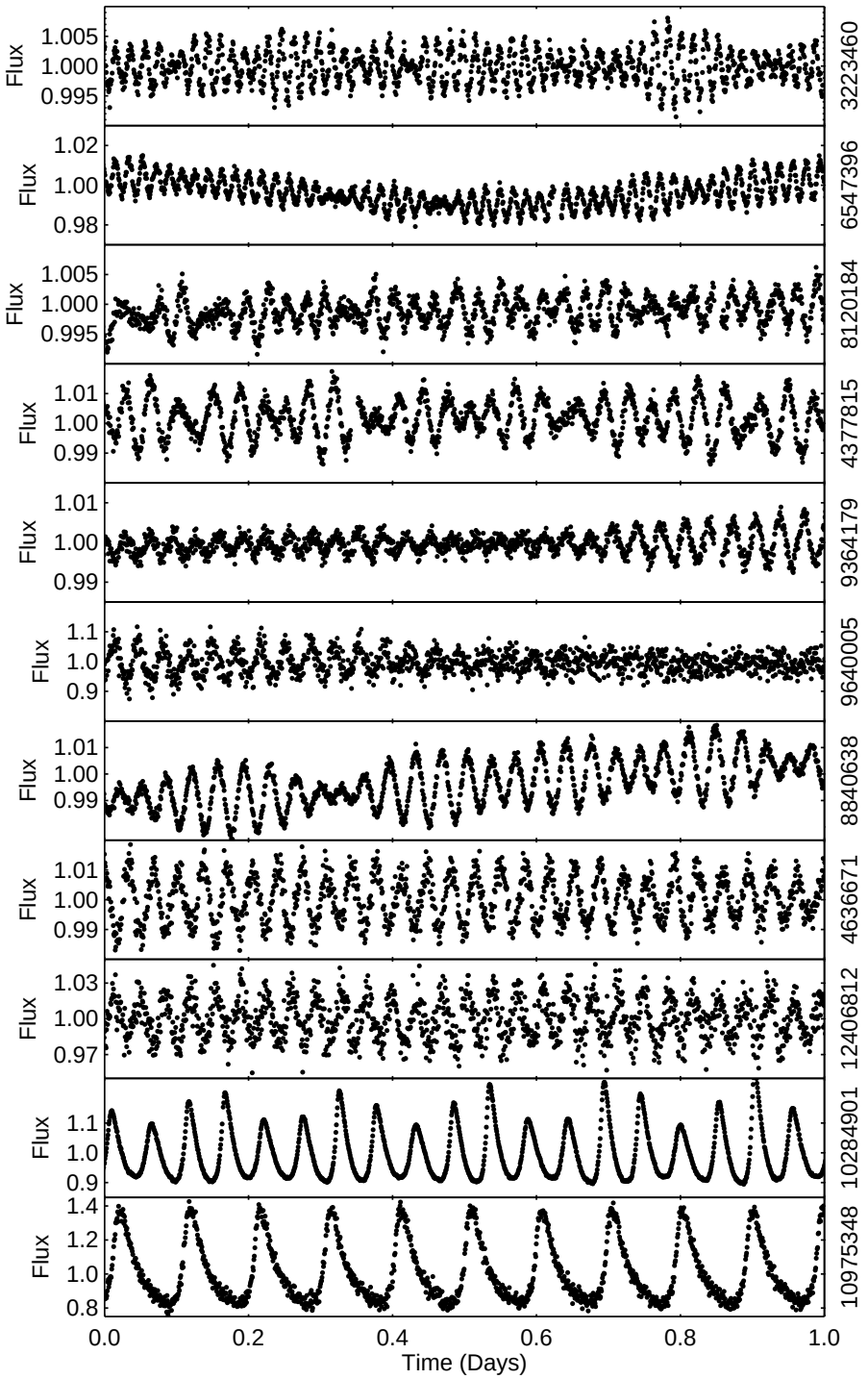

Figure 4.1: The *Kepler* SC light curves of the eleven sources which appear to be δ-Scuti type stars. They are ordered by the dominant period found in their *Kepler* light curves, with the shortest period shown at the top and the longest at the bottom. For clarity the light curves are shown covering only one day for each star. The KIC identifier for each star is shown on the right hand edge of each panel. Figure taken from (Ramsay et al., 2014).

at the extreme short period end of the δ-Scuti star distribution (18 mins marks the short period end, Uytterhoeven et al. (2011a)). The discovery of two δ-Scuti stars with such a short period will therefore provide an opportunity to discover the internal structure of these sources through asteroseismology. Eight of our sample, (KIC 8120184, 4377815, 9364179, 9640005, 8840638, 4636671 and 5623923), have a peak in their power spectra which lies in the range 42.6–50.5 mins. They have a best fit temperature in the range 7,660–7,950 K (Table 3.3) and cover an area towards the blue edge of the instability strip in the Hertzsprung-Russell diagram, as shown in Figure 4.4. All of the aforementioned sources seem to be low amplitude δ-Scuti stars, which typically exhibit a wider range of pulsation modes, including those that are not radially isotropic, which allows for a more rigorous testing of theoretical models. The longest period pulsators, KIC 10284901 (75.8 mins) and 10975348 (2.35 hrs) also show high amplitude variations and appear to be high amplitude δ-Scuti stars which occupy a restricted range of the instability strip (McNamara et al., 2000). Many of our δ-Scuti stars are likely to be too faint to identify their pulsation modes easily (even the brightest of our sources at g=13.7 is relatively faint for such an analysis), however, the frequency range and the stability of excited modes can lead to a better understanding of the pulsation mechanisms, provided the temperature is robustly determined, which will require higher resolution spectra than those which we have obtained.

4.2.2 KIC 5623923: a δ-Scuti in a Contact/Eclipsing Binary

KIC 5623923 was selected to be observed by *Kepler* as it appeared to be a δ-Scuti type star from its RATS-*Kepler* light curve (c.f. Figure 3.14). However, its

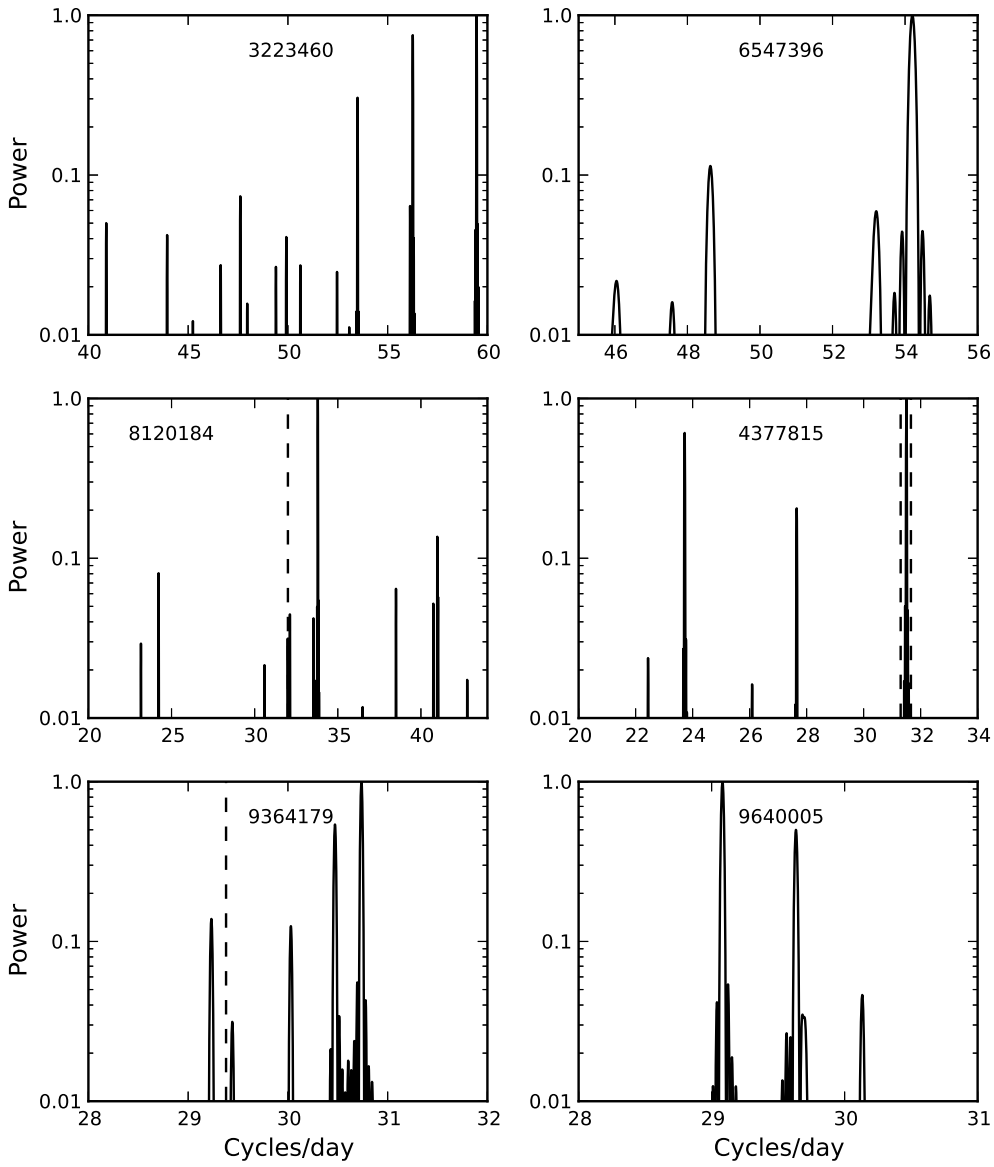

Figure 4.2: The power spectra of six of the sources shown in Figure 4.1. The power spectra have been normalised so that maximum power is unity, with a logarithmic y-scale, with the frequency range of interest for each star shown. The KIC identifier for each star is shown in each panel. The light curves for each star shown here cover one month of data, except for KIC 6547396 where the data were taken in month 1 of quarter 16 and only cover 5.2 days. Dashed vertical lines indicate known artifacts in the power spectra of *Kepler* SC data.

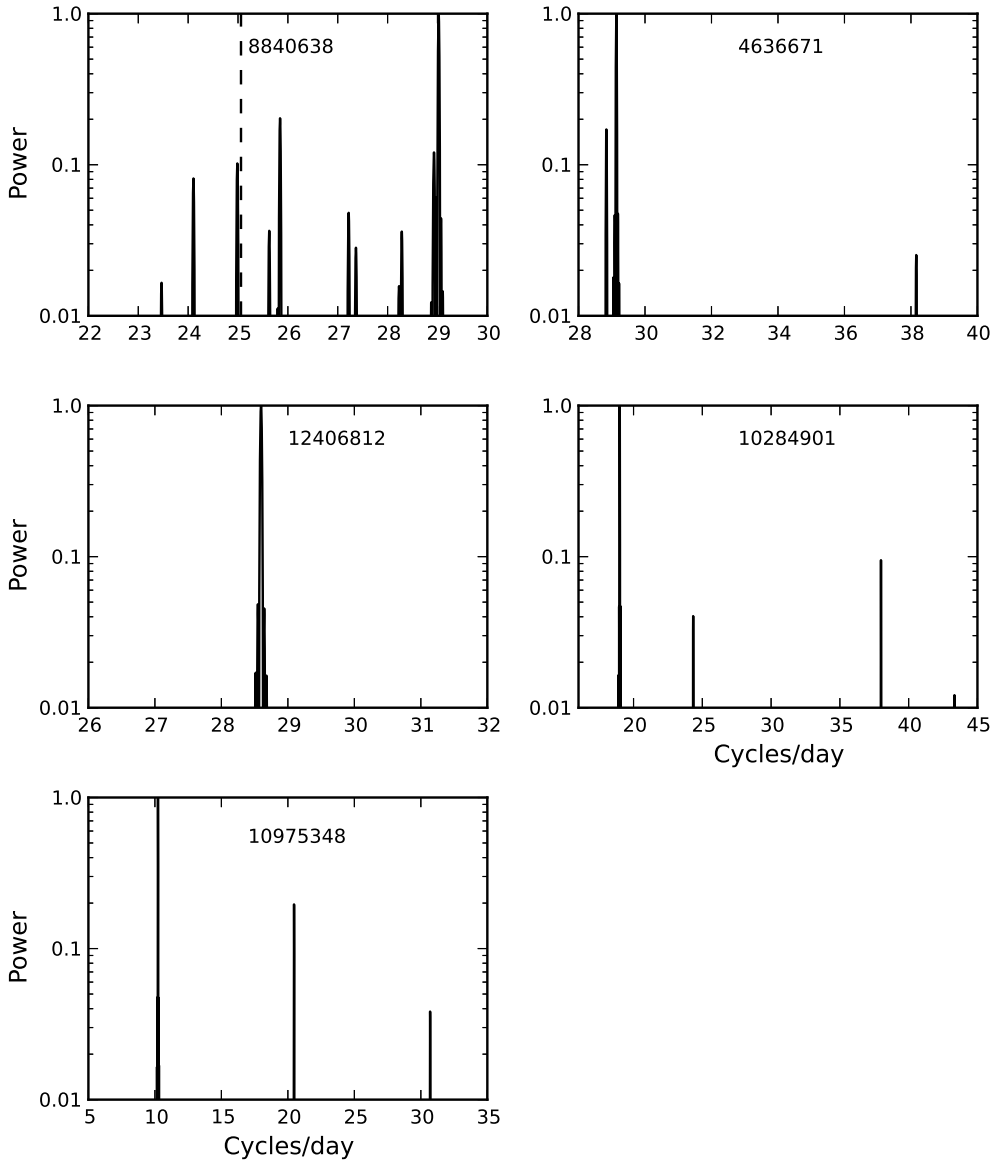

Figure 4.3: The power spectra of five of the sources shown in Figure 4.1. The power spectra have been normalised so that maximum power is unity, with a logarithmic y-scale, with the frequency range of interest for each star shown. The KIC identifier for each star is shown in each panel. The light curves for each star shown here cover one month of data. Dashed vertical lines indicate known artifacts in the power spectra of *Kepler* SC data.

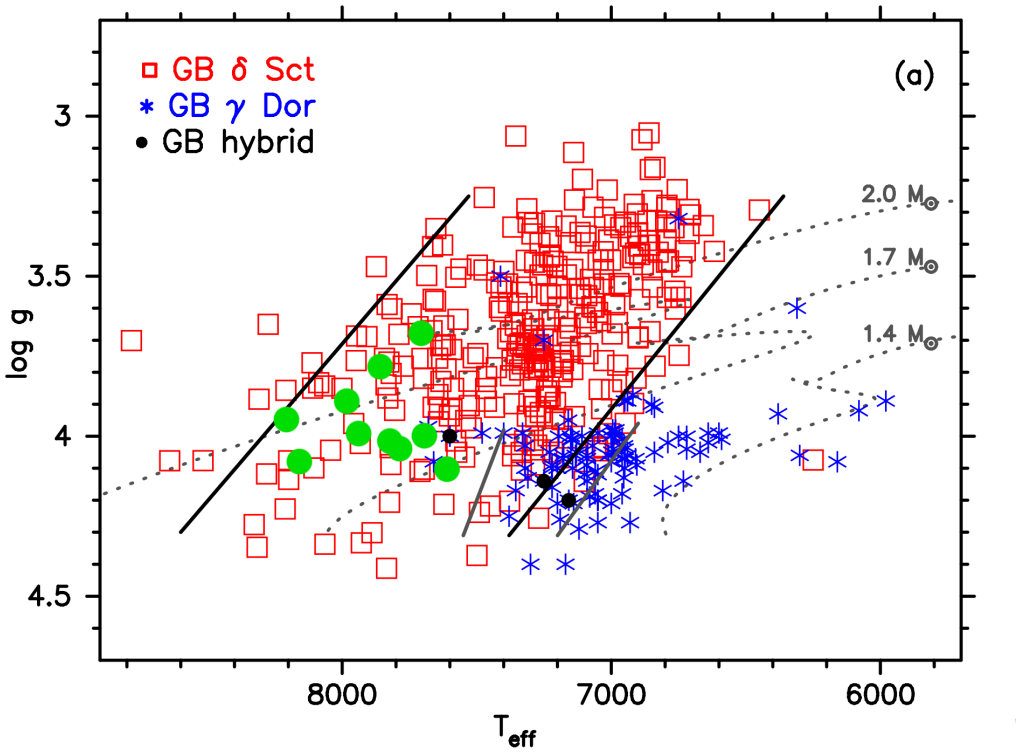

Figure 4.4: The location of our δ-Scuti sources which have been observed by *Kepler* plotted as green circles (T_{eff} and $\log g$ values obtained from our IDS and GTC spectra) on a figure of the δ-Scuti instability strip in the Hertzsprung-Russell diagram taken from (Uytterhoeven et al., 2011a) along with a number of δ-Scuti, γDororadus and 'hybrid' stars identified from ground-based observations. The solid thick black and light grey lines mark the blue and red edge of the observed instability strips of δ-Scuti and γDororadus stars, as described by Rodríguez and Breger (2001) and Handler and Shobbrook (2002), respectively. The evolutionary tracks were computed using the Code Liégeois d'Évolution Stellaire (CLES, Scuflaire et al. (2008).

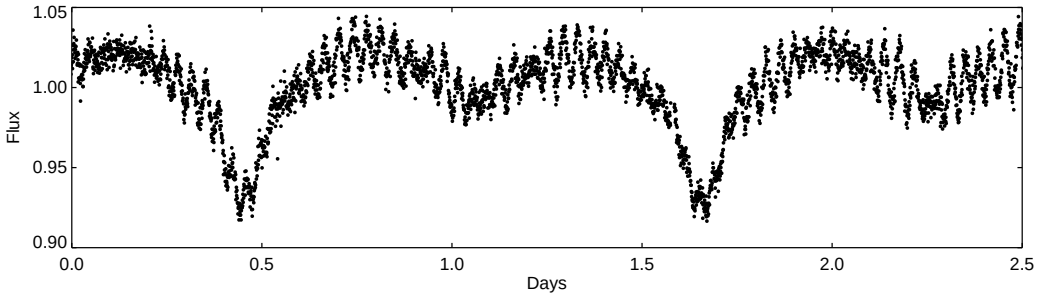

Figure 4.5: A short section of Q14 *Kepler* data of KIC 5623923. The binary component which is obscured during the secondary eclipse shows clear evidence of pulsations. Figure taken from (Ramsay et al., 2014).

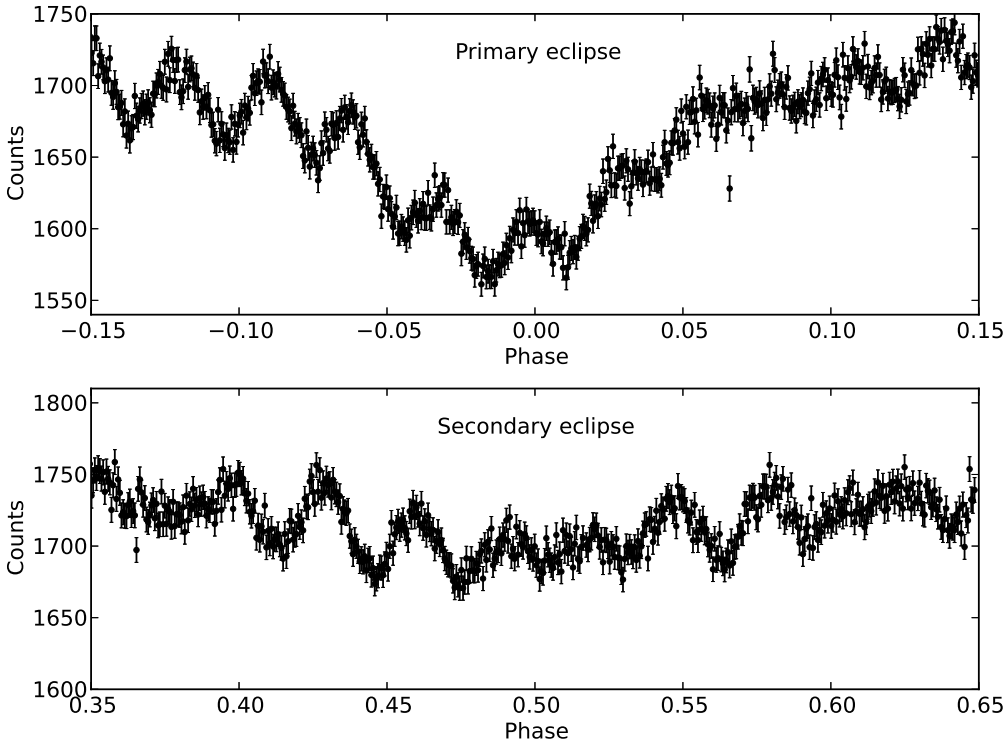

Figure 4.6: A close up of the light curve of KIC 5623923 showing a randomly selected primary eclipse and the secondary eclipse following it. Both light curves are phased and shown on the same scale in counts for easier comparison. Each light curve begins near the leading edge of the eclipse, with the primary and secondary eclipses centred on 0 and 0.5 respectively. There is clear evidence of pulsations in the primary eclipse, whereas they are obscured in the secondary eclipse.

Kepler light curve, a 2.5 day section of which can be seen in Figure 4.5, shows clear indication that this source is an eclipsing or contact binary system with an orbital period of 1.21 days. But, there are clear pulsations on a period of ∼50 mins superimposed on the light curve. As shown in more detail in Figure 4.6, the pulsations are not readily apparent during the secondary eclipses indicating that the secondary star (the less luminous of the binary components) is the source of the pulsations.

There are at least two other eclipsing or contact binary stars in the *Kepler* field which have a δ-Scuti component. These systems are particularly useful in testing our knowledge of δ-Scuti stars, as their binary nature allows for a direct measurement of their mass. KIC 4544587 is a binary system with a 2.18 day orbital period (Hambleton et al., 2013) while KIC 10661783 has an orbital period of 1.23 days (Southworth et al., 2011). Unlike KIC 5623923 where the secondary star is the pulsating component, in both KIC 4544587 and KIC 10661783 the primary is the pulsating star. It should be noted that the spectral fits suggest a temperature of 8,000 K (Table 3.3) although a single temperature has been fitted to a system which is clearly a binary. To determine parameters more stringently for this system, phase resolved spectroscopy is required.

The power spectrum of KIC 5623923 (Figure 4.7) shows many peaks in the 20-30 cycles/day frequency interval which are due to pressure (p) mode pulsations in the secondary star. Some of these peaks are separated by 0.83 cycles/day which is the orbital period. This implies that the amplitude of the δ-Scuti pulsations are correlated with the orbital period (Shibahashi and Kurtz (2012) gives a full discussion on how power spectra can be used to measure radial velocities in binary systems). The power spectrum of KIC 10661783 shows peaks in its power spectrum in a similar frequency range (Southworth et al., 2011) while the p-modes seen in KIC 4544587 (Hambleton et al., 2013) are at a higher frequency range (40-50 cycles/day). The differences and similarities between our system and those of Southworth et al. (2011) and Hambleton et al. (2013) provides a unique opportunity to probe theoretical models of these systems.

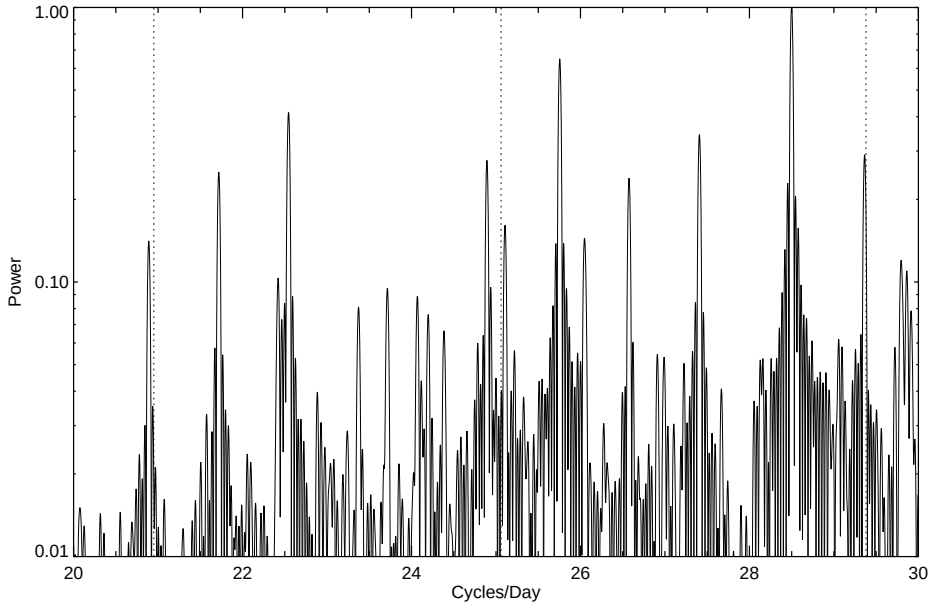

Figure 4.7: The power spectrum of the Q14 *Kepler* light curve of KIC 5623823. The spacing between some peaks correspond to the orbital frequency suggesting that the amplitude of the δ-Scuti pulsations are correlated with the orbital period. Dashed vertical lines indicate known artifacts in the power spectra of *Kepler* SC data. Figure taken from (Ramsay et al., 2014).

4.3 KIC 11911480: a Pulsating DA White Dwarf

As described in Section 1.2.4, around 97% of all stars are expected to end their lives as white dwarfs, meaning that the study of them and the galactic population of them is a key indicator of star formation in the galaxy and stellar evolution in general. The five classes of variable white dwarfs - DAV, DBV, GW Vir, DQV and ELMV - in particular offer the opportunity of probing many of their properties through asteroseismology, including the mass and composition of their degenerate cores and non-degenerate envelopes (Winget and Kepler (2008); Fontaine and Brassard (2008)); the extent of radiative levitation and diffusion of heavy metals (Charpinet et al., 2008); the neutrino flux from DBV white dwarfs (Bischoff-Kim and Østensen, 2011b); place constraints on the hydrogen-rich layer on the surface (Charpinet et al., 2007); the degree of internal differential rotation (Kawaler and Hostler, 2005); and to constrain the nuclear reaction rates (e.g. $^{12}C(\alpha,\gamma)^{16}O$, Metcalfe et al. (2002)). Dedicated studies of G29-38 ($T = 11690\,K$, $\log g = 8.11$) have shown that a detailed asteroseismological analysis of cool DAV stars requires observations extending over prolonged periods of time to capture as many of the amplitude-variable modes as possible (Kleinman et al. (1994, 1998)). With the limitations of ground-based observations, long baseline observations are essential to further test theoretical models and to aid in identification and removal of aliases found in ground-based data.

Prior to the launch of *Kepler* in 2009 only a small number of white dwarfs were known in the *Kepler* field (Borucki et al., 2010), none of which were found to be variable (Østensen et al., 2010a, 2011). By the time we began the RATS-*Kepler* survey, only one DAV star and one DBV star (Hermes et al. (2011); (Bischoff-Kim

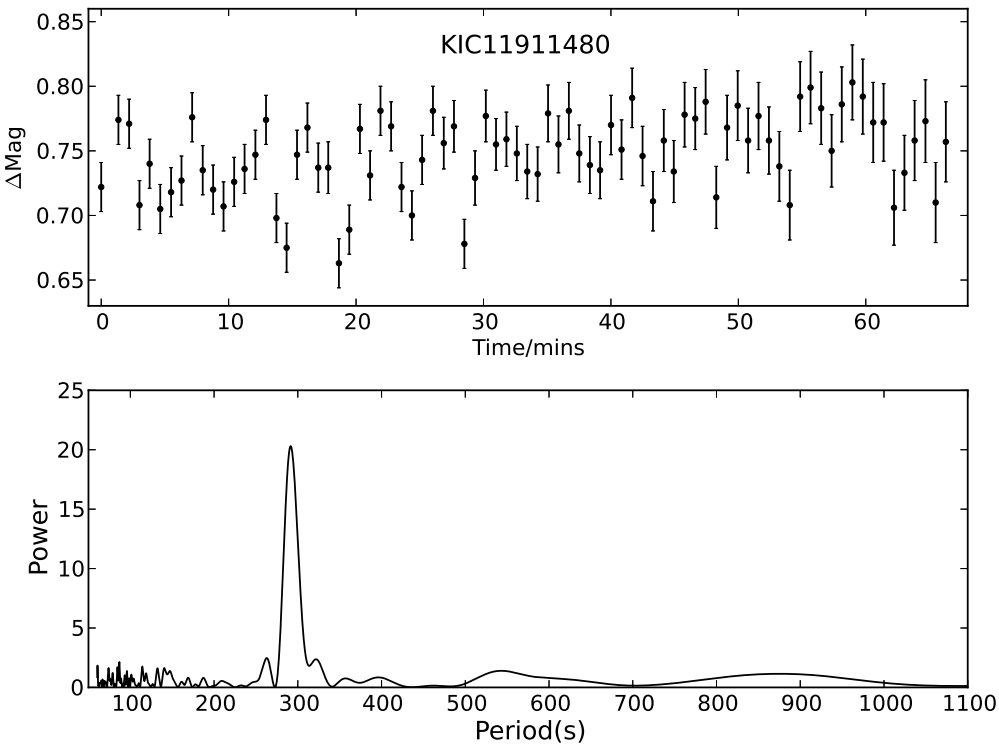

Figure 4.8: The RATS-*Kepler* light curve of the DA White dwarf KIC 11911480 (top) and its Lomb-Scargle power spectrum (shown in period space for clarity).

and Østensen (2011a)) were known in the *Kepler* field.

KIC 11911480 was found in our 1st set of observations made in July 2011 and stood out as a significantly variable object in the period-Log(FAP) plane at a period of ∼4 minutes. Analysis of its light curve (see Figure 4.8) showed dominant periodicity on a period of ∼290s and with a $g - r$ value of –0.048, it was clear that this was a highly likely candidate to be a degenerate compact pulsator.

The KIS (Greiss et al., 2012a,b), indicated colours of $g-r$=0.062, $U-g$=–0.393 and $r-\mathrm{H}_\alpha$=–0.155; placing it as a blue, UV excess, H_α deficient object well away

from the main sequence in the $(U-g)$–$(g-r)$ and $(r-i)$–$(r-\mathrm{H}_\alpha)$ colour-colour diagrams (c.f. Figures 3.11 and 3.12).

Further investigation (Greiss et al., 2014) placed it within the empirical instability strip in the $(U-g)$–$(g-r)$ colour-colour diagram (Gianninas et al., 2011) and close to the cooling tracks of a DA white dwarf with $\log g = 8$ in both the $(U-g)$–$(g-r)$ and $(r-i)$–$(r-\mathrm{H}_\alpha)$ colour-colour diagrams, as shown in Figure 4.9, with a spectrum eventually confirming it as a DA white dwarf with a temperature of $\mathrm{T}_{eff} = 12\,350 \pm 250\,\mathrm{K}$, $\log g = 7.96 \pm 0.10$ and $M_{WD} = 0.57 \pm 0.06 M_\odot$. This compares with values of $\mathrm{T}_{eff} = 11\,129 \pm 115\,\mathrm{K}$, $\log g = 8.34 \pm 0.06$ and $M_{WD} = 0.82 \pm 0.04 M_\odot$ for KIC 4552982, the DAV of Hermes et al. (2011). As shown in Figure 4.10, which shows KIC 11911480 and KIC 4552982 in the T_{eff}–$\log g$ plane alongside the sample of DA white dwarfs found by Gianninas et al. (2011), these values place KIC 11911480 and KIC 4552982 at the blue and red edges of the empirical DAV instability strip respectively. Both sources also have dominant periods typical of DAVs of their temperature, as can be seen in Figure 4.11, which shows KIC 11911480 and KIC 4552982 in the period-temperature plane alongside 35 DAVs found in the SDSS survey by Mukadam et al. (2004a). The discovery of KIC 11911480 therefore means that the unprecedented opportunites offered by *Kepler* can be used to probe two opposite extremes of the DAV distribution and hence, is an important discovery in improving our understanding of DAVs.

KIC 11911480 was the subject of a successful bid for observation in short cadence mode through the Director's Discretionary Time program and 6 months worth of near uninterrupted observations were obtained during quarters 12 and 16. Initial analysis (Greiss et al., 2014) identified a total of five independent

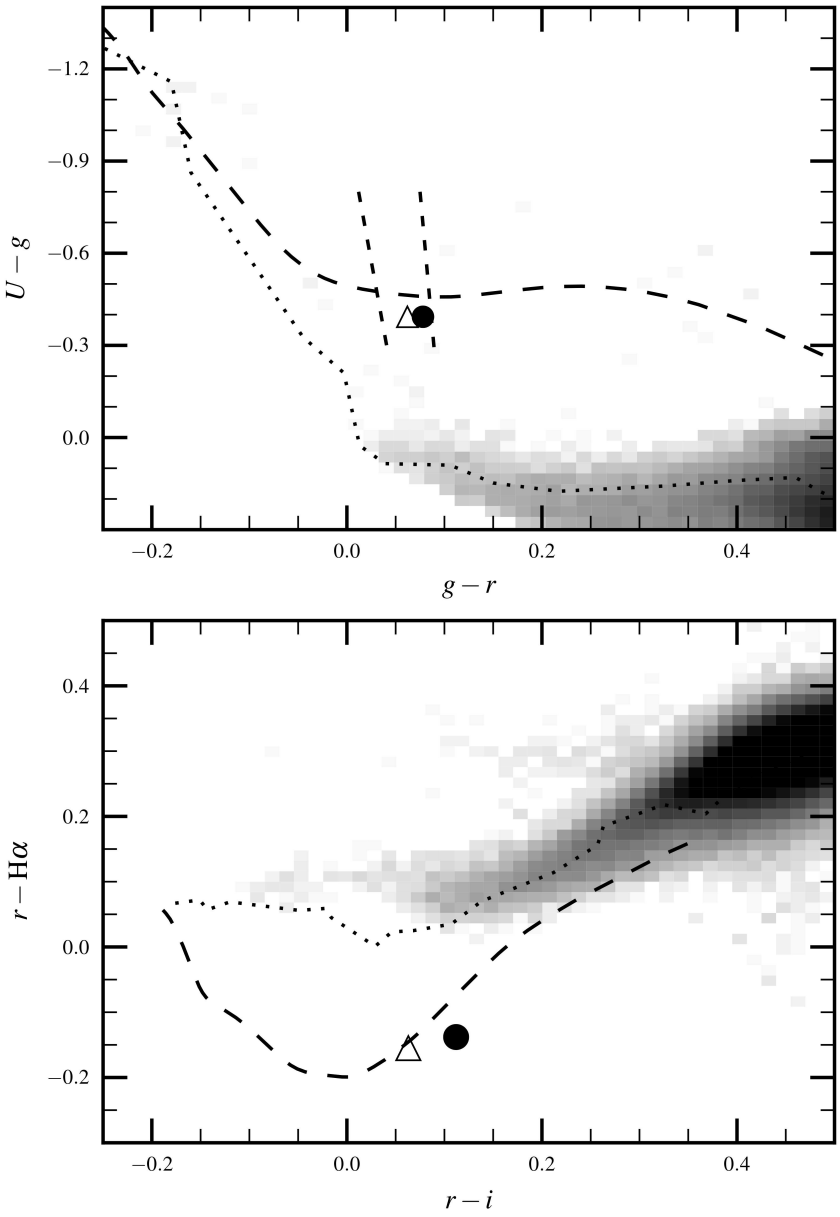

Figure 4.9: $(U-g)$–$(g-r)$ and $(r-i)$–$(r-\mathrm{H}_\alpha)$ colour–colour diagrams of stellar sources from the first half of the Kepler-INT survey (grey-scale, (Greiss et al., 2012a)). The cooling track for a Bergeron DA white dwarf with $\log g = 8$ is indicated by the dashed line and the dotted line indicates the Pickles main-sequence tracks which were both taken from Groot et al. (2009). The filled circle corresponds to KIC 4552982 (Hermes et al., 2011), whereas the open triangle marks KIC 11911480. They are clearly blue and H_α-deficient objects. The vertical dashed lines in the upper panel correspond to the empirical boundaries of the ZZ Ceti instability strip (Gianninas et al., 2011) projected in the $(U-g)$–$(g-r)$ colour space. Figure taken from Greiss et al. (2014).

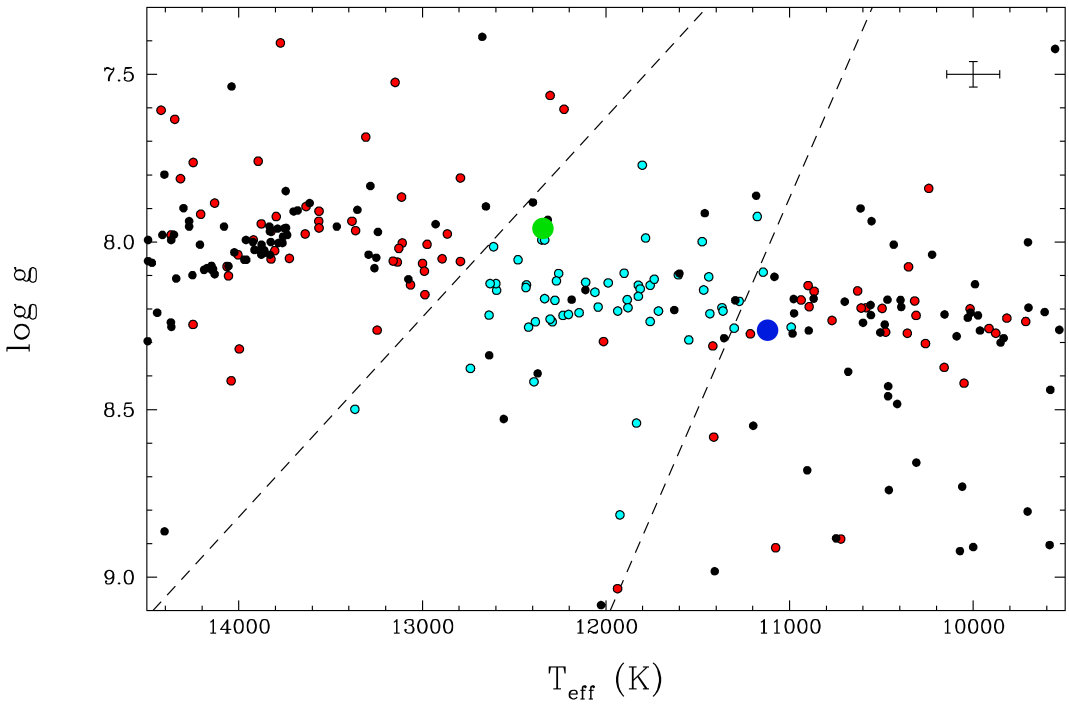

Figure 4.10: T_{eff} - $\log g$ distribution for the sample of DA white dwarfs with high-speed photometric measurements obtained by Gianninas et al. (2011). The cyan circles represent the 56 DAV stars in their sample, the red circles are the 145 photometrically constant DA stars in their sample and the black circles represent the stars for which they do not have any high-speed photometric data. The dashed lines correspond to the empirical boundaries of the DAV instability strip determined in Gianninas et al. (2011). The error bars represent the average uncertainties of their spectroscopic method in the region of the DAV instability strip. The green circle is the position of KIC 11911480, whilst the blue circle is the position of KIC 4552982. Figure taken from Gianninas et al. (2011).

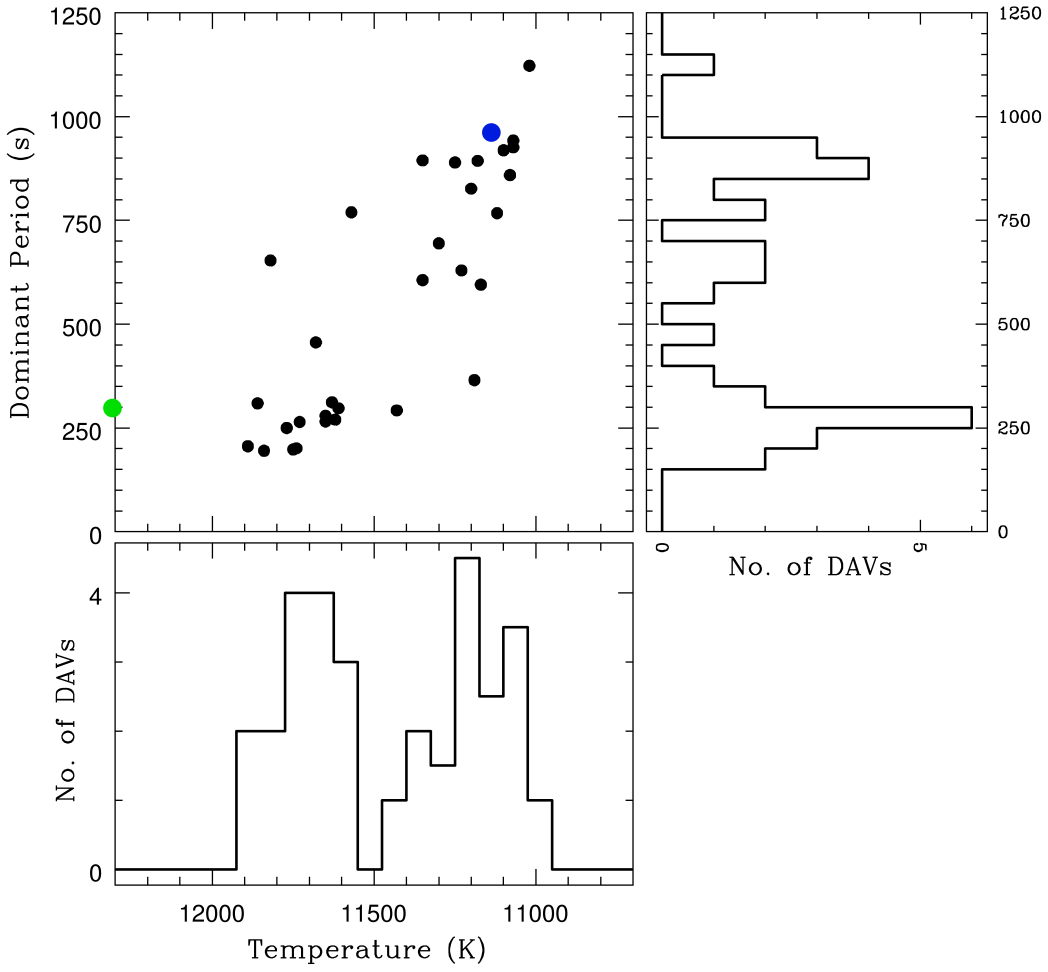

Figure 4.11: Period distribution of the 35 SDSS DAVs found by Mukadam et al. (2004a) as a function of temperature. The top left panel exhibits two distinct clumps consisting of the short-period hot DAVs and the long-period cool DAVs. The dominant period of a DAV is a seismological temperature indicator, and the histogram shown in the top right panel suggests a bimodal distribution. The green circle is the position of KIC 11911480, whilst the blue circle is the position of KIC 4552982. Figure taken from Mukadam et al. (2004b)

Mode	Period(s)	Frequency(μHz)	$\lvert\Delta f\rvert$(μHz)
$f_{1,-}$	290.9664(7)	3436.823(8)	1.947
$f_{1,0}$	290.8016(1)	3438.770(1)	
$f_{1,+}$	290.6322(4)	3440.775(5)	2.005
$f_{2,-}$	259.3731(2)	3855.451(3)	1.784
$f_{2,0}$	259.2531(2)	3857.235(3)	
$f_{3,-}$	324.529(1)	3081.39(1)	2.03
$f_{3,0}$	324.3152(9)	3083.420(9)	
$f_{3,+}$	324.1032(1)	3085.44(2)	2.02
$f_{4,-}$	172.9588(4)	5781.72(1)	1.96
$f_{4,0}$	172.9003(5)	5783.68(1)	
$2f_{1,0}$	145.4007(3)	6877.54(1)	
$f_{1,0} + f_{2,0}$	137.0610(2)	7296.02(1)	
$f_{4,0} - f_{1,0}$	426.936(3)	2342.27(2)	
$f_{4,-} - f_{2,-}$	519.600(4)	1924.56(2)	
$f_{4,0} - f_{2,0}$	519.110(4)	1926.37(1)	

Table 4.7: Periods, frequencies and $\lvert\Delta f\rvert$ of the rotational multiplets for the pulsation modes found in Q12 for the DA White dwarf KIC 11911480. Values in brackets represent the uncertainties. Values taken from Greiss et al. (2014).

pulsation modes and four modes which were non-linear combinations of the independent ones. Of these modes, four independent modes and four linear combinations were detected in the Q12 data, which are listed in Table 4.7, with the relevant power spectrum shown in Figure 4.12. The non-linear combinations are particularly useful for probing the physical conditions within the convection zone (Montgomery, 2005). Brickhill (1992) showed that these occur due to interaction between waves at the boundary between the convective and radiative zones at the base of the hydrogen ionisation zone, where the heat transport mechanisms change dramatically.

All modes exhibited rotational splitting, two examples of which are shown in Figure 4.13, which shows the splitting found in the two dominant modes in the

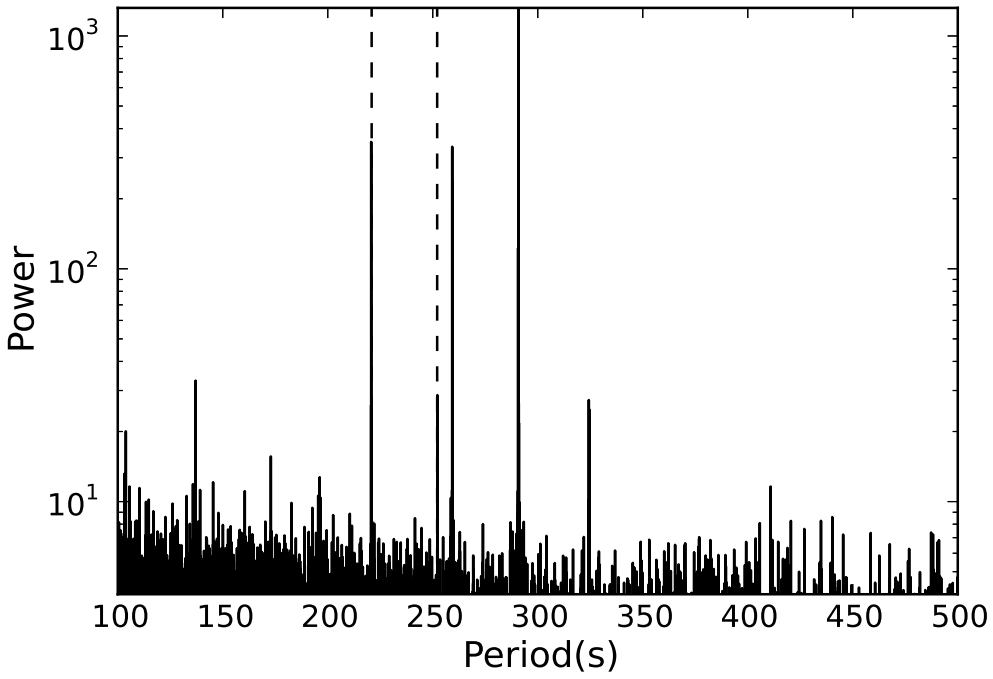

Figure 4.12: The Lomb-Scargle power spectrum of the *Kepler* Q12 light curve of the DA White dwarf KIC 11911480 made using the `VARTOOLS` suite of software. Dashed vertical lines indicate known artifacts in the power spectra of *Kepler* SC data.

power spectrum of the Q12 data. Note that not all modes of each rotationally split multiplet were detected in both quarters, though it is a common phenomena to not detect every mode in all epochs, see e.g. table 5 of Kepler et al. (2003). The rotation rate of the white dwarf can be derived from the difference in frequencies over these multiplets. The frequency difference between the frequency of one mode of indices n, ℓ, m, $\sigma_{n,\ell,m}$ (where n, ℓ, and m are the eigenvalues describing the spherical harmonics of the waves, c.f. Section 1.2), and the frequency in the non-rotating case, $\sigma_{n,\ell}$, i.e. the central peak of the multiplet, is:

$$\sigma_{n,\ell,m} - \sigma_{n,\ell} = m(1 - C_{n,\ell})\Omega \tag{4.1}$$

where $C_{n,\ell}$ comes from the Coriolis force term in the momentum equation and Ω is the rotation frequency (Winget et al. (1991); Vauclair (1997)). This yields a result of 3.0 ± 0.2 days, however this equation is only the classical first order expansion and only applies to g-modes when they are in the asymptotic limit, where $C_{n,\ell}$ only depends on the order of the mode and $C_{n,\ell} \approx \frac{1}{\ell(\ell+1)}$. However, most of the modes identified seem to be of low radial order, meaning that they are far from the asymptotic limit. Hence, the models of Romero et al. (2012), which include more realistic $C_{n,\ell}$ values, were used to make a more robust determination of the rotation period as being 3.5 ± 0.5 days.

The data await a full asteroseismic analysis, but with there being only one other DAV white dwarf having been observed with the previously unprecedented capabilities of *Kepler* it has the potential to significantly advance theoretical models of DAV white dwarfs.

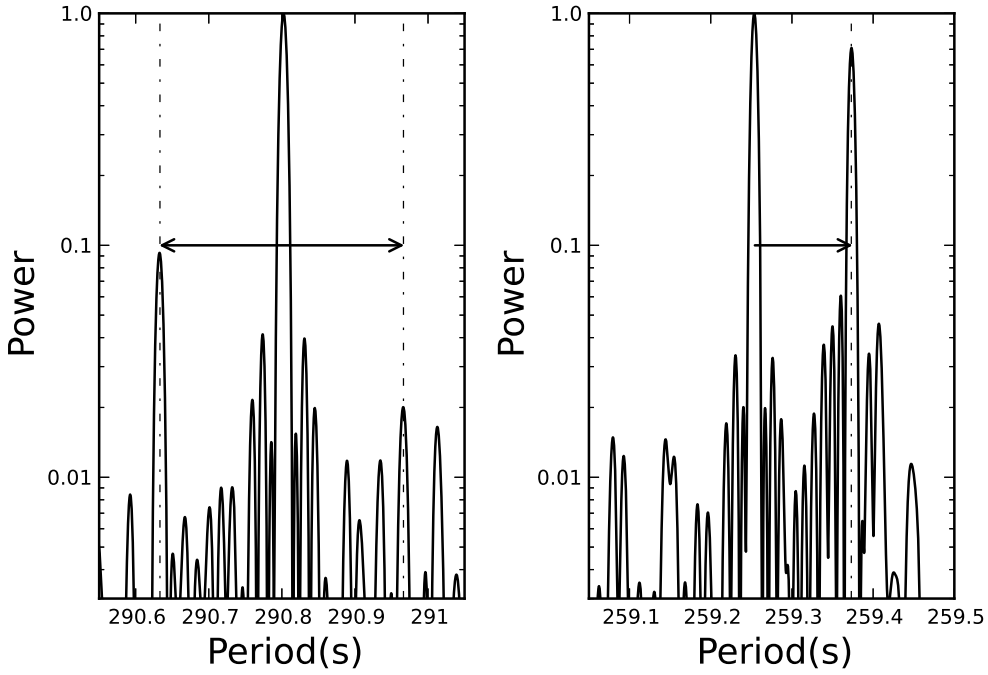

Figure 4.13: A close up of the Lomb-Scargle power spectrum for two of the dominant pulsation modes, f_1 (left) and f_2 (right), which exhibit rotational splitting. Rotationally split modes are indicated by a dashed-dotted line, with arrows emanating from the central peak of the rotational multiplet. Note that each plot has been normalised seperately.

4.4 KIC 7431243 (V363 Lyr): a Cataclysmic Variable

As described in Section 1.2.6 Cataclysmic variables (CV) are interacting binary systems composed of a white dwarf primary accreting matter from a secondary star. They exhibit both short-term and longer-term variability in the form of outbursts. Detailed investigations of these systems can help refine models of accretion, which can also be extended to other accreting sources such as active galactic nuclei, blackholes and X-ray binaries.

The RATS-*Kepler* light curve of KIC 7431243 showed evidence of flickering behaviour and quasi-periodic oscillations (QPO), similar to the CV identified by Ramsay et al. (2009) (RAT J1953+1859, a dwarf novae of the SU UMa type). Examination of its colours in the KIS (Greiss et al., 2012a,b) showed it to be a moderately blue, UV excess, H_α excess source ($g-r$=0.47, $U-g$=–0.94 and $r-H_\alpha$=0.79, c.f. Figures 3.11 and 3.12), which, consulting Figure 5 of Greiss et al. (2012a), occupies the same areas of the $(U-g)$–$(g-r)$ and $(r-i)$–$(r-H_\alpha)$ colour-colour diagrams as other published CVs, with its nature being confirmed spectroscopically by Scaringi et al. (2013). It matches the variable star V363 Lyr which was discovered as a CV by Hoffmeister (1967), whilst Kato et al. (2001) found that it shows outbursts of duration 7–8 days every ∼21 days. There are several dozen known CVs in the *Kepler* field (see Scaringi et al. (2013) and Howell et al. (2013)).

KIC 7431243 was observed using *Kepler* in Q16 for 5.2 days and no outbursts were seen (Figure 4.14), which is not surprising given the short observation length compared to the 21 day duration of its outburst cycle. The power spectrum of

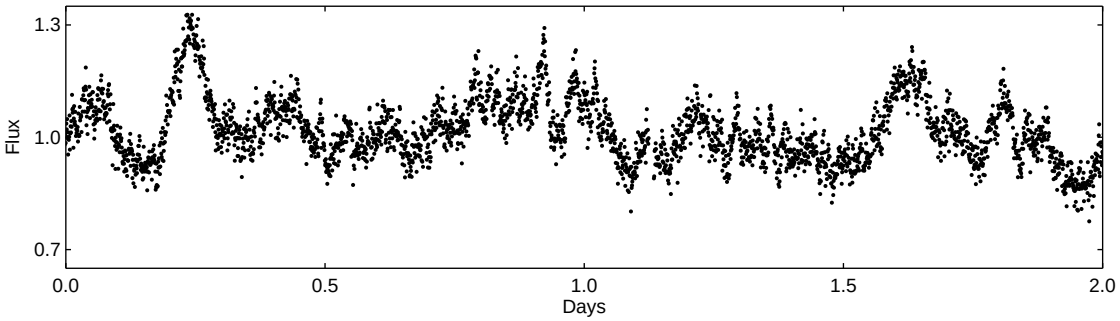

Figure 4.14: The *Kepler* short cadence light curve of KIC 7431243 (V363 Lyr) shown over a 2 day time interval. Figure taken from (Ramsay et al., 2014).

the light curve shows peaks corresponding to 4.68 hrs and 4.47 hrs. If the longer period is attributed to the super-hump period (super-humps are caused by the precession of the accretion disk) and the shorter period to the orbital period, then the fractional excess, $\epsilon^{+} = (P_{sh} - P_{orb})/P_{orb}$=4.7 percent. Using the relationship of Patterson et al. (2005) this would imply a mass ratio, $q = M_2/M_1 \sim 0.21$.

Using the secondary star mass (M_2)–orbital period relationship for CVs ($M_2 = 0.065 P_{hrs}^{5/4}$, Warner (1995)), for a CV with P_{orb}=4.47 hrs it can be found that, $M_2 = 0.42 M_{\odot}$ (or $0.45 M_{\odot}$ for P_{orb}=4.68 hrs). Super-humps are thought to be restricted to systems where the mass ratio, $q = M_2/M_1 < 0.33$, as detailed in Schreiber (2007). If super-humps are present in KIC 7431243 then this may suggest that the white dwarf in this binary has a mass $M_1 > 1.28 M_{\odot}$ assuming $M_2 = 0.42 M_{\odot}$ ($M_1 > 1.36 M_{\odot}$ for $M_2 = 0.45 M_{\odot}$). Given the potentially high mass of the white dwarf as compared to typical white dwarfs ($\sim 0.6 M_{\odot}$, Kepler et al. (2007)), it could potentially offer a unique test of theoretical models, which would require phase resolved optical spectroscopy.

4.5 Contact/Eclipsing Binaries

Contact binaries, or W Ursae Majoris systems (also known as W UMa binaries), are binary systems where the two stellar components are so close together as to be in physical contact with each other and account for ∼1% of main sequence star systems (Rucinski (1998), estimates are made excluding stars of spectral type K5 and later), with periods in the range of 0.21–0.7 days (Rucinski and Pribulla (2008); Pribulla et al. (2003)).

The RATS-*Kepler* light curves of the sources of KIC 7667885, KIC 9786165 and KIC 12553806 showed evidence that they were eclipsing or contact binary sources. This was confirmed by the *Kepler* data obtained for these three sources, which clearly indicate that they are eclipsing or contact binaries with an orbital period ranging from 0.315 days – 0.463 days. The *Kepler* Q14 SC data of these sources can be seen in Figure 4.15 where the data have been folded and binned on the orbital period for each system.

Prša et al. (2011) and Slawson et al. (2011) present an analysis of the first and second *Kepler* data release of 4,044 other eclipsing and contact binaries which have been observed by *Kepler*. Although the shape of the folded light curves of KIC 7667885 and KIC 12553806 are similar to that of semi-detached binaries (also known as β-Lyr binaries), their relatively short orbital period suggests that they are more likely to be contact binaries. The folded light curve of KIC 9786165 also implies it is a contact binary. Although some caution has to be applied in interpreting the results of the spectral fits made to these sources, since a single temperature model has been applied to sources which are clearly binary systems,

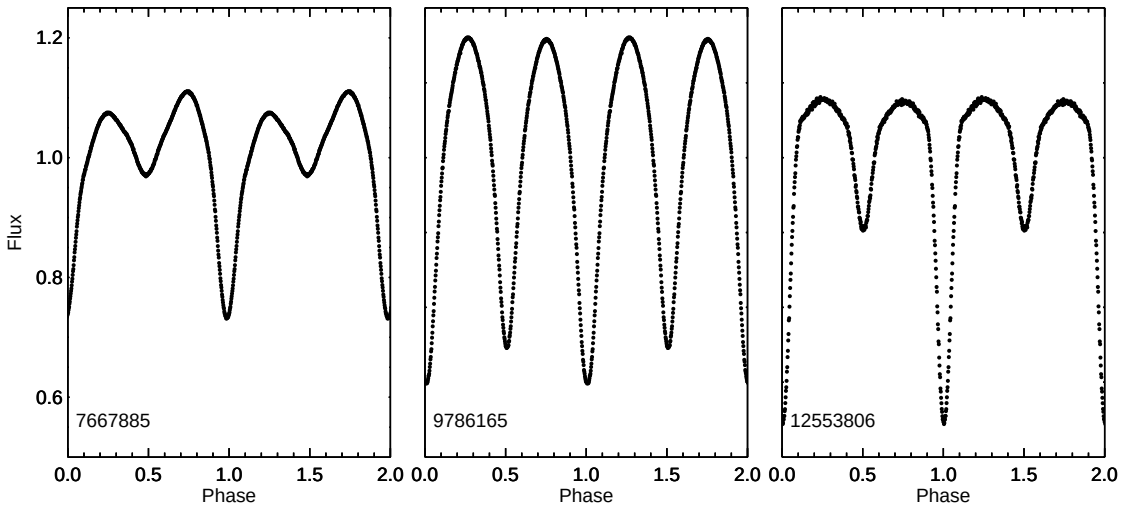

Figure 4.15: The *Kepler* short cadence light curve of the contact binaries KIC 7667885, KIC 9786165 and KIC 12553806. The data have been phased so that the primary eclipse is centered on ϕ=0.0 and the y-axis is plotted on the same scale in each panel. Figure taken from (Ramsay et al., 2014).

the temperatures which have been derived (Table 3.3) indicate they are contact binaries rather than semi-detached binaries which have B star components (and hence would be significantly hotter).

Unlike the three sources outlined here which have been observed using SC mode, none of the sources shown in Prša et al. (2011) or Slawson et al. (2011) have been observed in SC Mode. Since each of the three binaries has a high inclination, they are excellent data-sets to search for third bodies (such as exo-planets) in these systems.

4.6 KIC 5474065: an M Dwarf Flare Star

Flares with duration of a few to tens of minutes and energies of $\sim 10^{28-35}$ ergs have been observed on low mass dwarf stars for many decades (e.g. Bopp and Moffett (1973); Gershberg and Shakhovskaia (1983)). They are typically observed on stars of spectral type M, though they have also been observed in stars of earlier spectral type (e.g. Andrews (1967)). The origin of these flares is thought to be similar to Solar flares in that they are produced during magnetic reconnection events (e.g. Haisch et al. (1991)). Studying stellar flares from a wide range of stars can give important insight to how magnetic activity varies as a function of stellar mass and age. In more recent years, the effects of flares on the atmosphere of exo-planets around dwarf stars has been the subject of much interest (e.g. Segura et al. (2010)). This is because the transit of Earth-mass planets across lower radii stars is easier to detect and that the habitable zone is closer to the star and hence has a shorter orbital period, meaning more potential transit detections

Table 4.8: The absolute magnitude and luminosity of stars with spectral types M3 V–M5 V based on the data in Lépine and Gaidos (2011).

Spectral Type	M_V	L (erg s^{-1})
M3 V	11.2	1.1×10^{31}
M4 V	12.4	3.6×10^{30}
M5 V	13.5	1.4×10^{30}

in a given period of time. However, the prevalence of flaring in M-type stars could be a problem for the potential habitability of planets in the habitable zone of such stars (Segura et al., 2010).

The RATS-*Kepler* light curve of KIC 5474065 showed an ∼8 minute duration flare with an amplitude of 0.6 mag in the g band. Examination of the KIS (Greiss et al., 2012a,b) yielded colours of $g - r$=1.43, $U - g$=1.93, r−H$_\alpha$=0.79 and $r - i$=1.71, placing it as a late spectral type, main sequence star in the $(U - g)$–$(g - r)$ and $(r - i)$–$(r$−H$_\alpha)$ colour-colour diagrams (c.f. Figures 3.11 and 3.12). A spectrum was obtained using the GTC, as shown in Figure 3.16, which confirmed it to be an M4 V star and a successful bid to have it observed by *Kepler* in short cadence mode was made. In order to determine the energy of flares detected, the intrinsic luminosity needs to be determined, which required the V and J magnitudes. These were obtained from the UBV survey of the Kepler field ($V = 18.07$; Everett et al. (2012b)) and also the 2MASS survey ($J = 14.015$; Skrutskie et al. (2006)). Using the relationship between $(V - J)$ and absolute magnitude (M_V) outlined in the work of Lépine and Gaidos (2011) the mean M_V can be estimated for stars of spectral type M3 V–M5 V. If it is assumed that the Sun has $M_V = 4.83$ and $L_\odot = 3.8 \times 10^{33}$ erg s^{-1}, then the values shown in

Table 4.8 can be obtained.

The *Kepler* light curve of KIC 5474065, shown in Figure 4.16, exhibits two main features – one a clear quasi-sinusodial modulation with a period of 2.47 days and a semi-amplitude of ∼2 percent; and the presence of short but intense flares: two flares have an intensity $\Delta F/F$ ∼46 percent. For comparison, *MOST* observations of the dM3e star AD Leo (made using a 1 min cadence), show flares with $\Delta F/F$ ∼28 percent (Hunt-Walker et al., 2012), while 'super-flares' with amplitude of 8 percent are seen on Solar-type stars (Maehara et al., 2012). The rotational period of KIC 5474065 is typical of M4-5 dwarfs, e.g. YZ CMI has a rotational period of 2.78 days (Chugainov, 1974), while V577 Mon has a rotational period of 1.95 days.

To aid the analysis of KIC 5474065, we also extracted the light curve of KIC 9726699 which has also been observed using *Kepler* in SC mode, so that the results obtained can be put into a broader context. Savanov and Dmitrienko (2011) presented an analysis of these data, but concentrated on determining the extent and duration of spots on its photosphere and did not discuss the flares themselves. Like KIC 5474065 it has an M4 V spectral type (Reid et al., 2004), but it is more rapidly rotating (a rotation period of 0.593 days) which makes it similar to V374 Peg (0.45 days). The KIC (Brown et al., 2011b) gives g=13.9 for KIC 9726699 making it more than 5 mag brighter than KIC 5474065 and hence the *Kepler* data of this source have a much higher signal to noise than KIC 5474065.

KIC 9726699 has been observed using *Kepler* in SC mode in four quarters, but the comparitive analysis will be restricted to data only from Q6. Figure 4.17

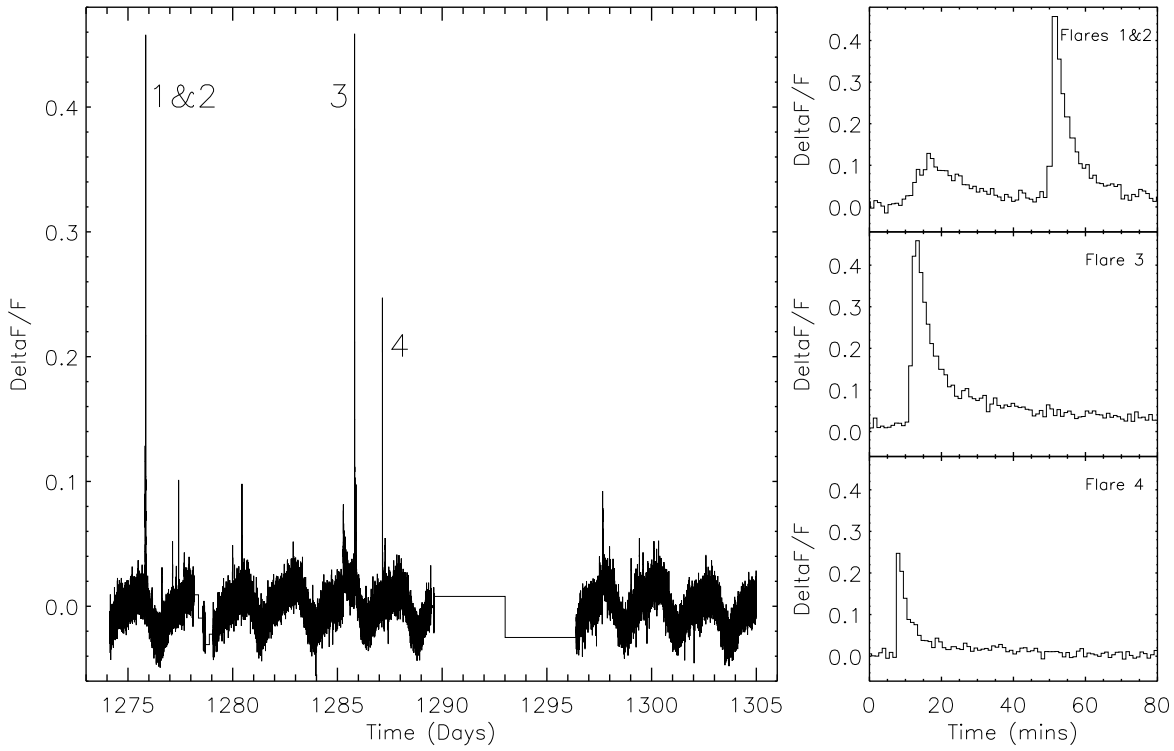

Figure 4.16: The *Kepler* Short Cadence light curve of KIC 5474065 made in Q14. ΔF/F is the ratio of the difference between the flux at any point and the mean flux. The rotational period of 2.47 days is clearly seen as are the short duration flares. The right hand panel shows a close up of four flares. Figure taken from Ramsay et al. (2013).

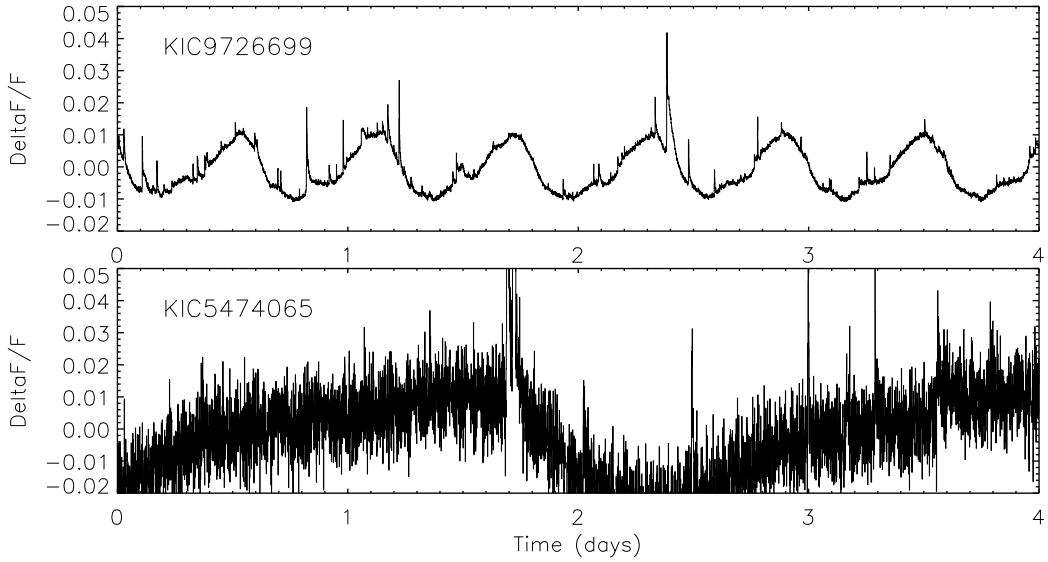

Figure 4.17: The top panel shows a section of the *Kepler* Short Cadence light curve of KIC 9726699 made in Q6. ΔF/F is the ratio of the difference between the flux at any point and the mean flux. For comparison the light curve of KIC 5474065 is shown in the lower panel on the same scales. The higher noise level in this light curve is immediately apparent and is due to KIC 5474065 being 5 magnitudes fainter than KIC 9726699. Figure taken from Ramsay et al. (2013).

shows a 4 day section of the light curve of KIC 9726699. It exhibits a relatively small number of large amplitude flares, but its light curve is dominated by short duration, low intensity, flares. By comparison, the light curve of KIC 5474065, also covering 4 days and on the same flux scale, is dominated by high amplitude flares, but shows fewer low intensity flares. Given that KIC 9726699 is very much brighter compared to KIC 5474065, it is possible that the difference in the number of short duration low intensity flares observed in KIC 5474065 is due to them being hidden in the noise.

To identify flares from KIC 5474065 in an automatic manner the effects of the

rotational modulation first needed to be removed. Then, a threshold increase in the flux above the mean flux needed to be determined which would find the right balance between detecting flares and reducing the false positive detection rate due to random noise in the data. After some experiment, this was defined as:

$$(f_i - \overline{f})/\sigma > 3 \tag{4.2}$$

where f_i is the flux of the ith point, $\overline{f}$ is the overall mean of the light curve and σ is the standard deviation of the overall light curve. If a lower threshold was defined for flare detection the flare rate goes up but the false positive rate also goes up as it becomes difficult to distinguish between a genuine flare and noise in the data. Through manual inspection of the selected events it was determined that this threshold provided an adequate balance. The resulting selected events were then manually inspected and points which were clearly part of the same flare were edited to ensure no 'double counting' of flares were made. This strategy found 27 flares in the SC light curve of KIC 5474065 – in otherwords, on average one flare was detected every 0.9 days, and on average there was one flare with an intensity $\Delta \mathrm{F}/\mathrm{F} > 0.2$ every 8 days. There was no evidence of any pre-flare dips such as that seen in V1054 Oph (Ventura et al., 1995). For KIC 9726699 it was more difficult to fully remove the effects of rotation so the flare detection threshold needed to be set higher at

$$(f_i - \overline{f})/\sigma > 8 \tag{4.3}$$

to adequately exclude false positive flare detections. However, over 260 flares

were identified in the Q6 data of KIC 9726699. The fact that KIC 9726699 appears to be more active compared to KIC 5474065 is consistent with the well known correlation between rotation period and stellar activity, (e.g. Noyes (1985)), although it should be noted that short duration, low energy flares would not have been detected in KIC 5474065 due to the much higher noise level.

To derive the flare frequency rate for these sources as a whole (as opposed to only those which have been observed), the equation found in Lacy et al. (1976) can be used:

$$E = \sum_{f} [(I_{f+o} - I_o)/I_o] \Delta T \tag{4.4}$$

where E is known as the flare equivalent duration, I_o is the stellar intensity of the star in its quiescent state, I_{f+o} the intensity during a flare and ΔT the integration time. Assuming an underlying luminosity of 3.6×10^{30} erg/s (Table 4.8), which is appropriate for an M4 V spectral type; this gave a range in flare energy for KIC 5474065 of $L = 1.1 - 7.3 \times 10^{32}$ ergs, whilst for KIC 9726699 the range was $L = 0.01 - 2.2 \times 10^{32}$ ergs (these energies will vary by a factor of three for one spectral sub-class either side of M4 V). For historical reasons the activity of flare stars is frequently measured in the U band, hence to compare these energies to other sources, it is required to estimate the equivalent energy of them in the U band. van den Oord et al. (1996) found $E_{opt}/E_U = 2.4$ where E_{opt} and E_U is the energy emitted in the optical UBV and U band respectively. In comparison, Lacy et al. (1976) find $E_{opt}/E_{WL} = 2.1$ where E_{WL} is the energy emitted in 'white light'. For these purposes we assume $E_{Kepler}/E_U = 2.4$ and note there will be a

Table 4.9: Flare rates for KIC 5474065, KIC 9726699 compared to AD Leo where the energies are the equivalent energy in the U band.

flare enery (ergs)	AD Leo flare rate (days)	KIC 5474065 flare rate (days)	KIC 9726699 flare rate (days)
10^{30}	0.09		0.3
10^{31}	0.29	0.2	0.6
10^{32}	1.5	8.7	117

$\sim$10 percent uncertainty in the values of E_U. Using this relationship we find that the flares for KIC 5474065 have a range between $L_U = 0.5 - 3 \times 10^{32}$ ergs and $L_U = 0.01 - 0.9 \times 10^{32}$ ergs for KIC 9726699. The energy and duration of these flares are at a lower energy than those detected on another M4 V flare star, AD Leo (Pettersen et al., 1986).

The cumulative flare-frequency distribution of the flares of KIC 5474065 and KIC 9726699 can be seen in Figure 4.18. This shows that on average KIC 5474065 shows a flare with energy $L = 10^{31}$ ergs every 0.2 days and a flare with energy $L = 10^{32}$ ergs every 8.7 days, with KIC 9726699 showing flares of these energies every 0.6 days and $\sim$117 days respectively. Comparitively AD Leo can produce a 10^{32} ergs flare every 1.5 days (see Table 4.9).

Figure 4.19 shows the light curve of both KIC 5474065 and KIC 9726699 folded on the stars rotational period together with the energy of each flare as a function of the rotational phase. Since the modulation in the light curve is caused by the rotation of stellar spots into and out of view, the minimum flux corresponds to the viewing phase when the fractional surface area covered by spots is at its greatest (since the spots are cooler and therefore less luminous

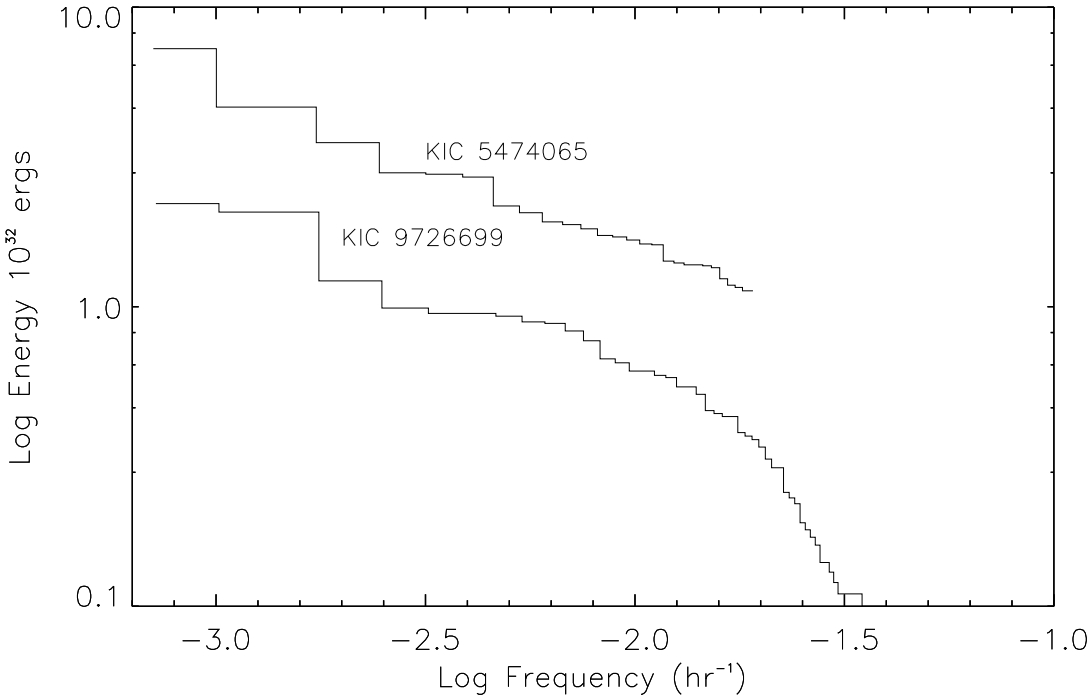

Figure 4.18: The cumulative energy distribution of flares (in the *Kepler* band-pass) as seen in KIC 5474065 and KIC 9726699. Figure taken from Ramsay et al. (2013).

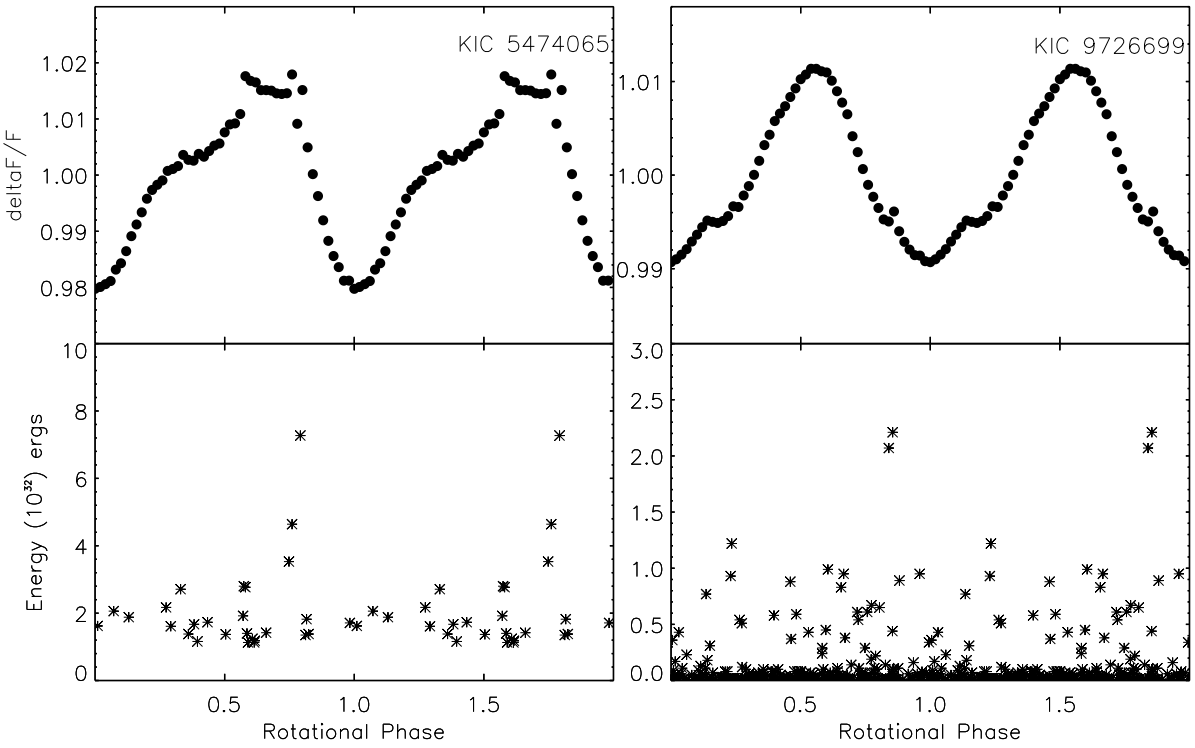

Figure 4.19: The upper panels show the mean light curve of KIC 5474065 (left) folded on T_o= BJD 2456106.97 + 2.47295492 E and KIC 9726699 (right) folded on T_o= BJD 2455371.310 + 0.593 E, where the light curves have been normalised so that the mean flux is unity and ϕ=0.0 is defined as photometric minimum and the light curves have been binned into 50 bins. The lower panels show the energy emitted in each flare as a function of rotational phase. Deviations from a smooth curve are a result of flares in the light curve. Figure taken from Ramsay et al. (2013).

than the surrounding photosphere).

In the case of KIC 5474065, the three most energetic flares were seen in a very short phase interval, ϕ=0.74–0.79. Coincidentally, in KIC 9726699 the two most energetic flares were also seen at a similar phase (ϕ=0.84–0.85) and separated by 6 rotational cycles. This indicates that the most active regions on the star are preferentially located in stellar longitude and last for timescales of (at least)

several weeks (a conclusion also reached by Savanov and Dmitrienko (2011)). In both sources, flares were seen at all rotational phases.

The monitoring of flares from M dwarf stars has been ongoing for the past 50 years, most of it in the Johnson U-band. Although all M dwarfs monitored over an extended timescale appear to show flares, only a few dozen have a well established flare-rate. Figure 4.20 summarises the results from several thousand hours of photometric monitoring (the caption indicates the original source of the data). Compared to the other M dwarf stars (which range from dM0 to dM8) shown in Figure 4.20, KIC 5474065 and KIC 9726699 show flares which are relatively energetic but occur less frequently.

KIC 9726699 also produces more frequent but less energetic flares than KIC 5474065, despite the fact that both have a dM4 spectral class. Generally speaking, stars of spectral class M4 and later are fully convective and therefore have a very different magnetic topology compared to stars with earlier spectral type. However, Morin et al. (2010) has shown this is not always the case as age may play a role in addition to mass and rotation period. Hence, the higher flare energies observed on KIC 5474065 despite its slower rotation rate are likely due to age. For example, V374 Peg has a similar rotation period to KIC 9726699, yet it can produce extremely energetic flares, e.g. Batyrshinova and Ibragimov (2001) detected an 11 mag superflare with an energy in excess of 10^{35} erg. A more plausible explanation may be the relative spot coverage on these two stars. For instance Notsu et al. (2013) found that the energy of superflares is related to the total coverage of starspots and therefore the amount of magnetic energy stored around starspots.

For those stars where monitoring exists over a number of years, the observed

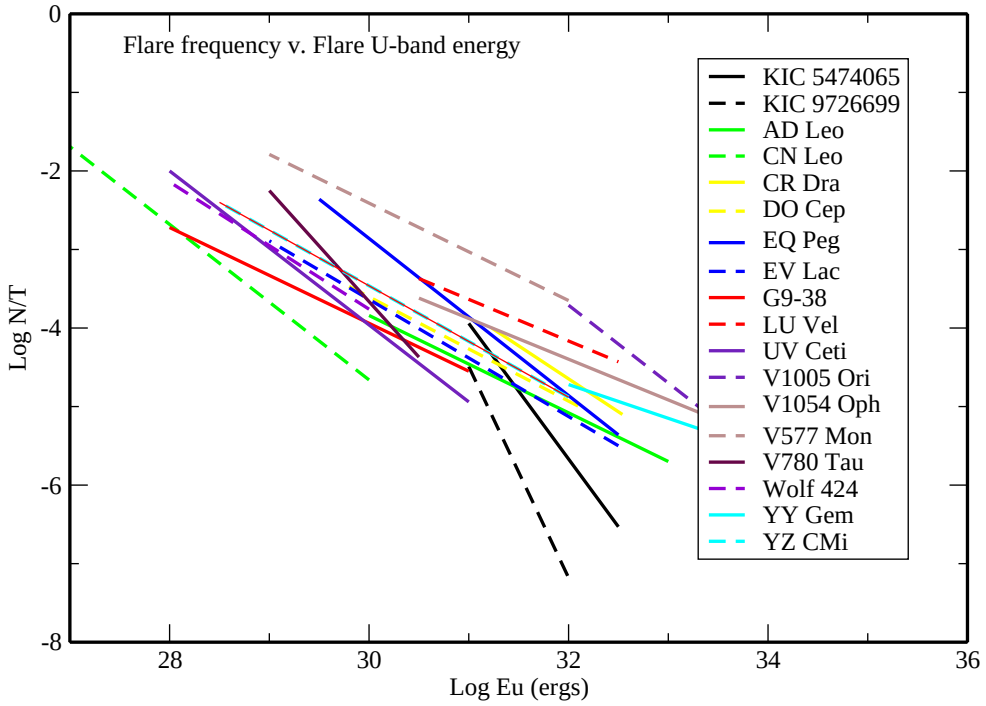

Figure 4.20: The cumulative flare frequency (in seconds) versus U-band flare energy (in ergs) for a large group of M dwarfs plus that for KIC 5464065 and KIC 9726699. These data have been compiled from work by Moffett (1974), Lacy et al. (1976), Byrne et al. (1984, 1985), Pettersen (1975b,a, 1981b,a, 1983, 1985a,b, 2006a,b), Pettersen et al. (1983, 1984, 1986), Pettersen and Sundland (1991), Doyle and Byrne (1986), Doyle et al. (1986, 1989, 1990), Hawley et al. (1989), Leto et al. (1997), Dal and Evren (2010, 2011) and Dal (2011, 2012). Figure taken from Ramsay et al. (2013).

seasonably variability can be a factor of two, perhaps indicating cycles similar to the Sun. This has been determined in a number of ways, but includes narrow band photometric filters centered on the Ca II H & K lines (e.g. Baliunas et al. (1995)) and spectropolarimetric observations (e.g. Donati et al. (2008)) spread over a considerable time interval. With the possibility of observing flare stars using *Kepler* with a cadence of 1 min for weeks at a time, it will be practical to map the activity of many stars over a timescale of years. This will also provide good motivation to re-examine the effects that stars which show many flares have on the chemistry of atmosphere's of exo-planets in the star's habitable zone.

The implications of stellar flares on the atmosphere of an exo-planet orbiting around a flare star are important for the development of life, as energetic flares could have a potentially hazardous influence on its habitability. These hazards come in a number of forms - high levels of ionising radiation and high energy protons which can cause cell damage and/or DNA mutation; and the high levels of UV radiation given off in flare events, which can cause photodissociation of atmospheric molecular gases, often leading to the production of highly reactive free radicals. These free radicals can then go on to affect other molecules necessary for an atmosphere to shelter life, sometimes even creating a chain reaction which leads to the continued destruction of these molecules. A well known recent terrestrial example of this is the effect that CFCs (Chloroflourocarbons) have had on our ozone layer in the upper atmosphere which is essential to shielding the surface of the planet from UV radiation. Photodissociation of the Carbon-Chlorine/Flourine bond at high atmospheric altitudes creates a free radical molecule which reacts with ozone and not only destroys ozone molecules, but leaves another free radical

as a reaction product, which then goes on to breakdown more ozone molecules. Examples from Earth's past, present and projected future; such as the current global warming being caused by large amounts of CO_2 being released into the upper atmosphere, the disruption of our ozone layer by the release of CFCs and global mass extinction events caused by excess sulphur dioxide in the atmosphere released through volcanic activity; show that the atmosphere required to support life as we know it on a planet is a delicate mix - one which could potentially be affected by excess flare activity on the host star.

For an M4 V dwarf star the habitable zone is roughly 0.04–0.14 AU (e.g. Kopparapu et al. (2013)). For instance Segura et al. (2010) determined the potential effect of a flare as seen on the dM3e star AD Leo in April 1985. This flare, which had a duration of 4 hrs, was found to have an energy of $L \sim 10^{34}$ ergs in the UV/Optical wave-band (Hawley and Pettersen, 1991), more than one order of magnitude greater than the largest flare seen on KIC 5474065. Segura et al. (2010) determined that such a flare was not a direct hazard for life (as we know it) on an exo-planet 0.16 AU distant from AD Leo. The flares which we report here are both less energetic but also of much shorter duration. For KIC 5474065 the total radiated U-band flare energy budget during the SC monitoring interval was $\approx 10^{27}$ erg s^{-1}. Assuming that the total radiated energy over all wavelengths is one order of magnitude greater (e.g. Doyle and Butler (1985)) implies a value two orders of magnitude less radiated energy than the large AD Leo flare referenced above which may suggest a minimum effect on any nearby planet. However, what effect a sequence of frequently occurring flares has still needs to be investigated, as this can have a long-term effect on the chemical stability of the

mixture of atmospheric gases. This is particularly important because exoplanets in the habitable zone of M-dwarfs are so close to their parent star that they will typically be tidally locked, hence atmospheric circulation models are very important in determining habitability of these planets.

Chapter 5

Summary of Thesis

In this thesis I have outlined the various types of stars which are variable on periods of 2 hours or less, the mechanisms driving their variability and what scientific goals can be achieved by making observations which improve our knowledge of these sources. I then go on to describe a number of variability surveys conducted in the past and introduce the unprecedented opportunities afforded by the precision and continuous pointing of the *Kepler* satellite. I then explore the limitations of surveys of the *Kepler* field conducted prior to its launch. I go on to outline the rationale for the survey we chose to initiate, RATS-*Kepler*, which aimed to maximise the scientific impact of *Kepler* in the field of short period variable stars by matching its cadence and depth. Hence we aimed to find previously undetectable sources to be the subject of proposals for observation time by *Kepler* in short cadence mode.

In chapter 2 I discussed how we took the proven observation strategy developed during the RATS project and adapted it to fit the differing needs of the RATS-*Kepler*

survey. I then go on to discuss how the use of a new difference imaging package, `DIAPL2`, required the production of a new data reduction pipeline which I produced and which also offered significant speed improvements over the previous pipeline used in the RATS project.

In chapter 3 I discuss a number of variability algorithms and the adaptations I made to the algorithm used by Barclay et al. (2011) to make an improved selection of variable sources, which offered improved detection of quasi-periodic sources and significantly reduced the false positive selection rate.

The most significant changes I made were to change the number of sources upon which the selection was made and the rectification of an error in the code which lead to a high number of false positive selections at longer periods. I also removed the condition for a source to be selected by both the Analysis of Variance and Lomb-Scargle algorithms to be classed as variable, as I found that the Analysis of Variance algorithm did not recover a known pulsating white dwarf in RATS data and I felt that the slight increase in false positive selections caused by the removal of this algorithm, was outweighed by the benefit of the increased selection of quasi-periodic sources and the general versatility of the Lomb-Scargle algorithm used alone.

I chose to maintain the use of the median and MAD to select outliers in the period-FAP plane as I was satisfied with its ability to provide a relative measure of the variance in the FAP values in each 2 minute period bin. However, I feel that this aspect of the variable selection could be improved by attempting to use a statistical model which adequately models the distribution of FAP values, such that selected sources can be attributed a formal statistical significance. One such

option which I briefly explored was the use of gamma functions to model the spread of FAP values. As such I have passed on my findings to the latest student in our working group, Ruxandra Toma, who is working on OmegaWhite data and encouraged her to pursue this avenue to improve variable selection. I also feel that whilst the Lomb-Scargle algorithm performed adequately for the purposes of this survey, which was to select sources which merited further investigation rather than aiming to uniquely characterise objects; there is the possibility for improved variable selection via the exploration of the use of other variability algorithms either in tandem or instead of this, especially where the aim is to more stringently define the parameters of an object, an opinion I have also passed on to Ruxandra.

In Chapter 4 I have presented the short cadence observations of the 18 sources from the RATS-*Kepler* survey which were selected as suitable targets for short cadence observations - 11 δ-Scuti stars, a δ-Scuti star in a contact/eclipsing binary, a pulsating DA white dwarf, a cataclysmic variable, 3 contact/eclipsing binaries and an M dwarf flare star. Some preliminary analysis was also presented, along with a discussion of how these observations can be used to advance our knowledge in these areas. The unprecedented quality of the data obtained by *Kepler* and the unique parameter space probed by the RATS-*Kepler* survey offer tantalising opportunities which either cannot be matched by other observations, or which are only matched by a small number of other observations. In this respect, we have been successful in our aim of exploiting the unique opportunities for the study of short period variable stars by expanding the scope of the variety of sources observed by *Kepler* beyond that which were otherwise available. It is likely that the full potential of these observations (and all those made by *Kepler*)

will continue to unfold for years to come.

This work has lead to the following publications being made:

- "*Short-duration high-amplitude flares detected on the M dwarf star KIC 5474065*" Ramsay, G., Doyle, J. G., Hakala, P., Garcia-Alvarez, D., Brooks, A., Barclay, T., and Still, M.:; et al 2013, MNRAS 434, 2451

- "*KIC 10449976: discovery of an extreme helium subdwarf in the Kepler field*" Jeffrey, C.S., Ramsay, G., Naslim, N., Carrera, R., Greiss, S., Barclay, T., Karjalainen, R., Brooks, A., and Hakala, P.: 2013, MNRAS 429, 3207

- "*RATS-Kepler, a deep high-cadence survey of the Kepler field*" Ramsay, G., Brooks, A., Hakala, P., Barclay, T., Garcia-Alvarez, D., Antoci, V., Greiss, S., Still, M., Steeghs, D., Gänsicke, B., and Reynolds, M.: 2014, MNRAS 437, 132

- "*KIC 11911480: the second ZZ Ceti in the Kepler field*" Greiss, S., Gänsicke, B. T., Hermes, J. J., Steeghs, D., Koester, D., Ramsay, G., Barclay, T., and Townsley, D. M.: 2014, MNRAS; et al 2014

With *Kepler* unable to observe the *Kepler* field with sufficient accuracy with only two of its original four reaction wheels operational, the original *Kepler* mission was unfortunately forced to come to an end on 11^{th} May 2013. However, a new mission has been devised to keep *Kepler* advancing the forefronts of astronomy and astrophysics into the future, which will be discussed in the next chapter.

Chapter 6

Kepler - Past, Present and Future

6.1 *Kepler* - An Overview of the Initial Mission

The *Kepler* satellite has been carrying out it's initial mission since early 2009 until it lost a 2^{nd} reaction wheel, causing the telescope to enter an automatic prolonged safe-mode, with attempts to bring it back to normal operation ceasing in June 2013. During this time it had a duty cycle exceeding 90% (Prsa et al., 2014), as detailed schematically in Figure 6.1. The primary aim of the *Kepler* mission was to detect exoplanets via their transit of their host star (Borucki et al., 2010) and has succeeded in detecting 1,703 confirmed planets around 1,033 stars, including 442 multi-planetary systems[1] (refereed journal articles: Borucki et al. (2011a,b); Batalha et al. (2013); Rowe and Kepler Team (2014)), with the scale of this increase shown in Figure 6.2 and their distribution in orbital period and size shown in Figure 6.3; this number is set to grow even further as the data

[1]retrieved from http://exoplanetarchive.ipac.caltech.edu/index.html on 26^{th} April 2014.

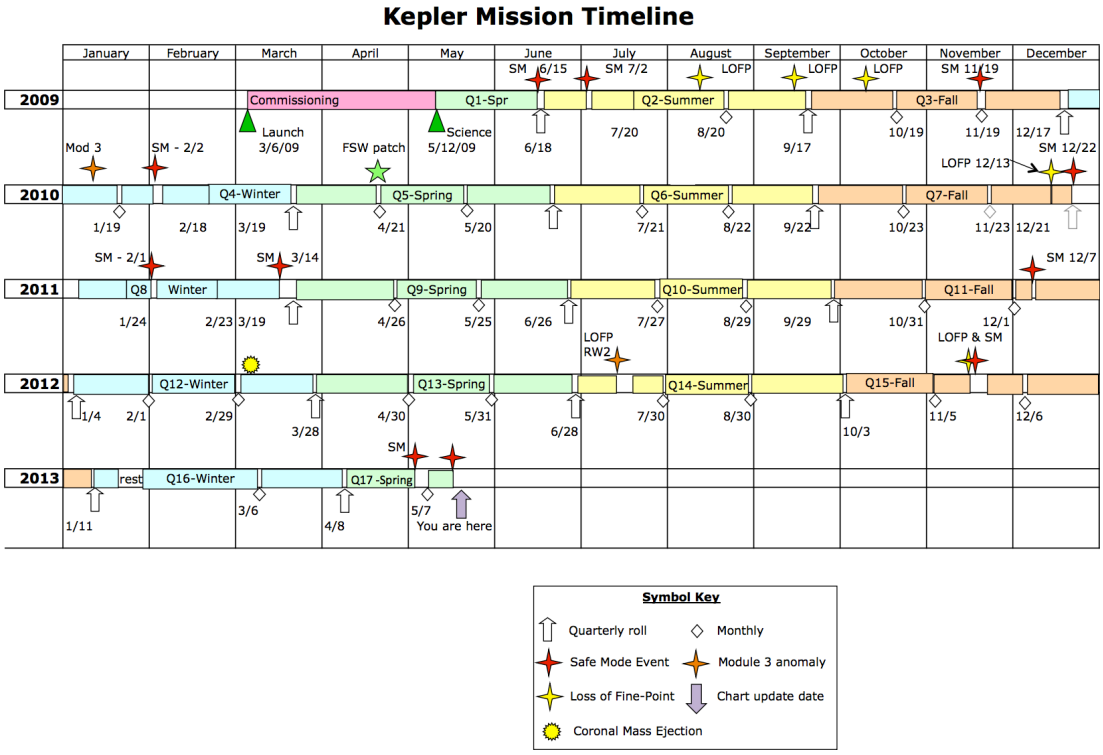

Figure 6.1: A schematic overview of the *Kepler* mission lifetime taken from *Kepler* data release 23, (Thompson et al., 2013).

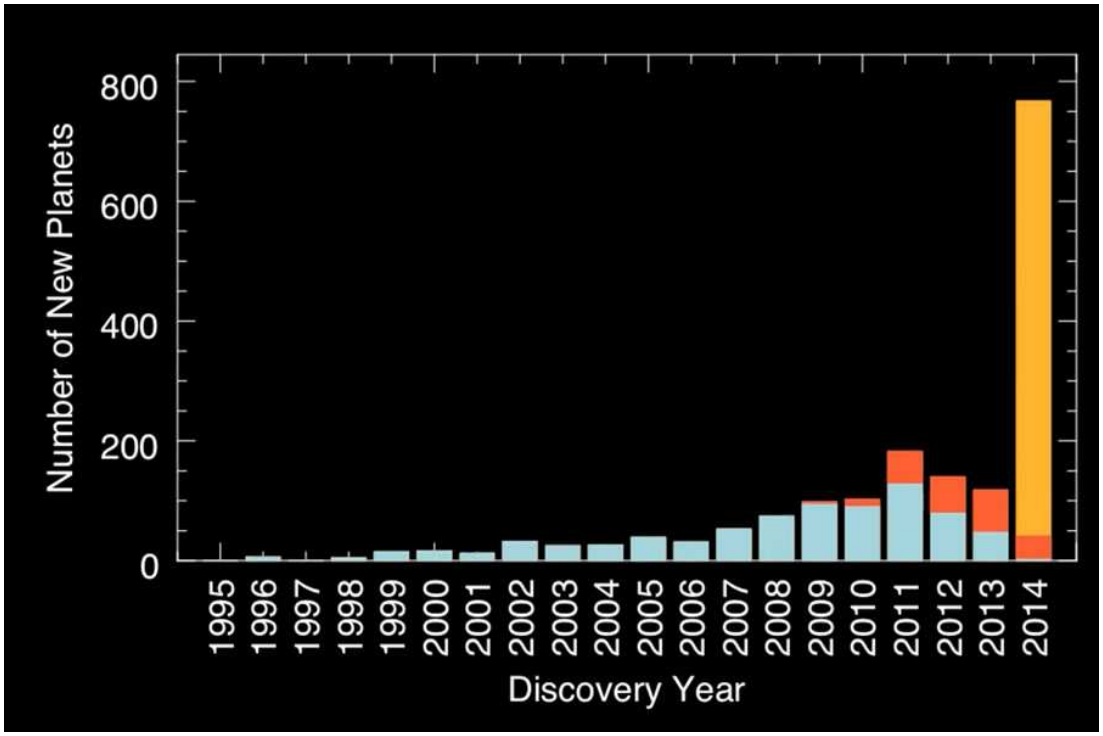

Figure 6.2: A histogram showing the number of exoplanet discoveries by year since 1995. The blue bar shows previous planet discoveries, the red bar shows previous *Kepler* planet discoveries, the gold bar displays the 715 new exoplanets in the most recent release of planetary candidates in February 2014 (Burke et al., 2014). Image taken from http://kepler.nasa.gov/news/nasakeplernews/index.cfm?FuseAction=ShowNews&NewsID=324 Image Credit: NASA Ames/SETI/J Rowe.

obtained continues to be mined. It has also found that multi-planetary systems with the planets orbiting in approximately the same plane, such as our own solar system, are commonplace and not the exception (e.g. Rowe et al. (2014)).

It also provided unprecedented opportunities for the study of variable stars, due to its continuous pointing and photometric precision of parts per million, with asteroseismology providing the means to probe the masses and compositions of stellar interiors; determine stellar internal rotation profiles; the extent of instability strips and therefore test models of stellar structure and evolution (e.g.

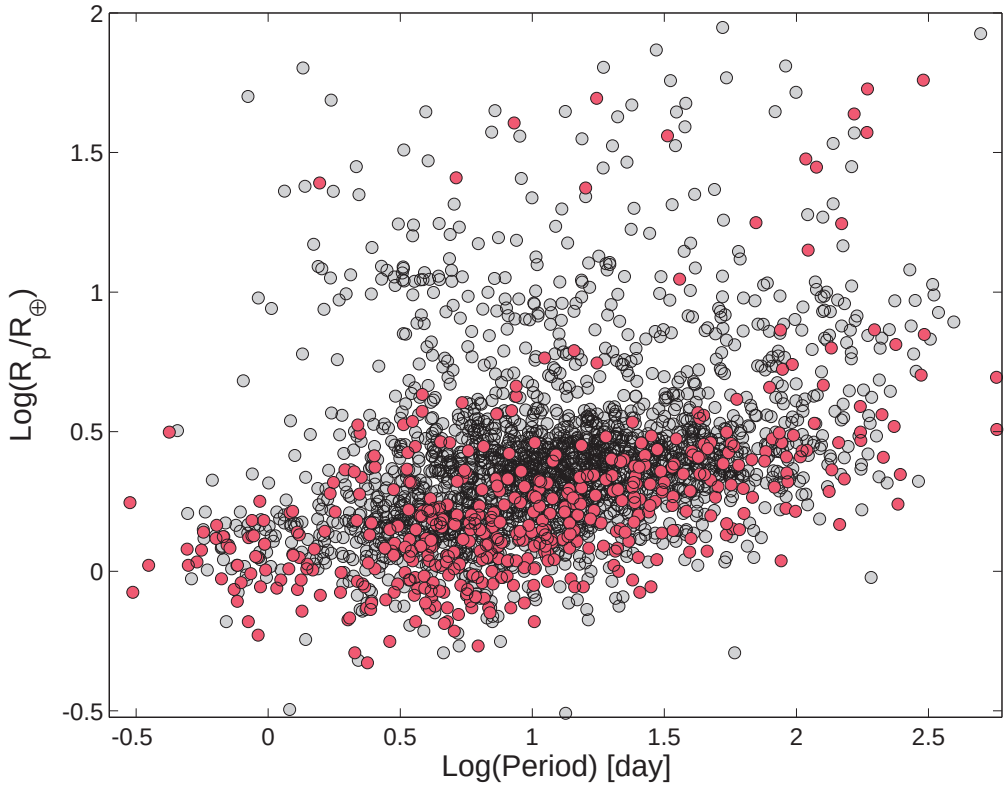

Figure 6.3: Resulting *Kepler* planet candidate radii relative to $R_\oplus$ from limb-darkened transit model fits for the most recent release of *Kepler* planet candidates (red points) and previously published *Kepler* planet candidates from Borucki et al. (2011a,b) and Batalha et al. (2013) (grey points) against orbital period. Note that both axes are on a log scale. Figure taken from Burke et al. (2014).

Chaplin et al. (2011)). It has lead to a wide range of exciting new results, such as those on main sequence B stars (Papics, 2013), solar-like oscillations in red giants (Gaulme et al., 2013), ensemble results on δ-Scuti stars (Uytterhoeven et al., 2011a), DB white dwarfs (Bischoff-Kim and Østensen, 2011a), DA white dwarfs (Hermes et al. (2011), Greiss et al. (2014)), to name but a few. Currently there are 432 refereed journal articles pertaining to exoplanets and 454 refereed journal articles pertaining to astrophysics related to the *Kepler* satellite[2]. With such a large treasure trove of high quality data having been obtained by *Kepler* in its initial mission phase, it will continue advancing the forefronts of astronomy and astrophysics into the future. With the spacecraft unable to keep sufficient pointing accuracy when observing the *Kepler* field with only 2 reaction wheels, it is sadly unable to continue with its initial mission profile. However, this does not mean that the spacecraft will have to be retired; a new mission has been devised so that the opportunites afforded by *Kepler* can continue to be utilised, as will be discussed in the next section.

6.2 *Kepler* - The Future and the K2 Mission

After *Kepler* could no longer continue with its original mission, a white paper call was issued to the community for ideas on how to utilise the *Kepler* satellite in a repurposed mission. The forerunner to come from this was the so called 'K2 mission' concept (Howell et al., 2014), which utilises the fact that pointing accuracy could be maintained in all three axes (Putnam and Wiemer, 2014) within

[2]Source: http://keplergo.arc.nasa.gov/PublicationsExoplanets.shtml and http://keplergo.arc.nasa.gov/PublicationsAstrophysics.shtml, accessed on 08/04/2014

+50° and −30° of its velocity vector in the orbital plane, which approximately corresponds to the ecliptic plane (Prsa et al., 2014). These limitations allow for *Kepler* to be able to point at the same field in the ecliptic plane for ∼83 days at a time, as shown in Figure 6.4, of which ∼75 days will be dedicated to science data collection, as shown in the campaign timeline schematic shown in Figure 6.5. In the proposed format the spacecraft has enough fuel to continue providing data for another 2–3 years.

The new mission concept has been submitted to NASA HQ and currently awaits approval in the 2014 Senior Review. Meanwhile the 1^{st} engineering observations using the new mission design concept were successfully obtained in October 2013, which proved it to be a viable science mission. The 1^{st} science run, dubbed 'campaign 0', began in March 2014, in a field close to the Galactic anti-centre, which includes M35 and NGC2304. The location of this field and those proposed for campaigns 0–9 are listed in Table 6.1 and shown in the ecliptic plane in Figure 6.6. Currently only the fields for campaigns 0 and 1 have been set, the rest are potentially subject to change depending on any community feedback or engineering needs.

With a slightly larger aperture required to perform aperture photometry in *Kepler's* new operational mode, only ∼10,000 targets will be observed at one time, rather than the >170,000 in the nominal mission (Howell et al., 2014), hence the amount of data obtained in a given campaign will be significantly less than was obtained in any one quarter in the nominal mission phase. If selected in the Senior Review, it is anticipated that *Kepler* will observe upwards of 40,000–80,000 targets during the first year across 4 different fields, with a potential to observe

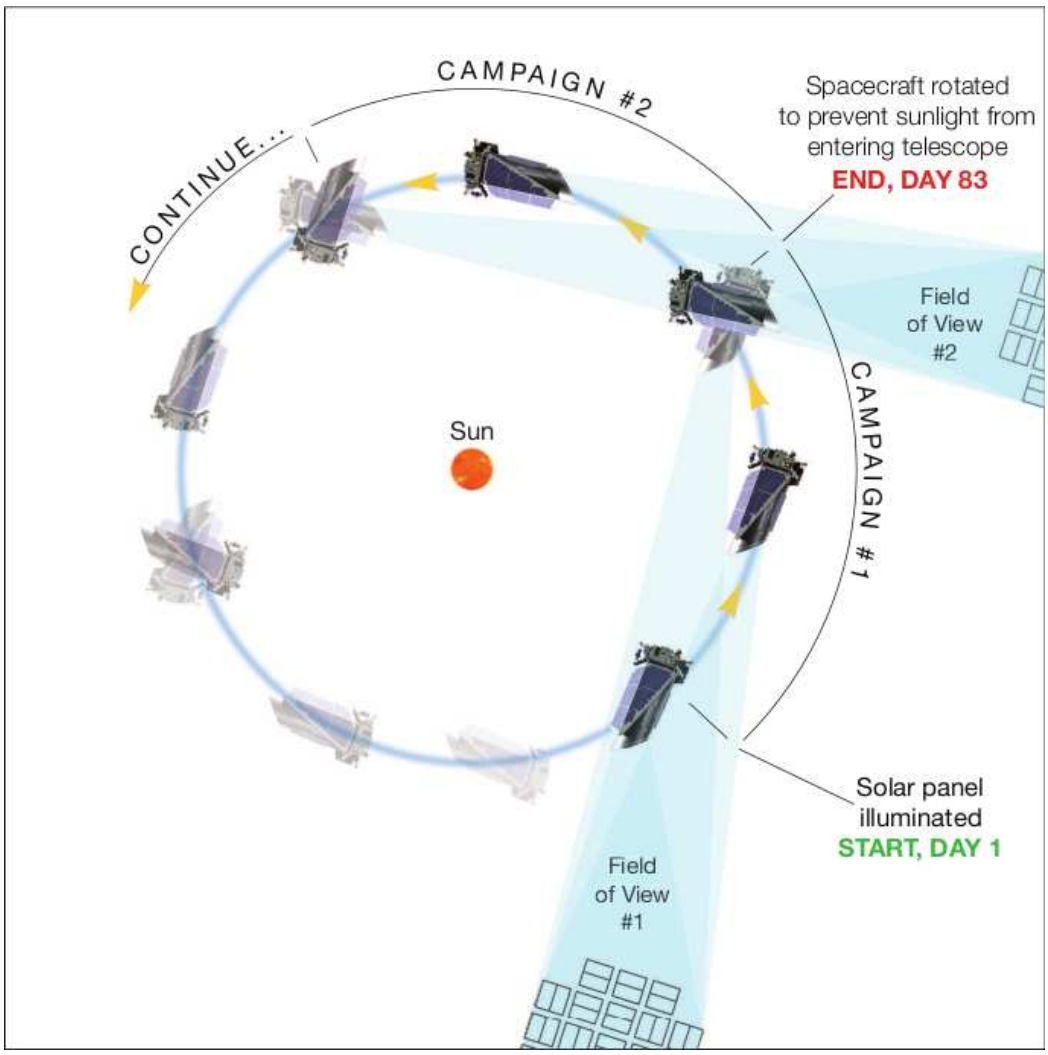

Figure 6.4: The K2 mission will observe sequential fields in the ecliptic plane for a duration of ∼83 days, where ∼75 days will be dedicated to science, as illustrated above. Figure taken from Howell et al. (2014).

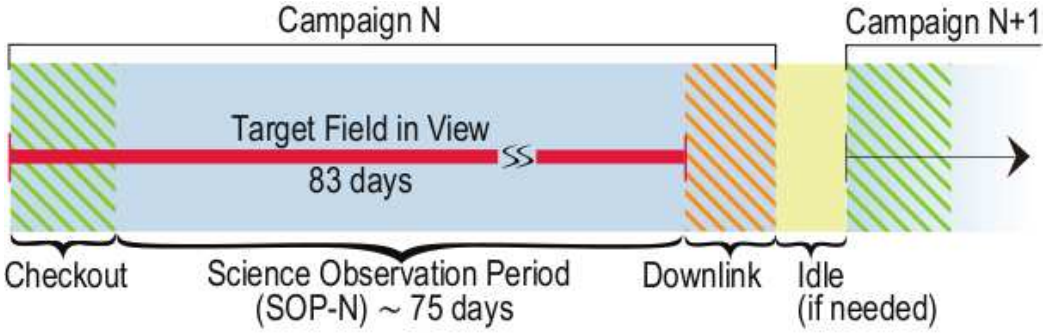

Figure 6.5: Schematic representation of a typical K2 campaign timeline, showing how each will provide a long, uninterrupted science observation period. An initial checkout period assures precise initial pointing, while all data are returned at the end of the campaign during an approximately 2-day downlink period. Idle time can be inserted between campaigns to allow flexibility in choosing the next field-of-view. Figure taken from Howell et al. (2014).

Table 6.1: Proposed K2 campaigns. At the time of writing, campaigns 0 and 1 have been set and the remaining campaigns are subject to change, depending on the engineering requirements and community feedback. Table taken from Prsa et al. (2014).

Campaign:	End Date:	Center α_{2000}	Center δ_{2000}	Comments:
0	2014-05-04	$06^{\rm h}\,46^{\rm m}\,59.58^{\rm s}$	$+21^\circ\,22'\,47.1''$	Near galactic anti-centre, M35, NGC2304
1	2014-07-23	$11^{\rm h}\,37^{\rm m}\,55.65^{\rm s}$	$+01^\circ\,11'\,19.7''$	North galactic cap
2	2014-10-14	$16^{\rm h}\,34^{\rm m}\,43.63^{\rm s}$	$-22^\circ\,48'\,49.0''$	Near galactic centre, M4, M80, M19
3	2015-01-05	$22^{\rm h}\,21^{\rm m}\,06.01^{\rm s}$	$-11^\circ\,36'\,59.4''$	South galactic cap, Neptune
4	2015-03-29	$03^{\rm h}\,45^{\rm m}\,59.04^{\rm s}$	$+18^\circ\,07'\,49.7''$	Pleiades (M45), Hyades, NGC1647
5	2015-06-20	$09^{\rm h}\,19^{\rm m}\,02.66^{\rm s}$	$+14^\circ\,11'\,41.0''$	Beehive (M44), M67
6	2015-09-11	$14^{\rm h}\,01^{\rm m}\,11.20^{\rm s}$	$-13^\circ\,16'\,02.8''$	North galactic cap
7	2015-12-03	$19^{\rm h}\,34^{\rm m}\,16.22^{\rm s}$	$-22^\circ\,38'\,23.4''$	Near galactic centre, NGC6717
8	2016-02-24	$01^{\rm h}\,04^{\rm m}\,43.18^{\rm s}$	$+05^\circ\,11'\,52.2''$	South galactic cap
9	2016-05-17	$18^{\rm h}\,23^{\rm m}\,35.72^{\rm s}$	$-24^\circ\,12'\,12.8''$	Galactic centre, Baade's window, M8

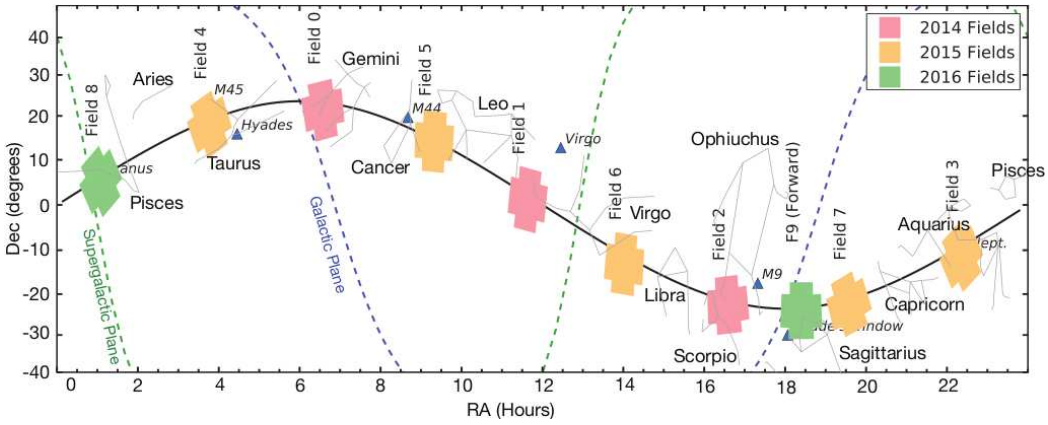

Figure 6.6: The K2 ecliptic observing field sequence was anchored by Field 4, which collects observations of the Pleiades and Hyades clusters in 2015 (see Table 6.1). Earlier and later fields march around the ecliptic in steps of 83 days as described in Figure 6.4. Field 9 is designed to observe along the spacecraft velocity vector (pointing toward the Earth), instead of the standard anti-velocity vector, to provide a unique K2 survey of Baade's window to be used for a microlensing study. This Earth-pointing orientation was chosen to allow simultaneous ground-based support. Figure taken from Howell et al. (2014).

$\sim$250,000 stars in total in its current proposed format (Prsa et al., 2014). K2 will do this in the same 58.89s short cadence and 29.4 minute long cadence modes as in its original mission and will produce 80ppm photometry for 12^{th} magnitude stars on 6 hour timescales (Howell et al., 2014). With the wide variety of stellar population distributions probed in this repurposed mission, it provides tantalising science opportunities across a wide range of science goals and looks set to continue in its legacy of advancing the forefronts of astronomy and astrophysics.

Bibliography

Alard, C. and Lupton, R. H.: 1998, ApJ **503**, 325

Alentiev, D., Kochukhov, O., Ryabchikova, T., Cunha, M., Tsymbal, V., and Weiss, W.: 2012, MNRAS **421**, L82

Amado, P. J., Moya, A., Suárez, J. C., Martín-Ruiz, S., Garrido, R., Rodríguez, E., Catala, C., and Goupil, M. J.: 2004, MNRAS **352**, L11

Andrews, A. D.: 1967, PASP **79**, 368

Antipin, S. V., Kolesnikova, D., Sat, L. A., Sokolovsky, K. V., and Korotkiy, S. A.: 2007, *Peremennye Zvezdy* **27**, 8

Antoci, V., Handler, G., Campante, T. L., Thygesen, A. O., Moya, A., Kallinger, T., Stello, D., Grigahcène, A., Kjeldsen, H., Bedding, T. R., Lüftinger, T., Christensen-Dalsgaard, J., Catanzaro, G., Frasca, A., De Cat, P., Uytterhoeven, K., Bruntt, H., Houdek, G., Kurtz, D. W., Lenz, P., Kaiser, A., van Cleve, J., Allen, C., and Clarke, B. D.: 2011, Nature **477**, 570

Antoci, V., Handler, G., Grundahl, F., Carrier, F., Brugamyer, E. J., Robertson, P., Kjeldsen, H., Kok, Y., Ireland, M., and Matthews, J. M.: 2013, MNRAS **435**, 1563

Astier, P., Guy, J., Regnault, N., Pain, R., Aubourg, E., Balam, D., Basa, S., Carlberg, R. G., Fabbro, S., Fouchez, D., Hook, I. M., Howell, D. A., Lafoux, H., Neill, J. D., Palanque-Delabrouille, N., Perrett, K., Pritchet, C. J., Rich, J., Sullivan, M., Taillet, R., Aldering, G., Antilogus, P., Arsenijevic, V., Balland, C., Baumont, S., Bronder, J., Courtois, H., Ellis, R. S., Filiol, M., Gonçalves, A. C., Goobar, A., Guide, D., Hardin, D., Lusset, V., Lidman, C., McMahon, R., Mouchet, M., Mourao, A., Perlmutter, S., Ripoche, P., Tao, C., and Walton, N.: 2006, A&A **447**, 31

Baker, N. and Kippenhahn, R.: 1962, ZAp **54**, 114

Baldry, I. K., Kurtz, D. W., and Bedding, T. R.: 1998, MNRAS **300**, L39

Baliunas, S. L., Donahue, R. A., Soon, W. H., Horne, J. H., Frazer, J., Woodard-Eklund, L., Bradford, M., Rao, L. M., Wilson, O. C., Zhang, Q., Bennett, W., Briggs, J., Carroll, S. M., Duncan, D. K., Figueroa, D., Lanning, H. H., Misch, T., Mueller, J., Noyes, R. W., Poppe, D., Porter, A. C., Robinson, C. R., Russell, J., Shelton, J. C., Soyumer, T., Vaughan, A. H., and Whitney, J. H.: 1995, ApJ **438**, 269

Balmforth, N. J., Cunha, M. S., Dolez, N., Gough, D. O., and Vauclair, S.: 2001, MNRAS **323**, 362

Baran, A. S., Gilker, J. T., Fox-Machado, L., Reed, M. D., and Kawaler, S. D.: 2011, MNRAS **411**, 776

Barclay, T.: 2011, *Ph.D. thesis*, Mullard Space Science Laboratory/Armagh Observatory

Barclay, T., Ramsay, G., Hakala, P., Napiwotzki, R., Nelemans, G., Potter, S., and Todd, I.: 2011, MNRAS **413**, 2696

Batalha, N. M., Rowe, J. F., Bryson, S. T., Barclay, T., Burke, C. J., Caldwell, D. A., Christiansen, J. L., Mullally, F., Thompson, S. E., Brown, T. M., Dupree, A. K., Fabrycky, D. C., Ford, E. B., Fortney, J. J., Gilliland, R. L., Isaacson, H., Latham, D. W., Marcy, G. W., Quinn, S. N., Ragozzine, D., Shporer, A., Borucki, W. J., Ciardi, D. R., Gautier, III, T. N., Haas, M. R., Jenkins, J. M., Koch, D. G., Lissauer, J. J., Rapin, W., Basri, G. S., Boss, A. P., Buchhave, L. A., Carter, J. A., Charbonneau, D., Christensen-Dalsgaard, J., Clarke, B. D., Cochran, W. D., Demory, B.-O., Desert, J.-M., Devore, E., Doyle, L. R., Esquerdo, G. A., Everett, M., Fressin, F., Geary, J. C., Girouard, F. R., Gould, A., Hall, J. R., Holman, M. J., Howard, A. W., Howell, S. B., Ibrahim, K. A., Kinemuchi, K., Kjeldsen, H., Klaus, T. C., Li, J., Lucas, P. W., Meibom, S., Morris, R. L., Prša, A., Quintana, E., Sanderfer, D. T., Sasselov, D., Seader, S. E., Smith, J. C., Steffen, J. H., Still, M., Stumpe, M. C., Tarter, J. C., Tenenbaum, P., Torres, G., Twicken, J. D., Uddin, K., Van Cleve, J., Walkowicz, L., and Welsh, W. F.: 2013, ApJS **204**, 24

Batyrshinova, V. M. and Ibragimov, M. A.: 2001, *Astronomy Letters* **27**, 29

Beauchamp, A., Wesemael, F., Bergeron, P., Fontaine, G., Saffer, R. A., Liebert, J., and Brassard, P.: 1999, ApJ **516**, 887

Bertin, E. and Arnouts, S.: 1996, A&AS **117**, 393

Bigot, L., Provost, J., Berthomieu, G., Dziembowski, W. A., and Goode, P. R.: 2000, A&A **356**, 218

Bischoff-Kim, A. and Østensen, R. H.: 2011a, ApJ **742**, L16

Bischoff-Kim, A. and Østensen, R. H.: 2011b, ApJ **742**, L16

Boas, M. L.: 2006, *Mathematical Methods in the Physical Sciences, 3rd edition*, John Wiley & Sons, Inc

Bochanski, J. J., Munn, J. A., Hawley, S. L., West, A. A., Covey, K. R., and Schneider, D. P.: 2007, AJ **134**, 2418

Bopp, B. W. and Moffett, T. J.: 1973, ApJ **185**, 239

Borucki, W. J., Koch, D., Basri, G., Batalha, N., Brown, T., Caldwell, D., Caldwell, J., Christensen-Dalsgaard, J., Cochran, W. D., DeVore, E., Dunham, E. W., Dupree, A. K., Gautier, T. N., Geary, J. C., Gilliland, R., Gould, A., Howell, S. B., Jenkins, J. M., Kondo, Y., Latham, D. W., Marcy, G. W., Meibom, S., Kjeldsen, H., Lissauer, J. J., Monet, D. G., Morrison, D., Sasselov, D., Tarter, J., Boss, A., Brownlee, D., Owen, T., Buzasi, D., Charbonneau, D., Doyle, L., Fortney, J., Ford, E. B., Holman, M. J., Seager, S., Steffen, J. H., Welsh, W. F., Rowe, J., Anderson, H., Buchhave, L., Ciardi, D., Walkowicz, L., Sherry, W., Horch, E., Isaacson, H., Everett, M. E., Fischer, D., Torres, G., Johnson, J. A., Endl, M., MacQueen, P., Bryson, S. T., Dotson, J., Haas, M., Kolodziejczak, J., Van Cleve, J., Chandrasekaran, H., Twicken, J. D., Quintana, E. V., Clarke, B. D., Allen, C., Li, J., Wu, H., Tenenbaum, P., Verner, E., Bruhweiler, F., Barnes, J., and Prsa, A.: 2010, *Science* **327**, 977

Borucki, W. J., Koch, D. G., Basri, G., Batalha, N., Boss, A., Brown, T. M., Caldwell, D., Christensen-Dalsgaard, J., Cochran, W. D., DeVore, E., Dunham, E. W., Dupree, A. K., Gautier, III, T. N., Geary, J. C., Gilliland, R., Gould, A., Howell, S. B., Jenkins, J. M., Kjeldsen, H., Latham, D. W., Lissauer, J. J., Marcy, G. W., Monet, D. G., Sasselov, D., Tarter, J., Charbonneau, D., Doyle, L., Ford, E. B., Fortney, J., Holman, M. J., Seager, S., Steffen, J. H., Welsh, W. F., Allen, C., Bryson, S. T., Buchhave, L., Chandrasekaran, H., Christiansen, J. L., Ciardi, D., Clarke, B. D., Dotson, J. L., Endl, M., Fischer, D., Fressin, F., Haas, M., Horch, E., Howard, A., Isaacson, H., Kolodziejczak, J., Li, J., MacQueen, P., Meibom, S., Prsa, A., Quintana, E. V., Rowe, J., Sherry, W., Tenenbaum, P., Torres, G., Twicken, J. D., Van Cleve, J., Walkowicz, L., and Wu, H.: 2011a, ApJ **728**, 117

Borucki, W. J., Koch, D. G., Basri, G., Batalha, N., Brown, T. M., Bryson, S. T., Caldwell, D., Christensen-Dalsgaard, J., Cochran, W. D., DeVore, E., Dunham, E. W., Gautier, III, T. N., Geary, J. C., Gilliland, R., Gould, A., Howell, S. B., Jenkins, J. M., Latham, D. W., Lissauer, J. J., Marcy, G. W., Rowe, J., Sasselov, D., Boss, A., Charbonneau, D., Ciardi, D., Doyle, L., Dupree, A. K., Ford, E. B., Fortney, J., Holman, M. J., Seager, S., Steffen, J. H., Tarter, J., Welsh, W. F., Allen, C., Buchhave, L. A., Christiansen, J. L., Clarke, B. D., Das, S., Désert, J.-M., Endl, M., Fabrycky, D., Fressin, F., Haas, M., Horch, E., Howard, A., Isaacson, H., Kjeldsen, H., Kolodziejczak, J., Kulesa, C., Li, J., Lucas, P. W., Machalek, P., McCarthy, D., MacQueen, P., Meibom, S., Miquel, T., Prsa, A., Quinn, S. N., Quintana, E. V., Ragozzine, D., Sherry, W., Shporer, A., Tenenbaum, P., Torres, G., Twicken, J. D., Van

Cleve, J., Walkowicz, L., Witteborn, F. C., and Still, M.: 2011b, ApJ **736**, 19

Bradley, P. A. and Winget, D. E.: 1994, ApJ **430**, 850

Brahe, T. and Kepler, J.: 1602, *Tychonis Brahe Astronomiae instauratae progymnasmata : quorum haec prima pars de restitutione motuum SOLIS et lunae stellarumque inerrantium tractat, et praeterea de admiranda nova stella anno 1572 exorta luculenter agit.*

Brassard, P., Fontaine, G., Wesemael, F., and Tassoul, M.: 1992, ApJS **81**, 747

Brecher, K., Fesen, R. A., Maran, S. P., and Brandt, J. C.: 1983, *The Observatory* **103**, 106

Breedt, E., Gänsicke, B. T., Marsh, T. R., Steeghs, D., Drake, A. J., and Copperwheat, C. M.: 2012, MNRAS **425**, 2548

Breger, M.: 1979, PASP **91**, 5

Breger, M. and Montgomery, M. (eds.): 2000, *Delta Scuti and Related Stars*, Vol. 210 of *Astronomical Society of the Pacific Conference Series*

Brickhill, A. J.: 1992, MNRAS **259**, 529

Brown, T. M., Latham, D. W., Everett, M. E., and Esquerdo, G. A.: 2011a, AJ **142**, 112

Brown, T. M., Latham, D. W., Everett, M. E., and Esquerdo, G. A.: 2011b, AJ **142**, 112

Brown, W. R., Kilic, M., Hermes, J. J., Allende Prieto, C., Kenyon, S. J., and Winget, D. E.: 2011c, ApJ **737**, L23

Budding, E., Erdem, A., Çiçek, C., Bulut, I., Soydugan, F., Soydugan, E., Bakiş, V., and Demircan, O.: 2004, A&A **417**, 263

Burke, C. J., Bryson, S. T., Mullally, F., Rowe, J. F., Christiansen, J. L., Thompson, S. E., Coughlin, J. L., Haas, M. R., Batalha, N. M., Caldwell, D. A., Jenkins, J. M., Still, M., Barclay, T., Borucki, W. J., Chaplin, W. J., Ciardi, D. R., Clarke, B. D., Cochran, W. D., Demory, B.-O., Esquerdo, G. A., Gautier, III, T. N., Gilliland, R. L., Girouard, F. R., Havel, M., Henze, C. E., Howell, S. B., Huber, D., Latham, D. W., Li, J., Morehead, R. C., Morton, T. D., Pepper, J., Quintana, E., Ragozzine, D., Seader, S. E., Shah, Y., Shporer, A., Tenenbaum, P., Twicken, J. D., and Wolfgang, A.: 2014, ApJS **210**, 19

Byrne, P. B., Doyle, J. G., Butler, C. J., and Andrews, A. D.: 1984, MNRAS **211**, 607

Byrne, P. B., Doyle, J. G., and Menzies, J. W.: 1985, MNRAS **214**, 119

Cameron, C., Matthews, J. M., Rowe, J. F., Kuschnig, R., Guenther, D. B., Moffat, A. F. J., Rucinski, S. M., Sasselov, D., Walker, G. A. H., and Weiss, W. W.: 2006, *Communications in Asteroseismology* **148**, 57

Campbell, L. C., J. L.: 1946, *The Harvard books of astronomy - The Story of Variable Stars*

Cannizzo, J. K., Smale, A. P., Wood, M. A., Still, M. D., and Howell, S. B.: 2012, ApJ **747**, 117

Carrington, R. C.: 1859, MNRAS **19**, 81

Carter, P. J., Steeghs, D., de Miguel, E., Goff, W., Koff, R. A., Krajci, T., Marsh, T. R., Gänsicke, B. T., Breedt, E., Groot, P. J., Nelemans, G., Roelofs, G. H. A., Rau, A., Koester, D., and Kupfer, T.: 2013, MNRAS **431**, 372

Cepa, J., Aguiar, M., Bland-Hawthorn, J., Castañeda, H. O., Cobos, F., Correa, S., Espejo, C., Fragoso, A. B., Fuentes, J., Gigante, J. V., González, J. J., González-Escalera, V., González-Serrano, I., Joven, E., López, J. C., Militello, C., Peraza, L., Pérez, A., Pérez, J., Rasilla, J. L., Sánchez, B., and Tejada, C.: 2003, in J. M. Rodriguez Espinoza, F. Garzon Lopez, and V. Melo Martin (eds.), *Revista Mexicana de Astronomia y Astrofisica Conference Series*, Vol. 16 of *Revista Mexicana de Astronomia y Astrofisica Conference Series*, pp 13–18

Chanmugam, G.: 1972, *Nature Physical Science* **236**, 83

Chaplin, W. J., Kjeldsen, H., Christensen-Dalsgaard, J., Basu, S., Miglio, A., Appourchaux, T., Bedding, T. R., Elsworth, Y., García, R. A., Gilliland, R. L., Girardi, L., Houdek, G., Karoff, C., Kawaler, S. D., Metcalfe, T. S., Molenda-Żakowicz, J., Monteiro, M. J. P. F. G., Thompson, M. J., Verner, G. A., Ballot, J., Bonanno, A., Brandão, I. M., Broomhall, A.-M., Bruntt, H., Campante, T. L., Corsaro, E., Creevey, O. L., Doğan, G., Esch, L., Gai, N., Gaulme, P., Hale, S. J., Handberg, R., Hekker, S., Huber, D., Jiménez, A., Mathur, S., Mazumdar, A., Mosser, B., New, R., Pinsonneault, M. H., Pricopi, D., Quirion, P.-O., Régulo, C., Salabert, D., Serenelli, A. M., Silva Aguirre, V., Sousa, S. G., Stello, D., Stevens, I. R., Suran, M. D., Uytterhoeven, K., White, T. R., Borucki, W. J., Brown, T. M., Jenkins, J. M., Kinemuchi, K., Van Cleve, J., and Klaus, T. C.: 2011, *Science* **332**, 213

Charbonneau, D., Brown, T. M., Latham, D. W., and Mayor, M.: 2000, ApJ **529**, L45

Charpinet, S., Fontaine, G., and Brassard, P.: 2001, PASP **113**, 775

Charpinet, S., Fontaine, G., Brassard, P., and Chayer, P.: 2008, *Communications in Asteroseismology* **157**, 168

Charpinet, S., Fontaine, G., Brassard, P., Chayer, P., Green, E. M., and Randall, S. K.: 2007, *Communications in Asteroseismology* **150**, 241

Charpinet, S., Fontaine, G., Brassard, P., Chayer, P., Rogers, F. J., Iglesias, C. A., and Dorman, B.: 1997, ApJ **483**, L123

Charpinet, S., Fontaine, G., Brassard, P., and Dorman, B.: 1996, ApJ **471**, L103

Chayer, P., Fontaine, G., and Wesemael, F.: 1995, ApJS **99**, 189

Chugainov, P. F.: 1974, *Izvestiya Ordena Trudovogo Krasnogo Znameni Krymskoj Astrofizicheskoj Observatorii* **52**, 3

Clark, D. H. and Stephenson, F. R.: 1982, in M. J. Rees and R. J. Stoneham (eds.), *NATO ASIC Proc. 90: Supernovae: A Survey of Current Research*, pp 355–370

Collins, II, G. W., Claspy, W. P., and Martin, J. C.: 1999, PASP **111**, 871

Cox, J. P.: 1980, *Theory of Stellar Pulsation*

Cunha, M. S.: 2002, MNRAS **333**, 47

Cunha, M. S.: 2006, MNRAS **365**, 153

Dal, H. A.: 2011, PASA **28**, 365

Dal, H. A.: 2012, PASJ **64**, 82

Dal, H. A. and Evren, S.: 2010, AJ **140**, 483

Dal, H. A. and Evren, S.: 2011, PASP **123**, 659

Devor, J.: 2005, ApJ **628**, 411

Djorgovski, S. G., Baltay, C., Mahabal, A. A., Drake, A. J., Williams, R., Rabinowitz, D., Graham, M. J., Donalek, C., Glikman, E., Bauer, A., Scalzo, R., and Ellman, N.: 2008, *Astronomische Nachrichten* **329**, 263

Donati, J.-F., Moutou, C., Farès, R., Bohlender, D., Catala, C., Deleuil, M., Shkolnik, E., Collier Cameron, A., Jardine, M. M., and Walker, G. A. H.: 2008, MNRAS **385**, 1179

Donoho, D. and Huber, P. J.: 1983, *The notion of breakdown point*, pp 157–184, Wadsworth Statist./Probab. Ser., Wadsworth, Belmont, CA

Dorman, B., Rood, R. T., and O'Connell, R. W.: 1993, ApJ **419**, 596

Doyle, J. G. and Butler, C. J.: 1985, Nature **313**, 378

Doyle, J. G., Butler, C. J., and van den Oord, G. H. J.: 1989, A&A **208**, 208

Doyle, J. G., Butler, C. J., van den Oord, G. H. J., and Kiang, T.: 1990, A&A **232**, 83

Doyle, J. G. and Byrne, P. B.: 1986, A&A **154**, 370

Doyle, J. G., Byrne, P. B., and Butler, C. J.: 1986, A&A **156**, 283

Drake, A. J., Djorgovski, S. G., Mahabal, A., Beshore, E., Larson, S., Graham, M. J., Williams, R., Christensen, E., Catelan, M., Boattini, A., Gibbs, A., Hill, R., and Kowalski, R.: 2009, ApJ **696**, 870

Drew, J. E., Greimel, R., Irwin, M. J., Aungwerojwit, A., Barlow, M. J., Corradi, R. L. M., Drake, J. J., Gänsicke, B. T., Groot, P., Hales, A., Hopewell, E. C., Irwin, J., Knigge, C., Leisy, P., Lennon, D. J., Mampaso, A., Masheder, M. R. W., Matsuura, M., Morales-Rueda, L., Morris, R. A. H., Parker, Q. A., Phillipps, S., Rodriguez-Gil, P., Roelofs, G., Skillen, I., Sokoloski, J. L., Steeghs, D., Unruh, Y. C., Viironen, K., Vink, J. S., Walton, N. A., Witham, A., Wright, N., Zijlstra, A. A., and Zurita, A.: 2005, MNRAS **362**, 753

Dufour, P., Fontaine, G., Liebert, J., Schmidt, G. D., and Behara, N.: 2008, ApJ **683**, 978

Dufour, P., Liebert, J., Fontaine, G., and Behara, N.: 2007, Nature **450**, 522

Dupret, M.-A., Grigahcène, A., Garrido, R., Gabriel, M., and Noel, A.: 2004, in D. Danesy (ed.), *SOHO 14 Helio- and Asteroseismology: Towards a Golden Future*, Vol. 559 of *ESA Special Publication*, p. 408

Dupret, M.-A., Théado, S., and Noels, A.: 2008, *Journal of Physics Conference Series* **118(1)**, 012052

Duquennoy, A. and Mayor, M.: 1991, A&A **248**, 485

Dziembowski, W. and Krolikowska, M.: 1990, Acta Astron. **40**, 19

Dziembowski, W. A. and Goode, P. R.: 1996, ApJ **458**, 338

Eaton, N., Draper, P., and Allan, A.: 2009, *Starlink User Note, 45*

Everett, M. E., Howell, S. B., and Kinemuchi, K.: 2012a, PASP **124**, 316

Everett, M. E., Howell, S. B., and Kinemuchi, K.: 2012b, PASP **124**, 316

Faulkner, J.: 1971, ApJ **170**, L99

Feldmeier, J. J., Howell, S. B., Sherry, W., von Braun, K., Everett, M. E., Ciardi, D. R., Harding, P., Mihos, J. C., Rudick, C. S., Lee, T.-H., Kutsko, R. M., and van Belle, G. T.: 2011, *The Burrell-Optical-Kepler-Survey (BOKS). I. Survey Description and Initial Results*

Fontaine, G. and Brassard, P.: 2008, PASP **120**, 1043

Fontaine, G., Brassard, P., and Bergeron, P.: 2001, PASP **113**, 409

Fontaine, G., Brassard, P., Charpinet, S., and Chayer, P.: 2006, Mem. Soc. Astron. Italiana **77**, 49

Fontaine, G., Brassard, P., Charpinet, S., Green, E. M., Chayer, P., Billères, M., and Randall, S. K.: 2003, ApJ **597**, 518

Fontaine, G., Brassard, P., and Dufour, P.: 2008, A&A **483**, L1

Fontaine, G. and van Horn, H. M.: 1976, ApJS **31**, 467

Fridlund, M.: 2007, in *European Planetary Science Congress 2007*, p. 807

Frieman, J. A., Bassett, B., Becker, A., Choi, C., Cinabro, D., DeJongh, F., Depoy, D. L., Dilday, B., Doi, M., Garnavich, P. M., Hogan, C. J., Holtzman, J., Im, M., Jha, S., Kessler, R., Konishi, K., Lampeitl, H., Marriner, J.,

Marshall, J. L., McGinnis, D., Miknaitis, G., Nichol, R. C., Prieto, J. L., Riess, A. G., Richmond, M. W., Romani, R., Sako, M., Schneider, D. P., Smith, M., Takanashi, N., Tokita, K., van der Heyden, K., Yasuda, N., Zheng, C., Adelman-McCarthy, J., Annis, J., Assef, R. J., Barentine, J., Bender, R., Blandford, R. D., Boroski, W. N., Bremer, M., Brewington, H., Collins, C. A., Crotts, A., Dembicky, J., Eastman, J., Edge, A., Edmondson, E., Elson, E., Eyler, M. E., Filippenko, A. V., Foley, R. J., Frank, S., Goobar, A., Gueth, T., Gunn, J. E., Harvanek, M., Hopp, U., Ihara, Y., Ivezić, Ž., Kahn, S., Kaplan, J., Kent, S., Ketzeback, W., Kleinman, S. J., Kollatschny, W., Kron, R. G., Krzesiński, J., Lamenti, D., Leloudas, G., Lin, H., Long, D. C., Lucey, J., Lupton, R. H., Malanushenko, E., Malanushenko, V., McMillan, R. J., Mendez, J., Morgan, C. W., Morokuma, T., Nitta, A., Ostman, L., Pan, K., Rockosi, C. M., Romer, A. K., Ruiz-Lapuente, P., Saurage, G., Schlesinger, K., Snedden, S. A., Sollerman, J., Stoughton, C., Stritzinger, M., Subba Rao, M., Tucker, D., Vaisanen, P., Watson, L. C., Watters, S., Wheeler, J. C., Yanny, B., and York, D.: 2008, AJ **135**, 338

Galilei, G.: 1635, *Systema cosmicvm, authore Galilaeo Galilaei ... ; in quo qvatvor dialogis, de duobus maximis mundi systematibus, Ptolemaico & Copernicano, vtriusq; rationibus philosophicis AC naturalibus indefinite propositis disseritur : EX italica lingua latine conuersum : accessit appendix gemina, qua SS. Scripturae dicta cum terrae mobilitate conciliantur .. ..*

Galilei, G.: 1953, *Dialogue concerning the two chief world systems, Ptolemaic & Copernican*

Galilei, G., Welser, M., and de Filiis, A.: 1613, *Istoria E dimostrazioni intorno alle macchie solari E loro accidenti comprese in tre lettere scritte all'illvstrissimo signor Marco Velseri*

Gänsicke, B. T.: 2005, in J.-M. Hameury and J.-P. Lasota (eds.), *The Astrophysics of Cataclysmic Variables and Related Objects*, Vol. 330 of *Astronomical Society of the Pacific Conference Series*, p. 3

Gänsicke, B. T., Dillon, M., Southworth, J., Thorstensen, J. R., Rodríguez-Gil, P., Aungwerojwit, A., Marsh, T. R., Szkody, P., Barros, S. C. C., Casares, J., de Martino, D., Groot, P. J., Hakala, P., Kolb, U., Littlefair, S. P., Martínez-Pais, I. G., Nelemans, G., and Schreiber, M. R.: 2009, MNRAS **397**, 2170

Gänsicke, B. T., Hagen, H.-J., and Engels, D.: 2002, in B. T. Gänsicke, K. Beuermann, and K. Reinsch (eds.), *The Physics of Cataclysmic Variables and Related Objects*, Vol. 261 of *Astronomical Society of the Pacific Conference Series*, p. 190

Gaulme, P., McKeever, J., Rawls, M. L., Jackiewicz, J., Mosser, B., and Guzik, J. A.: 2013, ApJ **767**, 82

Gershberg, R. E. and Shakhovskaia, N. I.: 1983, Ap&SS **95**, 235

Gianninas, A., Bergeron, P., and Ruiz, M. T.: 2011, ApJ **743**, 138

Green, E. M., Fontaine, G., Reed, M. D., Callerame, K., Seitenzahl, I. R., White, B. A., Hyde, E. A., Østensen, R., Cordes, O., Brassard, P., Falter, S., Jeffery, E. J., Dreizler, S., Schuh, S. L., Giovanni, M., Edelmann, H., Rigby, J., and Bronowska, A.: 2003, ApJ **583**, L31

Greiss, S., Gänsicke, B. T., Hermes, J. J., Steeghs, D., Koester, D., Ramsay, G., Barclay, T., and Townsley, D. M.: 2014, MNRAS

Greiss, S., Steeghs, D., Gänsicke, B. T., Martín, E. L., Groot, P. J., Irwin, M. J., González-Solares, E., Greimel, R., Knigge, C., Østensen, R. H., Verbeek, K., Drew, J. E., Drake, J., Jonker, P. G., Ripepi, V., Scaringi, S., Southworth, J., Still, M., Wright, N. J., Farnhill, H., van Haaften, L. M., and Shah, S.: 2012a, AJ **144**, 24

Greiss, S., Steeghs, D. T. H., Gänsicke, B. T., Martín, E. L., Groot, P. J., Irwin, M. J., González-Solares, E., Greimel, R., Gentile Fusillo, N. P., Still, M., and the KIS collaboration: 2012b, *ArXiv e-prints*

Groot, P. J., Verbeek, K., Greimel, R., Irwin, M., González-Solares, E., Gänsicke, B. T., de Groot, E., Drew, J., Augusteijn, T., Aungwerojwit, A., Barlow, M., Barros, S., van den Besselaar, E. J. M., Casares, J., Corradi, R., Corral-Santana, J. M., Deacon, N., van Ham, W., Hu, H., Heber, U., Jonker, P. G., King, R., Knigge, C., Mampaso, A., Marsh, T. R., Morales-Rueda, L., Napiwotzki, R., Naylor, T., Nelemans, G., Oosting, T., Pyrzas, S., Pretorius, M., Rodríguez-Gil, P., Roelofs, G. H. A., Sale, S., Schellart, P., Steeghs, D., Szyszka, C., Unruh, Y., Walton, N. A., Weston, S., Witham, A., Woudt, P., and Zijlstra, A.: 2009, MNRAS **399**, 323

Groot, P. J., Vreeswijk, P. M., Huber, M. E., Everett, M. E., Howell, S. B., Nelemans, G., van Paradijs, J., van den Heuvel, E. P. J., Augusteijn, T., Kuulkers, E., Rutten, R. G. M., and Storm, J.: 2003, MNRAS **339**, 427

Gutiérrez-Soto, J., Fabregat, J., Suso, J., Lanzara, M., Garrido, R., Hubert, A.-M., and Floquet, M.: 2007, A&A **476**, 927

Haisch, B., Strong, K. T., and Rodono, M.: 1991, ARA&A **29**, 275

Hambleton, K. M., Kurtz, D. W., Prša, A., Guzik, J. A., Pavlovski, K., Bloemen, S., Southworth, J., Conroy, K., Littlefair, S. P., and Fuller, J.: 2013, MNRAS **434**, 925

Hampel, F. R.: 1974, **69(346)**, 383

Han, Z., Podsiadlowski, P., Maxted, P. F. L., and Marsh, T. R.: 2003, MNRAS **341**, 669

Han, Z., Podsiadlowski, P., Maxted, P. F. L., Marsh, T. R., and Ivanova, N.: 2002, MNRAS **336**, 449

Handler, G. and Shobbrook, R. R.: 2002, MNRAS **333**, 251

Hartman, J. D., Bakos, G., Stanek, K. Z., and Noyes, R. W.: 2004, AJ **128**, 1761

Hartman, J. D., Gaudi, B. S., Holman, M. J., McLeod, B. A., Stanek, K. Z., Barranco, J. A., Pinsonneault, M. H., and Kalirai, J. S.: 2008, ApJ **675**, 1254

Hawley, S. L., Kowalski, A. F., Wisniewski, J. P., Hilton, E. J., Walkowicz, L. M., and Brown, A.: 2011, in *American Astronomical Society Meeting Abstracts*, p. 227.05

Hawley, S. L., Panov, K. P., Pettersen, B. R., and Sundland, S. R.: 1989, A&A **220**, 218

Hawley, S. L. and Pettersen, B. R.: 1991, ApJ **378**, 725

Heber, U.: 1986, A&A **155**, 33

Henry, G. W., Marcy, G. W., Butler, R. P., and Vogt, S. S.: 2000, ApJ **529**, L41

Hermes, J. J., Montgomery, M. H., Winget, D. E., Brown, W. R., Kilic, M., and Kenyon, S. J.: 2012, ApJ **750**, L28

Hermes, J. J., Mullally, F., Østensen, R. H., Williams, K. A., Telting, J., Southworth, J., Bloemen, S., Howell, S. B., Everett, M., and Winget, D. E.: 2011, ApJ **741**, L16

Hoffmeister, C.: 1967, *Astronomische Nachrichten* **289**, 205

Horne, J. H. and Baliunas, S. L.: 1986, ApJ **302**, 757

Howell, S. B., Everett, M. E., Seebode, S. A., Szkody, P., Still, M., Wood, M., Ramsay, G., Cannizzo, J., and Smale, A.: 2013, AJ **145**, 109

Howell, S. B., Nelson, L. A., and Rappaport, S.: 2001, ApJ **550**, 897

Howell, S. B., Sobeck, C., Haas, M., Still, M., Barclay, T., Mullally, F., Troeltzsch, J., Aigrain, S., Bryson, S. T., Caldwell, D., Chaplin, W. J., Cochran, W. D., Huber, D., Marcy, G. W., Miglio, A., Najita, J. R., Smith, M., Twicken, J. D., and Fortney, J. J.: 2014, *ArXiv e-prints*

Hu, H., Dupret, M.-A., Aerts, C., Nelemans, G., Kawaler, S. D., Miglio, A., Montalban, J., and Scuflaire, R.: 2008, A&A **490**, 243

Hu, H., Nelemans, G., Aerts, C., and Dupret, M.-A.: 2009, A&A **508**, 869

Huber, P. J.: 1981, *Robust statistics*, John Wiley

Hunt-Walker, N. M., Hilton, E. J., Kowalski, A. F., Hawley, S. L., and Matthews, J. M.: 2012, PASP **124**, 545

Ivezic, Z., Tyson, J. A., Acosta, E., Allsman, R., Anderson, S. F., Andrew, J., Angel, R., Axelrod, T., Barr, J. D., Becker, A. C., Becla, J., Beldica, C., Blandford, R. D., Bloom, J. S., Borne, K., Brandt, W. N., Brown, M. E., Bullock, J. S., Burke, D. L., Chandrasekharan, S., Chesley, S., Claver, C. F., Connolly, A., Cook, K. H., Cooray, A., Covey, K. R., Cribbs, C., Cutri, R., Daues, G., Delgado, F., Ferguson, H., Gawiser, E., Geary, J. C., Gee, P., Geha, M., Gibson, R. R., Gilmore, D. K., Gressler, W. J., Hogan, C., Huffer, M. E., Jacoby, S. H., Jain, B., Jernigan, J. G., Jones, R. L., Juric, M., Kahn, S. M., Kalirai, J. S., Kantor, J. P., Kessler, R., Kirkby, D., Knox, L., Krabbendam, V. L., Krughoff, S., Kulkarni, S., Lambert, R., Levine, D., Liang, M., Lim, K., Lupton, R. H., Marshall, P., Marshall, S., May, M., Miller, M., Mills, D. J., Monet, D. G., Neill, D. R., Nordby, M., O'Connor, P., Oliver, J., Olivier, S. S., Olsen, K., Owen, R. E., Peterson, J. R., Petry, C. E., Pierfederici, F., Pietrowicz, S., Pike, R., Pinto, P. A., Plante, R., Radeka, V., Rasmussen, A., Ridgway, S. T., Rosing, W., Saha, A., Schalk, T. L., Schindler, R. H., Schneider, D. P., Schumacher, G., Sebag, J., Seppala, L. G., Shipsey, I., Silvestri, N., Smith, J. A., Smith, R. C., Strauss, M. A., Stubbs, C. W., Sweeney, D., Szalay, A., Thaler, J. J., Vanden Berk, D., Walkowicz, L., Warner, M., Willman, B., Wittman, D., Wolff, S. C., Wood-Vasey, W. M., Yoachim, P., Zhan, H., and for the LSST Collaboration: 2008, *ArXiv e-prints*

Jeffery, C. S., Ramsay, G., Naslim, N., Carrera, R., Greiss, S., Barclay, T., Karjalainen, R., Brooks, A., and Hakala, P.: 2013, MNRAS **429**, 3207

Jeffery, C. S. and Saio, H.: 2006, MNRAS **372**, L48

Jeffery, C. S. and Saio, H.: 2007, MNRAS **378**, 379

Jester, S., Schneider, D. P., Richards, G. T., Green, R. F., Schmidt, M., Hall, P. B., Strauss, M. A., Vanden Berk, D. E., Stoughton, C., Gunn, J. E., Brinkmann, J., Kent, S. M., Smith, J. A., Tucker, D. L., and Yanny, B.: 2005, AJ **130**, 873

Kato, T., Nogami, D., Baba, H., and Masuda, S.: 2001, *Information Bulletin on Variable Stars* **5118**, 1

Kawaler, S. D. and Hostler, S. R.: 2005, ApJ **621**, 432

Keller, S. C., Schmidt, B. P., Bessell, M. S., Conroy, P. G., Francis, P., Granlund, A., Kowald, E., Oates, A. P., Martin-Jones, T., Preston, T., Tisserand, P., Vaccarella, A., and Waterson, M. F.: 2007, PASA **24**, 1

Kepler, J.: 1606, *De Stella nova in pede Serpentarii*

Kepler, S. O., Kleinman, S. J., Nitta, A., Koester, D., Castanheira, B. G., Giovannini, O., Costa, A. F. M., and Althaus, L.: 2007, MNRAS **375**, 1315

Kepler, S. O., Nather, R. E., Winget, D. E., Nitta, A., Kleinman, S. J., Metcalfe, T., Sekiguchi, K., Jiang, X., Sullivan, D., Sullivan, T., Janulis, R., Meistas, E., Kalytis, R., Krzesinski, J., Ogoza, W., Zola, S., O'Donoghue, D., Romero-Colmenero, E., Martinez, P., Dreizler, S., Deetjen, J., Nagel, T., Schuh, S. L., Vauclair, G., Ning, F. J., Chevreton, M., Solheim, J.-E., Gonzalez Perez, J. M., Johannessen, F., Kanaan, A., Costa, J. E., Murillo Costa, A. F., Wood, M. A., Silvestri, N., Ahrens, T. J., Jones, A. K., Collins, A. E., Boyer,

M., Shaw, J. S., Mukadam, A., Klumpe, E. W., Larrison, J., Kawaler, S., Riddle, R., Ulla, A., and Bradley, P.: 2003, A&A **401**, 639

Kilic, M., Allende Prieto, C., Brown, W. R., and Koester, D.: 2007, ApJ **660**, 1451

Kilkenny, D.: 2010, Ap&SS **329**, 175

Kilkenny, D., Koen, C., O'Donoghue, D., van Wyk, F., Larson, K. A., Shobbrook, R., Sullivan, D. J., Burleigh, M. R., Dobbie, P. D., and Kawaler, S. D.: 1999, MNRAS **303**, 525

King, A. R.: 1988, QJRAS **29**, 1

Kirkpatrick, J. D., Henry, T. J., and McCarthy, Jr., D. W.: 1991, ApJS **77**, 417

Kjeldsen, H., Christensen-Dalsgaard, J., Handberg, R., Brown, T. M., Gilliland, R. L., Borucki, W. J., and Koch, D.: 2010, *Astronomische Nachrichten* **331**, 966

Kleinman, S. J., Nather, R. E., Winget, D. E., Clemens, J. C., Bradley, P. A., Kanaan, A., Provencal, J. L., Claver, C. F., Watson, T. K., Yanagida, K., Dixson, J. S., Wood, M. A., Sullivan, D. J., Meistas, E., Leibowitz, E. M., Moskalik, P., Zola, S., Pajdosz, G., Krzesinski, J., Solheim, J.-E., Bruvold, A., O'Donoghue, D., Katz, M., Vauclair, G., Dolez, N., Chevreton, M., Barstow, M. A., Kepler, S. O., Giovannini, O., Hansen, C. J., and Kawaler, S. D.: 1994, ApJ **436**, 875

Kleinman, S. J., Nather, R. E., Winget, D. E., Clemens, J. C., Bradley, P. A., Kanaan, A., Provencal, J. L., Claver, C. F., Watson, T. K., Yanagida, K.,

Nitta, A., Dixson, J. S., Wood, M. A., Grauer, A. D., Hine, B. P., Fontaine, G., Liebert, J., Sullivan, D. J., Wickramasinghe, D. T., Achilleos, N., Marar, T. M. K., Seetha, S., Ashoka, B. N., Meistas, E., Leibowitz, E. M., Moskalik, P., Krzesinski, J., Solheim, J.-E., Bruvold, A., O'Donoghue, D., Kurtz, D. W., Warner, B., Martinez, P., Vauclair, G., Dolez, N., Chevreton, M., Barstow, M. A., Kepler, S. O., Giovannini, O., Augusteijn, T., Hansen, C. J., and Kawaler, S. D.: 1998, ApJ **495**, 424

Knigge, C.: 2006, MNRAS **373**, 484

Kolb, U. and Baraffe, I.: 1999, MNRAS **309**, 1034

Kopparapu, R. K., Ramirez, R., Kasting, J. F., Eymet, V., Robinson, T. D., Mahadevan, S., Terrien, R. C., Domagal-Goldman, S., Meadows, V., and Deshpande, R.: 2013, ApJ **765**, 131

Kowalski, A. F., Hawley, S. L., Hilton, E. J., Becker, A. C., West, A. A., Bochanski, J. J., and Sesar, B.: 2009, AJ **138**, 633

Kowalski, A. F., Hawley, S. L., Holtzman, J. A., Wisniewski, J. P., and Hilton, E. J.: 2010, ApJ **714**, L98

Kurtz, D. W., Cunha, M. S., Saio, H., Bigot, L., Balona, L. A., Elkin, V. G., Shibahashi, H., Brandão, I. M., Uytterhoeven, K., Frandsen, S., Frimann, S., Hatzes, A., Lueftinger, T., Gruberbauer, M., Kjeldsen, H., Christensen-Dalsgaard, J., and Kawaler, S. D.: 2011, MNRAS **414**, 2550

Kurtz, D. W., Shibahashi, H., Dhillon, V. S., Marsh, T. R., and Littlefair, S. P.: 2008, MNRAS **389**, 1771

Kurucz, R. L.: 1992, Rev. Mexicana Astron. Astrofis. **23**, 181

Lacy, C. H., Moffett, T. J., and Evans, D. S.: 1976, ApJS **30**, 85

Landolt, A. U.: 1968, ApJ **153**, 151

Lang, D., Hogg, D. W., Mierle, K., Blanton, M., and Roweis, S.: 2010, AJ **139**, 1782

Law, N. M., Kulkarni, S. R., Dekany, R. G., Ofek, E. O., Quimby, R. M., Nugent, P. E., Surace, J., Grillmair, C. C., Bloom, J. S., Kasliwal, M. M., Bildsten, L., Brown, T., Cenko, S. B., Ciardi, D., Croner, E., Djorgovski, S. G., van Eyken, J., Filippenko, A. V., Fox, D. B., Gal-Yam, A., Hale, D., Hamam, N., Helou, G., Henning, J., Howell, D. A., Jacobsen, J., Laher, R., Mattingly, S., McKenna, D., Pickles, A., Poznanski, D., Rahmer, G., Rau, A., Rosing, W., Shara, M., Smith, R., Starr, D., Sullivan, M., Velur, V., Walters, R., and Zolkower, J.: 2009, PASP **121**, 1395

Lemke, M.: 1991, *Department of Astronomy, Univ. Texas at Austin*

Lenz, P., Pamyatnykh, A. A., Zdravkov, T., and Breger, M.: 2010, A&A **509**, A90

Lépine, S. and Gaidos, E.: 2011, AJ **142**, 138

Leto, G., Pagano, I., Buemi, C. S., and Rodono, M.: 1997, A&A **327**, 1114

Lomb, N. R.: 1976, Ap&SS **39**, 447

Maehara, H., Shibayama, T., Notsu, S., Notsu, Y., Nagao, T., Kusaba, S., Honda, S., Nogami, D., and Shibata, K.: 2012, Nature **485**, 478

Marsh, T. R., Dhillon, V. S., and Duck, S. R.: 1995, MNRAS **275**, 828

Mas-Hesse, J. M., Giménez, A., Culhane, J. L., Jamar, C., McBreen, B., Torra, J., Hudec, R., Fabregat, J., Meurs, E., Swings, J. P., Alcacera, M. A., Balado, A., Beiztegui, R., Belenguer, T., Bradley, L., Caballero, M. D., Cabo, P., Defise, J. M., Díaz, E., Domingo, A., Figueras, F., Figueroa, I., Hanlon, L., Hroch, F., Hudcova, V., García, T., Jordan, B., Jordi, C., Kretschmar, P., Laviada, C., March, M., Martín, E., Mazy, E., Menéndez, M., Mi, J. M., de Miguel, E., Muñoz, T., Nolan, K., Olmedo, R., Plesseria, J. Y., Polcar, J., Reina, M., Renotte, E., Rochus, P., Sánchez, A., San Martín, J. C., Smith, A., Soldan, J., Thomas, P., Timón, V., and Walton, D.: 2003, A&A **411**, L261

Maxted, P. f. L., Heber, U., Marsh, T. R., and North, R. C.: 2001, MNRAS **326**, 1391

Mayor, M. and Queloz, D.: 1995, Nature **378**, 355

McGraw, J. T., Liebert, J., Starrfield, S. G., and Green, R.: 1979, in H. M. van Horn and V. Weidemann (eds.), *IAU Colloq. 53: White Dwarfs and Variable Degenerate Stars*, pp 377–381

McNamara, D.: 1997, PASP **109**, 1221

McNamara, D. H.: 2011, AJ **142**, 110

McNamara, D. H., Madsen, J. B., Barnes, J., and Ericksen, B. F.: 2000, PASP **112**, 202

McNamara, D. H. and Redcorn, M. E.: 1977, PASP **89**, 61

Metcalfe, T. S., Salaris, M., and Winget, D. E.: 2002, ApJ **573**, 803

Moffett, T. J.: 1974, S&T **48**, 94

Montgomery, M. H.: 2005, ApJ **633**, 1142

Montgomery, M. H., Williams, K. A., Winget, D. E., Dufour, P., De Gennaro, S., and Liebert, J.: 2008, ApJ **678**, L51

Mordasini, C., Alibert, Y., Georgy, C., Dittkrist, K.-M., Klahr, H., and Henning, T.: 2012a, A&A **547**, A112

Mordasini, C., Alibert, Y., Klahr, H., and Henning, T.: 2012b, A&A **547**, A111

Morin, J., Donati, J.-F., Petit, P., Delfosse, X., Forveille, T., and Jardine, M. M.: 2010, MNRAS **407**, 2269

Mukadam, A. S., Mullally, F., Nather, R. E., Winget, D. E., von Hippel, T., Kleinman, S. J., Nitta, A., Krzesiński, J., Kepler, S. O., Kanaan, A., Koester, D., Sullivan, D. J., Homeier, D., Thompson, S. E., Reaves, D., Cotter, C., Slaughter, D., and Brinkmann, J.: 2004a, ApJ **607**, 982

Mukadam, A. S., Winget, D. E., von Hippel, T., Montgomery, M. H., Kepler, S. O., and Costa, A. F. M.: 2004b, ApJ **612**, 1052

Napiwotzki, R., Yungelson, L., Nelemans, G., Marsh, T. R., Leibundgut, B., Renzini, R., Homeier, D., Koester, D., Moehler, S., Christlieb, N., Reimers, D., Drechsel, H., Heber, U., Karl, C., and Pauli, E.-M.: 2004, in R. W. Hilditch, H. Hensberge, and K. Pavlovski (eds.), *Spectroscopically and Spatially Resolving the Components of the Close Binary Stars*, Vol. 318 of *Astronomical Society of the Pacific Conference Series*, pp 402–410

Nather, R. E., Winget, D. E., Clemens, J. C., Hansen, C. J., and Hine, B. P.: 1990, ApJ **361**, 309

Nelemans, G., Portegies Zwart, S. F., Verbunt, F., and Yungelson, L. R.: 2001, A&A **368**, 939

Nelemans, G., Yungelson, L. R., and Portegies Zwart, S. F.: 2004, MNRAS **349**, 181

Nemec, J. and Mateo, M.: 1990, in C. Cacciari and G. Clementini (eds.), *Confrontation Between Stellar Pulsation and Evolution*, Vol. 11 of *Astronomical Society of the Pacific Conference Series*, pp 64–84

Notsu, Y., Shibayama, T., Maehara, H., Notsu, S., Nagao, T., Honda, S., Ishii, T. T., Nogami, D., and Shibata, K.: 2013, ApJ **771**, 127

Noyes, R. W.: 1985, Sol. Phys. **100**, 385

Oreiro, R., Ulla, A., Pérez Hernández, F., Østensen, R., Rodríguez López, C., and MacDonald, J.: 2004, A&A **418**, 243

Østensen, R. H., Bloemen, S., Vučković, M., Aerts, C., Oreiro, R., Kinemuchi, K., Still, M., and Koester, D.: 2011, ApJ **736**, L39

Østensen, R. H., Oreiro, R., Solheim, J.-E., Heber, U., Silvotti, R., González-Pérez, J. M., Ulla, A., Pérez Hernández, F., Rodríguez-López, C., and Telting, J. H.: 2010a, A&A **513**, A6

Østensen, R. H., Silvotti, R., Charpinet, S., Oreiro, R., Handler, G., Green, E. M., Bloemen, S., Heber, U., Gänsicke, B. T., Marsh, T. R., Kurtz, D. W., Telting,

J. H., Reed, M. D., Kawaler, S. D., Aerts, C., Rodríguez-López, C., Vučković, M., Ottosen, T. A., Liimets, T., Quint, A. C., Van Grootel, V., Randall, S. K., Gilliland, R. L., Kjeldsen, H., Christensen-Dalsgaard, J., Borucki, W. J., Koch, D., and Quintana, E. V.: 2010b, MNRAS **409**, 1470

Paczyński, B.: 1967, Acta Astron. **17**, 287

Paczyński, B. and Sienkiewicz, R.: 1981, ApJ **248**, L27

Paczyński, B. and Sienkiewicz, R.: 1983, ApJ **268**, 825

Papics, P. I.: 2013, *Ph.D. thesis*, Instituut voor Sterrenkunde, KU Leuven, Celestijnenlaan 200D, B-3001 Leuven, Belgium EMAIL: Peter.Papics@ster.kuleuven.be

Patterson, J.: 1998, PASP **110**, 1132

Patterson, J., Kemp, J., Harvey, D. A., Fried, R. E., Rea, R., Monard, B., Cook, L. M., Skillman, D. R., Vanmunster, T., Bolt, G., Armstrong, E., McCormick, J., Krajci, T., Jensen, L., Gunn, J., Butterworth, N., Foote, J., Bos, M., Masi, G., and Warhurst, P.: 2005, PASP **117**, 1204

Paunzen, E., Netopil, M., Rode-Paunzen, M., Handler, G., Božić, H., Ruždjak, D., and Sudar, D.: 2012, A&A **542**, A89

Pettersen, B. R.: 1975a, A&A **41**, 113

Pettersen, B. R.: 1975b, A&A **41**, 87

Pettersen, B. R.: 1981a, A&A **97**, 199

Pettersen, B. R.: 1981b, A&A **95**, 135

Pettersen, B. R.: 1983, A&A **120**, 192

Pettersen, B. R.: 1985a, A&A **147**, 328

Pettersen, B. R.: 1985b, A&A **148**, 151

Pettersen, B. R.: 2006a, *The Observatory* **126**, 397

Pettersen, B. R.: 2006b, MNRAS **368**, 1392

Pettersen, B. R., Coleman, L. A., and Evans, D. S.: 1984, ApJS **54**, 375

Pettersen, B. R., Kern, G. A., and Evans, D. S.: 1983, A&A **123**, 184

Pettersen, B. R., Panov, K. P., Ivanova, M. S., and Sandmann, W. H.: 1986, A&AS **66**, 235

Pettersen, B. R. and Sundland, S. R.: 1991, A&AS **87**, 303

Pinsonneault, M. H., An, D., Molenda-Żakowicz, J., Chaplin, W. J., Metcalfe, T. S., and Bruntt, H.: 2012, ApJS **199**, 30

Poggendorff, J. C.: 1863, *Biograpisch-Literarisches Handworterbuch zur Geschischte der Extacten Wissenschaften enhaltend nachwe isungen uber lebensverhaltinisse und Leistungen von Mathematikern*

Pojmanski, G.: 2002, Acta Astron. **52**, 397

Pollacco, D. L., Skillen, I., Collier Cameron, A., Christian, D. J., Hellier, C., Irwin, J., Lister, T. A., Street, R. A., West, R. G., Anderson, D., Clarkson, W. I., Deeg, H., Enoch, B., Evans, A., Fitzsimmons, A., Haswell, C. A., Hodgkin, S., Horne, K., Kane, S. R., Keenan, F. P., Maxted, P. F. L., Norton,

A. J., Osborne, J., Parley, N. R., Ryans, R. S. I., Smalley, B., Wheatley, P. J., and Wilson, D. M.: 2006, PASP **118**, 1407

Poretti, E., Clementini, G., Held, E. V., Greco, C., Mateo, M., Dell'Arciprete, L., Rizzi, L., Gullieuszik, M., and Maio, M.: 2008, ApJ **685**, 947

Press, W. H. and Rybicki, G. B.: 1989, ApJ **338**, 277

Press, W. H., Teukolsky, S. A., Vetterling, W. T., and Flannery, B. P.: 1992, *Numerical recipes in C. The art of scientific computing*, Cambridge: University Press, 1992, 2nd ed.

Pribulla, T., Kreiner, J. M., and Tremko, J.: 2003, *VizieR Online Data Catalog* **5119**, 0

Prsa, A., Robin, A., and Barclay, T.: 2014, *ArXiv e-prints*

Prša, A., Batalha, N., Slawson, R. W., Doyle, L. R., Welsh, W. F., Orosz, J. A., Seager, S., Rucker, M., Mjaseth, K., Engle, S. G., Conroy, K., Jenkins, J., Caldwell, D., Koch, D., and Borucki, W.: 2011, AJ **141**, 83

Putnam, D. and Wiemer, D.: 2014, *Journal of the Astronautical Sciences* **14**, 102

Quimby, R. M.: 2006, *Ph.D. thesis*, The University of Texas at Austin

Ramachandran, P. and Varoquaux, G.: 2011, *Computing in Science & Engineering* **13(2)**, 40

Ramsay, G., Brooks, A., Hakala, P., Barclay, T., Garcia-Alvarez, D., Antoci,

V., Greiss, S., Still, M., Steeghs, D., Gänsicke, B., and Reynolds, M.: 2014, MNRAS **437**, 132

Ramsay, G., Cannizzo, J. K., Howell, S. B., Wood, M. A., Still, M., Barclay, T., and Smale, A.: 2012, MNRAS **425**, 1479

Ramsay, G., Doyle, J. G., Hakala, P., Garcia-Alvarez, D., Brooks, A., Barclay, T., and Still, M.: 2013, MNRAS **434**, 2451

Ramsay, G., Hakala, P., Barclay, T., Wheatley, P., Marshall, G., Lehto, H., Napiwotzki, R., Nelemans, G., Potter, S., and Todd, I.: 2009, MNRAS **398**, 1333

Ramsay, G., Hakala, P., and Cropper, M.: 2002, MNRAS **332**, L7

Ramsay, G., Napiwotzki, R., Barclay, T., Hakala, P., Potter, S., and Cropper, M.: 2011, MNRAS **417**, 400

Ramsay, G., Napiwotzki, R., Hakala, P., and Lehto, H.: 2006, MNRAS **371**, 957

Rappaport, S., Joss, P. C., and Webbink, R. F.: 1982, ApJ **254**, 616

Rappaport, S., Verbunt, F., and Joss, P. C.: 1983, ApJ **275**, 713

Reid, I. N., Cruz, K. L., Allen, P., Mungall, F., Kilkenny, D., Liebert, J., Hawley, S. L., Fraser, O. J., Covey, K. R., Lowrance, P., Kirkpatrick, J. D., and Burgasser, A. J.: 2004, AJ **128**, 463

Ritter, H. and Kolb, U.: 2003, A&A **404**, 301

Rodríguez, E. and Breger, M.: 2001, A&A **366**, 178

Rodríguez, E., López-González, M. J., and López de Coca, P.: 2000, A&AS **144**, 469

Rodriguez, E., Rolland, A., and Lopez de Coca, P.: 1990, Ap&SS **169**, 113

Roelofs, G. H. A., Rau, A., Marsh, T. R., Steeghs, D., Groot, P. J., and Nelemans, G.: 2010, ApJ **711**, L138

Rogers, F. J. and Iglesias, C. A.: 1992, ApJS **79**, 507

Romero, A. D., Córsico, A. H., Althaus, L. G., Kepler, S. O., Castanheira, B. G., and Miller Bertolami, M. M.: 2012, MNRAS **420**, 1462

Rowe, J. and Kepler Team: 2014, in *American Astronomical Society Meeting Abstracts*, Vol. 223 of *American Astronomical Society Meeting Abstracts*, p. 228.02

Rowe, J. F., Bryson, S. T., Marcy, G. W., Lissauer, J. J., Jontof-Hutter, D., Mullally, F., Gilliland, R. L., Issacson, H., Ford, E., Howell, S. B., Borucki, W. J., Haas, M., Huber, D., Steffen, J. H., Thompson, S. E., Quintana, E., Barclay, T., Still, M., Fortney, J., Gautier, III, T. N., Hunter, R., Caldwell, D. A., Ciardi, D. R., Devore, E., Cochran, W., Jenkins, J., Agol, E., Carter, J. A., and Geary, J.: 2014, ApJ **784**, 45

Rowe, J. F., Matthews, J. M., Seager, S., Kuschnig, R., Guenther, D. B., Moffat, A. F. J., Rucinski, S. M., Sasselov, D., Walker, G. A. H., and Weiss, W. W.: 2006, ApJ **646**, 1241

Rucinski, S. M.: 1998, AJ **116**, 2998

Rucinski, S. M. and Pribulla, T.: 2008, MNRAS **388**, 1831

Saffer, R. A., Bergeron, P., Koester, D., and Liebert, J.: 1994, ApJ **432**, 351

Saio, H. and Gautschy, A.: 2004, MNRAS **350**, 485

Samus, N. N., Durlevich, O. V., and et al.: 2009, *VizieR Online Data Catalog* **1**, 2025

Savanov, I. S. and Dmitrienko, E. S.: 2011, *Astronomy Reports* **55**, 890

Scalo, J., Kaltenegger, L., Segura, A. G., Fridlund, M., Ribas, I., Kulikov, Y. N., Grenfell, J. L., Rauer, H., Odert, P., Leitzinger, M., Selsis, F., Khodachenko, M. L., Eiroa, C., Kasting, J., and Lammer, H.: 2007, *Astrobiology* **7**, 85

Scargle, J. D.: 1982, ApJ **263**, 835

Scaringi, S., Groot, P. J., Verbeek, K., Greiss, S., Knigge, C., and Körding, E.: 2013, MNRAS **428**, 2207

Schaller, G., Schaerer, D., Meynet, G., and Maeder, A.: 1992, A&AS **96**, 269

Schreiber, M. R.: 2007, A&A **466**, 1025

Schuh, S., Huber, J., Dreizler, S., Heber, U., O'Toole, S. J., Green, E. M., and Fontaine, G.: 2006, A&A **445**, L31

Schwabe, M.: 1844, *Astronomische Nachrichten* **21**, 233

Schwarzenberg-Czerny, A.: 1989, MNRAS **241**, 153

Schwarzenberg-Czerny, A.: 1996, ApJ **460**, L107

Scuflaire, R., Théado, S., Montalbán, J., Miglio, A., Bourge, P.-O., Godart, M., Thoul, A., and Noels, A.: 2008, Ap&SS **316**, 83

Segura, A., Walkowicz, L. M., Meadows, V., Kasting, J., and Hawley, S.: 2010, *Astrobiology* **10**, 751

Shibahashi, H. and Kurtz, D. W.: 2012, MNRAS **422**, 738

Shipman, H. L.: 1979, ApJ **228**, 240

Silvotti, R., Solheim, J.-E., Gonzalez Perez, J. M., Heber, U., Dreizler, S., Edelmann, H., Østensen, R., and Kotak, R.: 2000, A&A **359**, 1068

Skrutskie, M. F., Cutri, R. M., Stiening, R., Weinberg, M. D., Schneider, S., Carpenter, J. M., Beichman, C., Capps, R., Chester, T., Elias, J., Huchra, J., Liebert, J., Lonsdale, C., Monet, D. G., Price, S., Seitzer, P., Jarrett, T., Kirkpatrick, J. D., Gizis, J. E., Howard, E., Evans, T., Fowler, J., Fullmer, L., Hurt, R., Light, R., Kopan, E. L., Marsh, K. A., McCallon, H. L., Tam, R., Van Dyk, S., and Wheelock, S.: 2006, AJ **131**, 1163

Slawson, R. W., Prša, A., Welsh, W. F., Orosz, J. A., Rucker, M., Batalha, N., Doyle, L. R., Engle, S. G., Conroy, K., Coughlin, J., Gregg, T. A., Fetherolf, T., Short, D. R., Windmiller, G., Fabrycky, D. C., Howell, S. B., Jenkins, J. M., Uddin, K., Mullally, F., Seader, S. E., Thompson, S. E., Sanderfer, D. T., Borucki, W., and Koch, D.: 2011, AJ **142**, 160

Solheim, J.-E.: 2010, PASP **122**, 1133

Southworth, J., Gänsicke, B. T., Marsh, T. R., de Martino, D., Hakala, P., Littlefair, S., Rodríguez-Gil, P., and Szkody, P.: 2006, MNRAS **373**, 687

Southworth, J., Marsh, T. R., Gänsicke, B. T., Aungwerojwit, A., Hakala, P., de Martino, D., and Lehto, H.: 2007, MNRAS **382**, 1145

Southworth, J., Zima, W., Aerts, C., Bruntt, H., Lehmann, H., Kim, S.-L., Kurtz, D. W., Pavlovski, K., Prša, A., Smalley, B., Gilliland, R. L., Christensen-Dalsgaard, J., Kawaler, S. D., Kjeldsen, H., Cote, M. T., Tenenbaum, P., and Twicken, J. D.: 2011, MNRAS **414**, 2413

Steinfadt, J. D. R., Bildsten, L., and Arras, P.: 2010, ApJ **718**, 441

Szkody, P., Fraser, O., Silvestri, N., Henden, A., Anderson, S. F., Frith, J., Lawton, B., Owens, E., Raymond, S., Schmidt, G., Wolfe, M., Bochanski, J., Covey, K., Harris, H., Hawley, S., Knapp, G. R., Margon, B., Voges, W., Walkowicz, L., Brinkmann, J., and Lamb, D. Q.: 2003, AJ **126**, 1499

Szkody, P., Henden, A., Mannikko, L., Mukadam, A., Schmidt, G. D., Bochanski, J. J., Agüeros, M., Anderson, S. F., Silvestri, N. M., Dahab, W. E., Oguri, M., Schneider, D. P., Shin, M.-S., Strauss, M. A., Knapp, G. R., and West, A. A.: 2007, AJ **134**, 185

Takata, M. and Shibahashi, H.: 1994, PASJ **46**, 301

Takata, M. and Shibahashi, H.: 1995, PASJ **47**, 219

Tamuz, O., Mazeh, T., and North, P.: 2006, MNRAS **367**, 1521

Tamuz, O., Mazeh, T., and Zucker, S.: 2005, MNRAS **356**, 1466

The Opacity Project Team: 1995, *The Opacity Project, Vol. 1*, IoP, Bristol

Thompson, S. E., Christiansen, J. L., Jenkins, J. M., Caldwell, D. A., Barclay, T., Bryson, S. T., Burke, C. J., Campbell, J. R., Catanzarite, J., Clarke, B. D., Coughlin, J. L., Girouard, F., Haas, M. R., Ibrahim, K., Klaus, T. C., Kolodziejczak, J. J., Li, J., McCauliff, S. D., Morris, R., Mullally, F., Quintana, E. V., Rowe, J., Sabale, A., Seader, S., Smith, J. C., Still, M. D., Tenenbaum, J. D., Twicken, J. D., and Uddin, A. K.: 2013, *Kepler Data Release 23 Notes (KSCI-19063-001)*

Udalski, A., Soszynski, I., Szymanski, M., Kubiak, M., Pietrzynski, G., Wozniak, P., and Zebrun, K.: 1998, Acta Astron. **48**, 563

Udalski, A., Szymanski, M., Kubiak, M., Pietrzynski, G., Soszynski, I., Wozniak, P., and Zebrun, K.: 2000, Acta Astron. **50**, 307

Unno, W., Osaki, Y., Ando, H., and Shibahashi, H.: 1979, *Nonradial oscillations of stars*

Uytterhoeven, K., Moya, A., Grigahcène, A., Guzik, J. A., Gutiérrez-Soto, J., Smalley, B., Handler, G., Balona, L. A., Niemczura, E., Fox Machado, L., Benatti, S., Chapellier, E., Tkachenko, A., Szabó, R., Suárez, J. C., Ripepi, V., Pascual, J., Mathias, P., Martín-Ruíz, S., Lehmann, H., Jackiewicz, J., Hekker, S., Gruberbauer, M., García, R. A., Dumusque, X., Díaz-Fraile, D., Bradley, P., Antoci, V., Roth, M., Leroy, B., Murphy, S. J., De Cat, P., Cuypers, J., Kjeldsen, H., Christensen-Dalsgaard, J., Breger, M., Pigulski, A., Kiss, L. L., Still, M., Thompson, S. E., and van Cleve, J.: 2011a, A&A **534**, A125

Uytterhoeven, K., Moya, A., Grigahcène, A., Guzik, J. A., Gutiérrez-Soto, J., Smalley, B., Handler, G., Balona, L. A., Niemczura, E., Fox Machado, L.,

Benatti, S., Chapellier, E., Tkachenko, A., Szabó, R., Suárez, J. C., Ripepi, V., Pascual, J., Mathias, P., Martín-Ruíz, S., Lehmann, H., Jackiewicz, J., Hekker, S., Gruberbauer, M., García, R. A., Dumusque, X., Díaz-Fraile, D., Bradley, P., Antoci, V., Roth, M., Leroy, B., Murphy, S. J., De Cat, P., Cuypers, J., Kjeldsen, H., Christensen-Dalsgaard, J., Breger, M., Pigulski, A., Kiss, L. L., Still, M., Thompson, S. E., and van Cleve, J.: 2011b, A&A **534**, A125

van den Oord, G. H. J., Doyle, J. G., Rodono, M., Gary, D. E., Henry, G. W., Byrne, P. B., Linsky, J. L., Haisch, B. M., Pagano, I., and Leto, G.: 1996, A&A **310**, 908

Vauclair, C.: 1997, in J. Provost and F.-X. Schmider (eds.), *Sounding Solar and Stellar Interiors*, Vol. 181 of *IAU Symposium*, p. 367

Ventura, R., Peres, G., Pagano, I., and Rodono, M.: 1995, A&A **303**, 509

Verbunt, F. and Zwaan, C.: 1981, A&A **100**, L7

Walker, G., Matthews, J., Kuschnig, R., Johnson, R., Rucinski, S., Pazder, J., Burley, G., Walker, A., Skaret, K., Zee, R., Grocott, S., Carroll, K., Sinclair, P., Sturgeon, D., and Harron, J.: 2003, PASP **115**, 1023

Walkowicz, L. M., Basri, G., Batalha, N., Gilliland, R. L., Jenkins, J., Borucki, W. J., Koch, D., Caldwell, D., Dupree, A. K., Latham, D. W., Meibom, S., Howell, S., Brown, T. M., and Bryson, S.: 2011, AJ **141**, 50

Warner, B.: 1995, *Cataclysmic Variable Stars*, Cambridge University Press

Warner, B. and Robinson, E. L.: 1972, *Nature Physical Science* **239**, 2

Werner, K., Hammer, N. J., Nagel, T., Rauch, T., and Dreizler, S.: 2005, in D. Koester and S. Moehler (eds.), *14th European Workshop on White Dwarfs*, Vol. 334 of *Astronomical Society of the Pacific Conference Series*, p. 165

Wilson, E. R.: 1917, *Popular Astronomy* **25**, 88

Winget, D. E.: 1981, *Ph.D. thesis*, University of Rochester

Winget, D. E. and Kepler, S. O.: 2008, ARA&A **46**, 157

Winget, D. E., Nather, R. E., Clemens, J. C., Provencal, J., Kleinman, S. J., Bradley, P. A., Wood, M. A., Claver, C. F., Frueh, M. L., Grauer, A. D., Hine, B. P., Hansen, C. J., Fontaine, G., Achilleos, N., Wickramasinghe, D. T., Marar, T. M. K., Seetha, S., Ashoka, B. N., O'Donoghue, D., Warner, B., Kurtz, D. W., Buckley, D. A., Brickhill, J., Vauclair, G., Dolez, N., Chevreton, M., Barstow, M. A., Solheim, J. E., Kanaan, A., Kepler, S. O., Henry, G. W., and Kawaler, S. D.: 1991, ApJ **378**, 326

Winget, D. E., Robinson, E. L., Nather, R. D., and Fontaine, G.: 1982, ApJ **262**, L11

Winget, D. E., van Horn, H. M., Tassoul, M., Hansen, C. J., and Fontaine, G.: 1983, ApJ **268**, L33

Winkler, P. F., Gupta, G., and Long, K. S.: 2003, ApJ **585**, 324

Wolszczan, A.: 1994, *Science* **264**, 538

Wolszczan, A. and Frail, D. A.: 1992, Nature **355**, 145

Woudt, P. A. and Warner, B.: 2010, MNRAS **403**, 398

Wozniak, P. R.: 2000, Acta Astron. **50**, 421

Yau, K. K. C. and Stephenson, F. R.: 1998, QJRAS **29**, 175

Young, D. R., Smartt, S. J., Mattila, S., Tanvir, N. R., Bersier, D., Chambers, K. C., Kaiser, N., and Tonry, J. L.: 2008, A&A **489**, 359

Zhang, X. B., Zhang, R. X., and Fang, M. J.: 2002, A&A **395**, 587

Zhao, F.-Y., Strom, R. G., and Jiang, S.-Y.: 2006, Chinese J. Astron. Astrophys. **6**, 635